Production of Catalyst Supports by Twin Screw Extrusion of Pastes

Gemma Winstone

2011

EngD in Formulation Engineering

Abstract

The production of ceramic catalyst supports is commonly performed by the extrusion of a paste. The rheological properties of the paste as it passes through the extruder have a strong influence on the extrudate properties such as porosity and strength, which in turn affect the catalytic performance of the final product.

An assessment of the effect of acid type and strength and powder type on the rheological properties of concentrated boehmite slurries has been made. In particular, evidence of gel formation is looked for, and the surface chemistry is examined using zeta potential measurements. Further understanding of the observed rheological changes is obtained by performing nuclear magnetic resonance studies and cryogenic microscopy.

The effect of powder properties and acid type and strength on the saturation states of a formulation has been examined using mixer torque rheometry. The prediction of saturation states from bulk density measurements is discussed.

The predictive capability of the mixer torque rheometer with regards extrusion formulations is investigated. The effect of acid type and strength on successful extrusion formulations and extrudate properties is discussed.

For my family

Contents

List of Figures and Tables

List of Figures

List of Tables

Chapter 1 Introduction

1.1 Catalysis and Johnson Matthey

A catalyst is a material which increases the rate of a reaction step with no net consumption or generation of the catalyst by the reaction. Heterogeneous catalysis is crucial to a large number of industrial operations, over 90% of global chemical processes require or utilise a catalyst. Johnson Matthey is one of the world's leading catalyst companies, supplying catalysts across a wide variety of applications including emissions control technologies, synthesis gas and hydroprocessing catalysts.

Heterogeneous catalysis most commonly incorporates the use of a solid phase catalyst with products and reactants in the liquid or gaseous phase. The high commercial cost of catalytically active materials encourages the use of cheap, inert support materials, typically ceramics, in many applications. Johnson Matthey currently purchases a large portion of the supports required to meet the catalytic needs of their customers, however, changes in the market are encouraging the production of supports internally.

1.2 Catalyst Supports

For a catalyst support to be effective in application it must be highly porous to maximise the surface area available for supporting the catalytically active material. The pores must be of a suitable size for the supports' application and highly inter connected to allow for transport of reactants and products to and from active sites. The surface chemistry of the support also needs to be suitable for the particular active catalyst with which the support is to be loaded.

The successful manufacture of a catalyst support is a combination of the material formulation and the forming method used. A wide variety of forming techniques are available for support manufacture, including tabletting, granulation and extrusion, of which there are a number of types, principally ram extrusion and single or twin screw extrusion. The advantages of the twin screw extrusion process over ram or single screw extrusion is that it allows the mixing of a paste and forming into a shape to be combined into a single unit step and is suited to continuous operation, which is desirable for an industrial process. Extrusion also allows the formation of a variety of shapes by varying the design of the die, as opposed to granulation which is limited to the production of spheres.

1.3 Scope of Investigation

The aim of this thesis is to investigate the relationship between formulation parameters and extrudate properties of an alumina catalyst support, produced by twin screw extrusion of an acidic boehmite paste. In particular, it was desired to develop the capability to predict successful extrusion formulations from fundamental powder properties and acid strength, allowing plant managers to move towards operating on a feed-forward, rather than feedback, control basis, based on measurable feed properties, improving the control over issues associated with batch to batch variability.

Chapter 2 presents a more detailed backround and introduction to the prjoject work undertaken and description of factors to be considered throughout the project. A review of published literature pertaining to the topic of the thesis is presented in Chapter 3. Chapter 4 contains details of the materials, equipment and methods employed.

Characterisation of the powder properties such as particle and crystallite size, and dispersion and dissolution rates in acid are presented in Chapter 5.

Chapter 6 presents an assessment of the effect of acid type and strength and powder type on the rheological properties of concentrated boehmite slurries. In particular, evidence of gel formation is looked for, and the surface chemistry is examined using zeta potential measurements. Further understanding of the observed rheological changes is obtained by performing nuclear magnetic resonance studies and cryogenic microscopy.

The effect of powder properties and acid type and strength on the saturation states of a formulation has been examined using mixer torque rheometry, presented in Chapter 7. The prediction of saturation states from bulk density measurements is discussed.

Chapter 8 examines the capability of the mixer torque rheometer to predict successful extrusion formulations. The effect of acid type and strength on successful extrusion formulations and extrudate properties is discussed.

Chapter 9 contains project conclusions and suggestions for further work in the field. References can be viewed in Chapter 10.

Chapter 2 Background

2.1 General Introduction and Background

2.1.1 Alumina

Aluminium oxides and aluminium hydroxides are commonly called alumina. Alumina exists in many phases, including α, γ, δ, ε, θ, κ, and ρ, and various nomenclatures have been developed over the years. Each of the phases exhibit differences in physical and chemical properties, a detailed description of aluminas can be found in Wefers and Misra (1987). Alpha aluminium oxide ($\alpha - Al_2O_3$) is also commonly called corundum and it is the only thermodynamically stable form of aluminium oxide. It is a very abrasive material, which can be formed from the other phases of alumina, according to the transformation sequence seen in Figure 2.1, when exposed to high temperatures and pressures. This project considers the use of boehmite, ($\gamma - AlOOH$) as a raw material for the production of alumina catalyst supports.

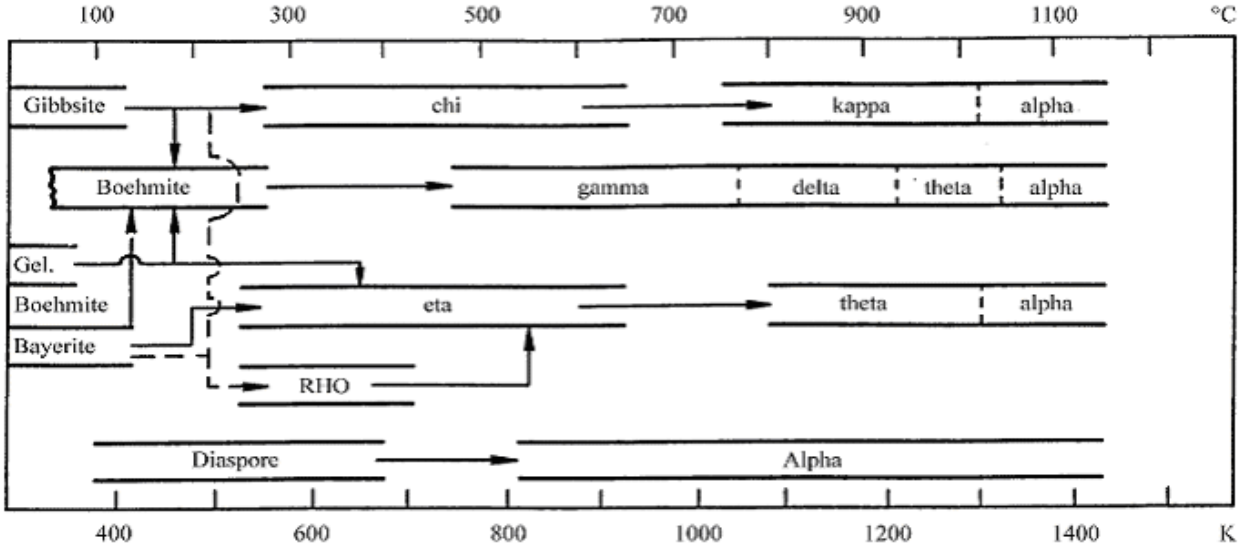

Figure 2.1: Transformation sequence of aluminas to alpha alumina (adapted from Wefers and Misra, 1987)

Boehmite or pseudoboehmite is a common choice of raw material for forming of catalyst supports. The term pseudoboehmite refers to a boehmite with which additional crystalline water is associated, (discussed further in Section 2.1.3). A large variety of boehmites are commercially available with different properties such as particle size distribution, crystallite size and impurity levels, resulting from the specific conditions of synthesis, (discussed in Section 3.4). The wide variety available is illustrated by Stoepler and Unger (1983) who performed an investigation on extrusion using more than 60 commercially available aluminas, principally gibbsites and boehmites. They found that the degree of crystallinity and the size distribution of the aggregates had a significant effect on the properties of the product.

2.1.2 Manufacture of Boehmites

Boehmite is produced from the ore bauxite. This material is converted to alumina trihydrate, $Al(OH)_3$ by the Bayer process, developed and patented over 100 years ago and described in detail by Hind *et al.* (1999). This can then be used to form boehmite by the sulphate route, chlorate route or organic route. The route of manufacture has a significant impact on the types and levels of impurities present and the specific synthesis conditions can determine the structure and properties of a boehmite crystal, (discussed in Section 3.4).

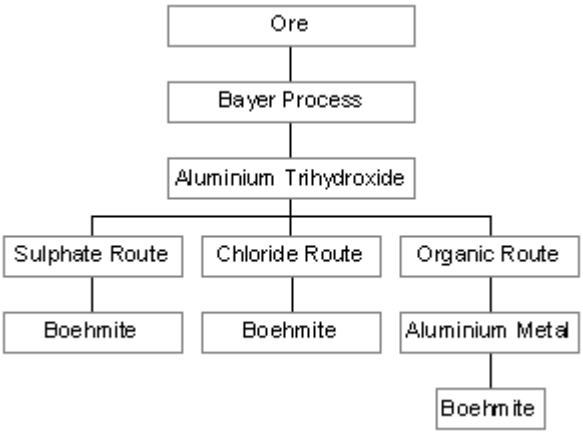

Figure 2.2: Routes of boehmite manufacture

Both the sulphate and chloride routes are acid precipitation methods which involve the alumina trihydrates being dissolved in sulphuric or hydrochloric acid respectively and precipitated out with a base, typically sodium hydroxide or sodium carbonate. Precipitation using nitric acid and ammonium nitrate, results in impurities which are volatile and as such can be easily removed. However, this process is rare due to the high cost and formation of an explosive side product, aluminium nitrate. A study by Guzmán-Castillo *et al.* (2005) indicated that boehmites produced by the sulphate route were less crystalline than those produced by the chloride route. They also observed differences in the types of acidity present in each case; boehmites produced by the chloride route displayed only Lewis acidity in the gamma phase, where as those produced by the chloride route displayed both Lewis and Brönsted Lowry sites, the ratio of which was a function of the crystallite size.

The organic route involves refining the alumina trihydrates to pure aluminium and then applying the Ziegler process to the aluminium to produce boehmite. This is also referred to as the alkoxide route and involves four steps; the formation of an organic aluminium compound, chain growth of the organic, oxidation and hydrolysis. This

process was originally used to produce long chain alcohols and boehmite was formed as a by-product. Boehmites from the long chain alcohol plants can have up to 2000 ppm titania present where as the boehmites from purpose built sites would typically have only a few hundred ppm.

Three boehmite powders have been studied in this project, each manufactured by different routes, though all three are precipitated boehmites. The boehmite G250 is manufactured by the sulphate route whilst the boehmite V250 by the chloride route, both of these boehmites are spray dried. The boehmite Dequagel HP is manufactured by precipitating aluminium hydroxide with CO_2 according to patent US4492682. The acid and base used for washing the precipitate are not specified, this boehmite is static dried.

2.1.3 Structure of Boehmite and Psuedoboehmite

Wefers and Misra (1987) present a description of the structure of boehmite, elucidated from a variety of previous published work, including one of the earliest and most commonly cited references regarding the structure of boehmite, Lippens (1961). The crystals consist of double layers in which the oxygen ions are packed cubically. Each of these double layers is composed of chains formed by double molecules of Al-OOH, seen in Figure 2.3 extending in the lengthwise direction. In these layers, the hydroxyl ions in one layer are located over the depression which occurs between the hydroxyl ions in adjacent layers, seen in Figure 2.4. The primitive unit cell can be seen within the dashed line in Figure 2.4, this was shown by Kiss *et al.* (1980) to comprise of 4 Al-OOH units using Raman spectroscopy. The double layers are linked by hydrogen bonds between neighbouring hydroxyl ions.

Pierre and Uhlmann (1986) describe how the oxygen octahedra in boehmite are arranged in parallel layers linked by hydrogen bonds. Each of these octahedral layers are composed of two octahedral sublayers. They examined the structure of boehmite gels formed from aluminium hydroxide sols using transmission electron microscopy (TEM) and scanning electron microscopy (SEM) and present a schematic representation of the gel consisting of folded layers of boehmite crystals, formed as a result of stacking defects in the octahedral sublayers.

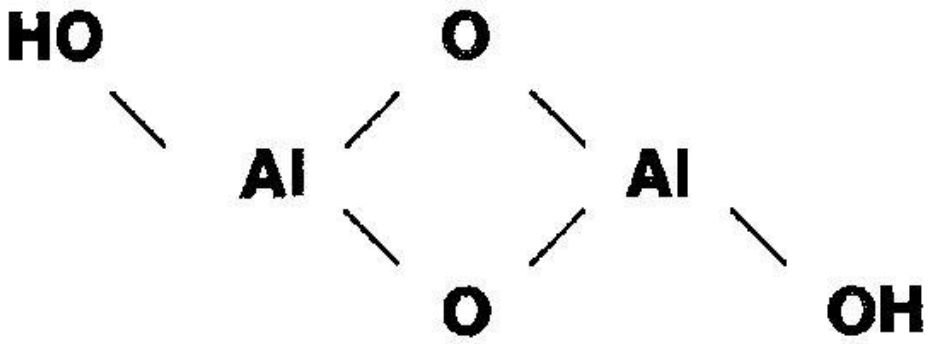

Figure 2.3: A 2-AlOOH molecule (adapted from Wefers and Misra, 1987)

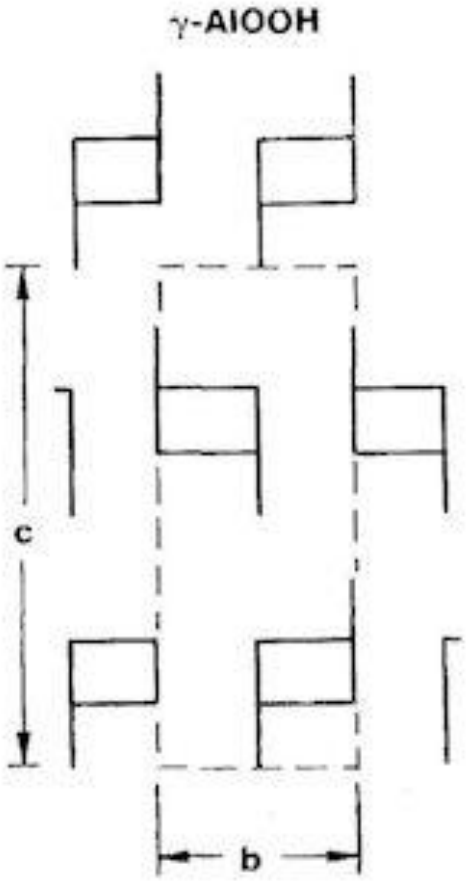

Figure 2.4: Structure of boehmite (adapted from Wefers and Misra, 1987)

Further descriptions and details of the structure of boehmite and psuedoboehmite are discussed by Bokhimi *et al.* (2001) who discuss the relationship between the formation conditions of boehmite and the resulting crystallite size. Lamberov *et al.* (2003) also discuss the effect of synthesis conditions on the physicochemical properties of aluminium hydroxides, additional studies into these relationships are discussed further in Section 3.4.

Most authors, (including Zakharchenya, 1996, Wefers and Bell, 1972, Music *et al.*, 1996 and Assin *et al.*, 1998) agree that boehmite and pseudoboehmite have the

same crystal structure, varying only in water content and degree of crystallinity, connected to the presence of excess water considered by these authors to be located in the hydrogen bonding layer, increasing the d spacing. Pseudoboehmite is described by Martens *et al.* (2001) as a hydrated form of boehmite with a larger d spacing. Loong and Ozawa (2004) examined the structure of boehmite and pseudoboehmite using small angle scattering (SANS), they identified proton delocalisation and disordered OH sites in psuedoboehmite microstructure.

It is proposed by Bokhimi *et al.* (2001) that boehmite and pseudoboehmite are the same phase of aluminium hydroxide but with different crystallite sizes, shown by examining the crystallography of boehmites with crystallite sizes ranging from 1 to 27 nm. Other publications such as Baker and Pearson (1974) and Okada *et al.* (2002b) discuss that the difference is due to excess water and lower crystallinity of pseudoboehmite.

Of particular interest in the discussion of boehmite structure is the issue of the location of excess water in a pseudoboehmite. Pseudoboehmite, poorly crystalline boehmite and gelatinous boehmite are used interchangeably in literature regarding this issue. The excess water is typically 15-30 wt%. A review of the proposed locations of this water is presented by Wefers and Misra (1987). Proposed locations include as a suface monolayer (Bye and Robinson, 1974) random intercalation (Pierre and Uhlmann, 1986) and as a link between the $(AlOOH)_2$ molecules seen in Figure 2.3 (Lippens, 1961). X-ray diffraction patterns show varying degrees of increase in the d-spacing, placing the water between the double layers, though the largest increase was observed in the b axis (Wefers and Misra, 1987). This location is argued by Guzman Castillo *et al.* (2001) who compared the crystallite dimensions

of boehmite and pseudoboehmite and found the same crystallite structure with a difference of only 0.0052 nm in the b axis, a difference which is not large enough to support this as the location of excess water.

Near-infrared spectroscopy can be used to study the water retention capacity of a material, and distinguish the energetic states of water within a material, Luukkonen (2001). Quasi elastic neutron scattering (QENS) has also been employed by Mitra *et al.* (2001) to study the dynamics of water contained in the pores of an alumina gel. They identified the presence of both localised water, bonded to the surface, and delocalised water free to diffuse.

Evidence of the presence of proton pairs in boehmite was obtained by nuclear magnetic resonance absorption spectra by Slade and Halstead (1980). Details of the preparation and structure of this deuterated form of boehmite can be seen in the paper by Corbato *et al.* (1985).

The surface polarity of peptised aluminas (not boehmite) was studied using gas chromatography by Hillerova *et al.* (1981), who concluded that the polarity varied with preparation conditions. The crystallinity of boehmite has been shown by Nortier *et al.* (1990) to affect the surface properties of the resulting gamma alumina. The structure of gamma alumina has been shown to vary depending on whether it has been formed from boehmite or gibbsite by Chen *et al.* (1992) who studied transition aluminas using solid state NMR and identified a much higher presence of pentahedral aluminium coordination in aluminas formed from boehmite.

2.1.4 Size Distribution and Packing Effects

Particle packing is important in the formation of ceramics by paste extrusion as it will affect the rheological behaviour of the paste during processing and also the properties such as strength and porosity of the resulting extrudate. The maximum packing fraction, also termed packing limit, of a system is an important parameter to consider in paste production and the packing structure is critical in determining the resulting pore structure of a formed product. Particle packing is strongly affected by particle size distribution, particle size and surface chemistry. Particle packing behaviour is also known to have a significant effect on the rheology of concentrated suspensions and pastes, the influence of particle packing on paste extrusion is discussed by Blackburn and Böhm (1993).

The contact polyhedra formed in particle systems, which were described by Bernal (1959), have formed the basis of many packing models developed since. Blackburn and Wilson (2008) review the packing theories for powders which are numerous and well reported. Jaeger and Nagel (1992) calculated that the maximum packing fraction of a unimodal distribution of spheres, ignoring colloidal interactions, is 0.64. Variations in size distribution, size and shape of particles will alter this value. Various studies have been performed on the packing of more complicated systems, such as the packing of continuous particle size distributions which was considered by Bark and Apte (1987), prediction of the maximum packing fraction of a multimodal non spherical system by Liu and Ha (2002), and the effect of surface chemistry on particle packing in alumina suspensions by Tseng and Wu (2003), A description of the effect of particle shape on particle packing is presented by Blackburn and Wilson

(2008). Packing in wet systems was studied by Ye *et al.* (2008) who developed a method which allowed a wet system to be considered as an imaginary dry system.

The discrete element method simulation technique has been applied by a number of authors (Sweeney and Martin, 2003, Chung *et al.*, 2005, Theuerkauf *et al.*, 2006) to understanding particle packing. Limitations of the technique mean that simulations fail to replicate real systems, studies focus on unimodal, dry, spherical particles, significantly larger than colloids. Fu *et al.* (2006) performed a DEM simulation of packing for a powder system containing 2000 180 - 300 μm particles. Their simulation was found to be in good agreement with observations made using X-ray microtomography, however the study is still a simplification of reality as it only considers a small number of spherical particles. Real particle systms contain a much larger number of non spherical particles which may exhibit properties not considered in the models, such as cohesivity, which will alter the packing behaviour from that predicted by the simulations.

2.1.5 Dispersion

Dispersion is known to occur by both mechanical and chemical means. Figure 2.5 shows a typical dispersion mechanism in which the agglomerates are first broken down by mechanical means into agglomerates, which can be dispersed into primary particles by chemical dispersion

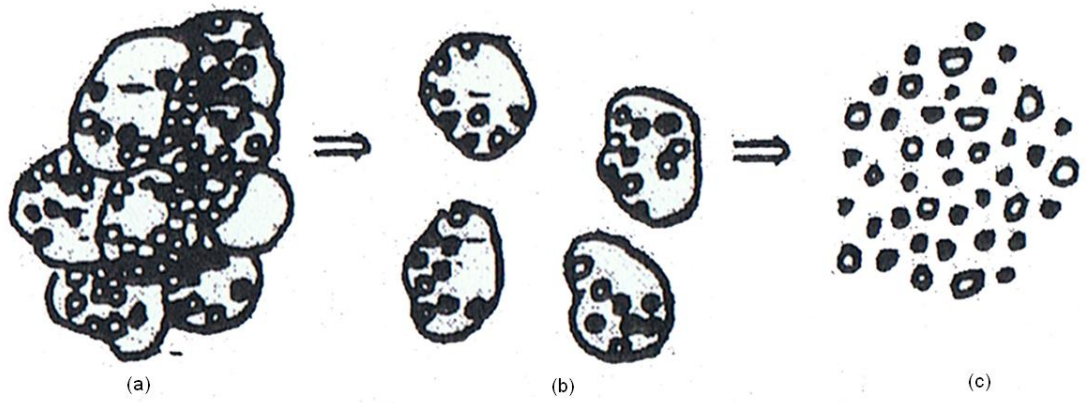

Figure 2.5: Dispersion mechanism of spray dried particles (a), to agglomerates (b) to crystallites (c) (adapted from UOP promotional literature)

Mechanical breakdown of particles can cause an alteration of the surface chemistry by exposing internal surfaces, and thus can encourage breakdown by chemical dispersion.

Boehmite powders can vary significantly in their tendency to disperse by both mechanical and chemical means, depending upon the conditions of their preparation. The variation in dispersibility is used as a marketing tool, targeting particular boehmite powders to specific markets.

2.1.6 Porosity

Pores are classified, according to their size, as either macropores, mesopores or micropores. Macropores are considered to be those pores which are larger than 50 nm. Mesopores, also called transitional or intermediate pores, are between 2 nm and 50 nm and micropores are those which are smaller than 2 nm. The origins of each of these types of pores are discussed by Johnson and Mooi (1968) who consider pores in the micropore range to be inherent within the boehmite crystals, the mesopores formed by dehydration during heat treatment steps and macropores

are the interparticle voids. The presence of macropores results in a loss of material strength as illustrated by the Griffiths crack theory which relates strength and toughness accounting for the presence and size of faults such as pores, (Griffiths, 1920). Based on Mooi's discussion of pore origin, micropores can be adjusted by control of raw material and chemistry affecting the crystallites, and mesopores can be controlled by adjustments in the formulation and forming process. The shapes of pores in aluminium oxide systems was studied by De Boer and Lippens (1964), by examining the nitrogen adsorption/desorption isotherms and concluded that pores with approximately rectangular shaped cross sections or needle-shaped pores were formed depending on the crystallinity of the boehmite used and the temperature to which samples were heated.

The control of pore size can be aided by the use of pore formers. Pore formers are effectively any material which will be removed during a post forming step, such as organic molecules or combustible solids. A pore former is also a formulation modifier, which are discussed in Section 2.1.7.

Investigation into the use of pore formers to control pore volume and pore size distribution in aluminas has been studied for many years, a review of the methods available to control pore size of alumina catalyst supports was presented by Trimm and Stanislaus (1986), citing 47 articles already published in this field 25 years ago, dating back to 1942, and work is ongoing.

Basmadjian *et al.* (1962) and Youssef (1976) added water soluble organic polymers to alumina gels. Youssef (1976) used vinyl pyrolidone polymer in concentrations of between 5 and 10 % by weight, resulting in a significant increase in the total pore

volume. The increase was proportional to polymer content, but not surface area, as the polymer was increasing pore size. Addition of 5 % increased pore size from 0.4 nm to 5 nm and addition of 10 % polymer by weight widened pores to 8 nm. The pore structure of a molybdena / alumina system was designed by Tischer (1981) using cellulose to form macropores and acid as a peptising agent. They found the resulting pore size was affected by the powder used, but independent of the acid type and processing conditions.

Absi-Halabi *et al.* (1993) found that the presence of ammonia vapour during the thermal treatment of boehmite gel enhanced the pore enlargement of the resulting alumina, where as the presence of acetic acid caused a suppression of the pore enlargement. The difference was attributed to the effect of the reagants on the hydroxylation of the Al-O-Al bonds.

Work by Han *et al.* (2003) on the fabrication of bimodal porous alumina ceramics involved combining the sponge method and the pore former method to obtain the desired pore size distribution. An aqueous phase was used as a binder and pore former and was burnt off after the sponge impregnation method. This report was principally aiming to investigate the effect of sintering temperatures on the strength of the formed ceramic foam but it highlights the use of pore formers being used to design the pore structure of a material. Phosphoric acid was successfully used to control the pore structure of titanium dioxide materials by Huang *et al.* (2005) who were able to control the modality of the distribution by altering acid concentration, the mechanism responsible for the control achieved was not discussed.

A series of works performed by Isobe *et al.* (2006a-d) examined the control of the microstructure of extrudates by uni-directionally orienting pores using solid pore formers such as nylon 66 fibres, carbon fibres and polyvinylacetate to produce pore sizes between 0.4 and 400μm, the size of the pore former correlated closely with the size of the pore formed. They achieved excellent pore orientation with pore formers and extrusion, though degree of orientation decreased with an increase in pore former concentration. The alignment of pores was found to increase the mechanical strength and permeability at a constant porosity. Mechanical strength was also increased by reducing the pore size.

2.1.7 Formulation Modifiers

Additives may be introduced to formulations to act as a binder or lubricating agent, or as mechanical promoters. It is rare that an additive will have a single effect on a formulation, the pore formers discussed in Section 2.1.6 will also act as rheology modifiers and additives included to act as a binder may also behave as a pore former. It is important to consider the full effects of any formulation additive, as effects may be detrimental, for example, Forzatti *et al.* (1998) found that an overuse of lubricating agents can lead to a severe loss of mechanical strength in the extrudate.

It is often preferable to introduce additives in the solid form to enable premixing with the solid component of the extrusion system, helping to ensure a uniform distribution. In general these components in their liquid form can be highly viscous and therefore difficult to mix uniformly with powders, (Forzatti *et al.* 1998). The mixing issues associated with the use of additives can complicate and increase the cost of a

process considerably, therefore it is preferable to avoid, or minimise, their use wherever possible.

Boehmite is often referred to and used as an extrusion aid, (Sunil Kumar *et al.*, 1997, and 1998, Ananthakumar *et al.*, 2001). The extrusion of boehmite commonly incorporates the use of nitric, or another acid which acts as a binder by behaving as a peptising agent. The significance of the acid used on the product properties was investigated by Jiratova (1981).

2.1.8 Forming of Ceramic Catalyst Supports

Catalysts and catalyst supports can be formed using techniques other than extrusion, such as tabletting or granulation. A review of the production of catalysts by granulation has been performed by Holt (2004). Extrusion is also suitable for forming a range of materials, illustrated by the extrusion of zeolites performed by Chapman and Blackburn (1991). The use of pillared clays as a raw material for producing catalyst supports was assessed by Mohino *et al.* (2005). Pillared clays are attractive in this application as they offer a high surface area and porosity, thermal stability, and suitable surface chemistry after thermal treatment.

The single screw extrusion of pastes was investigated by Burbidge and Bridgwater (1995) who coupled polymer extrusion models with paste rheology to improve the description of paste extrusion. Acknowledgment is made by the authors of the discrepancies between screw extrusion of polymers and ceramics, for example the materials exhibit the opposite relationship between channel depth and pressure. Botten *et al.* (2003) successfully developed a model to predict the pressure gradient in the extrusion of pastes through a single screw extruder, using the combination of a volume conservation equation and force balance solved for pressure as a function of

barrel length. The model was general and could be applied to all channel geometries, and all paste-like materials. Previdi *et al.* (2006) designed and tested a feedback control system for real-time control of polymer flow within a single screw extruder. The regulation achieved by the control system was effective and considered a cost effective alternative to mechanical volumetric pumps. The literature pertaining to the use of twin screw extrusion to produce catalyst supports is reviewed in Chapter 3.

The issue of temperature effects on forming operations is not considered by many authors. Tomita *et al.* (1994) investigated this effect in alumina slurries containing a dispersant and concluded that temperature had a significant effect on the absorption of the dispersant and therefore on the slurry rheology. No similar study has been published on the effect of temperature on the properties of acidic boehmite slurries or pastes.

A comprehensive review of the shaping of ceramics is presented by Blackburn and Wilson (2008), highlighting the importance of understanding paste instability by considering the propensity to phase migrate. Wilson and Rough (2006) present a detailed discussion of the curious characteristics of dense pastes, in particular wall slip, surface fracture and phase migration, both of these publications are discussed further in Chapter 3.

2.2 Introduction to Rheological Measurements

Rheology is defined as the flow of fluids, or deformation of solids, under stress or strain. The rheological properties of a soft material can be measured using a rotational rheometer, (though there are other types of rheometer) in which the

material of interest is placed between a stationary flat plate and a rotating geometry as shown in Figure 2.6. Geometries can be either flat or cone shaped and are available in a range of sizes and materials of construction and surfaces can be smooth or serrated. A rheological measurement is made by assessing the strain response to shear stress imposed on the sample, or vice versa.

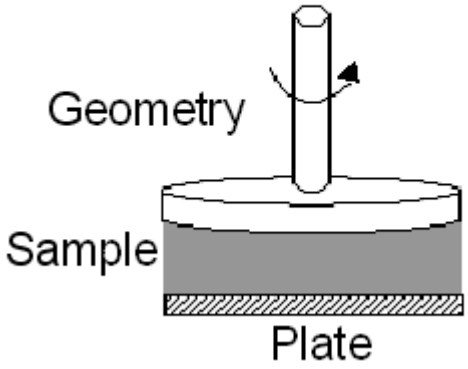

Figure 2.6: Schematic of a rotational rheometer (adapted from ciks.cbt.nist.gov)

Flow rheometry techniques can be used to determine the flow properties of a material such as apparent viscosity and yield stress. An alternative to this is oscillatory rheometry in which the oscillatory motion enables the microstructure of a material to be probed.

2.2.1 Rheological Behaviour of Suspensions

A simple liquid such as water displays Newtonian rheological behaviour, i.e. the viscosity is independent of shear rate. More complex, structured, liquids can exhibit either shear thinning or shear thickening behaviour, i.e. the apparent viscosity decreases or increases with shear rate respectively. These are termed power law fluids and behave according to equation 2.1

$\eta_{app} = k\dot{\gamma}^{n-1}$ ……..……..(equation 2.1)

where η_{app} is the apparent viscosity at a particular shear rate, k is a consistency term and n the flow behaviour index; n > 1 for shear thickening materials and n < 1 for shear thinning materials. Note that if $n = 1$ the material can be described as Newtonian. Materials with structure such as ketchup or paint are typically shear thinning, the imposed shear acts to break down the structure allowing flow to occur more easily, resulting in a reduced apparent viscosity. Similarly materials in which shear can act to build up structure can exhibit a higher apparent viscosity when shear is imposed, these are shear thickening materials.

A system of solid particles contained within a liquid medium can be considered as a dispersion, suspension, slurry or paste. There are no specific boundaries imposed on the use of these terms though each refers to a general range of solids contents listed here in order of increasing solids. The materials considered in this chapter fall within the range of suspensions to concentrated slurries.

At low shear rates suspensions are shear thinning due to the particles becoming aligned in the flow regime of the liquid medium and producing less resistance to flow. As the shear rate increases the kinetic energy of the particles can be sufficient to overcome the energy barrier provided by the repulsive interparticle forces and aggregation can occur, (these aggregates can be referred to as jamming clusters), leading to shear thickening. The shear rate at which shear thickening occurs is referred to as the ‘critical shear rate’ and at this point the shear forces in the system are equal to the interparticle forces (Boersma *et al.*, 1990). This phenomenon has the potential to yield quantitative data regarding the interparticle forces within a

material however it is not desirable in a formulation intended for an extrusion process as it would result in blockages occurring. Shear thickening can also be caused by an increase in the effective solids content of a system by aggregation of particles and entrapment of liquid. Particle shape and rotation can also alter the effective solids content of a system, with the effect of rotation increasing as the sphericity of particles decreases.

Some materials require a minimum amount of stress to induce flow; such materials are referred to as yield stress materials. Various rheological models exist for describing the behaviour of yield stress materials of which the Bingham (equation 2.2) and Herschel Bulkley (equation 2.3) models are the most common.

$\tau = \tau_0 + \eta\dot{\gamma}$ ……...……...(equation 2.2)

$\tau = \tau_0 + k\dot{\gamma}^n$ ……..…….....……(equation 2.3)

where τ is shear stress, τ_0 is yield stress, η is the Bingham plastic viscosity, k is the Herschel Bulkley consistency coefficient and n is the rate index (as described for the power law equation in equation 2.1).

The Bingham model considers that beyond the yield stress a material behaves as a Newtonian fluid where as the Herschel Bulkley model considers that beyond the yield stress the material is pseudoplastic in nature i.e. either shear thinning or shear thickening as described previously. Figure 2.7 shows the typical rheograms produced by materials according to each of the models discussed. In this example the power law model and Herschel Bulkley model are both displaying shear thinning behaviour.

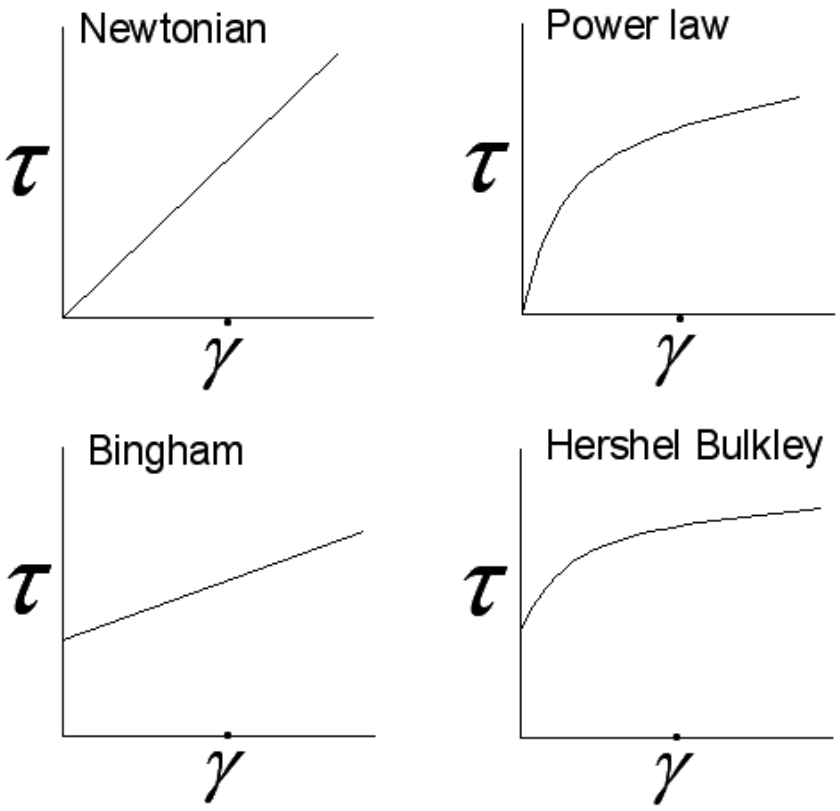

Figure 2.7: Typical rheograms

Another model commonly used is the Cross model (equation 2.4 and Figure 2.8) which is a simple but versatile model that can cope with a yield stress yet retain the extremes of a finite zero and infinite rate viscosity, (Barnes, 2000).

$$\eta = \eta_\infty + \frac{\eta_0 - \eta_\infty}{1 + (C\dot{\gamma})^m} \quad \text{.....(equation 2.4)}$$

where η is the apparent viscosity, η_∞ is the infinite shear viscosity, η_0 is the zero shear viscosity, C is the Cross time constant and m is the Cross rate constant. $m = 0$ for Newtonian materials and $m \to 1$ for perfect shear thinning materials.

The zero shear viscosity is the magnitude of the viscosity at the lower Newtonian plateau which can prove valuable in making assessments of suspension and

emulsion stability. The infinite shear viscosity describes how a material is likely to behave in very high shear processing situations and the reciprocal of C gives an indication of the shear rate at which shear thinning will occur. The rate constant m is dimensionless and is a measure of the degree of shear-thinning.

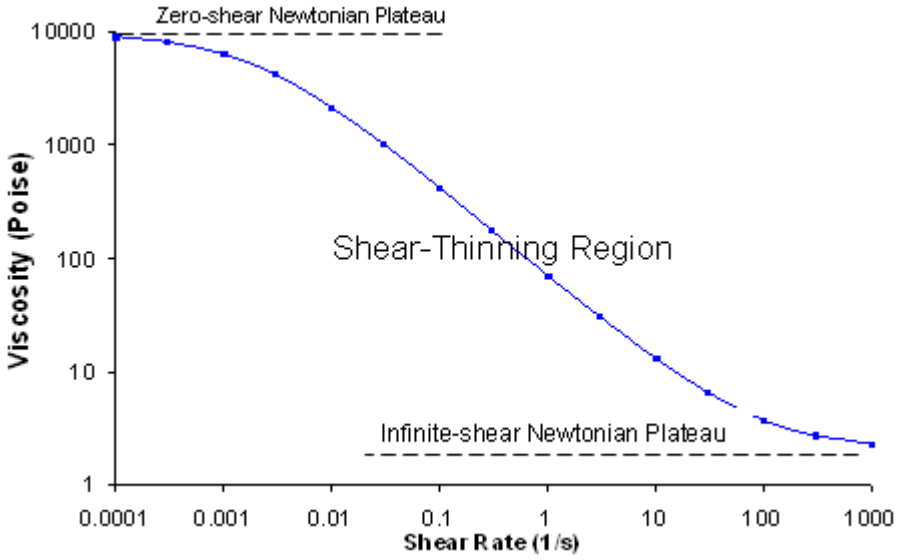

Figure 2.8: The Cross model (from www.rheologyschool.com)

Material rheology can be a function of time. A thixotropic material exhibits a reduction in viscosity over time at a constant shear rate and a material which displays an increase in viscosity over time at a constant shear rate is called rheopectic.

The concept of yield stress as a real phenomenon is debated within the rheological community. The debate developed from the consideration of how to best measure a yield stress fluid as there are various issues associated with the measurement of this parameter. It is argued that yield stress and thixotropy are fundamentally two effects from the same cause (Møller *et al.*, 2006), therefore, raising the issue of whether yield stress is itself a material property. In an engineering context the measurement of yield stress, or 'shear stress at which flow begins to occur', is useful when

designing equipment such as pumps and material conveying systems. This is also true when considering the flow of material within an extruder as the ability to retain shape is a particularly important property of a green extrudate. As such the rheological data and subsequent discussion presented in this chapter is not intending to enter into the debate of the fundamental cause, or existence of, yield stress but to use this measurement as a description of the materials under investigation.

2.2.2 Challenges of Characterising the Rheological Properties of Concentrated Suspensions

When solids are added to a liquid phase both the rheological properties and the measurement of these properties become more complex. When considering very dilute suspensions (solids content < 10 wt%) the Einstein equation (equation 2.5) can be applied to predict the viscosity of the suspension from the viscosity of the fluid and the volume of particles contained within the suspension. The idea of calculating a suspension's viscosity in this way was continued by Ball and Richmond (1980) who introduced the idea of a crowding factor; this model however is still only suitable for relatively dilute suspensions. The most commonly used expression describing the viscosity of suspensions is the Kreiger Dougherty equation (equation 2.6), which is valid for hard spheres. Over 100 equations attempting to describe this relationship are identified by Rutgers (1962).

$$\eta_{app} = \eta_0(1 + 2.5\phi) \quad \text{.....(equation 2.5)}$$

$$\eta_{app} = \eta_0\left(1 - \frac{\phi}{\phi_m}\right)^{-[\eta]\phi_m} \quad \text{.....(equation 2.6)}$$

where η_{app} is the apparent viscosity, η_0 is the viscosity of the liquid phase, $[\eta]$ is the intrinsic viscosity of the liquid phase, which is a function of the particle shape, ϕ is the volume fraction of the dispersed phase and $\phi_{\max}$ is the maximum packing fraction of the dispersed phase. The Kreiger Dougherty relationship describes how the viscosity of a suspension will increase with particle loading and that the increase will become more significant as the volume fraction approaches the maximum packing fraction. Particle packing theory (discussed previously in Section 2.1.4) shows how the maximum packing fraction, and therefore rheological properties, vary with the polydispersity of the dispersed phase (Zheng *et al.*, 1995).

The term wall slip is used to describe the issues caused by the disruption in local microstructure which occurs when a concentrated suspension is next to a wall or plate. A particle concentration profile is created from the centre of the sample to the wall at which point the concentration is zero. This results in the presence of a liquid rich lubricating layer (slip layer) near the wall, the extent of this effect is dependent on the particle size and size distribution and has been studied using total reflection infrared spectroscopy by Hartman Kok *et al.* (2004). The effect is most apparent when the disperse phase has a large unimodal size distribution. The occurrence of wall slip can be identified by performing shear rate variation experiments at a variety of gap sizes in parallel plate experiments where a significant variation in the position of the curve indicates the occurrence of wall slip. Wall slip in rotational geometries can be mitigated against by using a serrated geometry as the points of serration penetrate through the lubricating layer into the bulk of the material (Barnes, 2000). A similar and additional effect occurs with needle shaped particles where the random orientation of the particles is disrupted by the presence of a wall which enhances

alignment of the particles and reduces the apparent viscosity of the surface layer (Barnes, 2000). The formation of a particle concentration profile across the sample means that an appropriate gap size must be selected on an individual sample basis for accurate measurements to be taken. The particle concentration (for spheres) is found to equilibrate at a distance of around 5 particle diameters from the wall hence an appropriate gap size is considered to be between 5 and 10 times the largest particle diameter (Barnes, 2000).

Measurements performed over a long period of time are liable to experience additional problems associated with of evaporation of the liquid phase and settling of the solid particles. There are equipment and techniques available to mitigate each of these effects, however, they are not considered relevant due to the short time scale of the experiments performed in this project.

One of the issues with the measurement of yield stress is that of localised shear which is also referred to as shear banding. In a plate-plate type rheometer a gradient of shear rate naturally exists across the span of the sample (though this can be mitigated against with the use of a cone geometry) which can cause flow to be initiated in a portion of the sample rather than the bulk indicating an apparent yield stress smaller than if motion was initiated throughout the sample. This is a similar issue to that faced with wall slip; a segregation of the material leading to an inaccurate measurement of the bulk properties.

2.2.3 Controlling the Rheology of Concentrated Suspensions

Understanding the factors which affect the rheological properties of concentrated suspensions allows for attempts at controlling and designing these properties by manipulation of the formulation parameters.

The solids content contained within a suspension has a significant effect on the rheological properties particularly as the maximum packing fraction of the system is approached. Therefore, controlling the value of the maximum packing fraction by controlling particle size distribution is one way in which the rheology can be controlled. Research is ongoing in the field of particle packing behaviour and maximum packing fractions but it is considered well understood that the maximum packing fraction can be increased by increasing the polydispersity of a system as the smaller particles can fill the voids between the larger particles. The degree of polydispersity not only affects the magnitude of the apparent viscosity of a system but also the degree of shear thinning which it will exhibit due to variations in the ability to align with flow regimes. A system with a very narrow size distribution will exhibit the highest degree of shear thinning (Luckham and Ukeje, 1999).

Considering two systems with an equal mass of particles present and equal degrees of polydispersity, but different mean particle sizes, the system with the smallest particles will exhibit the highest viscosity due to the increased number of particles resulting in an increased number of particle-particle interactions and therefore an increased resistance to flow. This effect is more significant at very low shear rates as at higher shear rates the kinetic forces will overcome the interaction forces.

Variations in particle shape and deformability and the viscosity of the liquid phase will also affect the bulk rheological properties of a concentrated suspension. The rheological study performed by Martin *et al.* (2004) on talc-based paste discusses the occurrence of issues in rheological characterisation caused by particle shape.

Surface chemistry controls the interaction between, and the aggregation behaviour of, the particles. Zeta potential is a measurement of the charge at a particle's shear layer which is often considered as a very good approximation to the surface charge. A high surface charge (either positive or negative) will result in a stable suspension where as at low, or zero, surface charge the system is unstable and the particles are liable to aggregate. A loose aggregation of particles can result in a higher effective solids content due to entrapment of the liquid medium causing an increase in the effective viscosity considered academically previously but proven by Drouin *et al.* (1987). The pH at which the zeta potential is zero is termed the isoelectric point and is the pH at which the highest apparent viscosity of a system would be expected. This phenomenon is illustrated very clearly by work reported by Kukolev and Karaulov (1963) for inert alpha alumina systems and can be seen in Figure 2.9 (note that a zeta potential of nearly 200 mV is a very high charge, 20 mV is considered to be a stable charge though there is no indication why this charge is so high).

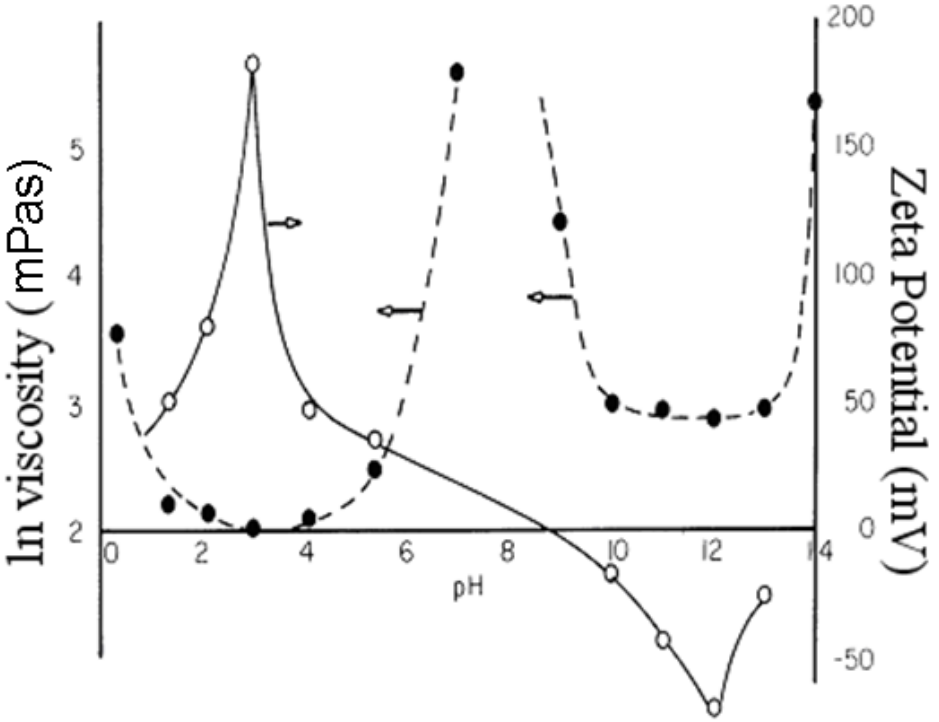

Figure 2.9: Relationship between zeta potential and viscosity of an alpha alumina system (adapted from Kukolev and Karaulov, 1963)

Quemada and Berli (2002) discuss how the arrangement of particles in a colloidal dispersion and hence its mechanical and rheological response is determined by the nature of the particle interaction forces. As particle size reduces, the electrical double layer and steric layer thickness play an increasingly important role. A similar useful review of the colloidal interactions of particles in liquid is presented by Liang *et al.* (2007).

2.2.4 The Peptisation Reaction between Boehmite and Acid

The term peptisation has previously been used in open literature in a number of contexts. It can refer to the dispersion of particles by either chemical or mechanical means, though in relation to boehmite and acid it is used in the literature to describe the reaction between these materials, which is though to result in the formation of a gelatinous phase. One definition of peptisation is: 'The term peptisation is

sometimes used in a general way to imply the reverse of coagulation, i.e. dispersion, especially where the process results in the formation of a colloidal sol. Peptisation is, however, generally restricted to a chemical means of dispersion in which the colloidal particles are stabilised by the adsorption of charged ions' (Sharp, 2003). In the context of this definition, the interaction chemistry between boehmite and acid is more than just peptisation. This will be considered and discussed further within the literature review, Section 4.2.

2.2.5 Using Oscillatory Rheology to Probe Microstructure

Oscillatory rheology is a technique that can be applied to examine the microstructure of a material. In some cases it is referred to as mechanical vibrational spectroscopy (Barnes, 2000). Ideally the movements during an oscillatory experiment are very small in order to cause minimal disturbance to the microstructure. An oscillatory motion is applied to the material and the rheometer measures the materials' response to this. If the response is perfectly in phase with the applied motion the material is considered to be perfectly elastic whilst being exactly out of phase implies that the material is viscous. These situations can be described by the spring and dashpot models respectively. The extent to which the response is in or out of phase with the input is quantified by considering the storage and loss moduli parameters which both vary with the applied frequency. The storage modulus (also called the elastic modulus), G', characterises the solid like component and the complementary loss modulus (also called the viscous modulus), G'', describes the liquid like component within a material. Other commonly quoted oscillatory parameters are the complex modulus, G*, which describes the overall resistance to material deformation and the tangent of the phase angle, tan δ, where the phase angle, δ, is the ratio of

the viscous modulus to the elastic modulus, or alternatively can be considered as a measure of the lag between the input and response. Combinations of the spring and dashpot models in various configurations such as the Maxwell, Kelvin - Voigt and Burger models can be used to describe viscoelastic materials.

2.2.6 Principles of Magic Angle Spinning Nuclear Magnetic Resonance (MAS NMR)

Nuclear magnetic resonance is a key analytical tool in identifying the species formed in the reaction between boehmite and acid due to its ability to distinguish the atomical coordination environment of a selected species. The spin behaviour of a nucleus within a strong magnetic field can be translated to yield information on the coordination number of a particular species. High resolution spectra can not be obtained within the solid state due to the dipole-dipole interactions not being averaged to zero as they are in the liquid or gaseous phase. This issue can be overcome by spinning at a specific angle (with respect to the magnetic field) of 54 º 44 `, described as the magic angle, θ. In this situation $\cos^2\theta = 1/3$ and the dipole-dipole interactions can be averaged to zero which allows high resolution spectra to be obtained.

2.2.7 Microscopy

Microscopy techniques are most effective when applied to a stable, dry, sample and often the technique involves a degree of sample preparation, such as gold sputtering in the use of scanning electron microscopy (SEM), which could potentially alter the structure of the material being observed. The development of environmental SEM (ESEM) allows the examination of samples in a wider range of environments, particularly in wet environments, but by far the most exciting technique currently

available for examining the microstructure of a material such as those of interest in this chapter is cryogenic SEM (cryo-SEM). This technique allows a sample to be cryogenically frozen, then sublimated within the microscope, minimising any effects on the existing microstructure of the sample allowing a visual examination of the variations in the microstructure and texture of materials.

2.3 Introduction to Mixer Torque Rheometry

2.3.1 Principles of Mixer Torque Rheology

The mixer torque rheometer (MTR) is an instrument which measures the torque required to rotate two intermeshing paddles through either a powder or a mixture of powder and liquid. This measurement allows an insight into the state of saturation of the material and the wetting properties of the powder and liquid combination, which provides valuable information for the formation of pastes by extrusion. The data obtained can also be related to the rheology of the material.

2.3.2 Saturation States

A solid material can exist in a variety of saturation states depending on the amount of liquid with which it is in contact. Four states of saturation have been identified, in order of increasing liquid content, pendular, funicular, and capillary, by Newitt and Conway-Jones (1958), and droplet, by Barlow (1968).

In the pendular state, discrete liquid bridges are formed between the particles, these exhibit strong forces due to surface tension which draws the particles together by hydrostatic pressure, resulting in an apparent reduction in the powder volume upon liquid addition. The bridges continue to grow in size, as liquid content is increased, until a continuous network of liquid is created which is interspersed with air, this is

the funicular state. The resistance to breaking of the liquid bridges increases with increased liquid content as the particles must be separated further in order to break the liquid bridge.

Increasing the contact between liquid and solid causes an increase in the cohesiveness of the mass and increase in torque. The point at which all air is expelled from the continuous liquid network is the capillary state of the material. This is the most cohesive state of the mass and there are concave menisci around the surface of the agglomerate. If liquid content is increased any further the discrete particles are suspended in a continuum of liquid and the mass can be considered to be a slurry, or in the droplet state. In the droplet state there are no longer any internal interfacial forces and only surface tension holds the drop together (Luukkonen, 2001).

Rumpf (1962) shows that the tensile strength of the pendular stage of saturation is only a third of that in the capillary condition and that the tensile strength, TS, of an agglomerate can be calculated according to equation 2.7.

$$TS = SC\frac{1-\varepsilon}{\varepsilon}\frac{\gamma}{d}\cos\theta \quad \text{.....(equation 2.7)}$$

where, S is the liquid saturation, C is a shape constant, ε is the agglomerate porosity, γ is the surface tension of the liquid phase, d is the particle diameter and θ is the contact angle between the liquid and solid phases. The liquid saturation depends on the amount of liquid present and the intragranular porosity, according to equation 2.8 as presented by Kristensen *et al.* (1984):

$$S = H\frac{(1-\varepsilon_{ig})}{\varepsilon_{ig}}\rho \quad \text{.....(equation 2.8)}$$

where, H is the ratio of the mass of liquid to the mass of solid, ε_{ig} is the intragranular porosity and ρ is the particle density. The intragranular porosity is defined as:

$$\varepsilon_{ig} = 1 - \frac{\rho_b}{\rho_s} \quad \text{.....(equation 2.9)}$$

where, ρ_b is the bulk density of the packed material and ρ_s is the skeletal density of the solid phase. The deficiencies of Rumpf's model, such as the lack of a viscous dissipation term and assumptions regarding failure mechanisms are discussed in Reynolds *et al.* (2005).

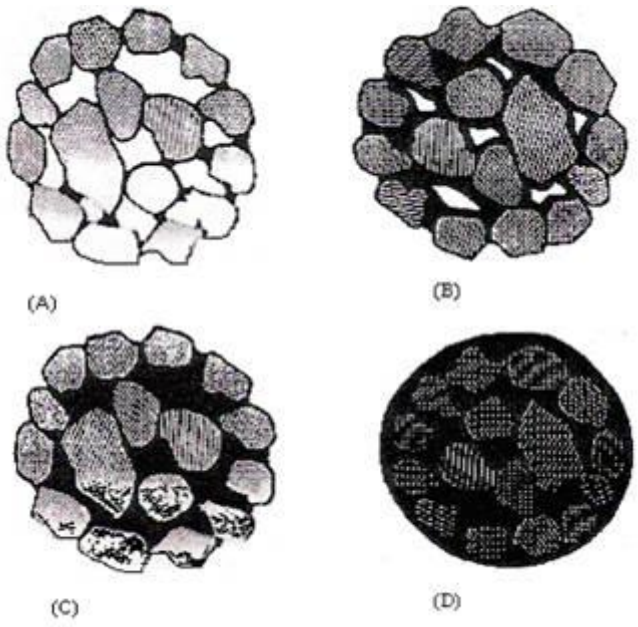

Figure 2.10: States of powder saturation. (A) – pendular, (B) – funicular, (C) – capillary, (D) – droplet. (adapted from Prabhakaran, 2009)

The extrusion process should be performed in the saturated condition, more specifically, at a liquid content just a little higher than the capillary state. Extruding at

this condition provides sufficient liquid for a lubricating layer to surround each of the solid particles whilst being sufficiently firm to retain shape post extrusion.

2.3.3 Mixer Torque Rheology Test Types

A multiple addition test (MAT) involves charging a dry powder to the mixing chamber and adding the appropriate liquid at a specified rate. An MAT records the change in torque required to rotate the paddles through the mixing chamber over time, allowing the change in saturation states to be observed and the capillary point of a material combination to be located. A typical curve resulting from such a test can be seen in Figure 2.11.

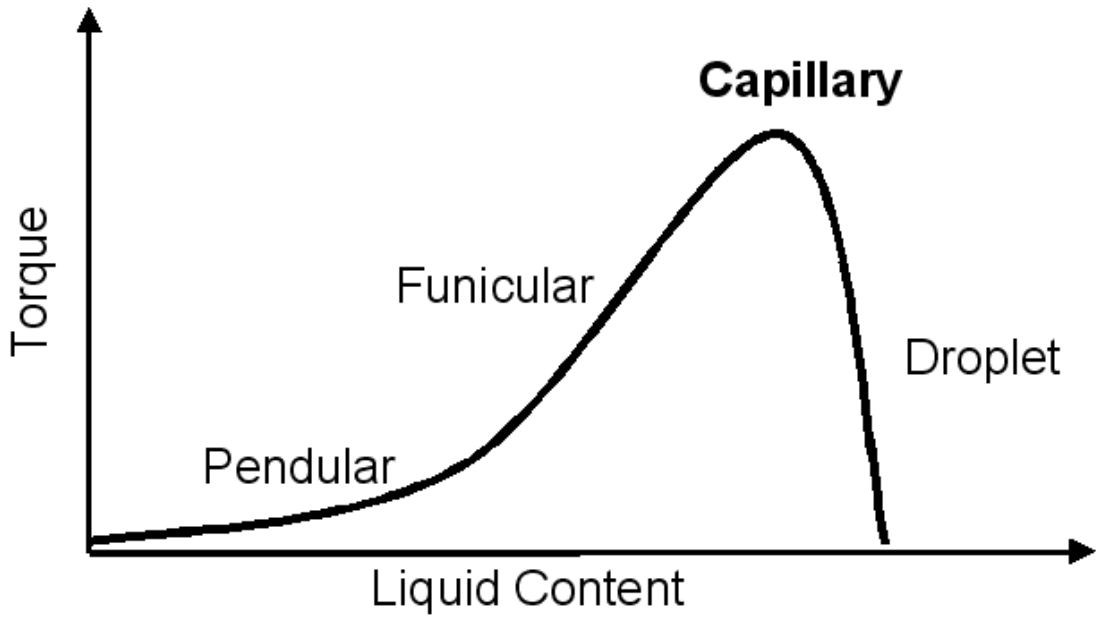

Figure 2.11: Typical relationship between liquid content and torque on MTR

The shape of the curve resulting from a MAT can be used as an indicator of the extrusion stability of a formulation by examining the gradient of the curve at the liquid content at which extrusion would be performed (between the capillary point and

droplet state). A steep curve suggests that the system may be too sensitive to liquid content to maintain the paste formulation in a range suitable for extrusion, a shallow curve would indicate a robust system.

A more accurate assessment of the interaction between a powder and liquid is the variable mixing time test (VMT). This differs from the MAT as the sample cell is initially charged with a mixture of liquid and powder rather than dry powder. No further additions of liquid are made during the experiment, and the variation of torque with time is measured, allowing examination of the effect of work input on the saturation state of a material (the significance of this is discussed in more detail in Section 2.3.4). This technique is considerably more time consuming than an MAT as a large number of experiments are required to achieve an understanding across a range of liquid contents, however, it can produce a more accurate representation of the effect of both work input and liquid content on the saturation state. Effectively an MAT curve of formulations at equilibrium with regard to work input can be derived by considering a large set of VMT data.

The analysis of data obtained from the MTR generally involves examining the position (in terms of liquid content, time and the magnitude) of the peak value of the mean torque and the peak value of the torque range. The mean torque describes the average resistance of the mass to shearing. The torque range is a measure of the amplitude of oscillations caused by inhomogeneities within the mass. Figure 2.12 shows a typical curve produced when an MAT is performed.

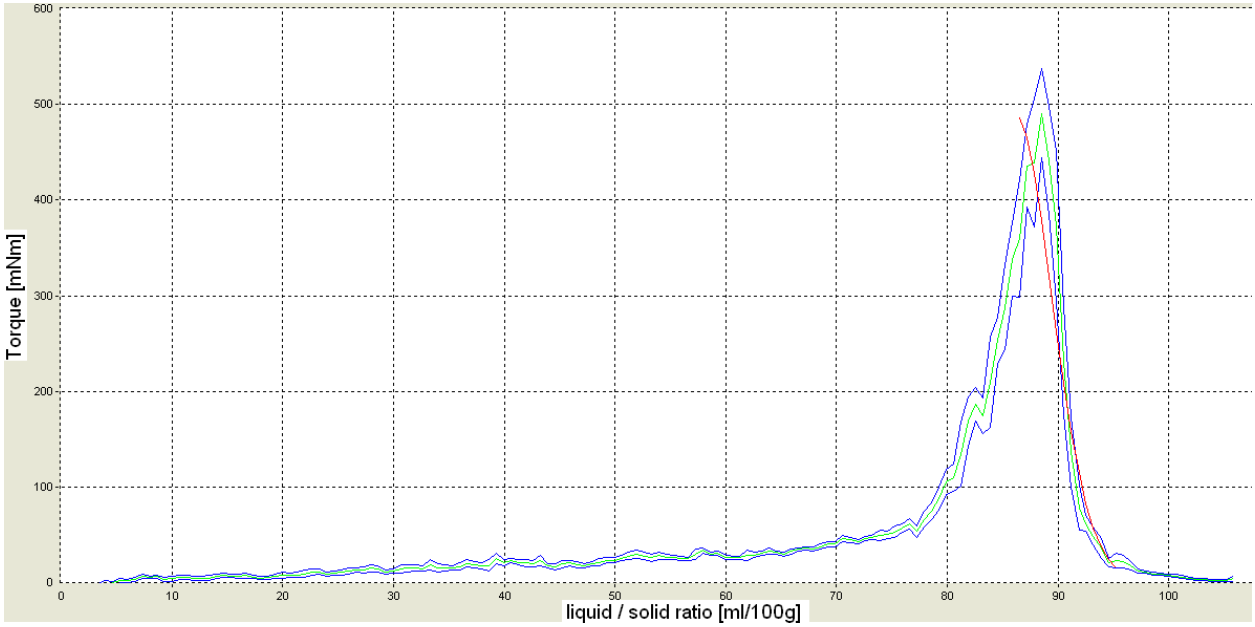

Figure 2.12: Typical MAT data, Torque vs Liquid Content (blue - torque range, green - mean torque, red – software curve fit)

2.3.4 Effect of Work Input

The description in Section 2.3.2 of the pendular, funicular, capillary and droplet conditions of a powder liquid mixture assumes that the powder and liquid are always well-mixed and in equilibrium, but in reality a transition can be made between the states of saturation without increasing the liquid content, but by applying work to the material. The act of applying work to a system can increase the particle packing density, reducing the voidage between particles. Therefore a system in the funicular state could transform to the capillary state without further liquid addition, by applying work to the system, and similarly, a system in the capillary state could transform to the droplet state.

The ability to transform between saturation states with work input, rather than liquid addition, means that care must be taken when using MTR data to aid in process design and scale up as the work input of the processing equipment must be

considered. It is when considering such issues that VMT data is much more reliable than MAT data. Understanding and analysing VMT data will be discussed further in Section 7.3.

2.3.5 Wettability

The wettability of a powder liquid system can be characterised by the apparent contact angle between the two materials when in equilibrium, it is a function of the surface tension of the liquid and the surface roughness of the powder. Contact angles can be measured using the spreading, condensational, immersional or capillary rise methods. In general these methods are more suited to measurements of the contact angle between a liquid and planar surface rather than a liquid and powder.

An instrument called a tensiometer has been developed which can measure the contact angle between a liquid and powder with a reasonable degree of accuracy, depending on the consistency of a powders' packing behaviour, using a capillary rise method. This method is based on the work of Laplace (1806), when a wetting liquid is present in a narrow channel (capillary) the contact between the liquid and the wall will be less than 90 º, therefore the liquid surface forms a concave meniscus. A capillary pressure is exerted on the meniscus due to surface tension and hydrostatic pressure effects according to equation 2.10.

$$\Delta P = \frac{2\gamma \cos\theta}{r} \quad \text{.....(equation 2.10)}$$

where, ΔP is the pressure difference between the gas and liquid phases, γ is the surface tension at the liquid gas interface, r is the capillary radius, and θ is the

contact angle between the liquid and solid phases. This technique will be discussed in more detail in materials and methods, Section 4.3.6.

2.4 Introdcution to Extrusion

2.4.1 Extruder Types

There are various types of extruders, ranging from a simple ram extruder to more complex screw extruders. The principle of extrusion remains the same across all extruder types, to exert a force on a material in order to push it through an orifice to form a shaped product. Ram extrusion involves the movement of a plunger through a barrel filled with the material to be extruded, the configuration of this equipment, seen in Figure 2.13, is such that it is only suited to batch processing, where as continuous operation is preferable in industrial processes. Screw type extruders are more suited to continuous operation, particularly the twin screw extruder which is capable of mixing a paste and forming an extrudate in a single unit step. A single screw extruder requires a pre-mixed paste as a feed, but can be operated in continuous mode.

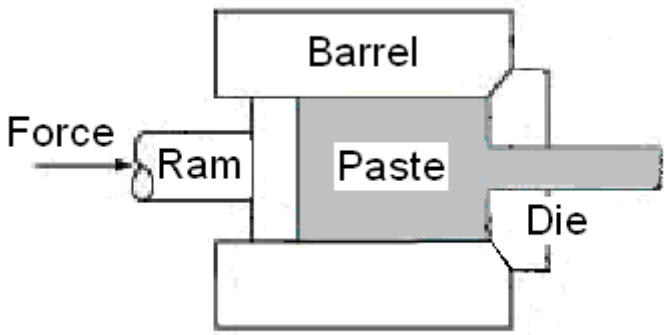

Figure 2.13: Ram extrusion.

2.4.2 Description of an Intermeshing Twin Screw Extruder

Twin screw extruders consist of two screws, within a barrel, which rotate either in the same direction (co rotating) or opposite directions (counter rotating) to each other, as shown in Figure 2.14, the term intermeshing refers to the overlapping configuration of the screw flights. Shah and Gupta (2004) present a comparison of the two modes of operation with polymeric materials, finding differences such as the maximum velocity occurring at a different location in the geometry and improved mixing performance in a co-rotating configuration. A similar study examining the differences in the extrusion of ceramic materials, to the authors knowledge, has not been published. A comparison of co and counter rotating extruders has been performed by Rauwendaal (2004) who determined that extruder performance is dominated by the intermeshing region of the screws, implying that analysis of extruders should centre around this region. He identified the co rotating extruder to be most suited to melt blending operations, and the counter rotating to dispersing solid fillers in a polymer mix due to the differences in flow regimes in the intermeshing region.

This project studies the use of a co rotating extruder, which is the more widely used configuration, (Wiedmann and Holzel, 2007) and all further discussions pertain to this equipment configuration.

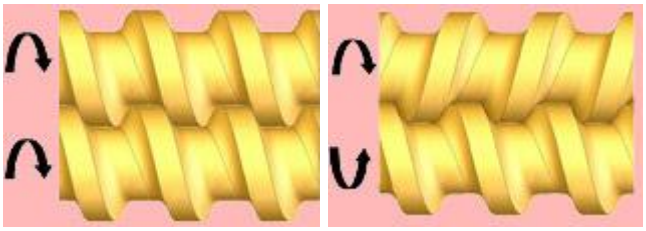

Figure 2.14: Conveying configuration within a fully intermeshing co rotating (left) and counter rotating (right) twin screw extruder (adapted from http://www.mprus.com)

The rotating action moves material down the barrel towards a die and generates pressure to push the material through the die. Theoretically, a combination of conveying and mixing elements, seen in Figure 2.15, enables powders and liquids to be mixed in situ to form a paste. The screw configuration should contain a suitable combination of these to allow the appropriate compromise between mixing and pressure generation to be achieved. As the names suggest, the conveying elements primary task is to move material along the barrel, where as the mixing elements knead the materials into a paste.

Figure 2.15: Types of screw elements. left: conveying right: mixing (30º forward)

The mixing of materials can be described as distributive or dispersive. Distributive mixing can be considered as the spatial distribution of components and is reasonably simple to achieve. Dispersive mixing involves the mixing at a smaller length scale, such as the dispersion of agglomerates, generally more difficult to achieve than distributive mixing. It is discussed by Gramann and Rauwendaal (2004) that mixing in a twin screw extruder is achieved in the region between the screw flight and the barrel, as this is where elongational flow is present, which is more effective at dispersive mixing than shear flow. A large flight helix angle, seen in Figure 2.16 along with other screw configuration dimensions, increases the amount of elongational flow (Gramann and Rauwendaal, 2004). The use of mixing elements effectively produces a very large flight helix angle, increasing as the degree of

stagger is increased, hence, 30 º forwards elements are believed to deliver the gentlest mixing action, followed by 60 º forwards, 90 º, 30 º backwards and 60 º backwards being considered the most aggressive mixing elements, schematics of the degrees of stagger can be seen in Figure 2.17. Literature pertaining to the mixing effectiveness and conveying action of screw configurations is discussed in Section 3.4.4.3.

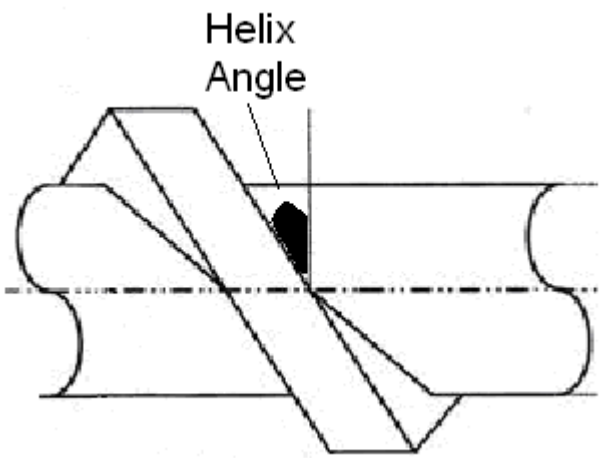

Figure 2.16: Dimensions of screw geometry, (adapted from http://www.slscrewbarrel.com/UploadFile/201063191736307.jpg)

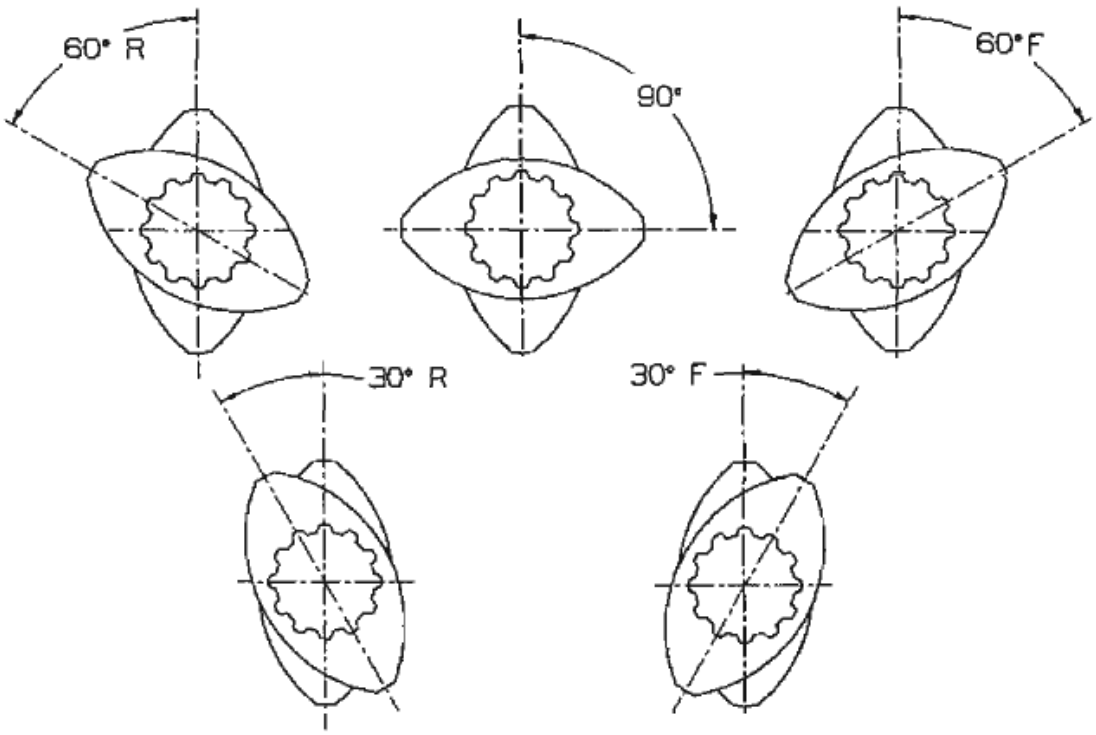

Figure 2.17: Mixing elements, 60 º reverse, 30 º reverse, , 90 º, 30 º forwards, 60 º forwards (adapted from APV training manual)

2.4.3 Relationship between Extrusion Parameters

There are a number of formulation and processing parameters of interest during ceramic extrusion, which are interrelated. Input parameters such as liquid and powder feed rates and screw rotation rate can be varied to give a range of processing output parameters such as throughput, fill level, residence time, pressure generation and torque whilst also enabling the production of a range of paste formulations. The variation of an input parameter results in a transition period before steady state operation is re-established. The duration of the transition period is related to the residence time under the conditions of operation. The expected qualitative relationships between extrusion input and output parameters mentioned above are as follows:

An increase in total feed rate at a constant screw speed results in an increase in fill level and throughput compared to the original state and both torque and work input to the material will increase due to the increase in fill level. Similarly, if screw speed is maintained and total feed rate reduced, the fill level, throughput, torque and work input will reduce. In each case the residence time is not expected to alter.

Maintaining total feed rate and increasing screw speed will reduce the fill level, torque and work input. The residence time will reduce, and throughput remains constant. Reducing screw speed with a constant feed rate will increase fill level, torque, work input and residence time, and throughput will remain constant.

2.4.4 Controlling Extrudate Properties with Extrusion Parameters

As discussed in Chapter 1 an effective catalyst support is required to be mechanically strong and highly porous with a compromise between these two properties often necessary. Both paste formulation and processing parameters affect the resulting product properties. The effect of formulation parameters on extrudate properties is discussed in Section 2.4.5.

The pressure at the die during forming has been considered to be a good indicator of the strength of an extrudate and has been used as a control parameter by Russel *et al.* (2003). However, high pressures can lead to processing issues such as phase migration, discussed further in Section 3.4.4.5. The throughput, torque, fill level and paste rheology all affect the pressure generated in an extruder.

The degree of mixedness of the paste achieved during extrusion can be related to product properties, in particular poor dispersive mixing is considered to be detrimental to the extrudate properties due to the increased presence of defects.

In a chemically active system, the residence time affects the extent to which chemical reactions occur, although reactions may continue after forming until further processing steps are taken, such as drying.

2.4.5 Controlling Extrudate Properties with Formulation Parameters

Paste formulations typically include a solid phase and a liquid, binding phase, in this study the liquid phase is comprised of water and varying amounts (and type) of acid. Additives such as pore formers or rheology modifiers can also be included in a formulation as discussed previously in Section 2.1.7, however such additives are not used in this study.

The rheological properties of a paste determine the flow behaviour within the extrusion process. Varying formulation parameters such as solids content, powder type or acid content of an acidic boehmite paste alters the rheological properties, which in turn affects the resulting extrudate properties. The results presented in Chapter 4 address this issue in more detail.

The particle packing behaviour is a significant factor in determining the rheological properties of a material containing solids, and will affect the extrudate properties such as strength and porosity. This is strongly affected by the particle size distribution of the powder and any dispersion, mechanical or chemical, occurring in the process which affect this distribution. The variation of packing of hard spheres with size and size distribution is reasonably well understood and is discussed previously in Section 2.1.4. What is not so well understood is how well this theory translates to inert particles within a liquid phase and even less so, chemically reactive particles in a liquid phase.

2.4.6 Characterisation of Pastes for Extrusion

Characterisation of the rheological properties of suspensions and slurries was discussed previously in Section 2.2.1. The characterisation methods and rheological properties of pastes vary quite significantly from those used on more dilute systems. Ceramic pastes exhibit many behavioural similarities to soils, hence the studies performed on mechanics of soils have been instrumental in the development of paste characterisation models. The extensive use of extrusion in polymer processing has also aided studies in the field of ceramic extrusion, though variations in polymeric and ceramic flow behaviour mean that care must be taken when applying learning from polymeric extrusion to ceramic extrusion.

The most commonly accepted method of rheologically characterising pastes is the Benbow Bridgwater method, the development of which is described in Section 3.4.3. The technique involves measuring the force required to extrude a paste through a number of (typically 3) cylindrical dies with varying ratios of length to diameter at a variety of (typically 5) speeds. The force required to perform each of these extrusions can be used to calculate the parameters as described in equation 2.11. The data can be fitted to the Benbow Bridgwater 4 or 6 parameter model. Equation 2.11 shows the 4 parameter model, details of the more complicated 6 parameter model can be found in Benbow and Bridgwater (1993).

$$P = P_e + P_1 = 2(\sigma_0 + \alpha V)\ln\left(\frac{D_0}{D}\right) + (\tau_0 + \beta V)4\left(\frac{L}{D}\right) \quad \text{.....(equation 2.11)}$$

where, P = total pressure drop, P_e = pressure drop at die entry, P_l = pressure drop along die land, σ_0 = yield stress, α = velocity factor, V = paste velocity, D_0 =

diameter of barrel, D = diameter of die , τ_0 = wall shear stress, β = wall velocity factor, L = length of die land. The bulk velocity exponent is a paste parameter that determines the dependence of the bulk paste yield stress on the velocity. Similarly the wall velocity exponent is a paste parameter that determines the dependence of the wall shear stress on the velocity. A full discussion of the physical implications of these parameters is discussed in Benbow and Birdgwater (1993). Obtaining the experimental data required to perform this analysis is laborious and time consuming and this method has therefore been considered unsuitable for the large number of pastes characterised in this formulation development work.

Chapter 3 Literature Review

3.1 Boehmite Formation and Properties

3.1.1 Effect of Formation Conditions on Properties of Boehmite

Martens *et al.* (2002) propose a model for the crystallite packing in pseudoboehmmite in which platelike psuedoboehmite crystallites are stacked in a 'sharing edges only' configuration, a stacking structure which produces pore sizes approximately equal to the crystallite size of the hydrolysates, and ageing of the hydrolysate allows the crystallites to grow. Okada *et al*. (2002b) found that the crystallite size of boehmite increased when precipitated at higher pH, higher temperature or for a longer ageing time. Their observations are in agreement with previous works by Tottenhorst and Hoffman (1980), Tsukada *et al.* (1999) and Mishra *et al.* (2000). The relationship observed between aging time and crystallite size has also been reported previously by Music *et al.* (1999). The relationship between synthesis conditions and physicochemical properties of aluminium hydroxides is also discussed by Lamberov *et al.* (2003). Martens *et al.* (2002) also observe the correlation between crystallite size and ageing time, commenting that this relationship is due to an increase in the d spacing with ageing time.

Tsukada *et al.* (1999) investigated the effect of the crystallite size of boehmite on subsequent thermal phase changes, they report that phase transitions to gamma and alpha alumina occur at higher temperatures with larger crystallites. A similar study was performed by Okada *et al.* (2002) who report on the shift in the temperature of the phase change from gamma to theta and theta to alpha, which decrease and increase respectively with an increase in crystallite size. They investigated crystallite sizes ranging from 2.9 to 24.4 nm (measured by x ray

diffraction) and found that a crystallite size of 5 nm gave the highest specific surface area, of interest in the field of catalysis. This relationship between crystallite size and bond length and temperature of phase transformations was also observed by Guzman Castillo *et al.* (2001).

It has been reported by Okada *et al.* (2003) that a larger crystallite size of boehmite results in an alumina ceramic with a greater sinterability, based on an examination of the microstructure of pelleted gamma alumina produced from boehmite. The effect of crystallite size on the bond length and bond angles of boehmites has been investigated for crystallite sizes between 1 and 27 nm. The crystal dimensions were found to determine the bond length and local symmetry, as crystallite size decreased the Al-OH interaction increased and the angle between these bonds tended to a tetrahedral system. Both the hydrogen bond which sustains the crystal structure and the bonds between the oxygen atoms and hydroxyls in the octahedra double layer are weakened as crystallite size is reduced. This could explain the previously discussed reduction of phase transition temperature at smaller crystallite sizes.

Guzmán-Castillo *et al.* (2005) also observed an increase in crystallite size with an increase in synthesis temperature. They studied the effect of the salt used in boehmite synthesis on the resulting physicochemical properties and subsequent phase transitions. Boehmites produced by both the sulphate and chloride route described in Section 2.1.2 were examined and found that due to residual sulphates delaying crystallisation, boehmites manufactured using sulphates generally exhibited smaller crystallites than those produced by the chloride route. The transition temperature to gamma alumina and alpha alumina were also affected by the salt used in synthesis.

The variation of crystallite size of the powders of interest in this project is not significant enough to consider the effects discussed by these authors. All of the crystallite sizes are close to 5 nm, previously indicated as the crystallite size with the maximum specific surface area by Okada *et al.* (2002).

3.1.2 Solubility of Boehmite

A number of authors report on the solubility of boehmite at high temperatures, most recently Benezeth *et al.* (2008) and previous to that Palmer *et al.* (2001), Benezeth *et al.* (2001, Panias *et al.* (2001) and Bourcier *et al.* (1993). These authors all measure solubility of boehmite, and other mineral materials, under a variety of conditions using a hydorgon electrode concentration cell (HECC). There is however no reported data specifically pertaining to the solubility of boehmite in nitric acid at room temperature.

3.1.3 Dispersibility

The importance of achieving good dispersion on producing a high quality ceramic product is highlighted by DeLiso *et al.* (1988) who examined the dispersion of an alumina / zirconia system and related the rheological properties and powder packing of this system to the zeta potential curves.

Alumina dispersions were stabilised with carboxylic acids by Graule *et al.* (1991) who identified that an optimum concentration of dispersant is required to achieve the most effective dispersion, as overdosing leads to instabilities due to excess salt compressing the diffuse layer. The dispersion efficiency of carboxylic acids was seen to increase with the acid size due to the increased tendency to form chelat complexes. The interaction between boehmite and carboxylic acids was examined by Schefe *et al.* (2009) using X ray adsorption near edge structure spectroscopy

(XANES), they found strong bonding between the materials, though the presence of phosphorous prevented any bonding suggesting site competition between these materials.

3.2 Rotational Rheology

3.2.1 Characterisation and Modelling Rheology of Concentrated Suspensions

Characterising the rheological properties of concentrated suspensions is non-trivial as discussed in Section 2.2. It also has significant industrial relevance, such as in the food industry and not least in the ceramics industry, where processes such as wet grinding, slip casting and spray drying, amongst others, are heavily dependent on slurry rheology. As such this is a topic which has been studied and reported on extensively.

Various reviews of this subject area have been written over the years, including Cheng (1984), Chander (1998), Mewis and Wagner (2009) and most recently Holek and Mendoza (2010). Many of the issues identified in early reviews have been examined and reported on but are still not fully understood. The difficulty of relating the properties of dilute systems to the characteristics of concentrated systems is discussed by Chander (1998).

Many theoretical and numerical works have been performed on the rheology of concentrated suspensions examining both the physical and chemical influences on rheological properties. A particularly useful introductory article on the connection between particle size, size distribution and rheology has been presented by Fletcher and Hill, of Malvern Instruments, (Malvern, UK) which illustrates how a smaller

absolute size or higher volume fraction of solids increases viscosity and how unimodal systems exhibit a higher viscosity than polydisperse systems. In addition to this article Malvern have also published a user-friendly guide 'Ten Ways to… Control Rheology by Changing Particle Properties' which covers both physical and chemical control of rheology.

A large number of works have studied the effect of particle size distribution on the rheological properties of concentrated suspensions of specific materials, for example, Dabak and Yucel (1987) studied the effect of particle size distribution and concentration on a variety of material systems and Ramal Jr. *et al.* (2002) found the rheological preroperties of refractory castables to be highly affected by variations in particle size distribution.

Models for concentrated suspension rheology typically consider non-reactive hard spheres, though the majority of real situations require understanding of anisometric shapes and chemically active systems. Consideration of the effect of deformable particles as opposed to hard spheres was made by Frith and Lips (1995) who found that the deformability did not significantly affect the high shear limiting viscosity, but did affect the dilatant transition. A similar article by Snabre and Mills (1999) found that the deformation – orientation interaction of viscoelastic particles under flow increased the maximum packing fraction of particles, leading to non-linear rheological behaviour. The rheology of a dilute suspension of hard spheres in a viscoelastic medium was studied by Patankar and Hu (2001) who show the migration of particles to the centre line of flow and found the materials to exhibit shear thinning behaviour despite the non-shear thinning behaviour of the medium.

The examination of fibre suspensions has been considered by Petrie (1999) who examined dilute suspensions of fibres to clarify some pre-existing confusions, and Pabst *et al.* (2006) who investigated the rheology of short fibre systems and present a simple relationship for the dependence of intrinsic viscosity on aspect ratio which approximates to the highly sophisticated Brenner equation (Brenner, 1974), details of which can be seen in Pabst *et al.* (2006), with reasonable precision for many practical situations.

The effect of the solid liquid interface on rheological properties was studied by Van Kao (1975) and the effect of surface chemistry by Leong and Boger (1989). Authors who have considered the DLVO (Derjaguin – Landau – Verwey - Overbeek) theory in conjunction with rheological properties include Zhou *et al.* (2001), who report on the effect of surface chemistry and particle physics on the rheology of metal oxide suspensions, and Johnson *et al.* (2000) who examined the relationship between surface chemistry and rheology of concentrated mineral suspensions of alumina, zirconia and kaolin. The DLVO theory considers the combined effects of the attractive van der Waals forces and repulsive double layer forces around a particle. Controlling the rheological properties by using dispersants to shift the isoelectric point of yttria suspensions has been investigated by Jin *et al.* (2009), enabling the desired rheological properties to be obtained at the required pH.

Published works relating the rheological properties of concentrated suspensions to operating conditions in a variety of processes are also numerous including Anklekar *et al.* (1998) on milling, Tsesekou *et al.* (2001) on slip casting, tape casting and spray drying and He *et al.* (2004) on wet grinding applications.

Ceramic suspensions were investigated by Bergstrom (1998) who found that the high shear form of the Cross model, presented in Figure 2.8 and equation 2.4 in Section 2.2.1 described the behaviour of the materials adequately. He also commented that the dependence of rheology on volume fraction fitted a modified version of the Krieger Doherty model therefore yielding values for the maximum packing fraction of the system. Significant differences were observed in the maximum packing value for systems containing particles of difference shapes.

Rheological properties of bimodal gibbsite and boehmite suspensions were investigated by Bruinsma *et al.* (1997) using nanometer sized boehmite particles with micron sized gibbsite particles in 0.1 M sodium nitrate. This work confirms that the presence of small particles can have a significant effect on the rheological properties of suspensions by enabling the solids content to be increased without significantly increasing viscosity. The effect is attributed to the small particles coating the larger particles (shown by TEM) and providing steric repulsion. Addition of boehmite above the level required to coat the larger gibbsite particles exacerbates the shear thinning behaviour of the material. This work highlights the importance of fully understanding the particle size distribution within a slurry particularly the very small particles which may not be detected with standard particle sizing methods.

The gelling of aluminium soaps has been studied by Wang and Rackaitis (2009). The original mechanism for this phenomenon was thought to be similar to that of gels formed in the peptisation of boehmite i.e. the formation of polymeric chains with aluminium atoms linking along the centre (this is discussed further in Section 3.2.2), however, their studies of the rheological properties of gelled aluminium soaps along with high resolution microscopy has confirmed this mechanism to be incorrect.

Instead the mechanism has been shown to be the formation of spherical micelles which aggregate into highly fractal and jammed structures. Mao *et al.* (2009) studied gelation kinetics of an epoxy resin gel system using oscillatory rheology and evaluating the storage modulus as a function of time. An alternative technique for measuring gelation kinetics is laser tweezer microrheology, such as is used by Meyer *et al.* (2006). Dickinson (1999) discusses the accepted models of reversible and irreversible gelling of colloidal particles and the arbitrariness of this distinction due to its dependence on time scale. Rheologically a complex real particle gel may behave as either a transient network or a covalent cross linked network. Laxton and Berg (2005) studied the use of gel trapping as a technique to stabilise systems pertinent to the food industry using a combination of sedimentation and rheometric techniques.

The effect of pH on rheological properties of sodium bentonite suspensions has been investigated by Benna *et al.* (1999). A vane rheometer was used to measure the yield stress which increased significantly as pH reduced below that of the isoelectric point. This was attributed to the edges being positively charged and face-edge interactions dominating causing a three dimensional structure to form within the gel in a card-house style. When the medium becomes very acidic the yield stress reduces significantly as the high ionic strength causes significant compression of the double layers and reduces the face-edge interaction leading to the breakdown of the structure. This effect is likely magnified by the structure of the clay being attacked by protons.

The difficulty of measuring yield stress is examined by Møller *et al.* (2006) who propose that the difficulties of measuring yield stress are removed when the

thixotropy of a material is also taken into account. They demonstrate an experimental protocol which allows for reproducible data to be obtained and conclude that yield stress is not a material property as it is dependent on the shear history of a sample and can be accounted for by thixotropy. It has been demonstrated by James *et al.* (1987) that a variety of yield stress magnitudes can be obtained depending on the method used to make the measurement. The use of a vane rheometer to determine the yield stress has been validated for a variety of solid like materials (Servais *et al*., 2003). Servais *et al.* used flow visualisation as a validation tool. They validated the use of vane rheology to measure yield stress within the linear viscoelastic region, and concentric cylinder or vane rheology to determine viscosity at high shear rates.

Nguyen and Boger (1992) state that: 'despite the controversial concept of the yield stress as a true material property… there is generally acceptance of its practical usefulness in engineering design and operation of processes where handling and transport of industrial suspensions are involved.' This is the view taken by the present author with regards to the work performed and presented by taking measurement of yield stress in a consistent manner the results are deemed to have validity as a tool for comparing samples.

Although suspensions are generally known to display shear thinning behaviour shear thickening (dilatancy) can also be observed. It is proposed by Barnes (1989) that all suspensions will display shear thickening, however, only some will display this at a shear rate measurable in rheometers. In the case of monodisperse systems the phenomenon is attributed to an order-disorder transitions. However, the cause in polydisperse systems remains unclear (Boersma *et al.* (1990)). It is proposed by

Boersma *et al.* (1990) that shear thickening occurs in the condition when the interparticle forces are equal to the shear forces applied to a suspension and the shear rate at which this occurs is termed the critical shear rate. This proposal has been experimentally validated on a range of dispersed systems.

As with rheology the measurement of zeta potential also becomes a more complex issue at higher solids contents. Electrophoretic techniques are limited to dilute, non turbid systems. The development of electroacoustic measurement methods has overcome many of the limitations of the electrophoretic techniques. Greenwood (2003) provides a comprehensive review of the measurement of zeta potentials in concentrated aqueous suspensions using electroacoustics.

Johnson *et al.* (1998) studied the relationship between the zeta potential measured by electroacoustic methods and yield stress measured using the vane method as described by Nguyen and Boger (1983). Their data clearly shows the peak yield stress occurring at the pH of the isoelectric point. The correlation between the yield stress (normalised to the maximum yield stress) and the zeta potential (squared) was used to calculate the interparticle separation according to a model described by Scales *et al.* (1998) and detailed in their publication. The results suggest that the interparticle separation is constant over the range of solids loadings investigated (0.2 - 0.3). Their experimental work also highlights the effect of solids loading on the measured zeta potential and the effectiveness of the Acoustosizer corrections made to compensate for this effect.

The effect of temperature on the point of zero charge of an alumina system was investigated by Akratopulu *et al.* (1986) who found that the point of zero charge increases with temperature within the range 10 °C and 50 °C

3.2.2 Previous Examination of Acidic Boehmite Systems

Acidic boehmite systems have been studied previously by a number of authors using a variety of techniques (Drouin *et al.*, 1988, Strenge and Bollman, 1991, Morgado *et al.*, 1995, Sunil Kumar *et al.*, 1997 and more). In general the studies aim to further the understanding of the interaction between boehmite and acid, most commonly nitric acid though others have been studied, and of the product formed when these materials are combined.

Ramsay *et al.* (1978) first described the formation of an Al_{13} cation as a product of the reaction between boehmite and nitric acid, and described this as a peptisation reaction. Micro electrophoresis, along with light and neutron scattering, was used to identify the species present. This is described as surface chemical changes leading to partial dissolution of particles giving rise to the formation of hydrolyzed, polymeric cations as detailed by Ramsay *et al.* (1978). The polymeric cations are proposed to be located on the surface of the particles causing short range repulsion. A complementary study to this work was performed by Drouin *et al*. (1988) who report on the rheological properties and structure of acidic boehmite systems using oscillatory rheology, proton NMR, thermoporosimetry and BET measurements. This study by Drouin *et al.* (1988) confirmed the formation of polymeric cations as suggested by Ramsay *et al.* (1978).

Jiratova and Janacek (1980) peptised boehmite with sulphuric, hydrochloric, nitric, hydrofluoric, trichloroacetic, phosphoric, oxalic, lactic and formic acid. They

concluded that the size of the boehmite particles was directly proportional to the amount of peptising agent. Organic and inorganic acids were considered to peptise differently due to the differences in the polarity, essentially inorganic acids are more effective as peptising agents due to the higher polarity of the anions which are therefore more easily absorbed by the particles.

Lee and Sohn (1985) prepared and characterised peptised alumina. They defined a peptisation index as the time taken for a specific formulation of 10 wt% solids with a specific concentration of formic acid to reach a viscosity of 5000 cp (5 Pa.s) measured using a Brookfield viscometer. However, there is no additional characterisation of the materials to confirm the structure or species present when this viscosity is reached.

An alternative definition of peptisability is given by Morgado Jr. *et al.* (1995) who describe the peptisation mechanism as a chemical disaggregation of large particles and propose that the degree of peptisation can be indicated by the reduction in the average particle size to the submicrometer range. They investigated the effect of the preparation method of boehmite on peptisability and find that the rate of the crystallisation, which controls the intercrystallite bond strength, correlated well with their measure of peptisability.

Pierre and Uhlmann (1986) investigated the acidic gelation of aluminium hydroxide sols and found that the preparation conditions determined whether the gels were crystalline or amorphous. This work deals with the preparation of boehmite or other alumina phases from aluminium hydroxide sols rather than the gelation of boehmite.

Beattie *et al.* (1996) studied the anomalous aggregation behaviour of aluminium oxyhydroxides at acidic pHs in the presence of chloride ions. It was observed that boehmite displayed anomalous stability which was not related to the pH and electrolyte dependence of the zeta potential. Gamma alumina was found to display similarly anomalous stability, the mechanism of which was attributed to the presence of anions due to the addition of salts such as KCl or NaCl. However, gibbsite was found to display normal stability, in that agglomeration occurred even at very low salt concentrations. Gamma alumina and boehmite both remain stable at reasonably high salt concentrations; once agglomeration begins to occur it is increased by increasing the concentration of salt in the formulation. Similar anomalous stability has been observed in silica and rutile systems. There is no mention in Beattie *et al.* (1996) of the formation of a polymeric cation causing the anomalous stability.

Van Bruggen *et al.* (1999) also investigated the anomalous stability of boehmite in an acidic system. This work concludes that the anomalous stability can be attributed to the presence of the polymeric cation species previously described. It is suggested in this work that the species form and absorb onto the surface of the boehmite in a reversible process in agreement with propositions made by Ramsay *et al.* (1978) and Drouin *et al.* (1988) with the additional proposition that the species can reversibly adsorb and desorb from the surface.

Evidence of the short range repulsion discussed by those authors proposing the presence of polymeric cations on the surface of particles in peptised systems was found using atomic force microscopy by Karaman (1997) who studied the interaction between alumina coated silica spheres and flat alumina substrates.

An investigation into the effect of acid on the flow rheology of boehmite systems was performed by Strenge and Bollmann (1991). Their work examined slurries with a solids content of between 35 and 42 % (w/w) and molar ratios of acid to boehmite of between 0.03 and 0.08. Their findings are particularly pertinent to the results displayed and discussed in Chapter 5. They reveal that as acid content is increased, all else being equal, the apparent viscosity of a boehmite slurry initially reduces, passes through a minimum and then increases as more acid is added. Unfortunately they do not present pH data which would have allowed for direct comparisons between the data sets. Their results highlight the shear thinning nature of the materials, and a sharp increase in viscosity, was observed as the solids content approached that of the maximum packing fraction between 39 and 42 wt% solids.

Mills and Blackburn (2002) investigated the rheological properties of alumina pastes using ram extrusion and found the rheological behaviour to be strongly related to the packing behaviour of the particulate phase despite the high moisture content. Pastes contained gamma alumina with peptised boehmite, and acetic acid, as a binder. Pastes were observed to age considerably over a time scale of days and an increase in acid content was observed to result in a significant reduction of bulk yield stress. Hence the molar ratio of acid to boehmite was kept constant throughout the investigation. The void fraction, relative bulk volume and ratio of particle sizes of gamma alumina to boehmite have been considered with reference to conventional particle packing theory, and the constraints imposed by the errors in these parameters are discussed by the authors.

A chemical review performed by Casey (2005) describes and presents schematic structures for large aqueous aluminium oxide hydroxide molecules, including various phases (ε and δ) of an Al_{13} cation.

The zeta potential of boehmites has been studied by relatively few authors. Jiratova (1981) studied the isoelectric point of modified aluminas and found i.e.p values of between 4.5 and 9.8 depending on the type and level of impurities present. They also refer to work by Parks (1965) and Stumm *et al.* (1976) who identified variations in the isoelectric point of alumina with crystallographic structure and preparation method respectively. The work of Drouin *et al.* (1988) quotes the isoelectric point of boehmite at pH 8.6, measured with a Laser Zec Meter. Wood *et al.* (1990) studied the electrochemistry of the boehmite – water interface using electrophoretic techniques, and demonstrated that the two pK triple layer site binding model gives a good representation of this. They identified the point of zero charge and isoelectric point of boehmite and found these to be at pH 8.5 and 9.1 respectively. The two pK triple layer binding site model is a surface chemistry model which assumes a sorbent to be homogeneous with respect to functional groups and particle geometry, although these assumptions are often unrealistic it is a popular model. Further details on the equations pertaining to the model can be seen in Lűtzenkirchen (1998).

Two nuclear magnetic resonance studies were performed in the late 80s by Olson and Bauer (1986) and Nazar and Klein (1988). Olson and Bauer identified three species present in the system. The first species was identified as $Al(H_2O)_6^{3+}$; a monomer represented by a single narrow peak that remained constant over time. The other two species were not specifically identified but it was shown that one

disappeared over time whilst the other grew. Nazar and Klein supported their findings but also found two additional peaks one of which was assigned to a colloidal species and the other suggested as $Al_2(OH)_2(H_2O)_8^{4+}$.

Drouin *et al.* (1988) found a minimum relaxation time at an acid content corresponding to the maximum storage modulus using proton NMR which they showed was the result of chemical phenomena.

A detailed study of peptised boehmite systems was performed by Morgado Jr. *et al.* (1997) who examined the materials with both solution and solid state NMR, particle size by dynamic light scattering, pH and viscometry. This work continued to support the findings of Olson and Bauer (1986) and Nazar and Klein (1988) in that there were no tetrahedrally coordinated species observed. They confirmed the presence of the monomer described by Olson and Bauer. A mass balance was performed on the system showing that the monomer and its hydroylsed version accounted for less than 10% of the aluminium present. A more significant amount of aluminium was identified as being present in an unidentified high molecular weight species with relatively symmetrical sites this was sensitive to pH. It is also suggested that this species can aggregate. Solid state NMR performed on freeze dried sols showed no significant difference between peptised and non peptised materials.

The formation of an aluminium gel comprising an Al_{13} molecule was studied by Bradley *et al.* (1993) who formed aluminium gels by base hydrolysis of Al^{3+} solutions with NaOH, a model of the Al_{13} unit is described. They observe a psuedoboehmite structure formed as an intermediate when gels formed in this way are aged. Fresh

gels were characterised using solid state NMR and found to contain both tetrahedrally and octahedrally coordinated aluminium species.

There is evidence of mechanically induced chemical changes occurring in aluminas which are referred to as mechanochemical changes. In the process of milling the large stresses acting on the particles and high local temperatures at impact points have been observed to cause changes from alumina to alumina hydroxide (Stenger *et al.*, 2005)) and the surfaces of milled alumina particles have been shown to become activated and form AlOOH (Yasuoka, 1992). Mackenzie *et al.* (2000) monitored the structural changes occurring when boehmite was milled for 60 minutes, using XRD, thermal analysis and ^{27}Al MAS NMR. Grinding was not observed to cause dehydration of boehmite but did result in a loss in crystallinity of the structure and the formation of an amorphous phase displaying pentahedral and tetrahedral coordinations.

Omura *et al.* (2006) compared the novel technique of wet jet milling to ball milling as a method of preparing alpha alumina slurries. They found that the wet jet mill produced a slurry with a lower viscosity compared to that produced by the ball mill and that the surface of the particles remained unaltered. The resulting ceramic had a higher green density than those from slurries prepared on a ball mill. Subsequent works support these findings; Hotta *et al.*, 2008, Hotta *et al.*, 2009 and Sato *et al.*, 2009. Hotta *et al*. (2009) found the use of a ball mill resulted in the formation of gibbsite at the alumina surface, the use of a planetary ball mill resulted in the formation of bayerite at the surface, and confirmed the surface had remained intact by wet jet milling. Sato *et al.* (2009) presented scanning and transmission electron microscopy images showing the variations in the surface.

Rosenberg *et al.* (1995) used cryogenic scanning electron microscopy techniques to obtain a direct visualisation of gel texture. They were able to identify textural differences between peptised, non peptised and intermediate alumina pastes. Fauchadour *et al.* (1999) examined cryotechniques applied to transmission electron microscopy, a technique intrinsically more suited to dilute systems than scanning electron microscopy. They assessed the effect of three cryofixation techniques on the structure of boehmite pastes and concluded that both liquid propane immersion cooling and slam freezing resulted in the loss of structural information due to rearrangement of the particles by the ice crystals which was not the case when the material was cooled by high pressure.

3.3 Mixer Torque Rheology

3.3.1 Development and Modelling of Mixer Torque Rheology

Mixer torque rheometry was initially used to measure the consistency and processability of plastics. Goodrich and Porter (1967) characterised a variety of polymers using a Brabender torque rheometer and modelled the torque rheometer as two adjacent concentric cylinder rheometers and converted the data obtained from a torque rheometer to that from a capillary rheometer for a material exhibiting Newtonian behaviour. Their analysis yielded relationships of the form: viscosity = f (torque, rotation speed) and shear stress = f (torque). This model was extended by Blyler and Danne (1967) who presented a general analysis to allow the determination of shear rate and viscosity from batch mixer rotor speed and torque data, to include non-Newtonian fluids and derived equation 3.1:

$$M = C(n)KN^n \quad \text{.....(equation 3.1)}$$

where, M is torque, $C(n)$ is a constant, N is roller speed (rpm), and K and n are parameters such as in the power law equation for fluid rheology as described in Section 2.2.2. They concluded that 'log (M) vs. log (N)' from the torque rheometer and 'log (τ) vs. log ($\dot{\gamma}$)' from a capillary rheometer should exhibit the same slope for a polymer melt, where τ is shear stress and $\dot{\gamma}$ is shear rate . A similar approach was taken by Lee and Purdon (1969) but the constant $C(n)$ used by Blyler and Danne (1967) was related to experimentally determined instrumental constants. Lee and Purdon commented that as a consequence of their work the Brabender Plastograph could now be regarded as a formal viscometer. Their approach was modified by Marquez *et al.* (1996) who simplified the calculation of $C(n)$. Further development on this model was performed by Mallette and Soberanis (1998) who employed a third order polynomial and further simlplified the calculation of $C(n)$. Cheng *et al.* (1999) introduced a reduced $C(n)$ and eliminated the effect of geometrical parameters.

Bousima *et al.* (1999) have continued the idea of modelling the torque rheometer as a concentric cylinder rheometer and introduced the concept of an effective internal radius R_i into the $C(n)$ term in equation 3.1. A significant finding when relating their modelling work to real experimental data was that R_i was insensitive to the material properties and only affected by the geometry and gearing of the mixing vessel, hence the definition of R_i for Newtonian fluids was also found to work for Non-Newtonian fluids. All of this work was performed based on examination of polymer behaviour, not ceramic pastes. Cheng *et al.* (2001) developed a new empirical equation describing the rheological parameters of polymer melts in a torque rheometer. They consider the effect of rotor speed, temperature and, unlike

previous authors, the apparent degree of fill on torque. The resulting rheological parameters were found to be in good agreement with those measured by capillary rheometry, which was not the case with the model developed by Bousima *et al.* (1999), suggesting that the model developed by Cheng *et al.* (2001) is more accurate.

Xu and Hilmas (2006) recently examined the applicability of Bousima's model for the torque rheology of ceramic/polymer mixtures and pure ceramic pastes. Their results were not encouraging as they found that the graphical similarity between data described by Blyler and Daane no longer held true and that the experimental data obtained showed significant deviations from Bousima's model.

There has been much investigation into the use of mixer torque rheometry took place in the pharmaceutical industry which has used the technique to investigate the granulation properties of pharmaceutical formulations in order to facilitate scale up of various processes. An initial investigation was performed by Rowe and Sadeghnejad (1987) on a mixture of microcrystalline cellulose powder and water in which the variation of torque observed by the technique was commented on, they also observed that steady state equilibrium conditions were attained after 3 - 5 minutes of mixing. A number of studies in the following years (Parker, York and Rowe, 1990, Parker and Rowe, 1991 and Parker, York and Rowe, 1992), in which the authors performed MTR studies along with additional characterisation, began to validate the technique as a useful characterisation tool by showing strong correlations between the observed rheological properties from the MTR and the variations in material properties.

During the same period this same group published an article (Hancock, York, Rowe and Parker, 1991) assessing the effect of instrument geometry on the characterisation of wet masses and found that different gearing resulted in variations in the mean torque values, though torque range was unaffected. This observation was attributed to the difference in mixing intensities achieved in each of the geometries. This was further investigated and reported on by Hancock, York and Rowe (1992). All previous work had studied the rheological properties of mixtures after a fixed period of time and assumed equilibrium, this investigation allowed mixing to continue until an equilibrium torque was observed, which was always within 12 minutes. An increase in torque was observed with a more viscous binder but varying the surface tension in binders with equal viscosities resulted in no change in torque.

Landin *et al.* (1995) reported on the nonlinear effects of shaft speed and sample weight and found that for small amounts of sample the shaft speed had little effect on the mean torque. Rowe (1996a) reported that the blade orientation has a significant effect on the measured torque responses, again attributed to the difference in the intensity of mixing achieved, as was the case with the study of the effect of instrument geometry. In this investigation it was also suggested than in order to compare torque rheology data with capillary rheometry data the mean torque must be converted to shear stress and the shaft speed to shear rate, an observation which agrees with the various works published regarding modelling MTR data.

Work by Hancock (1991) showed that the peak in mean torque always occurred at a higher liquid saturation than the peak in torque range, which, along with an assumption that the shear from the mixing blades would only shear void and liquid

bridges and not fracture powder, led to a number of important conclusions being drawn. These were that the torque range peaks when there are both voids and capillary bridges present in the wet mass, i.e. at the funicular state of liquid saturation. The mean torque reaches a peak when there are the most capillary bridges present, i.e. at the capillary state of liquid saturation. The further apart these two peaks are, the more readily wettable a system is and the magnitude of each of these peaks depends on the relative strength of the cohesive and adhesive forces within the mass. A large magnitude of the peak torque range indicates heterogeneously distributed interactions between the powder and liquid, i.e. a poorly mixed system indicative of poor spreading and wetting. A high mean torque peak implies a strong interaction between the powder and liquid phase with good spreading and wetting. These slightly speculative conclusions were validated with a number of model systems comprised of glass ballotini and polymeric binders.

Rheological models used to analyse mean torque data from a torque rheometer have included the logarithmic model, Herschel Bulkley model and Casson model. It was suggested by Landin *et al.* (1995) that the Herschel Bulkley model was most suited to the description of wet masses characterised by torque rheometry, it has been demonstrated by Rowe (1996a) that the Casson model is in fact the most appropriate. The Casson model takes the same form as the Bingham model seen in Section 2.2.1, with all components raised to the half power. The application of these models has led to calculated values of yield stress and kinematic viscosity being consistent with those generated by capillary rheometry (Rowe, 1996b). All of these works have focused on polymeric rather than ceramic systems.

Following on from the work detailed above there are a large number of examples from the late 90s through to recent years of the technique being used within the pharmaceutical field to characterise formulations for granulation, to help with scale up of the granulation process and to predict the properties of granulated products with some convincing correlations observed, (Landin *et al.*, 1996, Faure *et al.,* 1998, Chatlapalli, 1998, and 2002, Soh *et al.,* 2006). In general these studies concluded that the technique was useful as a predictive tool in developing formulations for the granulation process.

A correlation between near infrared spectroscopy (NIR) and MTR data has been investigated by Luukkonen (2001). NIR spectroscopy can be used to study the retention capacity of a material, and distinguish the energetic states of water within a material. They found that a plateau in the baseline corrected water bands heights from NIR correlated with the maximum torque values reported from MTR experiments. Some differences were observed between the two methods, which were attributed to the difference in the amount of shear imposed on the system. The results suggested that NIR could be used for end point detection in real time process measurements. This work also compared the results obtained from capillary rheometery and the MTR. They identify a significant difference in the techniques response to an increase in liquid content and comment that the MTR is only able to measure the liquid saturation state, not classical rheological parameters such as yield stress or viscosity constants.

3.3.2 Use of Torque Rheology in Ceramics

There are a limited number of examples of the mixer torque rheometer being used to characterise materials outside of the fields of polymers or pharmaceuticals, though of

those that are available, the majority pertain directly to the use of boehmite in extrusion.

Tischer (1981) used a torque rheometer as a mixer to prepare boehmite / molybdena pastes for ram extrusion. Acid was used as a peptising agent and the torque was observed to correlate with the degree of peptisation, quantified by acid concentration.

Sunil Kumar *et al.* (1994) produced a ceria zirconia ceramic by extrusion of a ceramic polymer mixture. The formulation for this extrusion was examined using a Brabender Plastograph which is essentially a continuous MTR. The instrument was used to identify optimum ceramic loadings at temperatures of 120 and 130 ºC.

Sunil Kumar *et al.* (1997) used torque rheology to investigate the properties of an alumina boehmite mixture for extrusion. Sunil Kumar *et al.* (1998) also published work on the extrusion of an alumina – zirconia (12 mol% ceria) composite using boehmite as an extrusion aid, however their experimental technique did not involve the use of torque rheology methods.

Ananthakumar *et al.* (2001) characterised the rheology of alumina paste for extrusion, which contained varying amounts of boehmite gel as a binder, using a mixer torque rheometer. In this study the rotor speed was varied from 10 – 40 rpm and the apparent viscosity was calculated by dividing the torque by the rotation speed. Ananthakumar and Warrier (2001) studied an extrusion formulation containing alumina – aluminium titatate with boehmite as a binder. Work continued in this field with Ananthakumar *et al.* (2004) publishing work on the effect of

boehmite and organic binders on the extrusion of alumina using the Brabender Plasticorder to examine the viscosity and torque behaviour of the formulations.

Liu and Chou (2000) have used viscosity measurements from a Brookfield rheometer to determine the critical powder volume concentration (cpvc) for ceramic powders (kaolin and alumina) and verified that the cpvc could be used as the minimum solids content required for successful extrusion formulations. They identify the cpvc as the maximum volume loading of powder in fluid that yields a stiff paste, as defined by Pierce and Holsworth (1965), and calculate the value as the reciprocal value of the crowding factor from the Mooney equation relating relative viscosity to solids loading. The critical powder volume concentration is also referred to by Sunil Kumar (1994, 1997) where it is identified as the solids loading at which the torque value from the mixer torque rheometer begins to increase sharply, although Markhoff *et al.* (1984) defined the cpvc as being the solids loading at which the maximum torque occurred. Due to the apparent inconsistencies in literature and possible confusion the term cpvc is not used in discussions within this project.

As mentioned in Section 3.3.1, the technique has been used recently by Xu and Hilmas (2007) to examine a ceramic / polymer mixture for co-extrusion. Although models for polymer materials in MTRs exist and characterisation of ceramic paste materials has begun there is currently no successful model of ceramic pastes in a mixer torque rheometer.

3.3.3 Wettability Measurements

Lazghab *et al.* (2005) present and compare various methods of measuring the wettability of finely divided solids such as spreading, capillary rise, condensational and immersional. They identify the use of capillary rise methods as an attractive

option for the measurement of the contact angle of bulk solids, (as opposed to individual particle), due to the low cost and ease with which the measurement can be taken, though the inability to accurately quantify the packed bed constant can pose a serious limitation to the technique.

3.4 Extrusion

3.4.1 Extrusion

Extrusion has been studied and reported on extensively in a variety of fields, including food, pharmaceuticals, agriculture and ceramics. This literature review focuses on the extrusion of ceramic materials.

The first commercially available twin screw extruder was produced and patented by Robert Columbo in 1938. Extruders available today are still of the same form though with some improvements in materials of construction and control technology. A more detailed review of the history and development of the twin screw extruder can be seen in McGuire (2008).

Perhaps one of the most impressive and widely used ceramic extrusion products is the monolithic ceramic catalyst support which is widely used across the automotive industry and in stationary NOx emissions controllers. Forzatti *et al.* (1998) studied the preparation and characterisation of these and identified the usefulness of capillary rheometry in prediciting the extrudability of ceramics pastes. They discuss the effect of paste composition on the mechanical properties of the paste, particularly the use of organic and inorganic materials to act as binders and mechanical promoters respectively. Das *et al.* (2002) characterised cordierite materials using the Benbow Bridgwater model, described previously in Section 2.4.6.

The use of a twin screw extruder (TSE) as a continuous granulator has been investigated by Keleb *et al.* (2002) who concluded that this was a robust process which may offer an alternative to high shear granulation within the pharmaceutical industry. This was also investigated by Djuric *et al.* (2009) who compared the effect of two similar twin screw extruders used as continuous granulators on the properties of the granules produced. They found that the equipment used had a significant effect on the granule properties, the reasons for which are not fully understood and require further investigation, highlighting the difficulties of interchanging between extruders.

The use of a twin screw extruder as a three phase reactor was investigated by Moshkabad and Winterbottom (1999) who immobilised palladium on the screw. Their results confirmed that the TSE performed as a superior reactor, achieving a gas liquid transfer coefficient 10 times greater, than the conventional stirred tank. Powell and Blackburn (2010) successfully extruded a 5 layer tubular structure for use as a solid oxide fuel cell. It was considered imperative in this extrusion application to unify the rheological properties of the 5 paste streams in order to achieve a successful extrusion.

3.4.2 Extrusion of Boehmite

Acidic boehmite materials were extruded and examined by Jiratova and Janacek (1980) who concluded that the anion affected the specific surface area of the resulting extrudate and that the mechanical strength achieved increased with both the mixing time and the acidity of the peptising agent.

The extrusion of molybdena / alumina incorporating boehmite as an extrusion aid was performed by Tischer (1981) and Stoepler and Unger (1983). They identified

that ‘unfavourable extrusion properties can be overcome by addition of boehmite’. Stoepler and Unger (1983) performed a large study examining the behaviour of 60 commercial aluminas, including boehmites, formed by ram extrusion. They concluded that 6 factors affect the product properties; the degree of powder dehydration, particle size and size distribution, shape of aggregates, crystallite size and specific surface area. Chen and Cawley (1989 and 1991) indicated the usefulness of boehmite as an extrusion aid for alumina systems. This was assessed further by Sunil Kumar *et al.* (1997) who studied both gamma and alpha alumina systems. They concluded that boehmite was useful in alumina systems as a binder and a sintering aid, with the advantage of avoiding any residual impurities as the boehmite becomes part of the alumina matrix.

The use of boehmite as an extrusion aid in a more complex extrusion system of alumina – zirconia (12 mol% ceria) composite was studied by Sunil Kumar (1998). The formulation was successfully extruded with boehmite and the addition of boehmite was found to improve the particle packing and the sintered density of the product.

A similar study was performed by Prabhakaran *et al.* (1999) who investigated the use of boemhite as a binder in an alumina system, specifically for use in the gel casting process. Both this study and Ananthakumar *et al.* (2001) concluded that boehmite has advantages such as good matrix compatibility, good workability and better green strength in an alumina system.

Kolenda *et al.* (2003) used a simple squeezing test to assess the extrudablility of a paste, with particular focus on whether the test could identify issues with phase

migration within a formulation. They experimented with titanium oxide and boehmite, in both cases using nitric acid as a peptising agent to generate repulsive interaction forces between primary particles. It was concluded that the boehmite paste, unlike the titanium oxide paste, behaved independently of compression speed in the test and exhibited no signs of phase migration, indicating that 'this type of paste will not generate extrusion problems'.

3.4.3 Paste Characterisation

Cone penetration is a simple technique which can be used to measure the bulk yield strength of a material, but fails to give any indication of the flow properties of the paste. This technique is described and employed by Benbow and Bridgwater (1987). Briscoe and Özkan (1997) employed a similar method, the indentation hardness test, to characterise the plasticity of alumina pastes. The use of oscillation techniques hold potential to increase the understanding of paste structure and behaviour (Chandler *et al.*, 2002), but as yet little is published in this area.

Squeeze flow has been used to assess the extrudability of pastes by Kolenda *et al.* (2003), the test was considered valuable in the task of formulating pastes for extrusion. They describe the use of a two parameter model suitable for describing the extrusion of pseudoplastic ceramic pastes. Tang and Kalyon (2004) combined capillary and squeeze flow methods to determine the Herschel Bulkley parameters and the relationship between wall slip velocity and wall shear stress. Although the combination of the techniques was an improvement on using a single technique, it was still found to be difficult to elucidate all 5 desired parameters from the experimental data.

The radial flow of pastes and gels was examined by Bates and Bridgwater (2000) using flow visualisation techniques and squeeze flow. They observed almost uniform radial outflow, with some velocity variations in the outermost material. The strains created in the material were found to result in the loss of contact between the paste and the wall, identified by the lack of a pressure signal from pressure transducers located in the plates.

The most commonly accepted method of characterising pastes for extrusion is by studying capillary flow and applying the Benbow Bridgwater equation, displayed in Section 2.4.6 and described in detail in Benbow and Bridgwater (1993). This model developed from some earlier work performed by Ovenston and Benbow (1968) investigating the effects of die geometry on the extrusion behaviour of clay like materials. They confirmed the occurrence of plug flow in dies with a uniform cross section, i.e. square entry dies, but found the description of flow in conical entry dies more complicated. Flow in conical entry dies was shown to be described by the same mechanics as those applicable in understanding square entry dies by Benbow (1971), this meant that for either category of die geometry the relationship between pressure gradient and volume output rate can be described by 3 material constants which could be adequately determined by ram extrusion through a number of dies. The results of this work were used as the design basis for numerous dies for the manufacture of catalyst supports.

Around the same time, Worrall and Khan (1972) used ram extrusion as a tool for characterising the plasticity of clay materials, though they recognised the limitation of the technique not fully describing all the parameters contributing to plasticity.

The relationship between paste formulations and extrusion parameters was investigated by Benbow *et al.* (1987, 1988) using a ram extruder. They identified two important extrusion parameters, the yield value and wall stress, and illustrated the considerable effect of the particle size distribution and liquid phase content on the extrusion parameters. The popularity of the model is evident from the extensive published works which use this model to characterise materials, a list of examples can be seen in Wilson and Rough (2006). The model was referred to in over 40 published articles within a ten year period from 1994 to 2004. The equation has its flaws and critiques of the model can be found in Blackburn *et al.* (2000) and Basterfield *et al.* (2005)

Horrobin and Nedderman (1998) used the large deformation elastic plastic finite element method to examine the pressure drop at the die entry region and predicted pressure drops which were in good agreement with the experimental data. They discuss that the uniaxial yield stress is overestimated by the Benbow Bridgwater equation due to the over simplification in assuming the variable to be independent of geometry. However, they employed a rate independent model, therefore assuming a velocity factor of zero, which is not applicable to the real extrusion of pastes.

Draper *et al.* (1999) examined the effect of paste preparation method on the resulting rheological properties. They minimised the effect of solids content by applying the equation described by Chong (1971), similar to the Kreiger Doherty equation discussed in Section 2.2.2, which allows the prediction of the viscosity of a concentrated suspension from the solids content, maximum packing fraction and binder viscosity. In order to apply this technique the maximum packing fraction was calculated by preparing pastes at various solids contents and characterising using

the Benbow Bridgwater method. This allowed the authors to prepare pastes of similar consistencies with different formulations. The Herschel Bulkley model was found to accurately describe the rheological properties of these pastes.

The stress relaxation of an alumina paste, (a ceramic catalyst mimic) was shown by Chou *et al.* (2003) to be rapid, resulting in residual stresses which were in good agreement with the Benbow Bridgwater model, unlike the behaviour of a talc paste, which was also studied by Martin *et al.* (2004), who also found the rheological properties a talc paste difficult to characterise.

3.4.4 Studies of the Extrusion Process

3.4.4.1 Understanding Flow in Extrusion

Ram extrusion is a comparatively simple process compared with screw extrusion, lending itself to characterisation techniques that are more difficult to apply to a twin screw extruder.

Götz *et al.* (1993) used nuclear magnetic resonance (NMR) to detect structural changes and flow patterns in extrusion pastes. They were able to confirm the occurrence of phase migration and identify the presence of a radial moisture profile across the barrel. They also confirmed that prior to the die entry region only displacement and compression occur, not shear, with the exception of shear deformation in close proximity to the barrel wall. The ability of NMR to distinguish between free and bound water as they exhibit different magnetic relaxation times, and to indicate bond type was used as an indication of the occurrence of ‘so-called peptisation’, with results suggesting that the strongest bound water was present on the solid surface, indicating that the material was a gel. They describe their raw material as an oxide ceramic based on alpha alumina. Götz *et al.* (1994) confirmed

the use of NMR to establish velocity profiles in concentrated suspensions and pastes.

The use of magnetic resonance imaging to study the velocity profiles in a ram extruder has been applied by Barnes *et al.* (2006). They observed variations in the flow regime which were dependent on distance from the die. Plug flow with slip at the barrel wall was observed away from the die, then as the die was approached the flow converged towards the centre of the barrel and stagnant static zones were observed adjacent to the walls. The shape of the velocity profile was found to be material dependent, but independent of ram speed and die length within the range studied. The build up of stagnant zones as the die is approached is also considered to be possible in a twin screw extruder, though a similar study has not been performed on this equipment.

Wildman *et al.* (1999) used positron emission particle tracking (PEPT) to monitor the flow of pastes in a ram extruder, the barrel was constructed from nylon to allow the tracking of particles. Irradiated glass ballotini tracking particles were placed at intervals across the barrel diameter and flow into the die monitored. Finite element analysis was applied to quantify the stress and strain rate, the strain rate was shown to be greatest at positions closest to the barrel wall.

PEPT is not a technique which readily lends itself to studying extrusion as the majority of extruder barrels are thick metal which prevents or affects the receiving of the radioactive signal from the tracer. A collaborative European research project (Collaborative publicity article, 2009) has successfully tracked the flow of polymer through a twin screw extruder in real time and under realistic processing conditions.

The successful application of this technique will lead to significant advancements in the field of modelling twin screw extrusion. Previous attempts to fully understand the flow of materials within a twin screw extruder have included the use of acrylic barrels, viewing windows and stop-start techniques. The issue of metal absorbing the gamma photons was overcome by the installation of a section (100 mm in length) of aluminium in the barrel which is reasonably transparent to photons.

3.4.4.2 Residence Distributions

A large number of studies have been conducted examining the residence time distribution (RTD) within twin screw extruders, particularly within the food and pharmaceutical industries. The first consideration of RTDs, i.e. flow through a vessel not being either plug flow or perfectly mixed, was made by Danckwert (1953), a useful outline of which is reviewed in McGuire (2008). One of the earliest studies of the RTD of a twin screw extruder was performed by Eise *et al.* (1983) who used an iron tracer coupled with conductivity measurements to assess the RTD of a polymer melt system. A significant change in the approach of considering residence distributions was made by Gasner *et al.* (1999) and Gao *et al.* (1999), both of whom identified that residence time distribution was not always a valid measure due to volume variations (fill level) and that an accurate understanding of the residence distribution should involve the normalisation of data to account for this. Data was normalised with respect to screw speed by Gasner *et al.* (1999) to produce a residence revolution distribution (RRV) and with respect to volumetric flow rate by Gao *et al.* (1999) to produce a residence volume distribution, (RVD).

A full discussion of the importance of normalising data and an illustration of the inaccuracies resulting from erroneously analysed data can be found in McGuire

(2008) who comments that a full understanding of the extrusion process requires consideration of all three distributions.

Unfortunately many studies on the residence distribution of a twin screw extruder have continued to focus entirely on the RTD with no consideration of the degree of screw fill or data normalisation. Examples of such studies up to 2008 are detailed in McGuire (2008), more recent examples include Kumar *et al.* (2008), Baron *et al.* (2010) and Villmow *et al.* (2010).

One of the principle reasons for studying residence distributions in a process is to elucidate an understanding of the degree of mixing occurring. Many published works study the effect of screw geometry and operating parameters on the RTD of a twin screw extruder, and draw conclusions from the resulting data regarding the factors affecting the degree of mixing achieved. There is conflict in the conclusions drawn and concern regarding the accuracy of conclusions based on the aforementioned issue of normalising data. Further discussion regarding these conclusions and the effect of equipment and operational parameters on mixing are discussed in Section 3.4.4.3.

3.4.4.3 Mixing and Agglomerate Breakdown

As discussed previously in Section 2.4.2 mixing can be considered as either distributive or dispersive. Gramann and Rauwendaal (2004) showed distributive mixing is achieved by elongational flow, caused by changes in cross sectional area. Distributive mixing can occur in the radial or axial direction in a twin screw extruder, i.e. across the screw cross section or along the barrel length. Section 3.4.4.2 presented literature studying the effect of screw configuration and operational parameters on mixing in twin screw extruders, inferred by examining the residence

time distribution, an unsatisfactory analysis which does not produce robust conclusions.

The publication by Vainio *et al.* (1995) is an example of using RTD to evaluate mixing effectiveness and being found to be a poor indicator. This study concluded that radial mixing was achieved with kneading elements and axial mixing was achieved with conveying elements, and particularly with reverse elements introducing backflow.

Van Zuilichem *et al.* (1999) studied the mixing effectiveness of screw elements using a combination of flow visualisation and RTD measurements in an extruder with a full length translucent barrel. They found a significant difference in the mixing behaviour of a kneading paddle and a reverse element, with reverse elements causing stagnancy not observed in flow within kneading paddles. In a block of kneading paddles the most significant mixing action is achieved by the first kneading paddle, with flow through a long block of paddles tending towards plug flow. Axial mixing was found to be unaffected by screw speed and paste rheology, probably due to operating in a flooded regime, but was affected by screw geometry. A similar conclusion was drawn by Gao *et al.* (1999) that axial mixing is independent of operational parameters, again they ran at a flooded regime. Carneiro *et al.* (1999) showed how the positioning of a reverse element downstream of kneading blocks creates greater eddie formation and improved both radial and axial mixing.

The dependence of the behaviour of screw sections on other screw sections remains undetermined, with contradictory studies being performed by Shearer and Tzoganakis (2001 a, b), one claiming that sections behave independently of each

other and the other concluding that the behaviour of a section is affected by the upstream configuration.

Mixing studies performed by McGuire (2008) concluded that the most effective configuration for distributive mixing was 4 d of 30 ° backwards kneading elements, where d is the barrel diameter. He defined a parameter for characterising the degree of distributive axial mixing achieved, defined by the volume of paste in which the first 2/3 of tracer were contained, hence neglecting the 'tail' commonly observed in tracer experiments. Mixing effectiveness is referred to in the review of ceramic shaping Blackburn and Wilson (2008) who highlight that mixing is best achieved by large strains rather than high strain rates.

Agglomerates have been shown to have a detrimental effect on the final strength of an extruded ceramic (Lange, 1989), and also significantly effects the flow behaviour (Benbow *et al.,* 1987). The breakdown of agglomerates can effectively be considered as dispersive mixing of particles.

Böhm and Blackburn (1994) and Wildman and Blackburn (1998) studied agglomerate breakdown using coloured agglomerates and optical microscopy, concluding that the breakdown of agglomerates was position (therefore shear rate) independent, but that the distributive mixing which followed was position (shear rate) dependent. Böhm and Blackburn (1994) also identified that agglomerate breakdown could be identified by monitoring pressure signals, though this analysis is limited by the qualitative nature of the data produced.

X-ray imaging of thin slices of material was used by Ess *et al.* (1984) to distinguish between agglomerates and the bulk paste, a technique which was extended into 3D

by McGuire *et al.* (2007) who demonstrated x-ray tomography, a technique developed for medical imaging, to be a useful tool in the imaging of extrusion pastes. They found that a TSE was more effective at achieving agglomerate breakdown than a Z-blade mixer / ram extrusion process. The volume of agglomerates broken down was found to be dependent on, and the final size of the broken agglomerates independent of, the operating conditions of the extruder.

3.4.4.4 Wall Slip

Understanding slip flow requires a quantification of the slip velocity and the dimensions of the slip layer. The pioneering study of wall slip was performed by Mooney (1931) who developed a model for calculating slip velocity which is now commonly accepted and remains the most popular model used to describe this phenomenon. The model considers slip flow as an abnormally large velocity gradient adjacent to the confining wall. The approach is relatively simplistic as it unrealistically considers the slip layer to be of uniform thickness and composition.

Despite the long standing acceptance of the Mooney model, it has been shown in a number of studies, including Khan *et al.* (2001) to be unsuitable, producing negative values of slip velocity. Various adjustments have been made to the model, such as the Jastrezebski modification, which in some cases has been used preferentially to the classical Mooney model, however there is no physical grounding behind the Jastrezebski approach and it is strongly recommended by Martin and Wilson (2005) that use of this approach cease. They advocate the use of the Tikhonov regularization of the Mooney model, described in their publication.

The Hatzikiriakos method, proposed by Hatzikiriakos and Dealy (1992) is advantageous compared to the Mooney approach as it requires data from only one

capillary. This method was successfully employed by Huzzard and Blackburn (1998) to study the slip flow in concentrated alumina suspensions, although some irrational values of slip velocity were obtained at very low shear rates.

The slip layer is proposed by Yilmazer and Kalyon (1991) to have a width of the same order of magnitude as the diameter of particles contained in the material. The width of the slip layer has generally received much less attention than calculation of the slip velocity. Wilson and Rough (2006) display images obtained by magnetic resonance velocity imaging to directly visualise the occurrence of wall slip and present a discussion of their studies of wall slip.

3.4.4.5 Phase Migration

The application of stress to a paste system can result in the preferential displacement of the liquid phase, resulting in liquid maldistribution and a variation in the pastes moisture profile. This effect, often termed phase migration, has been identified and observed by authors including Yaras *et al.* (1994) and Burbidge *et al.* (1995). Phase migration occurs due to the fact that the stresses imposed on a paste system are unevenly distributed by the phases, being predominantly borne by the liquid phase (Martin *et al.*, 2004).

Yu *et al.* (1999) confirmed the maldistribution of liquid by sectioning, weighing and drying an extruded paste. The use of a squeezing test was demonstrated to be successful in distinguishing between pastes which exhibited significant phase migration and those that did not (Kolenda *et al.,* 2003).

Rough *et al.* (2002) developed a model to predict phase migration based on a liquid drainage model. Patel *et al.* (2009) assessed the validity of using a modified version

of the Cam – Clay model (from soil mechanics theory) to describe the maldistribution of liquid in a system comprising glass spheres in a highly viscous Newtonian fluid. The model was shown to be acceptable but with significant room for refinement. Phase migration was shown to be dependent on the speed of extrusion, formulation and to a lesser extent, the extruder geometry.

3.4.4.6 Controlling Extrusion

Chen *et al.* (1998) and Böhm and Blackburn (1994) report that fluctuations in the pressure signals observed at the die were indicative of the quality of the paste. The fluctuations are identified by Amarasinghe and Wilson (1998) as being due to either the release of entrapped gas, the rupture of agglomerates, poor mixing or surface fracture. The use of signal processing methods to characterise the ram extrusion process using pressure data was investigated by Amarasinghe and Wilson (1998) with positive results. Russel *et al.* (2003) continued this investigation assessing the suitability of various statistical techniques for the analysis of such data, they found that outliers resulting from the rupture of air pockets of agglomerate breakdown could be identified and that the signal noise could be related to the mixedness of the paste. A further study by Russel *et al.* (2004) assessed the applicability of such analysis developed for the ram extrusion process to a twin screw extrusion process and found a good correlation between the results and extrudate quality, though with some limitations due to the sensitivity of the analysis.

A feed forward control approach, using pressure as a controlled extrusion variable, has been explored by Li and Bridgwater (2000) who assessed the use of an artificial neural network (ANN) for predicting the extrusion pressure in a ram extruder. They found that the ANN model was capable of predicting the extrusion pressure well, so

long as the influential extrusion parameters were accurately identified. In the prediction of the mean extrusion pressure they identified the following input parameters; the paste composition, the ratio of the die land to the die diameter, and the extrudate velocity. The application of a back propogation training process using these parameters and a set of 'training data' resulted in very good predictions of the mean extrusion pressure.

Köster and Thommes (2010) discuss the usefulness of torque measurements as a tool for monitoring twin screw extrusion, they reveal a linear relationship between torque and water content in a wet extrusion process, though the material studied is not specified.

3.4.4.7 Modelling

The geometry of self wiping twin screw extruder screw elements is described mathematically by Booy (1978); this work has formed the basis of much of the subsequent modelling work on extruders. This description, and details of modelling performed up to 2008 can be seen in McGuire (2008). The twin screw extruder has been considered and modelled by McGuire (2008) who examined the effect of screw speed, flow rate and paste rheology on the pressure drop across reverse elements. The model was validated using a variety of pastes and is considered accurate enough to be useful in the design process. The model developed to predict fill level was not considered to be so accurate. Barrera *et al.* (2008) performed 3-D modelling of flow curves in co rotating TSE elements and found a good match between their model and experimental data.

Vergnes and Berzin (2000) describe the issues associated with modelling reactive systems within a twin screw extruder, more specifically, the requirement to couple

flow simulation in a complex geometry with reaction kinetics and evolutionary rheological behaviour. They have developed models with good accuracy based on continuum mechanics for systems for which accurate kinetic data and rheokinetic laws exist. The use of such models is advantageous in dealing with scale up problems, even when imperfections exist.

A series of studies on the velocity distributions of liquids within various regions of a twin screw extruder have been performed by Bakalis and Karwe (1996, 1997, 1998 and 2002). Velocity distributions and volume flow rates through the nip and translational regions of a twin screw extruder have been studied by Bakalis and Karwe (2002). Two velocity components were measured simultaneously, using laser Doppler anemometry, over a range of mass flow rates (controlled by screw speed, ensuring that the fill level was maintained) and it was found that the volume flow rate in the nip region was roughly four times higher than in the translational region.

Chapter 4 Materials and Methods

4.1 Material Characterisation

4.1.1 Materials

Boehmite powder G250 was provided by BASF (Germany), V250 from UOP (USA) and Dequagel HP from Dequenne Chimie (Belgium).

BET surface area measurements were performed on Micromeritics ASAP 2420 and Micromeritics Tristar 3000 instruments using the ASTM method D 4222-83 using around 0.5 g of powder. The sample was initially outgassed using dry nitrogen at 140 ºC for a minimum of 1 hour before cooling to 77 K using dry nitrogen. The nitrogen adsorption desorption isotherm was measured between the relative pressures (P/P_0) 0.0035-0.95 and P_0 was measured at every point on the isotherm. The surface area was calculated by the Brunauer–Emmett–Teller (BET) method between pressures 0.05 and 0.2 using 5 data points. The equipment accuracy is within 0.5% with regards pressure measurement and ± 0.25 °C with regards temperature.

The BET surface areas for the boehmites G250, V250 and Dequagel HP, measured as described above, were 340, 280 and 300 m^2g^{-1} respectively, with an approximate error of ± 30 m^2g^{-1} based on variations in data observed over a range of samples. The losses on drying at 110 ºC measured on 2 g (± 0.01 g) of sample using a Mettler Toledo HG63 moisture analyzer were 8.3, 6.6 and 8.4 % respectively. Manufacturer quotes repeatability on a 2 g sample as ± 0.05%.

Demineralised water, unless otherwise specified, was produced by an Elga Option 3 water purifier. Dilute nitric and acetic acid were both produced from the respective concentrated acid provided by Alfa Aesar.

4.1.2 Particle Size and Shape

Three methods, each described below, have been used to measure the particle size distribution of the ‘as received’ boehmite powders.

A Malvern Mastersizer 2000 with a Hydro 2000g wet dispersion unit, pump speed was 1250 rpm, stirrer speed 500 rpm and no ultrasonics were used for dispersion. The optical properties in the selected operating procedure were; refractive index of the particles of 1.78, absorption index of 0.01 and refractive index of the medium (water) of 1.33. Three measurements were performed on each sample with a 5 second delay between measurements. The Malvern Mastersizer 2000 was also used with a Scirocco dry dispersion unit. The vibratory feeder was set at 50 % of the maximum with dispersive air pressure of 0.25 bar. The optical properties in the selected operating procedure were; refractive index of the particles of 1.78 and absorption index of 0.01. Measurement time was 15 seconds, with 15,000 measurement snaps and background time was 30 seconds with 30,000 background snaps.

Particle size distribution and sphericity were measured using a Sympatec dynamic image analyser. The lens allowed detection of particles between 5 and 1705 µm. The pixel resolution (1024 x 1024 pixels) and frame rate of 500 frames per second result in shape evaluation not being possible on particles less than 20 µm. Dispersion was performed by an Oasis VIBRI feeder at 25 %, 2 bar pressure and 71 mbar vacuum. Revolution and cascade were both zero. Calculations were performed on QICPIC software in EQPC calculation mode.

4.1.3 X-ray Diffraction

A Seimens D5000 diffractometer has been used to measure the crystallite size of boehmite. The powdered sample was pressed into a sample holder and loaded into the autosampler. The copper K alpha wavelength was 1.5406 angstroms, 2 theta started at 2 º and finished at 70 º using a step size of 0.02 º and step time of 1 second. X ray current was 30 mA and voltage 40 kV. Eva Version 8.0 and PDFMaint Version 8.0, both from Bruker were used to determine the phases present and crystallite size was calculated using Topas Version 2.0, also from Bruker. Instrument reproducibility and accuracy are both quoted as ± 0.0005 ° by the manufacturers.

4.1.4 Rate of Dissolution of Boehmite in Nitric Acid

A solution containing 25 g (± 0.01 g)of boehmite powder (G250 or V250) or 12.5 g (± 0.01 g) of powder (Dequagel HP) and 250 ml (± 0.5 ml) of demineralised water was manually titrated with 10 wt% nitric acid to a pH of just slightly below the desired pH (2 or 4) measured with a VWR 662 1762 pH probe. The pH of the solution was then maintained at pH 2 or 4 with the use of a Schott TA50 plus autotitrator and 10 wt% nitric acid. The conductivity was measured using a Hanna instruments MI 8733 conductivity meter. The experiment was monitored for 8 hours, recording the time elapsed (± 1 minute), pH (± 0.1 pH unit), volume of acid required to maintain pH (± 0.1 ml) and conductivity (± 1 %). In the case of Dequagel HP the volume of acid required to maintain pH has been altered to account for the presence of a smaller mass of powder.

4.1.5 Dispersibility of Boehmite in Acid

Acidic solutions of 5 wt% boehmite were prepared by addition of 10 g (± 0.01 g) of powder to 165 ml (± 0.2 ml) of demineralised water and 25 ml (± 0.2 ml) 1.0 M nitric or acetic acid. The solution was sheared for 5 minutes (± 10 s) using a Silverson mixer fitted with a high shear work head, as shown in Figure 4.1. 20 ml (± 0.2 ml) of the sheared solution was centrifuged at 3000 rpm (± 200 rpm) for 20 minutes (± 10 s) using an MSE Centaur 2. The supernatant was collected by pouring immediately after centrifuging and calcined at 1000 ºC (± 10 °C) for 3 hours (± 10 mins). The temperature was increased at a rate of 5 ºC min^{-1} and cooled at a natural rate.

Figure 4.1: High shear work head for Silverson mixer

4.1.6 Adsorption of Vapour

A Dynamic Vapour Sorption Advantage was used to measure the boehmites' ability to uptake moisture. The instrument was purged with nitrogen for 24 hours prior to the commencement of an experiment. The balance (accurate to 1 µg) was tared with a clean empty sample pan and 10 - 20 mg of sample charged to the pan. The sample pan was handled with tweezers to minimise the risk of contamination or equipment damage. The sample was dried at 120 ºC in 0 % relative humidity (accurate to ± 0.5 % relative humidity) for 2 hours to ensure complete moisture removal prior to uptake measurements. A double cycle was performed on each powder at 30 ºC. The relative humidity was varied from 10 % to 90 % and back to 10

% in increments of 10 %. Full equilibration was allowed at each humidity step, requiring the mass to remain constant to 0.001 g for 5 minutes.

4.2 Rheological Study and Gel Investigation

4.2.1 Sample Preparation

Samples have been prepared by milling on a Fritsch Planetary Micro Mill Pulverisette 7. Milling was performed at speed setting 7 with 3 media present in each of the vessels. The internal dimensions of the mill pots were 40 mm x 50 mm and the media were spherical with a diameter of 15 mm. The pots and media were both Fritsch “Syalon”, 90 % silicon nitride. Powder was weighed using a Mettler Toledo PR5002 Datarange balance located within a dust booth and liquids measured using 2.5, 5 or 10 ml plastic syringes from Beckton Dickinson. 6 g (± 0.1 g) of the appropriate boehmite powder was charged to the mill pot (with the media already in place) followed by 14 ml (± 0.2 ml) of liquid, containing the appropriate amount of dilute acid to obtain the desired overall acid content, producing samples containing 30 wt % (± 0.6 wt%) boehmite. Milling was carried out for 1, 14, 15, 30, 45, 60 and 90 minutes (± 10 s) for samples prepared with the boehmite G250 and for 1, 4 and 30 minutes (± 10 s) for samples prepared with the boehmites V250 and Dequgael HP.

4.2.2 Rheological Measurements

Rheological characterisation was performed using an AR 2000 from TA Instruments, Crawley, UK. A Julabo AWC100 chiller unit was used to control the peltier plate temperature which was maintained at 20 ºC. A 40 mm stainless steel cross hatched (serrated) plate with solvent trap was used for measurements (with solvent trap in place but no solvent present). The gap size was 1000 µm. The cross hatched plate

was used to mitigate against the occurrence of wall slip, a standard check for wall slip performing experiments at a variety of gap sizes was carried out to confirm that the occurrence of wall slip under these experimental conditions was minimal.

Both varied shear rate (shear rate ramp) and constant shear rate (shear rate hold) experiments were performed on each sample. Varied shear rate experiments were performed first, ramping from 0.001 s^{-1} to 1000 s^{-1} over a period of 1 minute each way, completing a total of 3 cycles. No pre-shear was performed and a 30 second equilibration time was allowed prior to commencement of the first shear rate ramp. The shear rate hold was performed without reloading of the sample. The sample was held at a shear rate of 1000 s^{-1} for either 3 or 5 minutes. The sample was pre-sheared at 100 s^{-1} for 1 minute, in accordance with suggestion by the instrument manufacturers, TA Instruments, to remove any memory the material may have of the shear rate ramp performed previously. Another 30 second equilibration time was allowed prior to the commencement of the shear rate hold.

Where oscillatory measurements have been made both varied shear stress (stress sweep) and varied frequency (frequency sweep) experiments were performed. A shear stress sweep was performed first, sweeping from an oscillatory stress of 0.01 Pa to 100 Pa in log mode at a frequency of 0.1 Hz, recording 3 points per decade. No pre-shear was performed and a 30 second equilibration time was allowed. This allowed identification of the linear viscoelastic region in which the frequency sweep could be performed. The frequency sweep was performed without reloading of the sample. A frequency sweep was performed at a frequency of 0.1 Hz from 0.01 to 100 Hz in log mode taking 10 points per decade. No pre-shear was performed and a 30 second equilibration time was allowed.

4.2.3 pH and Particle Size

pH measurements have been taken with a variety of probes over the course of the experiments. In each case a calibration was performed using Thermo Electron Corporation perpHect® pH buffers (pH 4 ± 0.01 @ 25ºC, pH 7 ± 0.01 @ 25ºC and pH 10 ± 0.02 @ 25ºC). The probes used include a VWR 662-1759 and an Orion PI10/S8 serial number 21054/001 with an Orion Research model 701A/digital Ionalyser meter, and a VWR 667-1761 probe with a Jenway 3051 pH meter. In some cases additional measurements were taken using pH strips from Alfa Aesar readable to 0.2 - 0.3 pH. Any quantitative analysis on pH data has been performed using the measurements made with a probe rather than a pH strip.

Particle size was measured using a Malvern Mastersizer X with a MS17 presentation unit and a 100 mm lens (which will detect particles between 0.5 and 180 µm). All samples were dispersed in demineralised water for analysis. The presentation unit settings were: pump at 50 %, stirrer at 50 % and ultrasonics at 10 % of maximum values. The optical properties in the selected presentation code (2QJD) were; refractive index of the particles of 1.7290, absorption index of 1.000 and refractive index of the medium of 1.3300. Microscopy images confirmed the presence of particles smaller than 0.5 µm, the use of a 45 mm lens would have allowed particles down to 0.1 µm to be viewed, this would however have not considered particles larger than 80 µm.

4.2.4 Zeta Potential

A Colloidal Dynamics Zetaprobe was used. The conductivity, electroacoustic spectral analysis (ESA) and pH probes were calibrated according to standard calibration procedure prior to carrying out the experiments. The ESA probe was

calibrated using a solution of potassium α-silicotungstate (KSiW). Potentiometric titrations were performed on each of the 3 boehmite powders with 1.0 M nitric acid, 1.0 M acetic acid and 1.0 M sodium hydroxide. Titrations were performed from the material's natural pH in demineralised water (from an Elga Purelab Option purifier) to pH 0.5 for the acidic titrations and pH 11 for the basic titration in increments of 0.5 pH. An equilibration time of 2 minutes was allowed for each measurement. A preliminary study was performed to confirm this as a suitable equilibration time. Dispersions containing ~1 wt% powder were prepared by weighing ~2.5 g accurately to 0.001 g using a Sartorious type 1425 balance into a glass 250 ml volumetric flask which was then filled with demineralised water from an Elga Purelab Option purifier. The sample was stirred at 250 rpm throughout the titration to prevent settling. The temperature was not controlled during the measurements, though temperature readings were recorded throughout.

4.2.5 Nuclear Magnetic Resonance

Samples have been prepared by milling on a Fritsch Planetary Micro Mill Pulverisette 7. Milling was performed for 30 minutes at speed setting 7 with 3 media present in each of the vessels. The internal dimensions of the mill pots were 40 mm x 50 mm and the media were spherical with a diameter of 15 mm. The pots and media were both Fritsch "Syalon", 90 % silicon nitride. Powder was weighed using a Mettler Toledo PR5002 Datarange balance located within a dust booth and liquids measured using 2.5, 5 or 10 ml plastic syringes from Beckton Dickinson. 6 g the boehmite G250 was charged to the mill pot (with the media already in place) followed by 14 ml of liquid, either demineralised water or 1.0 M nitric acid, producing samples

containing 30 wt % boehmite. Samples were dried at room temperature for 72 hours and crushed once dry.

NMR studies were performed by John Hanna and Gregory Rees of the Magnetic Resonance Group at Warwick University. Measurements were performed on a 600 MHz Chemagnetic magnet with a Bruker Avance II console and a Bruker MAS 4 mm probe with a spinning speed of 10 kHz. 3600 scans were completed per sample. Calibration was completed with 1.1 M aluminium nitrate (0.00 ppm) solution and the Magic Angle was confirmed with yttrium aluminium garnet. Later samples were doped with various amounts of MgO to dry them and hence quantitative aluminium comparison is not possible so all the peaks present have been normalised to 1 to allow for comparison.

The spectra were fitted using DMFIT to achieve a comparison and then simulated with pNMRsim and GSIM to check no anomalies or errors were gained when fitting. The agreement between all three programs suggest an accurate fit and the simulation confirmed this – errors have not been considered as this is an average fit of all the samples run.

4.2.6 Cryomicroscopy

Water-based and acidic slurries and pastes were prepared and viewed on the cryomicroscope. Slurries were prepared on a DAC 150 FVZ-K speed mixer, supplied by Synergy Devices Limited, manufactured by Hauschild. Samples were mixed for 15 minutes at a speed setting of 20. 45 mm x 48 mm plastic mill pots were used with three 15 mm Fritsch “Syalon” 90 % silicon nitride media.

Rheological characterization of samples prepared for cryomicrsocopy was performed on a TA Instruments AR2000 as described in Section 4.2.2.

Samples were frozen by immersing in liquid ethane and transferred to the microscope using the Baltec Cryo system. Observations were first made at –138 ºC, then the temperature was raised to –110 ºC prior to cutting the dome of the frozen sample using a baltec cryo-plane. Analysis was performed in the frozen condition, and then sublimated at 60 ºC for 10 – 20 minutes.

Samples were examined in a Zeiss ultra 55 field emission electron microscope equipped with in lens secondary electron and backscattered detectors. Two imaging modes were used: compositional analysis and low resolution general imaging, and high resolution low voltage imaging. Compositional analysis and low resolution general imaging was performed at an accelerating voltage of 10 – 20 kV, with a 30 micron aperture at a working distance of 7 – 8 mm using standard secondary electron and standard backscattered electron detectors. High resolution low voltage imaging was performed at an accelerating voltage of 3.6 kV, with a 20 – 30 µm aperture at a working distance of 2 – 3 mm using in-lens secondary electron and in-lens backscattered electron detectors.

4.3 Mixer Torque Rheometry

4.3.1 Description of Torque Rheometer Equipment

The instrument used as a torque rheometer was the Brabender Absorptometer ‘C’ with a Schott Titronic Universal Piston Burette (Model TZ 3160, systematic error 0.1 %, random error 0.05 %) were used along with a Julabo F34 temperature control

unit. Powder samples were weighed using an Ohaus ARD110 top pan balance accurate to 0.1 g.

The mixing chamber and paddles are shown in Figures 4.2, 4.3 and 4.4, the chamber has a capacity of 100 ml, with a chamber width of 70 mm and depth of 45 mm. There is no lid on the chamber allowing for expansion of material as mixing is performed. The mixing paddles are driven by a fixed ratio gearbox producing paddle rotations at a ratio of 2:1.

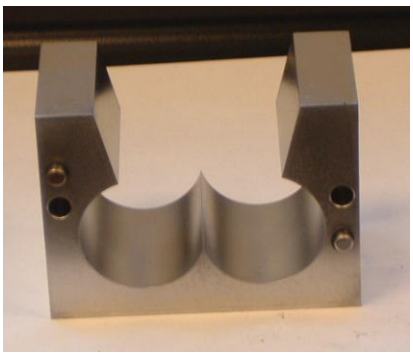

Figure 4.2: MTR sample chamber

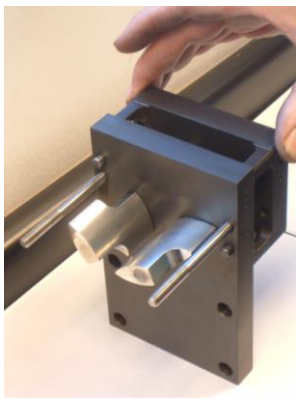

Figure 4.3: MTR mixing paddles and back plate

Figure 4.4: MTR mixing paddles, back plate and sample chamber

4.3.2 Taguchi Experimental Design

Taguchi orthogonal array factorial design was used to ascertain the relevance of parameters in the technique. The effect of five, two level factors on two outputs was assessed, these factors and the conditions of the levels can be seen in Table 4.1. The experiments were designed according to an L8 Taguchi matrix (shown in Table 4.2). Each experiment consisted of charging the mixing chamber with 20 g of the appropriate powder and adding the specified liquid at the required rate and temperature. The torque required to rotate the paddles at the specified rotation rate was measured. The matrix in Table 4.3 summarises the experimental conditions examined as a result of combining the parameters in Table 4.1 with the array in Table 4.2. A deficiency of the Taguchi experimental design method is that the interaction between two variables is not considered in the analysis, however it allows the effect of a large number of variables to be examined in a small number of experiments, allowing further experiments to be focussed on the most influential parameters.

Table 4.1: The 5, 2 level factors assessed by experimental design

Variable	Parameter	Units	Condition 1	Condition 2
1	Temperature	ºC	10	20
2	Paddle rotation rate	Rpm	50	150
3	Liquid addition rate	$ml.min^{-1}$	1	10
4	Powder type	n/a	Boehmite	Alpha alumina
5	Acid strength	M	0	1

Table 4.2: Variable conditions in Taguchi experimental matrix

Experiment Number	Variable Number						
	1	2	3	4	5	6	7
1	1	1	1	1	1	1	1
2	1	1	1	2	2	2	2
3	1	2	2	1	1	2	2
4	1	2	2	2	2	1	1
5	2	1	2	1	2	1	2
6	2	1	2	2	1	2	1
7	2	2	1	1	2	2	1
8	2	2	1	2	1	1	2

Table 4.3: Taguchi designed experiments

Experiment Number	Temperature	Paddle Rotation Rate	Liquid Addition Rate	Powder Type	Acid Strength
	ºC	Rpm	$ml.min^{-1}$		M
1	10	50	1	Boehmite	0
2	10	50	10	Alpha	0
3	10	150	1	Boehmite	1
4	10	150	10	Alpha	1
5	20	150	1	Alpha	0
6	20	150	10	Boehmite	0
7	20	50	1	Alpha	1
8	20	50	10	Boehmite	1

4.3.3 Test Type and Formulations

4.3.3.1 Multiple Addition Test

During the multiple addition test 20 g (± 0.01 g) of dry powder was charged to the mixing chamber and liquid added at a specified rate (4 $ml.min^{-1}$) to the chamber whilst recording the torque required to rotate the paddles through the powder at a rate of 125 rpm. The temperature was maintained at 20 ºC. The duration of the experiment varied, with the end point being determined when a peak mean torque had been observed and fallen to 50 % of the peak value.

A range of formulations has been examined using the multiple addition test described here, similar to those discussed and characterised by rotational rheometry presented in Chapter 6. Formulations included the combination of three boehmite

powders, (G250, V250 and Dequagel HP) with a variety of liquid phases; water, a variety of concentrations of nitric acid (0.36 M, 0.72 M and 1.0 M) and 1.0 M acetic acid. Repetitions of experiments was not possible due to equipment availability.

4.3.3.2 Variable Mixing Time Test

The variable mixing time test involves charging the mixing chamber with 20 g of the required powder and commencing paddle rotation to take background torque measurements. The specified amount of liquid phase (which varied in each experiment) was dosed to the mixing bowl at a rate of 99.9 $ml.min^{-1}$ using the Schott piston burette as described in Section 4.3.1, or by hand and the time at which the dose was added was recorded. The torque required to rotate the paddles at a rate of 125 rpm was measured for a period of time at 20 ºC. The time period varied for each experiment. The software would stop the experiment if a peak was observed in the torque magnitude and torque magnitude then reduced to only 50 % of the peak torque. Alternatively the operator could stop the experiment if the results showed visually that an equilibrium torque magnitude had been achieved.

The formulations selected for the variable mixing time tests were based on the results from the multiple addition tests. Four tests were performed on each of the 15 combinations of powder and liquid. A formulation exactly comparable to that at which the peak mean torque occurred in the multiple addition test, (i.e. at 100 % of the liquid content of the MAT peak mean torque), and three further formulations containing 90, 80 and 70 % of the liquid content of the MAT peak mean torque were measured. In each case the molar ratio of acid to boehmite was maintained at a value equal to that at the peak mean torque in the MAT, in order to minimise the number of variables across the experiments.

4.3.4 Densities of Powders

Poured and tapped bulk densities were measured using a plastic 250 ml volumetric measuring cylinder, with a diameter of 30 mm, and a Mettler Toledo PB8001 – L balance, accurate to 0.1 g. A measured mass of powder was poured into the cylinder and the volume recorded to calculate the poured bulk density. The cylinder containing the known mass of powder was tapped 2000 times on a Copley JV 2000, the volume measured and used to calculate the tapped bulk density. Additional experimental data confirmed that no significant further compaction occurred when tapped for a further 2000 taps. Density measurements made in this way are accurate to ± 0.5 gm^{-3}.

Skeletal density was measured using a Micromeritics AccuPyc 1330 helium pycnometer. Samples were prepared by drying at 115 ºC overnight prior to measurements being made.

4.3.5 Contact Angle Measurements

A Dataphysics Tensiometer with Dataphysics glass tubes with frit bottoms was used to measure the contact angle of water, 1.0 M nitric acid and 1.0 M acetic acid on each of the three boehmite powders of interest.

Figure 4.5: A Dataphysics Tensiometer

5 frit bottomed glass tubes, with a diameter of 10 mm were filled with the same, known mass of powder (± 0.01 g) measured using a Mettler Toledo XP205 balance. These were mounted on a device designed to allow all tubes to be tapped at the same time on a JBT tapping machine. The tubes were tapped 5000 times, examined and the volume of each tube recorded using the scale on the tubes. The tubes were then tapped a further 5000 times and the volume recorded. In the case of Dequagel HP the tubes were tapped a further 5000 times as adequate consistency of packing was not obtained with only two sets of taps. This is in disagreement with the consistent packing observed whilst performing tapped bulk

density tests, described previously in Section 4.3.4, this is believed to be due to the significant differences in the diameter of the tapping column and the difference in the significance edge effects on packing caused by this.

The packing consistency of each powder was assessed by characterising a full set of five tapped tubes with hexane as the test liquid. This also allowed calculation of a value containing the effective pore radius term of the Washburn equation (equation 2.10 in Section 2.3.5) as hexane is completely wetting (i.e. contact angle can be assumed to be 0 º) and the surface tension is known. By establishing the effective pore radius for a particular powder the contact angle with various liquids can be measured.

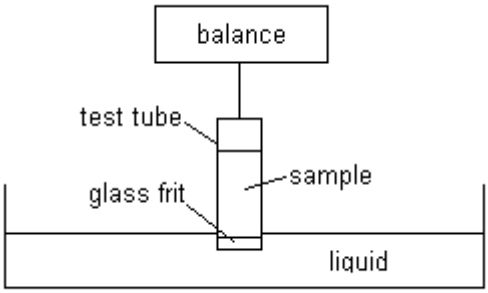

Figure 4.6: Schematic of tensiometer

Samples for subsequent tests with each of the liquids of interest were prepared using the same method of loading and tapping in sets of 5. The first 2 tubes were tested with hexane to ensure consistency of the term incorporating the effective pore radius. The further 3 tubes were tested with the liquid of interest. Calculations of contact angles were performed using the Dataphysics SCAT 32 software.

4.3.6 Reduction in Volume of Powders upon Liquid Addition

The reduction in powder volume upon the addition of liquid has been discussed previously in the Section 2.3.2 and is attributed to the capillary forces between the liquid and powder. Attempts have been made to quantify this phenomenon within each of the powders of interest, though these have been mainly unsuccessful with the equipment available. A qualitative analysis of the degree to which the phenomena occurs has been successfully performed on the powders. An equal volume of each powder was charged to a small glass vial. An equal volume of water was added to each of the vials and visual assessment made of the change in volume.

4.3.7 pH of Formulations in Capillary Saturation State

The nature of the MAT in the MTR does not allow for pH measurements to be made during the experiment. Each of the formulations at the MAT peak mean torque were reproduced using a Fritsch Planetary Micro Mill Pulverisette 7 as described in Section 4.2.1 at speed 7 with 3 media present for 15 minutes. This level of work input allowed the formulation to be pushed slightly past the capillary point into a thick slurry state allowing a pH measurement to be taken using a Jenway 3051 pH meter.

4.3.8 Effect of Particle Size Distribution on Torque Rheology Data

Some additional measurements were required when the Brabender Absorptometer was permanently unavailable. These measurements were performed on a Caleva Mark 1 MTR. This instrument is similar in design principle to the Brabender Absorptometer, though the mixing chamber is fitted with a lid causing containment of the sample, rather than allowing expansion. Additions and measurements are made in a discrete rather than continuous mode. 19 additions of 1.5 ml of liquid were made

with 2 minutes of mixing and 20 seconds of data logging between each addition. A Haake recirculating water bath, Type 001-0505, was used to maintain the mixing chamber temperature at 20 ºC for all experiments.

Comparison between the MAT of an 'as received' and milled powder sample was made in order to investigate the effect of particle size distribution. A Fritsch Planetary Micro Mill Pulverisette 7 as described in Section 4.2.1 at speed 7 with 3 media present was used to prepare the milled sample by dry milling 6 g in each pot for 15 minutes.

Particle size distribution was measured using a Malvern Mastersizer 2000 with a Hydro 2000g wet dispersion unit. Pump speed was 1250 rpm, stirrer speed 500 rpm and no ultrasonics were used in the dispersion unit. The optical properties in the selected operating procedure were; refractive index of the particles of 1.78, absorption index of 0.01 and refractive index of the medium of 1.33. Three measurements were performed on each sample with a 5 second delay between measurements.

4.4 Extrusion

4.4.1 Forming of Extrudates

In order to limit the number of uncontrolled variables pastes were prepared on a twin screw extruder and extruded using a ram extruder, allowing the study to focus on the effects of paste formulation rather than extrusion conditions.

An APV intermeshing co rotating twin screw extruder was used with a barrel diameter (d) of 19 mm, and length 40 d. The distance between the screw centres was 15 mm and the liquid feed port was 20.5 d from the die end. The barrel is

constructed of carbide coated stainless steel and the screws of nitron 60 stainless steel. The full length of the barrel is chilled using pressure hoses and a combination of mains water and chilled water from an Industrial Cooling Systems chiller unit. The length of barrel upstream of the liquid feed point is chilled with mains water and downstream of the liquid feed point with water supplied by the chiller unit. A Watson Marlow 505S peristaltic pump was used to supply the liquid feed. Initially a Brabender volumetric powder feeder with a twin screw and stirring agitator was used, which was replaced with a gravimetric feeder with the same configuration (Brabender Congrav S) to improve accuracy in later experiments. Table 5.1 shows which formulations were produced with which powder feeder. Both the liquid and powder feeders were calibrated with the appropriate materials prior to extrusion of each formulation.

Figure 4.7: The twin screw extruder

Table 4.4: Feeder type used for each formulation

Volumetric feeder	Gravimetric feeder
G250 and water	G250 and acetic acid
G250 and 0.36 M nitric acid	V250 and water
G250 and 0.72 M nitric acid	V250 and 0.36 M nitric acid
G250 and 1.0 M nitric acid	V250 and 0.72 M nitric acid
Dequagel HP and 0.72 M nitric acid	V250 and acetic acid
Dequagel HP and 1.0 M nitric acid	Dequagel HP and water
	Dequagel HP and 0.36 M nitric acid
	Dequagel HP and acetic acid

The screw configuration used can be seen in Figure 4.8. Each square indicates 1 screw diameter of the screw length (i.e. 19 mm). 'c' indicates a conveying section. A number denotes a mixing section with paddles staggered at the degrees indicated by the number, staggered in the forwards (f) direction.

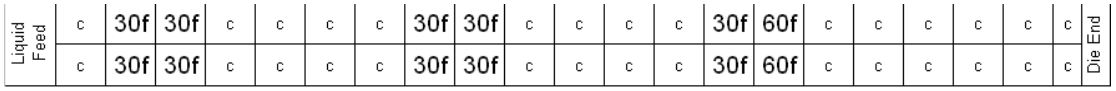

Figure 4.8: Screw configuration

The screw speed of the extruder was maintained at 125 rpm, (though this value had a tendency to drift between 120 and 130 rpm). During start up a wet formulation was extruded, ensuring low torques were maintained, the solids content of the formulation was then gradually increased by reducing the liquid flow rate resulting in an increase in torque. Solids content was increased until a paste with a suitable

consistency for extrusion was formed, (this was determined visually with previous experience of successful extrusion pastes).

As discussed in Section 3.4.4.2 the measurement and analysis of the residence time distribution of an extruder is non-trivial. An indication of residence time was made by implementing a step change to each process input and observing the time taken for the change to take effect at the die end. The residence time observed in this way at 100 rpm indicated that a change in any feed rate took full effect at the die end within 3 minutes. Based on this, an equilibration time of 5 minutes was allowed between changes made and sample collection.

Pastes were collected from the twin screw extruder in plastic bags and sealed to remain air tight until formed into extrudates using a ram extruder later the same day.

Extrudates were formed by ram extrusion on an Instron 5500r with an 85 hole, 1.2 mm trilobe die, with a land length of 12.7 mm. Internal barrel diameter was 35 mm and the length 250 mm though only ~100 mm of this length could be utilised on each extrusion run due to physical constraints of the equipment.

The paste was loaded into the barrel either by rolling into balls with a diameter slightly less than that of the barrel or by pouring through a funnel, depending on the consistency. Wetter pastes tended to be rolled and drier, granular feeds poured. The loaded barrel was then placed on the load frame, consistently at its maximum height to ensure repeatability across all samples. Extrusion was performed at a speed of 0.5 mms^{-1} until the barrel was almost empty. The force of extrusion was recorded when displacement from the initial position was 50 mm (extrusion tended to commence at a displacement of around 30 mm). Where possible three barrels of

each formulation were extruded allowing repeat measurements. The resulting extrudates were transferred to a drying tray gently by hand. The barrel and die were not cleaned between extrusions of the same formulation. When changing between a formulation the die was removed, the barrel, plunger and die washed in warm water, cooled in cold water and dried before being reassembled for extrusion of the next formulation.

Extrudates were dried and calcined in an oven with extraction capability. Prior to being placed in the oven the extrudates were left to air dry overnight in the lab. Drying was performed by ramping temperature to 110 ºC at a rate of 5 ºCmin^{-1}, holding at 110 ºC for 2 hours, then ramping at 5 ºCmin^{-1} to 550 ºC, holding for 2 hours and reduced back to 20 ºC at a natural cooling rate.

4.4.2 Characterisation of Extrudates

Crush strength measurements were performed on an Engineering Systems CT5, 0.5 tonne testing machine using a 50 kg load cell and 25 mm platens. Each extrudate length was measured using digital callipers. In some cases samples snapped rather than crushed, identifiable by a very low force and by visual inspection upon raising the platen. This was most likely due to curvature of the extrudates, this data has not been included in the quoted crush strength. Strength measured in this way is quoted as Nmm^{-1} rather than Nmm^{-2} as the second length dimension is ambiguous and varies for different catalyst support shapes, this unit for strength is standard within the catalyst industry.

Loss on attrition tests were performed using attrition tubes. Approximately 50 ml of extrudates were accurately weighed using a Mettler Toledo PR 5002 Datarange balance and placed in a stainless steel attrition tube with an internal diameter of 38

mm and length 250 mm. The tubes were tumbled at 60 rpm for 30 minutes on equipment designed in house. Fines below 1 mm were separated using a mesh sieve and weighed accurately to calculate the mass loss during the attrition test. Fines below 1 mm were also removed prior to the test commencing to ensure accurate measurement of the loss experienced. In some cases attrition testing was not considered practical as the extrudates were clumps rather than individual extrudates.

Nitrogen physisorption measurements were performed on Micromeritics ASAP 2420 and Micromeritics Tristar 3000 instruments using the ASTM method D 4222-83 using around 0.5 g of powder. The sample was initially outgassed using dry nitrogen at 140 ºC for a minimum of 1 hour before cooling to 77 K using dry nitrogen. The nitrogen adsorption desorption isotherm was measured between the relative pressures (P/P_0) 0.0035-0.95 and P_0 was measured at every point on the isotherm. The surface area was calculated by the Brunauer–Emmett–Teller (BET) method between pressures 0.05 and 0.2 using 5 data points. The pore size distribution is based on adsorption using the the Barrett, Joyner and Halenda (BJH) method, as desorption is complicated by network and percolation effects. The pore volume is taken at the final point on the isotherm which is typically 0.995 P/P_0. The average pore diameter is calculated from the BET area using the equation 4V/A where V is the pore volume and A is the BET area.

4.4.3 Particle Size Distribution Profile of Twin Screw Extruder

An intermeshing co-rotating twin screw extruder with chiller unit as described in Section 4.4.1 was used. The screw configuration was designed and altered to ascertain the effect of each type of configuration on the particle size distribution.

Extrusion was performed with the boehmite G250 and water. Configuration 6 was also profiled using the boehmite G250 and 1.0 M nitric acid.

Six screw configurations were designed, as seen in Figure 4.9. Each square indicates 1 screw diameter (19 mm) of the screw length, ‘c’ indicates a conveying section. A number indicates the degrees at which the paddles in a mixing section are staggered, either forwards or backwards, denoted by f or b respectively. Grey shading indicates a sample collection at the end of the screw element shaded. Particle size measurements were also made at the liquid feed point for configurations 1-5.

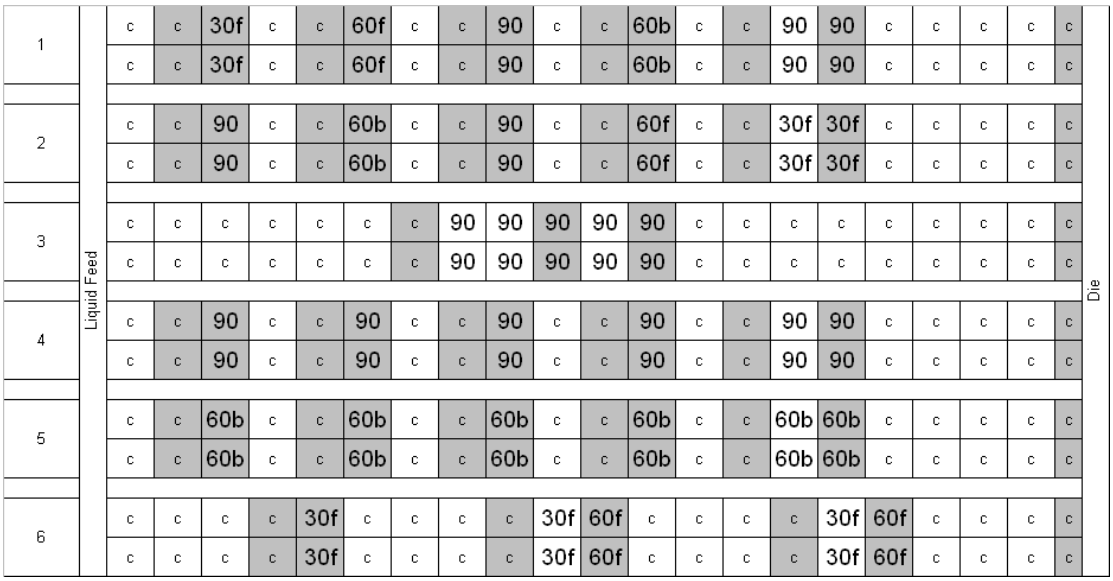

Figure 4.9: Screw configurations for particle size distribution profile

The combination of screw configurations 1 and 2 allowed assessment of the effect of each type of mixing section prior to and following each other type of mixing section, this would allow assessment of whether a less aggressive mixing element would have an effect at all if following a more aggressive mixing element. Screw configurations 3 and 4 only contain conveying elements and mixing sections with a

90° stagger. Comparison of the profiles of these two configurations would yield information about the comparative effectiveness of a number of short mixing section compared with one long mixing section. Configuration 5 is theoretically the most aggressive mixing configuration, containing a number of 60° backwards mixing elements. Screw configuration 6 is of historical interest within the company.

The operating conditions of the extruder during particle size distribution profile experiments is given in Table 4.5.

Table 4.5: Extruder operating conditions during particle size distribution profile experiments

Configuration Number	Throughput	Solids Content	Screw Speed
	$kghr^{-1}$	wt %	Rpm
1, 2, 3	4.49	51.5	153
4	4.89	53.4	188
5	4.79	54.5	184
6	4.89	53.4	160

Particle size distributions were measured using a Malvern Mastersizer 2000 with a Hydro 2000g wet dispersion unit. Pump speed 1250 rpm, stirrer speed 500 rpm and no ultrasonics were used in the dispersion unit. The optical properties in the selected operating procedure were; refractive index of the particles of 1.78, absorption index of 0.01 and refractive index of the medium of 1.33. Three

measurements were performed on each sample with a 5 second delay between measurements. Pastes from the die end were collected and air dried overnight in a fume cupboard and characterised by nitrogen physisorption on a Micromeretics ASAP 2420 and Micromeretics Tristar 3000 as described previously in Section 4.4.3.

Chapter 5 Material Properties

5.1 Particle Size and Shape

Significant discrepancies are observed in the size distributions reported by each of the analytical techniques employed.

The differences observed for the boehmites G250 and V250 (both spray dried powders) are similar, the results vary with the dispersion technique employed; when measured using wet dispersion a single peak at ~100 µm is observed, where as results obtained for both powders using both dry dispersion techniques indicate a particle size an order of magnitude smaller than this. This could be due to sample presentation by wet dispersion failing to achieve appropriate dispersion, or causing agglomeration of primary particles. Alternatively, dry dispersion may be causing the breakdown of particles.

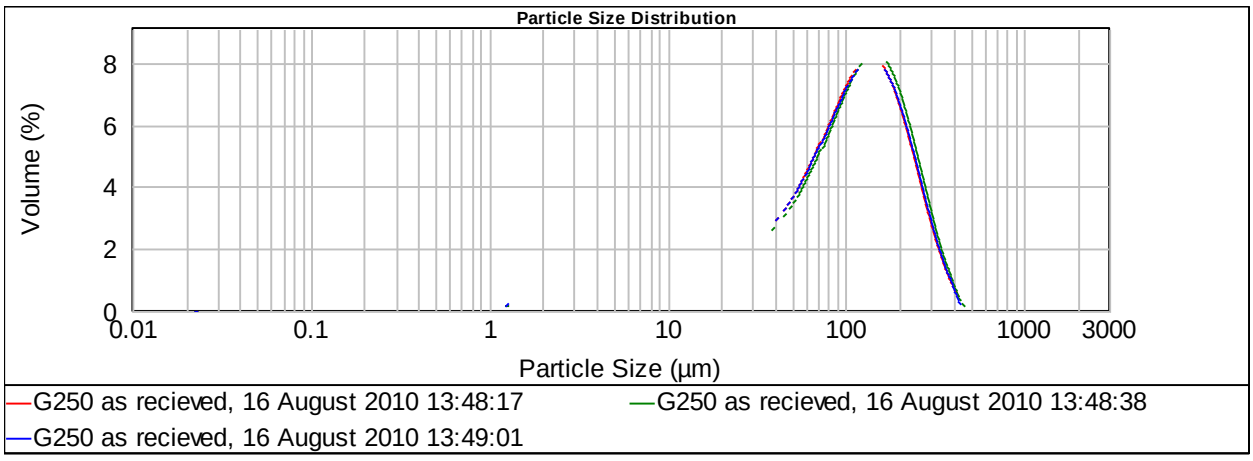

Figure 5.1: PSD of G250 using wet dispersion and Malvern Mastersizer

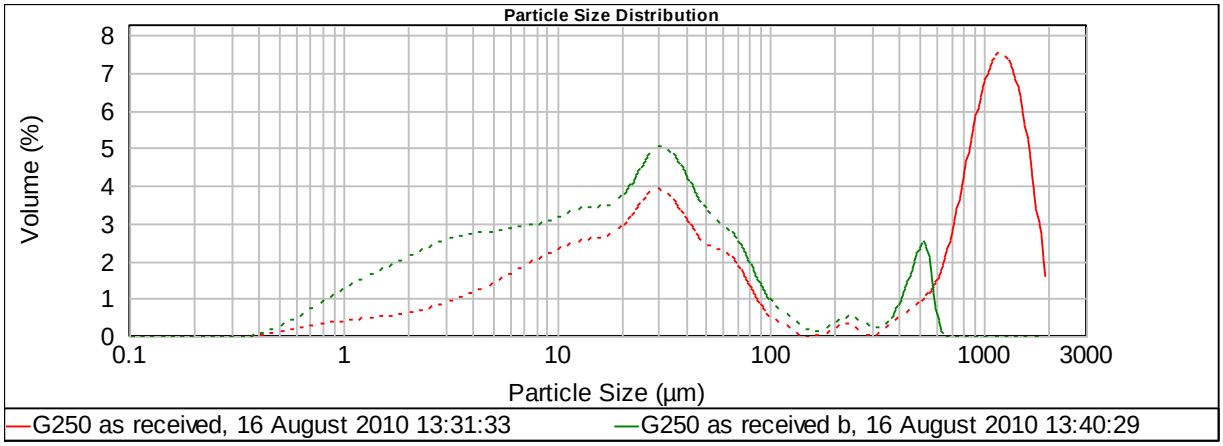

Figure 5.2: PSD of G250 using dry dispersion and Malvern Mastersizer

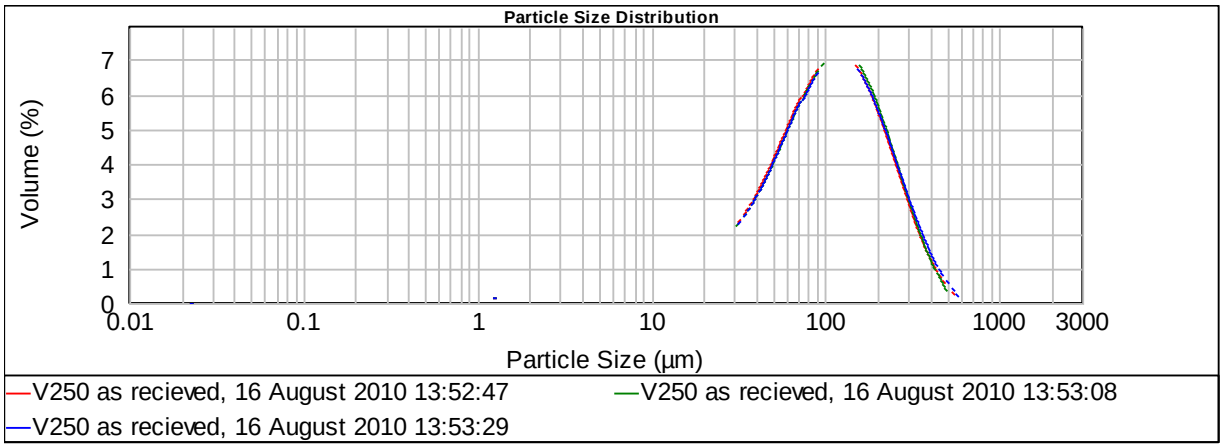

Figure 5.3: PSD of V250 using wet dispersion and Malvern Mastersizer

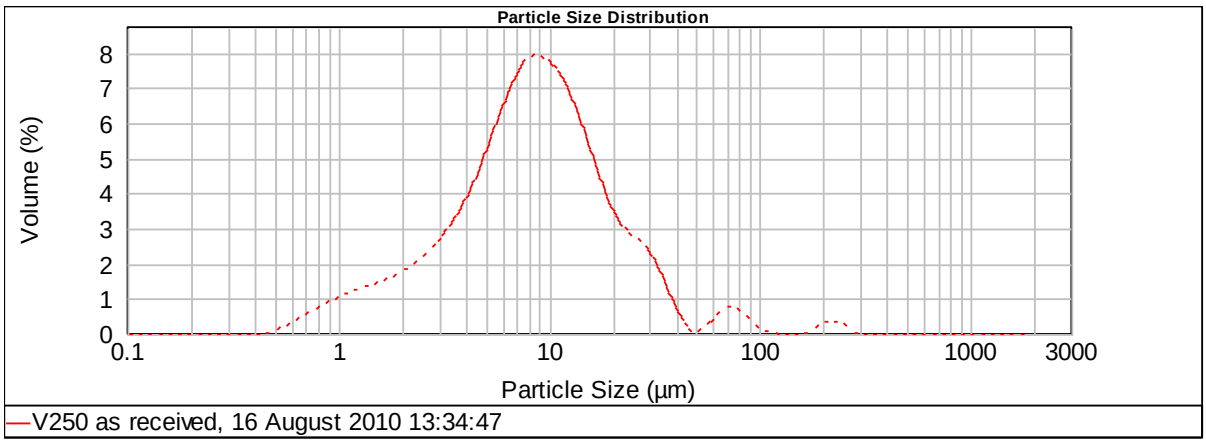

Figure 5.4: PSD of V250 using dry dispersion and Malvern Mastersizer

The discrepancies observed with the boehmite Dequagel HP appear to be linked to the measurement method rather than the dispersion technique. Results obtained on the Malvern using either dispersion technique display similar PSD's, a bimodal distribution with peaks in the same positions (at 3 and 300 µm) but differing in magnitudes, dry dispersion indicates a larger volume of the smaller particles is present. However, in the Sympatec only the larger peak is observed, with no evidence of particles below 10 µm, this is most likely due to a physical limitation of the technique, as the lens in the equipment is unable to observe particles below 5 µm.

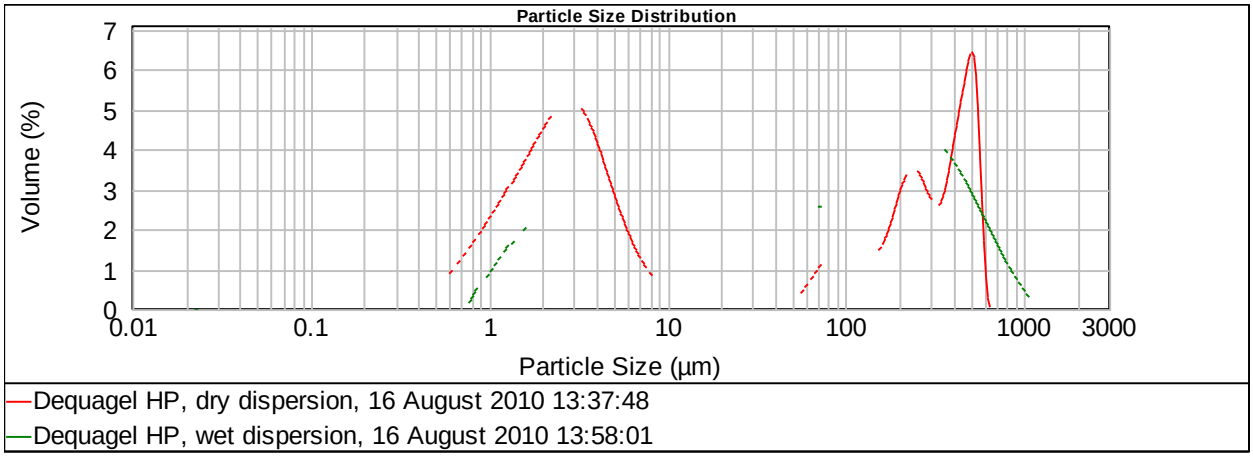

Figure 5.5: PSD of Dequagel HP using wet and dry dispersion and Malvern Mastersizer

Particle shape can be described by sphericity, circularity, roundness, or aspect ratio. Descriptions of these terms can be found in Bowman *et al.* (2000). Particle shape here has been described in terms of the aspect ratio, which is the ratio of the length of a particle to the width. A sphere or a cube would exhibit an aspect ratio of 1, the measurement does not take account of the shape of the surface, simply the characteristic lengths between surfaces. The results displayed in Figure 6.8 show each of the powders have similar aspect ratios, between 0.72 and 0.82 across the

size range of 20 – 200 µm. Limitations of the technique render measurements below 20 µm too unreliable to be considered for analysis. The boehmites G250 and V250 exhibit an increase in aspect ratio as the particle size increases within this size range, with G250 consistently displaying a higher aspect ratio. The aspect ratio of Dequagel HP reduces as size increases within this range. A wider range of aspect ratios is present in particles larger than 200 µm in all boehmite powders.

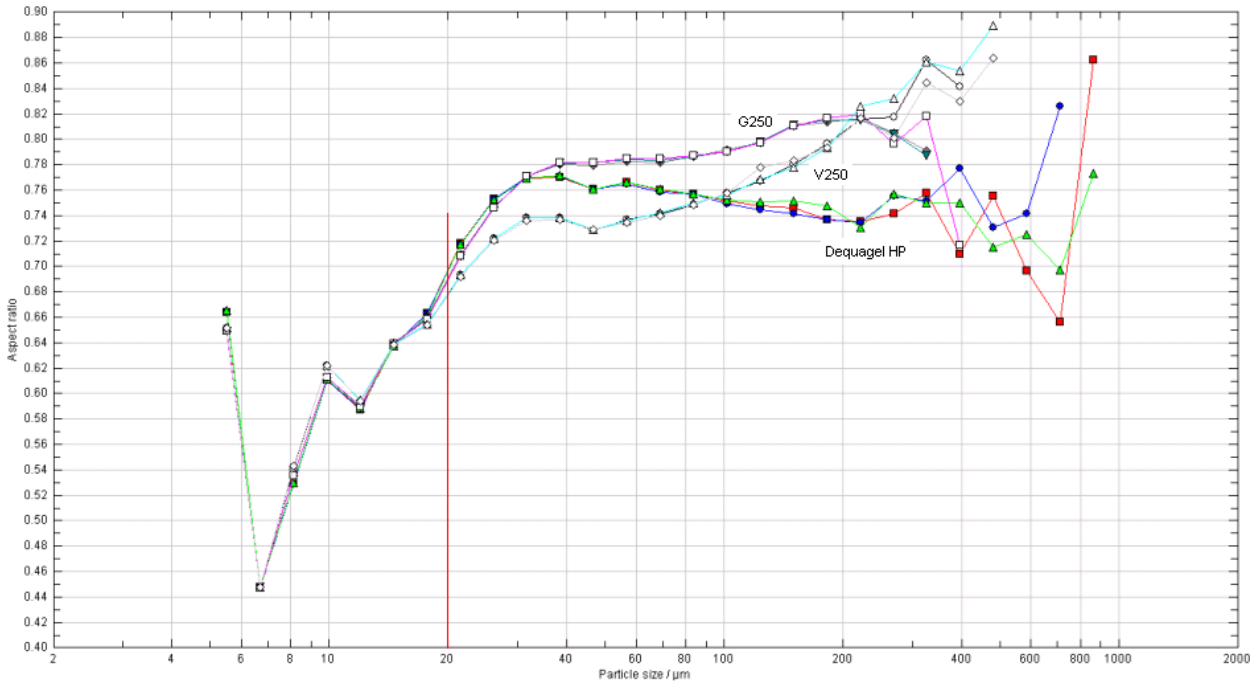

Figure 5.6: Aspect ratio of boehmite powders

5.2 Crystallite Size

Crystallite sizes of each of the boehmite powders, as measured by X-ray diffraction, are shown in Table 5.1. Note that all of the crystallite size, which is the size of the primary units forming the particle, are around 5 nm, which is discussed by Okada *et al.* (2002) as providing the highest specific surface area, therefore most suitable for catalytic applications. The effect of crystallite size on various properties of boehmite

has been discussed in Section 3.1, however, the size variation of less than 1 nm between these three powders is not considered large enough to have significant effects, when considered that the ranges investigated and reported in the literature discussed in Section 3.1 were generally larger than 20 nm.

Table 5.1: Crystallite size of boehmite powders measured by X-ray diffraction

	G250	V250	Dequagel HP
Crystallite size (nm)	4.7	5.1	5.6

X-ray diffraction inherently measures the shortest dimension of a crystal, given that boehmite is known to contain needle-shaped crystallites (Wefers and Misra, 1987). The use of transmission electron microscopy has not been suitable for measuring crystallite size of these materials as the vacuum conditions required for the sample presentation results in a phase transformation of boehmite to gamma alumina.

5.3 Dissolution Rate of Boehmite in Nitric Acid

The dissolution of boehmite results in the release of OH^- groups into solution, increasing the pH. Therefore the rate of acid addition required to maintain a constant pH indicates the rate at which boehmite powders dissolve at a given pH. The conductivity of the solutions increases steadily with the addition of acid, indicating the presence of more ions, as boehmite dissolves and releases Al^{3+} ions and OH^- ions, although the OH^- ions are neutralised by the addition of H^+ ions the Al^{3+} ions are still present and contributing to conductivity.

Figure 5.7 shows the volume of acid required to maintain a solution containing 10 wt% boehmite at pH 2. Initially the powders G250 and V250 show very similar behaviour, though beyond ~180 minutes V250 continues to dissolve at a faster rate than G250. The boehmite Dequagel HP dissolves initially at a faster rate than the other two boehmites and requires more acid to maintain pH 2 over the whole time period. The gradient of the curve suggests that further acid dissolution would have occurred had the experiment continued. This is in contrast to the results obtained for dissolution at pH 4, seen in Figure 5.8. The final gradient indicates that no further dissolution of boehmite is occurring. The initial rate of dissolution however is faster at pH 4 than at pH 2, which may be due to a mass transfer limitation at pH 2, this is supported by the increase in viscosity observed at pH 2, presented in Chapter 6.

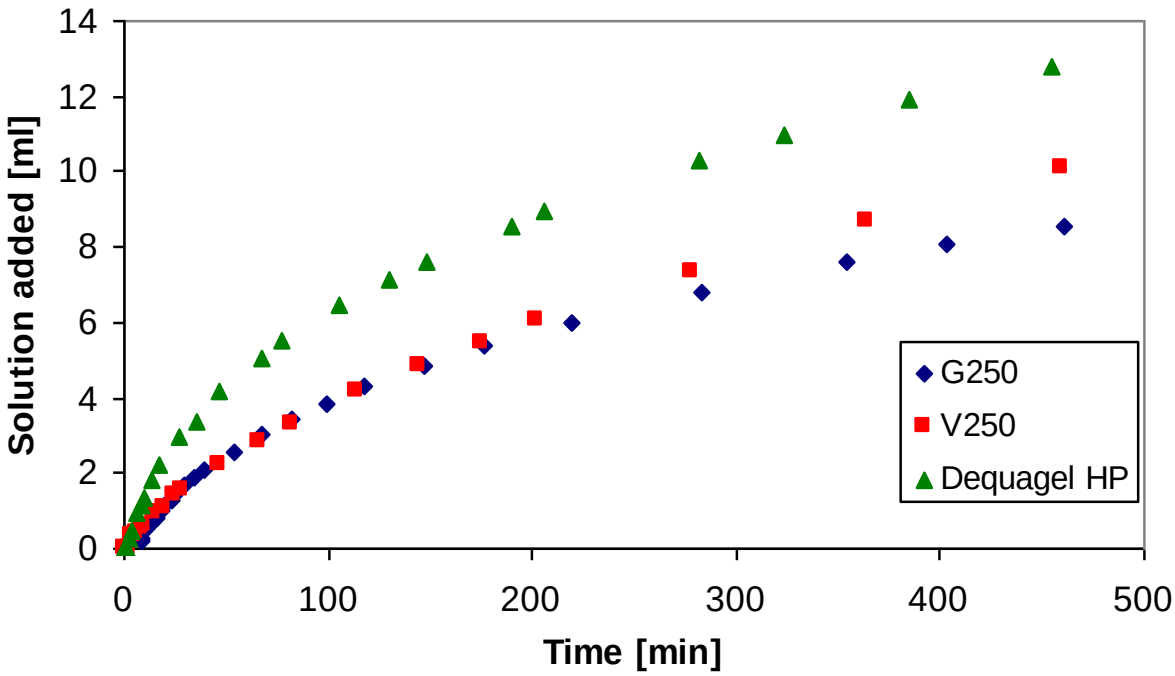

Figure 5.7 Dissolution rate of boehmite in nitric acid at pH 2

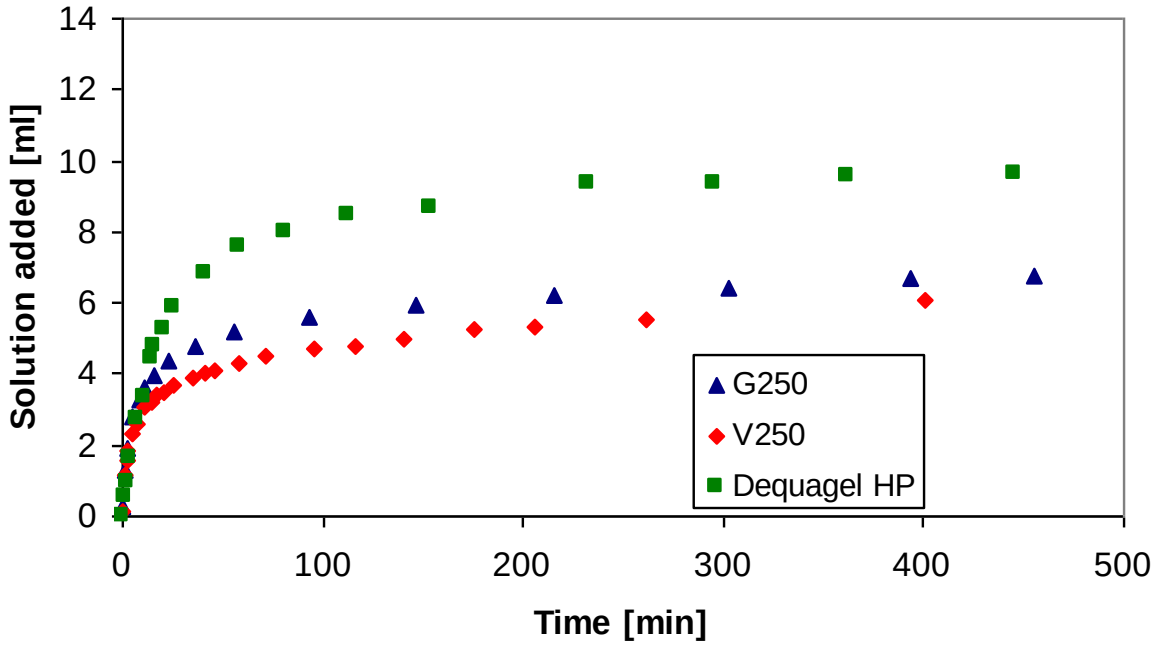

Figure 5.8: Dissolution rate of boehmite in nitric acid at pH 4

5.4 Acid Dispersibility

A well dispersed powder will contain a large portion of small particles which will remain stable in the supernatant during centrifuging. Figures 5.9 and 5.10 display the dispersibility of each boehmite powder, described by the percentage of the original mass of material present in the supernatant after centrifuging. These figures also contain data on the dispersibility implied by the shift in the solids content at the capillary point with pH exhibited on the MTR, discussed in Chapter 7. This value is quoted as the difference in the solids content at the capillary point measured on the MTR using water and 1.0 M acid, a large shift in this value implies significant acid dispersion. This simplified calculation assumes a linear relationship between pH and solids content at the MAT peak and ignores the variation in pH's between the

powders.

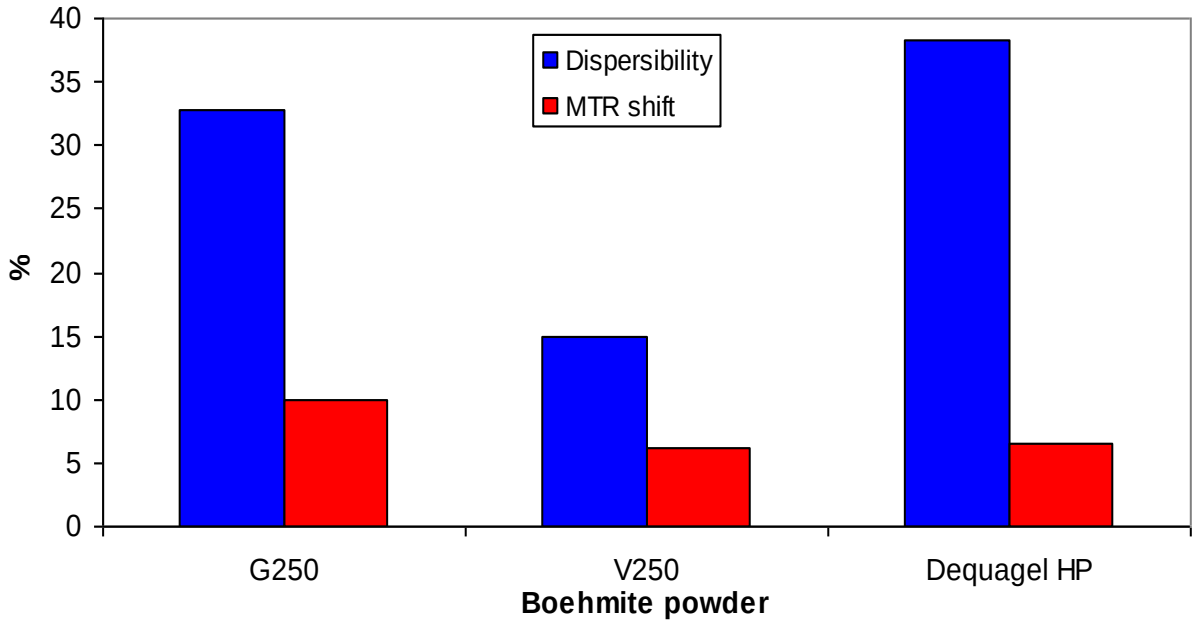

Figure 5.9: Dispersibility of boehmite with nitric acid

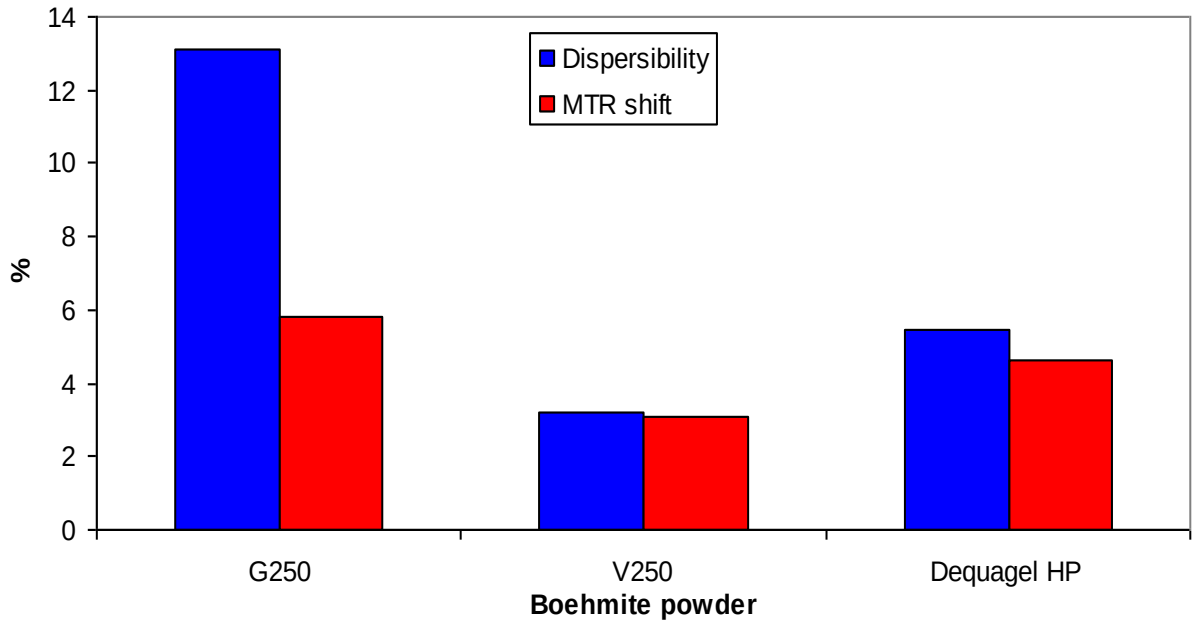

Figure 5.10: Dispersiblity of boehmite with acetic acid

According to the dispersibility test performed the boehmite Dequagel HP is the most readily dispersed with nitric acid and the boehmite G250 has a comparable degree of

dispersibility. The boehmite V250 is much less dispersible with nitric acid. Each of the boehmites are significantly less dispersible in acetic acid than nitric acid. The boehmite G250 is the most dispersible in acetic acid, with Dequagel HP and V250 displaying comparably low dispersiblity.

The dispersibility implied by the MTR results show that the boehmite G250 is the most readily dispersed by nitric acid, followed by the boehmite Dequagel HP, this is in contrast with the results of the dispersibility test. The MTR data implies the boehmite V250 to be the least dispersible in nitric acid, which is in agreement with the results of the dispersibility test.

The dispersibility of each powder in acetic acid measured by the dispersibility test and implied from MTR results show good agreement, with the boehmite G250 being the most dispersible, followed by Dequagel HP and V250 being the least dispersible.

5.5 Adsorption of Vapour by Boehmite Powders

Table 5.2 shows the rate of vapour adsorption by each boehmite powder. Boehmite G250 is capable of adsorbing the largest percentage of its own dry mass in water vapour and adsorption occurs at the fastest rate. The V250 powder has the lowest adsorption capacity but adsorbs at a high rate and Dequagel HP adsorbs at a slow rate compared to the other two powders but adsorbs more than V250. These results suggest that there are more open pores and less resistance to mass transfer in the G250 powder than the other two powders.

Table 5.2: Adsorption of vapour by boehmite powders

	G250	V250	Dequagel HP
mass gain (as % of dry mass)	42.2	37.2	40.5
Rate of mass uptake ($gmin^{-1}$)	$6.5x10^{-3}$	$5.0x10^{-3}$	$3.7x10^{-3}$

5.6 Conclusions

The particle size distribution measured for each powder varies with measurement technique and dispersion method. Boehmites G250 and V250 exhibit particle size distribution differences under different sample presentation methods and the boehmite Dequagel HP shows variations with the measurement technique. The sphericity of each of the powders, described by aspect ratio is similar, with aspect ratios between 0.72 and 0.82 for particles between 20 and 200 μm.

The crystallite size of each of the powders, measured by X ray diffraction vary by only 1 nm between all powders, This is insignificant compared to the ranges of crystallite sizes studied in the literature discussed in Section 3.1.

The boehmite Dequagel HP displayed a faster initial rate of dissolution in nitric acid at pH 2 than the boehmite powders G250 and V250, which displayed similar initial dissolution rates. All three boehmite powders display a very similar initial dissolution rate in nitric acid at pH 4. The dissolution rate at pH 4 is faster than at pH 2, which is thought to be due to a mass transfer limitation effect at pH 2, supported by the rheological changes observed and discussed previously in Chapter 6.

All boehmite powders have been shown to be more readily dispersed by nitric acid than acetic acid. The boehmite powder V250 is the least dispersible in both acids. The correlation between the dispersibility measured by the dispersibility test and the dispersibility implied by the magnitude of shift in the MTR capillary point strongly suggests that chemical dispersion is responsible for the observed shift.

Chapter 6: Identifying and Examining the Gelatinous Product of Peptisation

6.1 Rheological Characterisation

The Rheological Advantage Data Analysis software has been used to fit the experimental data obtained from samples milled for 1 minute to the Herschel Bulkley (HB) model, (equation 6.1).

$$\tau = \tau_0 + k\dot{\gamma}^n \quad \text{.....(equation 6.1)}$$

where τ is the measured stress, τ_0 is the yield stress, k is a constant relating to the viscosity, $\dot{\gamma}$ is the shear rate and n is the rate index.

The model has been fitted to the data obtained from the second increasing ramp in shear rate of each experimental set as calculation of a yield stress is more accurate from initiation rather than cessation of flow and the 1st increasing shear rate ramp tends to exhibit atypical behaviour due to material memory. Table 6.1 shows the standard error calculated in fitting the model, a reasonable fit is considered to be a standard error less than 20 (TA Instruments, 2010). Standard error, expressed as a percentage of the data range, is calculated by the software according to equation 6.2.

$$\frac{\sqrt{\frac{\sum\left(x_m - x_c\right)^2}{n-2}}}{range} \times 100 \quad \text{.....(equation 6.2)}$$

where, x_m is the measured value, x_c is the calculated value and n is the number of data points.

Many of the samples prepared exhibit a good fit to the HB model, indicated by the green data in Table 6.1, those not displaying a good fit to the model are indicated in red italic. The sample prepared with the boehmite V250 and water shows a particularly bad fit to the HB model, this sample however shows a reasonable fit to the Cross model, described in Section 2.2.2, with a standard error of 17.0. Similarly, the most acidic samples prepared with the boehmite V250 and nitric acid display poor fits to the HB model but good fits to the Cross model. Samples containing the boehmites G250 and Dequagel HP also exhibit a good fit to the HB model at lower acid contents (including samples prepared with water) and poor fits at the highest acid contents where the Cross model is a better description of the data. The standard errors based on fitting data to the Cross model can be seen in Table 6.5.

With a few exceptions, the HB model fits the data produced by the samples prepared with acetic acid. The sample prepared with the boehmite G250 showing a poor fit to the HB model also does not fit the Cross model. Examination of the data suggested that the poor fit may be due to anomalous behaviour at very low shear rates, however, altering the limits of the model fit to exclude data below 0.1 s^{-1} did not improve the accuracy of the fit. Similarly the samples prepared with the boehmite Dequagel HP and acetic acid that do not fit the HB model do not fit the Cross model, displaying standard errors of >50 in each case. No other rheological model has been found to fit these data sets.

The trend of poor fits of the HB model to the samples indicates the poor applicability of the model to chemically altered, or gelled, systems. The samples which do fit the Hershel Bulkley model can all be considered as classical colloidal suspensions. They all exhibit very low yield stresses (which can be approximated to 0 Pa in the majority of cases) and as such these materials could be adequately modelled by the power law model as described in Section 2.2.2. The apparent small yield stresses could be a due to the analysis being performed on the second shear rate ramp, the structure will have been broken down during the first shear rate ramp and may not have had sufficient time to rebuild prior to commencing the second ramp. Analysis has not been performed on the first shear rate ramp as this data consistently displays atypical behaviour. Some samples display an apparent negative yield stress, a physical impossibility; however these occur in samples which exhibit a poor fit to the model and as such can be ignored.

The viscosity term of the HB model describes the magnitude of the plastic viscosity, or the consistency. All samples which fit the HB model have viscosity constant values which approximate to 0, as do those which do not fit the model prepared with water or acetic acid.

The rate index term in the HB model describes deviation from Newtonian behaviour of a material. When the rate index is 1 the behaviour beyond the yield stress is Newtonian, and the material is effectively behaving according to the Bingham model. A value of < 1 describes a shear thinning material and $n > 1$ a shear thickening material. As such the samples are expected to have a rate index < 1, however, this is not the case. The majority of samples display a rate indec of 1, indicating Newtonian behaviour.

Table 6.1: Standard error in data fitting to Herschel Bulkley model

molar ratio of acid to boehmie	nitric acid			acetic acid		
	G250	V250	Dequagel HP	G250	V250	Dequagel HP
water	7	100	6	7	100	6
0.02	4	6	5	8	5	5
0.036	6					
0.048	9	4	10	50	5	20
0.06	2	4	3	6	5	30
0.072	4					
0.084	50	50	6	5	5	90
0.096	60					
0.1			100	7		5
0.13		200		10	5	6
0.25				10		7

Table 6.2: Yield stress (Pa) according to Herschel Bulkley model

molar ratio of acid to boehmie	nitric acid			acetic acid		
	G250	V250	Dequagel HP	G250	V250	Dequagel HP
water	0	100	0	0	100	0
0.02	0	0	0	0	0	0
0.036	0					
0.048	0	0	0	2	0	0
0.06	0	0	0	0	0	1
0.072	0					
0.084	-900	-40,000	0	0	0	2
0.096	400					
0.1			800,000	0		0
0.13		-2,000		0	0	0
0.25				0		0

Table 6.3: Viscosity constant, k, according to Herschel Bulkley model

molar ratio of acid to boehmie	nitric acid			acetic acid		
	G250	V250	Dequagel HP	G250	V250	Dequagel HP
water	0	0	0	0	0	0
0.02	0	0	0	0	0	0
0.036	0					
0.048	0	0	0	0	0	0
0.06	0	0	0	0	0	1
0.072	0					
0.084	900	40,000	0	0	0	0
0.096	100					
0.1			800,000	0		0
0.13		3,000		0	0	0
0.25				0		0

Table 6.4: Rate index according to Herschel Bulkley model

molar ratio of acid to boehmie	nitric acid			acetic acid		
	G250	V250	Dequagel HP	G250	V250	Dequagel HP
water	1	1	1	1	1	1
0.02	1	1	1	1	1	1
0.036	2					
0.048	1	1	1	1	1	1
0.06	1	1	1	1	1	1
0.072	1					
0.084	0	0	1	1	1	1
0.096	-1000					
0.1			0	1		1
0.13		0		1	1	1
0.25				1		1

Table 6.5: Standard error in data fitting to Cross model

molar ratio of acid to boehmie	nitric acid			acetic acid		
	G250	V250	Dequagel HP	G250	V250	Dequagel HP
water	~	17	~	~	17	~
0.02	~	~	~	~	~	~
0.036	~					
0.048	~	~	~	78	~	>50
0.06	~	~	~	~	~	>50
0.072	~					
0.084	15	~	~	~	~	>50
0.096	2					
0.1			9	~		~
0.13		17		~	~	~
0.25				~		~

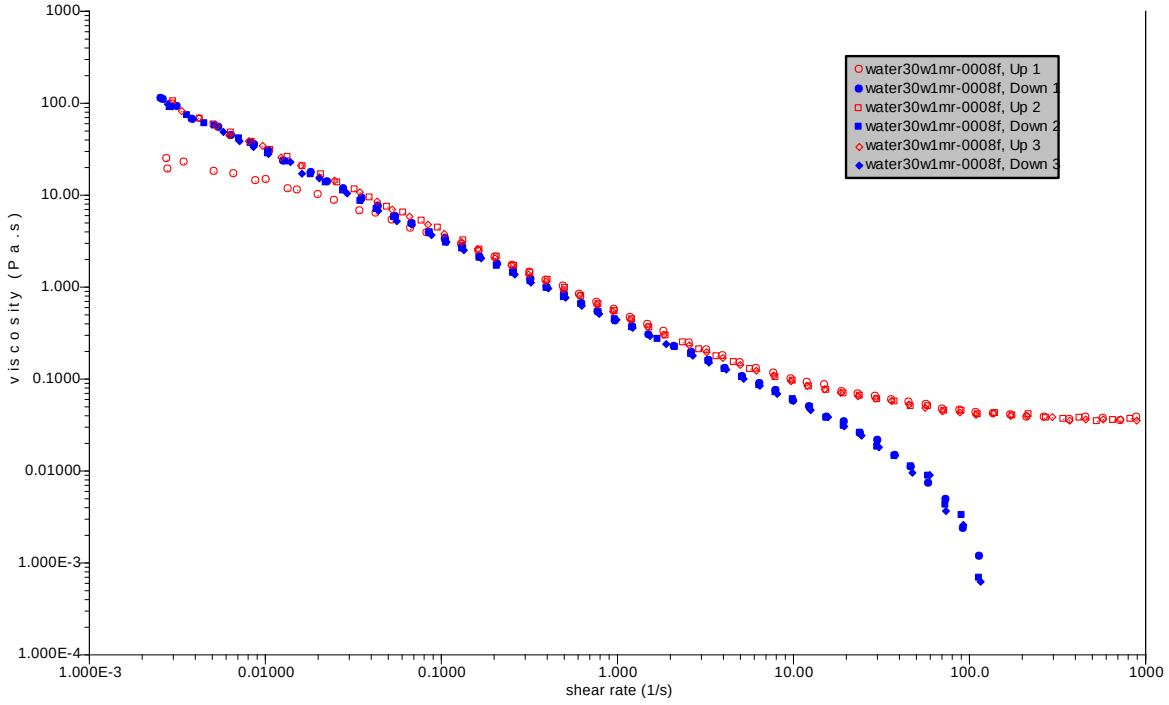

Figure 6.1: Example of a flow curve showing a good fit to the Hershel Bulkley model. Sample prepared with boehmite G250 and water

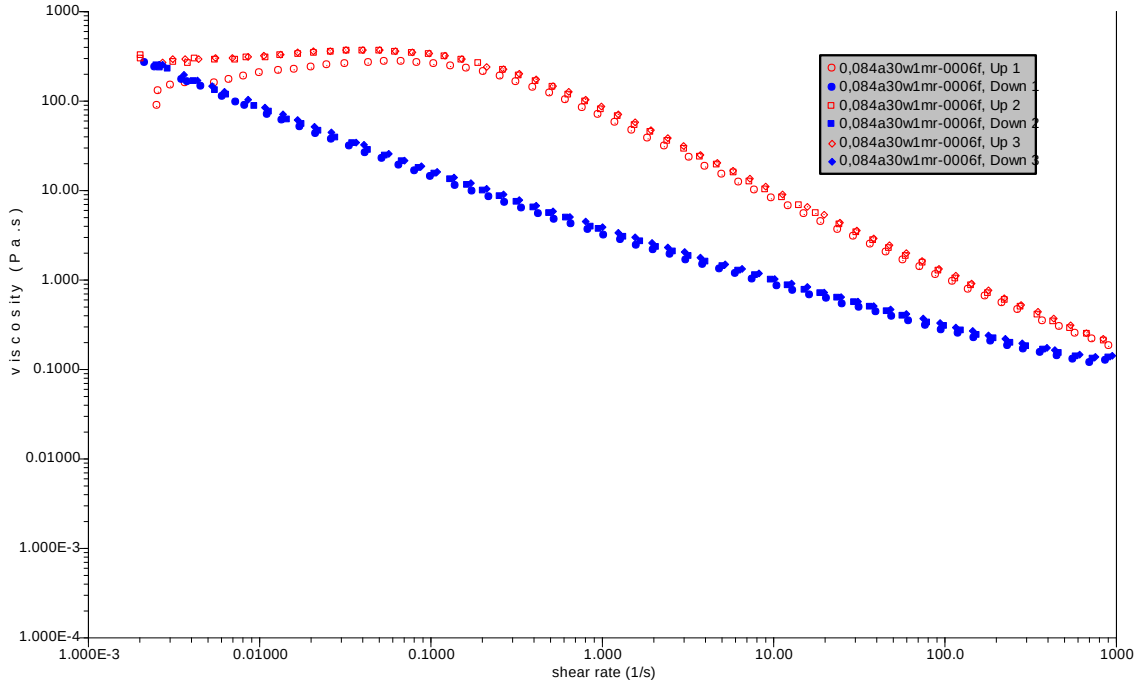

Figure 6.2: Example of a flow curve showing a bad fit to the Herschel Bulkley model. Sample prepared with boehmite G250 and 0.084 moles of acid per mole of boehmite

Figure 6.1 and 6.2 show typical flow curves produced by samples which show a good fit and a bad fit to the Herschel Bulkley model respectively. In Figure 6.1 there is consistency between the increasing and decreasing shear rate ramps at low shear rates, with the exception of the first up ramp which displays a slightly lower viscosity at low shear rates. It is normal for the initial up ramp to display slightly anomalous behaviour. At high shear rates there is evidence of a degree of slip occurring, suggested by the hysteresis between the up and down ramps. The shape of the curve indicates that the slip does not occur as the shear rate is increased; these curves consistently show a progression towards Newtonian behaviour at high shear rates. As the shear is reduced a sudden reduction is observed in the viscosity, implying the material has slipped against the geometry or plate. The red curves showing the increasing shear rate ramp in Figure 6.2 show shear thinning behaviour at high shear rates and a consistent viscosity at lower shear rates. This sample

displays a significant and consistent hysteresis between the increasing and decreasing shear rate ramps.

Due to the issues and inconsistencies of the application of rheological models to the range of data obtained an alternative method quantifying yield stress and apparent viscosity has been used to allow analysis of the trends in behaviour. As discussed previously in Sections 2.2.3 and 3.2.1 there are issues surrounding the accurate measurement of a yield stress value, the 'yield stress' has been quoted as the stress at which the shear rate is 0.1 s^{-1} indicating a certain amount of movement is occurring within the sample. The viscosity discussed is the apparent viscosity at 1000 s^{-1}, quoted as the average viscosity from the shear rate hold performed at 1000 s^{-1} for 3 or 5 minutes. It is possible that measuring the apparent viscosity at such a high shear rate may have broken down any existing material structure, however, the use of a high shear rate can minimize the effects of wall slip (Ekere *et al.*, 2001).

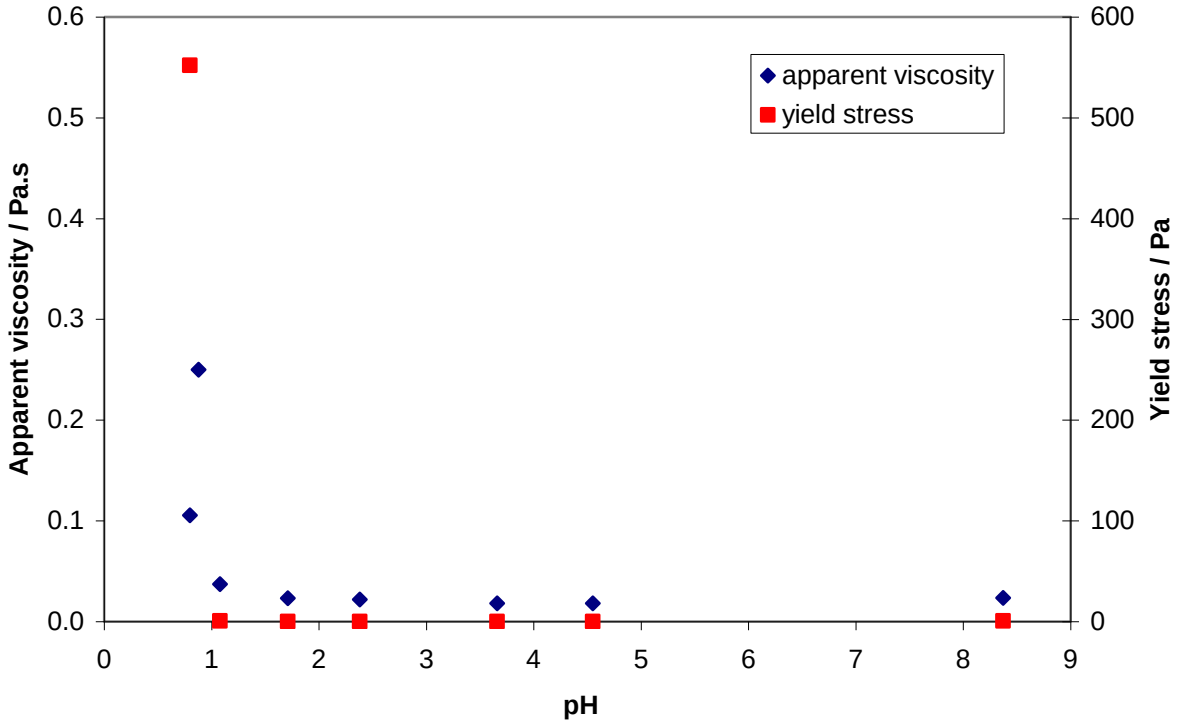

Figure 6.3: G250 and nitric acid, 1 minute mix

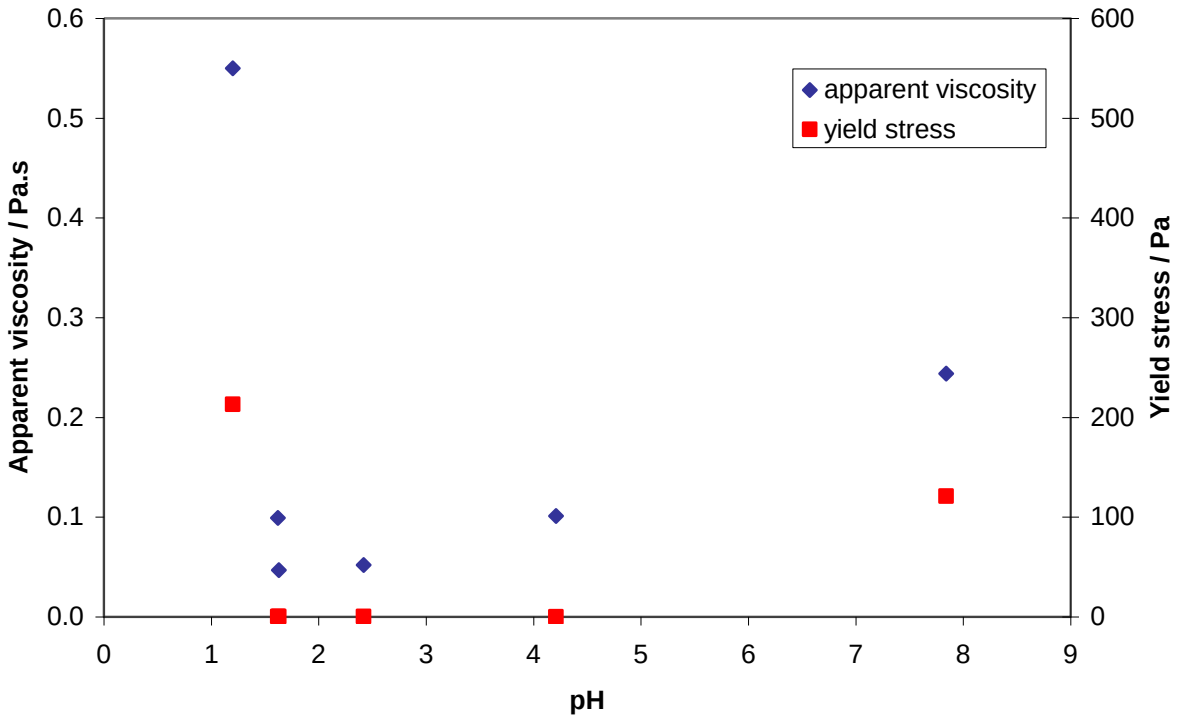

Figure 6.4: V250 and nitric acid, 1 minute mix

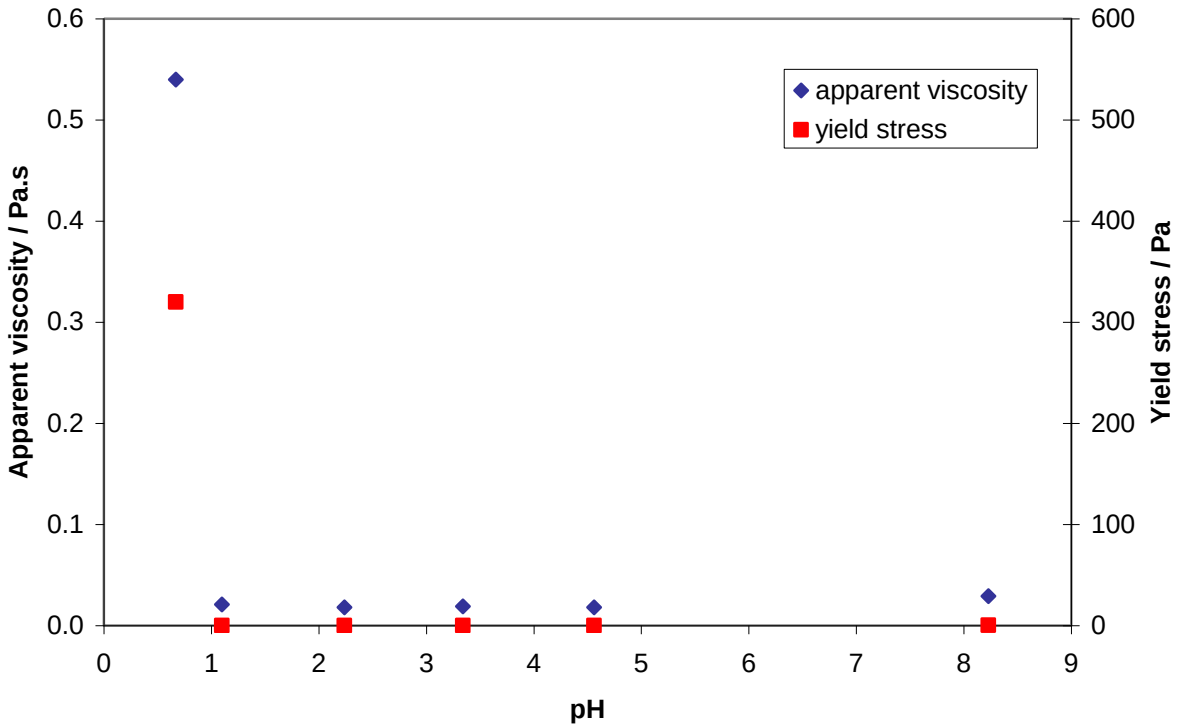

Figure 6.5: Dequagel HP and nitric acid, 1 minute mix

The variation of apparent viscosity at 1000 s^{-1} with nitric acid content is similar for all three boehmite powders studied. In water the pH is ~8, a small addition of acid (0.02 moles of acid per mole of boehmite) results in a significant decrease in the pH with minimal alteration to the rheological properties, particularly for samples prepared with boehmite G250 and Dequagel HP, though boehmite V250 exhibits a most significant alteration of rheological properties. This is due to the dispersive effect of acid on boehmite which is examined and discussed previously in Chapter 5. Further addition of acid, reducing pH below 2, results in an increase in both apparent viscosity and yield stress of the materials. Both the increase in yield stress and apparent viscosity at 1000 s^{-1} with nitric acid content indicate the existence of a microstructure which is present at both high and low shear rates in strongly acidic conditions. Boehmites V250 and Dequagel HP both display more of an increase in

apparent viscosity at 1000 s^{-1} than in yield stress, where as the yield stress of the acidic G250 sample increases more than the apparent viscosity at 1000 s^{-1}.

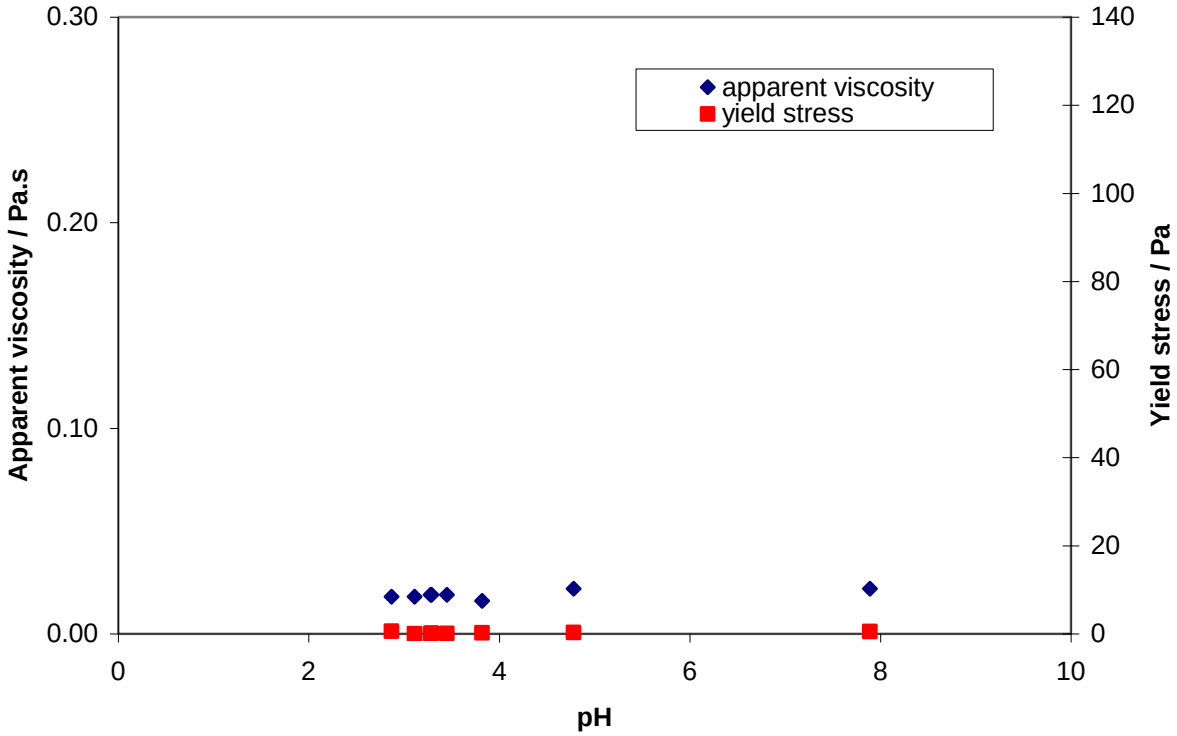

Figure 6.6: G250 and acetic acid, 1 minute mix

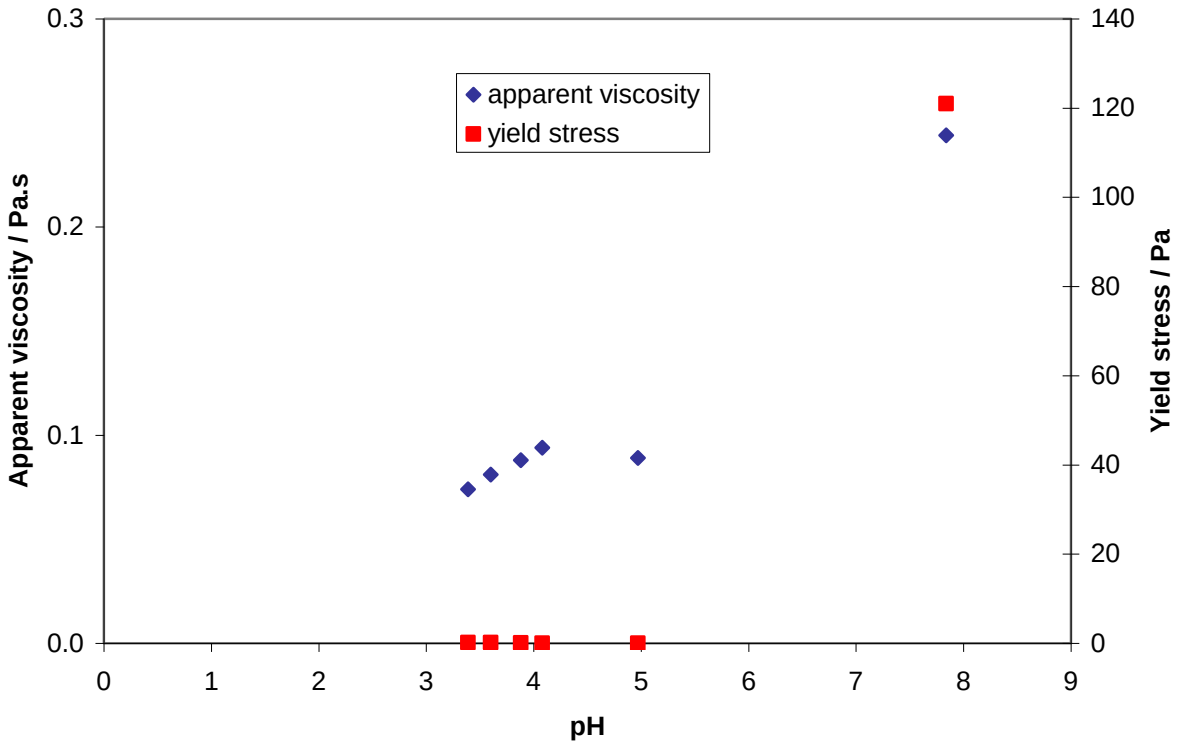

Figure 6.7: V250 and acetic acid, 1 minute mix

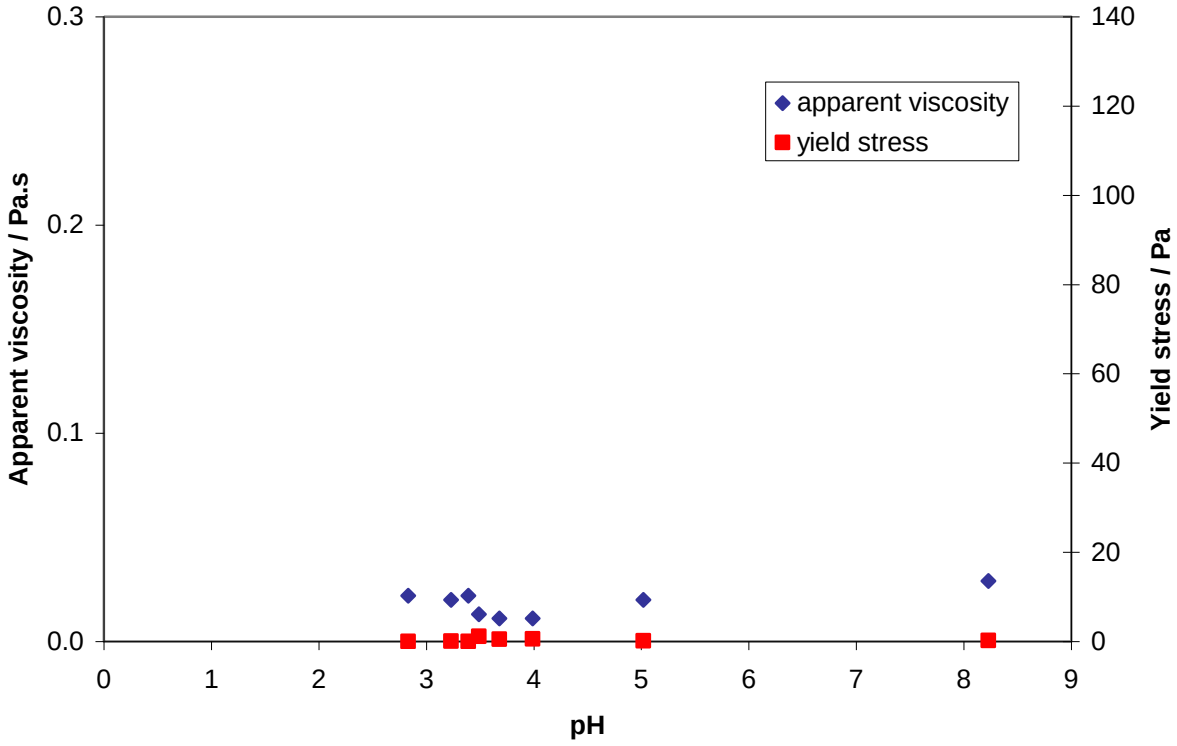

Figure 6.8: Dequagel HP and acetic acid, 1 minute mix

The results observed with acetic acid differ from those observed with nitric acid. Initial addition of 0.02 moles of acid per mole of boehmite results in a significant reduction in pH, however, with further additions of up to 0.13 moles of boehmite the pH reduces in only very small increments due to the weak nature of acetic acid. No increase in apparent viscosity or yield stress is observed at the lowest pHs, as a low enough pH has not been reached for any transitional chemistry to occur. It is not certain whether the change in rheological properties observed with nitric acid would be observed with acetic acid if the pH of the slurry could be reduced sufficiently.

6.2 Surface Chemistry Effects

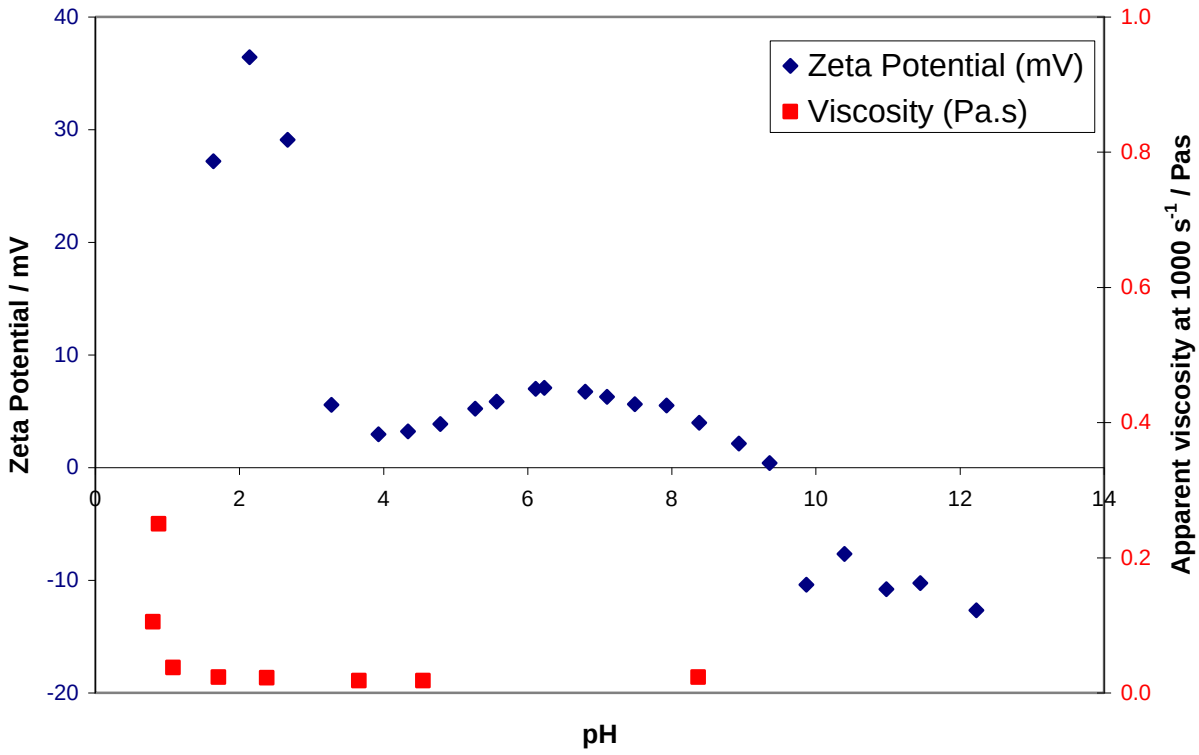

Figure 6.9: Zeta potential and rheology of boehmite G250 (milled 1 minute)

It is evident from the data presented in Figure 6.9 that the expected correlation between zeta potential and apparent viscosity at 1000 s^{-1} is not observed, as the apparent viscosity increases under conditions at which the surface chemistry implies

a more stable suspension. This data indicates that observed rheological changes of boehmite slurries at acidic pHs are not a result of surface charge effects.

The boehmites have produced zeta potential curves with an interesting shape shown in Figure 6.10. Only one data set has been collected for each powder at basic pHs using sodium hydroxide (shown with block symbols), where as titrations were performed with both nitric and acetic acid to acidic pHs (shown with open and block symbols respectively). Each titration was performed starting with the boehmite dispersed in demineralised water and titrating in one direction, slight variations in the pH of the demineralised water has resulted in a gap in the data at around pH 6-7. At basic pHs the materials display typical behaviour, and all exhibit similar isoelectric points, shown in Table 6.6. The pH of each of the boehmites in water is similar (between 6.5 and 7.5), though their zeta potential at this condition varies, with G250 and V250 both exhibiting a low zeta potential indicating an unstable suspension whilst Dequagel HP has a high zeta potential. As the pH reduces from 7 to 4 (using either nitric or acetic acid) the behaviour becomes atypical as zeta potential reduces. In all cases the zeta potential reaches a minimum at ~ pH 4 and rises to a zeta potential indicating a stable suspension below ~ pH 2.

Table 6.6: Isoelectric points of boehmites

Powder	G250	V250	Dequagel HP
pH of i.e.p	9.5	10.0	9.7

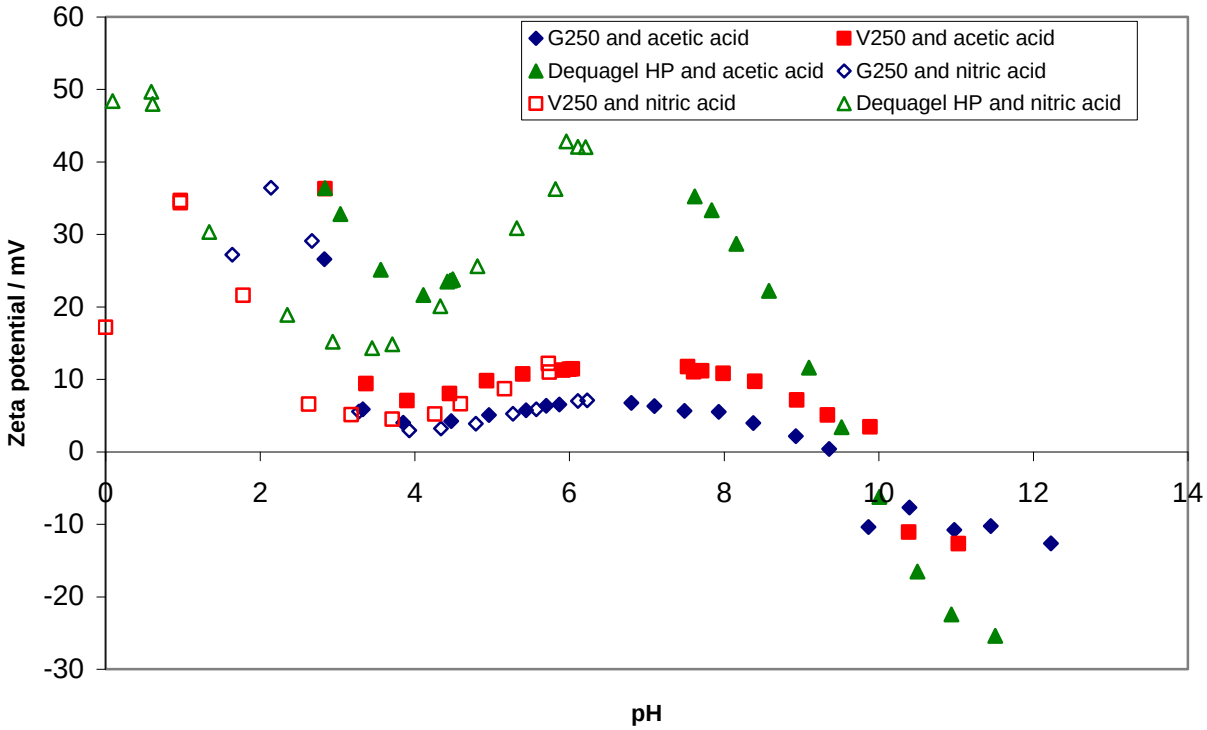

Figure 6.10: Zeta potential of boehmites

The anomalous behaviour of the zeta potential between pH 3 and 7 can be rationalised by the occurrence of dissolution - adsorption chemistry such as that expected in the gelation of boehmite by acid. The proposed mechanism is that at weakly acidic pHs the surface dissolves into the solution, reducing the positive charge on the surface. As the concentration of ions in solution increases they form polymeric cationic species which can readsorb onto the surface resulting in an increase in the positive charge at the surface. Compression of the double layer in highly concentrated ionic solutions will exacerbate the extent of this effect as the apparent charge on the surface appears reduced under these conditions. The conductivity of each solution increases sharply below pH 2 when the titration was performed with nitric acid and below pH 4 when the titration was performed with

acetic acid. The increase in conductivity indicates the presence of free ions in the solution.

6.3 Particle Packing Effects

There is no significant change in mean particle size or particle size distribution with pH, seen in Figures 6.14 - 6.16. A direct examination of the relationship between rheological parameters and particle size for each of the 6 systems under investigation has revealed that there is no strong correlation between these parameters and therefore particle size is not responsible for the observed rheological changes in acidic samples.

6.4 Rate of pH Change

The initial rate of reaction between boehmite and nitric acid has been calculated by considering the change in pH between samples milled for 1 and 4 minutes. In all cases it can be considered that boehmite is in excess. The rates calculated by this method have low accuracy due to the time taken for measurements to be made (loading and unloading sample from the mill) combined with the inherent issues associated with measuring the pH of a concentrated suspension.

Results displayed in Figure 6.11 confirm that a faster rate of consumption of nitric acid occurs at higher initial acid contents. All 3 boehmite powders display similar rates of acid consumption under these preparation conditions up to an initial acid content of ~ 0.08 moles of acid per mole of boehmite at which point the boehmite G250 exhibits a significant increase in the rate of consumption. Note that this coincides with the initial acid content at which significant variation in the rheological behaviour of concentrated suspensions prepared with this boehmite are observed.

The boehmite V250 also exhibits a significant rate increase at an initial acid content of 0.13 moles of acid per mole of boehmite, though the boehmite Dequagel HP consumes at a consistently low rate.

The rate of consumption of acetic acid is extremely slow when compared with those of nitric acid, though there is a clear increase in rate with initial acid contents. In this case all powders display very similar reaction rates.

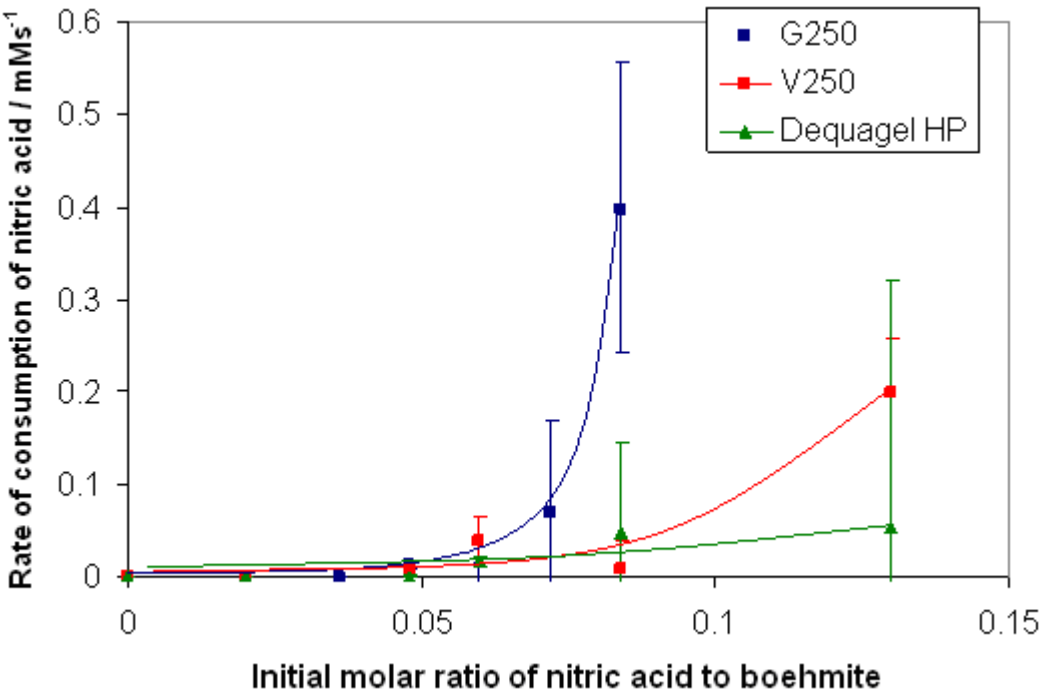

Figure 6.11: Rate of consumption of nitric acid by boehmite

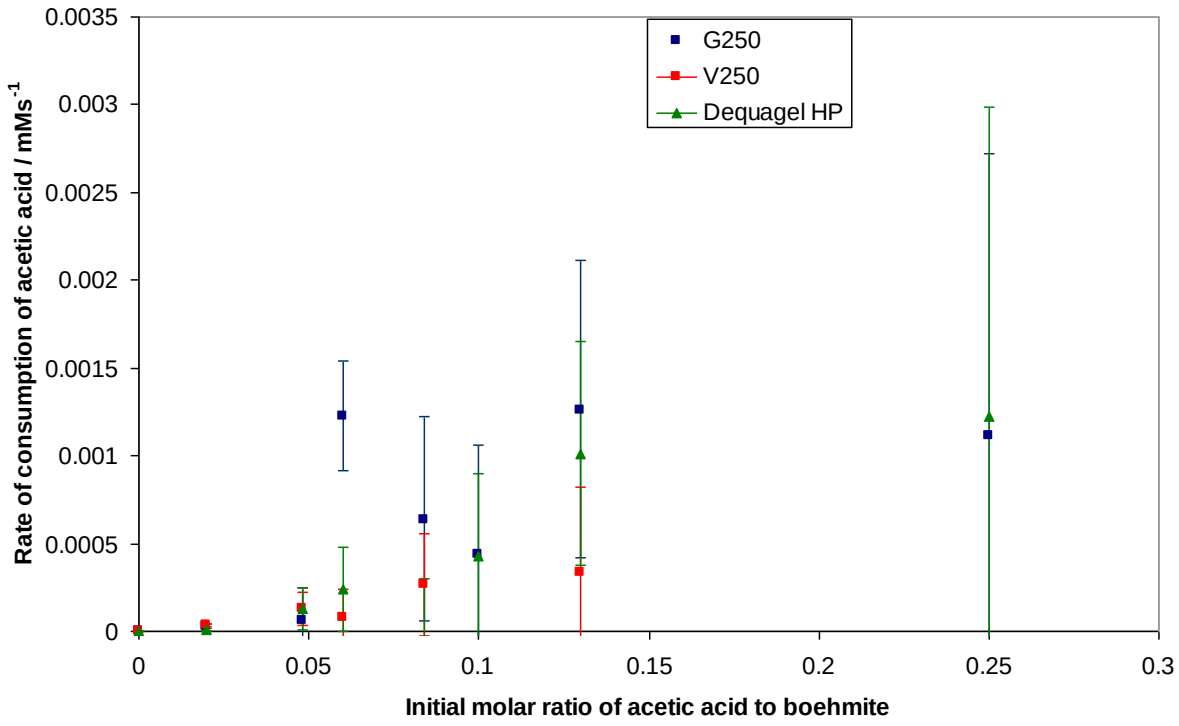

Figure 6.12: Rate of consumption of acetic acid by boehmite

The pH data collected for the boehmite G250 prepared with nitric acid has been fitted to the first order kinetic model (equation 6.3). It was found that the model fits well for samples with an initial acid content of above 0.06 moles of acid per mole of boehmite.

$$rate = k_1[H^+] \quad \text{.....(equation 6.3)}$$

where k_1 is the rate constant and $[H+]$ is the concentration of hydrogen ions. A second order model fit (equation 6.4) was also attempted, though with the exception of one formulation the first order model was found to be a better fit, this data is shown in Figure 6.13 and Table 6.7.

$$rate = k_2[H^+]^2 \quad \text{.....(equation 6.4)}$$

where k_2 is the rate constant and $[H+]$ is the concentration of hydrogen ions. This indicates that the rate of consumption of acid is first order with respect to the concentration of acid present, at least in cases where initial acid content is at least 0.06 moles of acid per mole of boehmite. In formulations containing less acid than this an additional phenomena such as mass transfer limitations may be contributing to the observed rate of consumption. The observed differences in rates may simply be due to whether or not the acid is present in excess.

Similar model fitting was not feasible with the other powders and acetic acid as pH measurements at 1, 4, and 30 minutes result in a consistently high value of r^2, simply due to the clustered nature of the data.

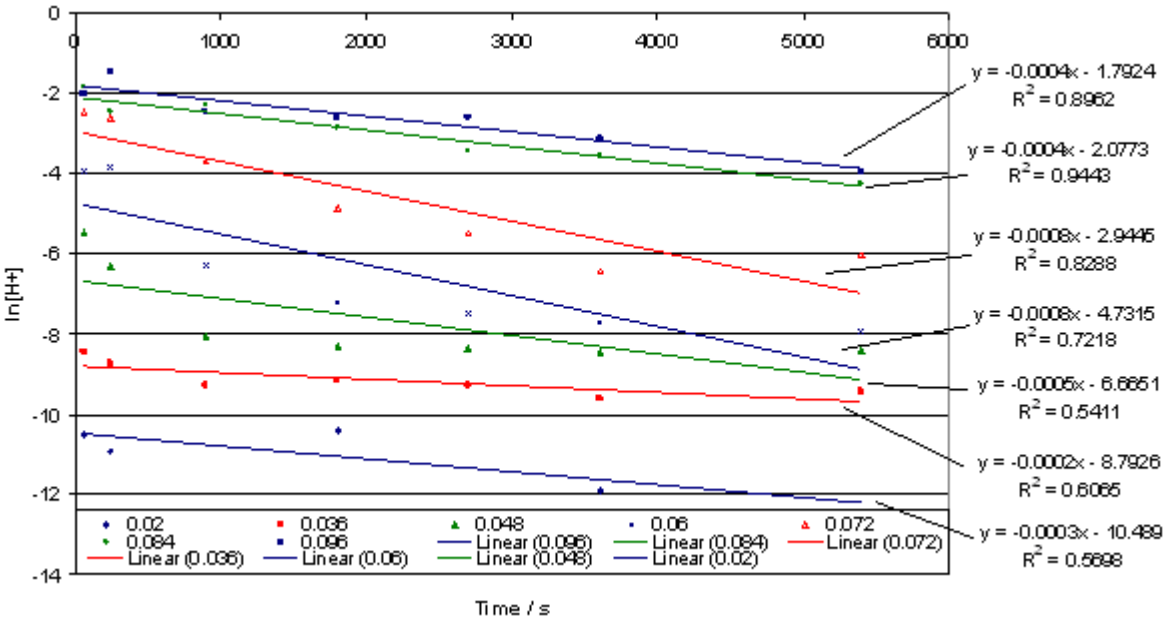

Figure 6.13: Fitting pH data for G250 and nitric acid to first order kinetic model

Table 6.7: Fitting pH data for G250 and nitric acid to first and second order kinetic models

Molar ratio of acid to	r^2 first order kinetics	r^2 second order kinetics
0.036	*0.53*	0.57
0.048	*0.45*	0.60
0.060	*0.69*	0.97
0.072	0.99	0.82
0.084	0.97	0.95
0.096	0.94	0.82

6.5 Effect of Increasing Milling Time

The most comprehensive study of the effect of mixing time on rheological properties has been performed on the boehmite G250 with nitric acid, where milling durations of 1, 4, 15, 30, 45, 60 and 90 minutes have been investigated. The results of this study can be seen in Figure 6.14.

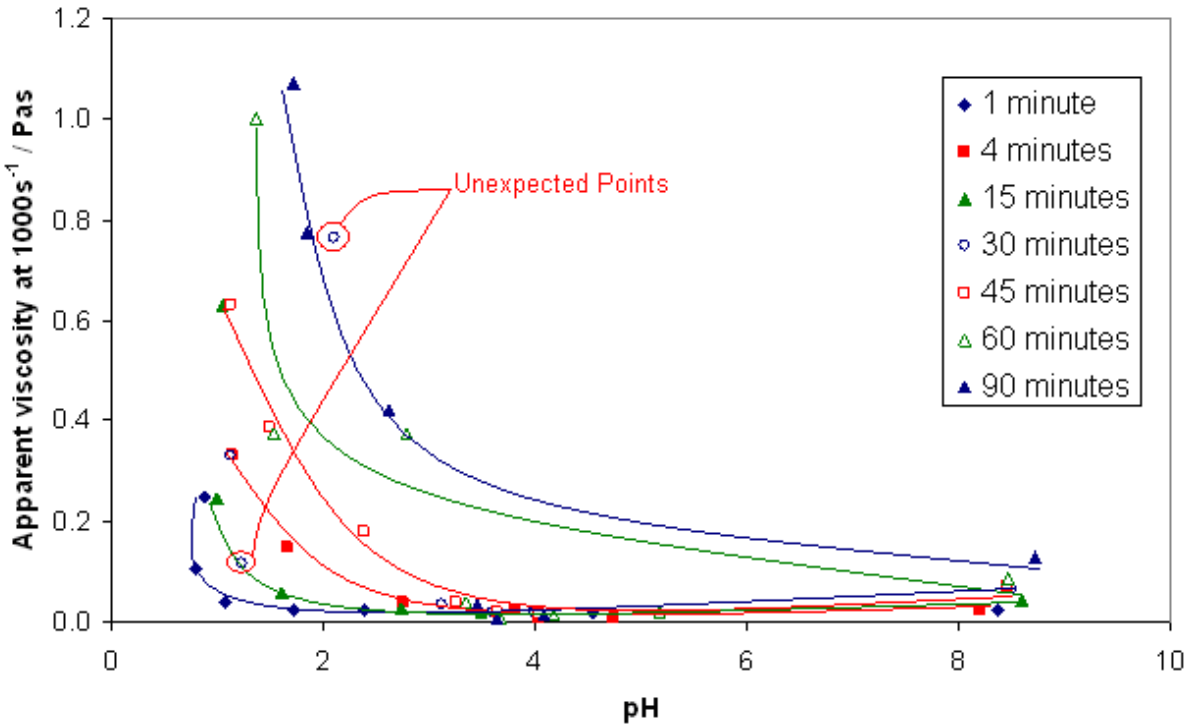

Figure 6.14: Relationship between pH and apparent viscosity for G250 with nitric acid samples at various milling times

The effect of milling time on the rheological properties of slurries is dependent on the pH of the slurry. Samples at pH 8 - 9 prepared with water and samples below pH 3 exhibit an increase in apparent viscosity at 1000 s^{-1} as milling time is increased. Within the pH range of 3 – 5, where apparent viscosity at 1000 s^{-1} is very low, the effect of milling time on the apparent viscosity at 1000 s^{-1} varies.

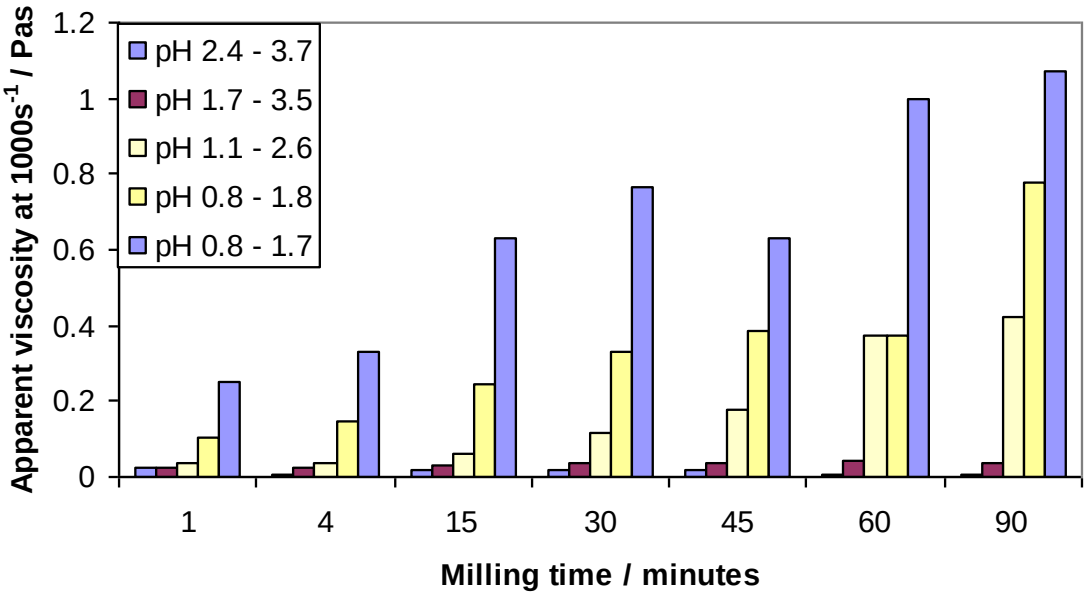

Figure 6.15: Relationship between apparent viscsoity and milling time for G250 samples at variety of pH's

The volumetric moment mean, d(4,3), has been quoted in Figure 6.16 as a description of the particle size of the samples as the measurement technique used is volumetric and particle volume is significant to the rheological properties. The use of the surface area moment mean, d(3,2), seen in Figure 6.17, can also be considered valid and produces similar conclusions, though the particle size increase at low pH and long milling time is not as evident from this data. Figure 6.18 presents a better visualisation of the increase in particle size at low pH and long milling times, these apparent increases in particle size are thought to be due to the presence of large gelatinous species which remain intact during the measurement technique.

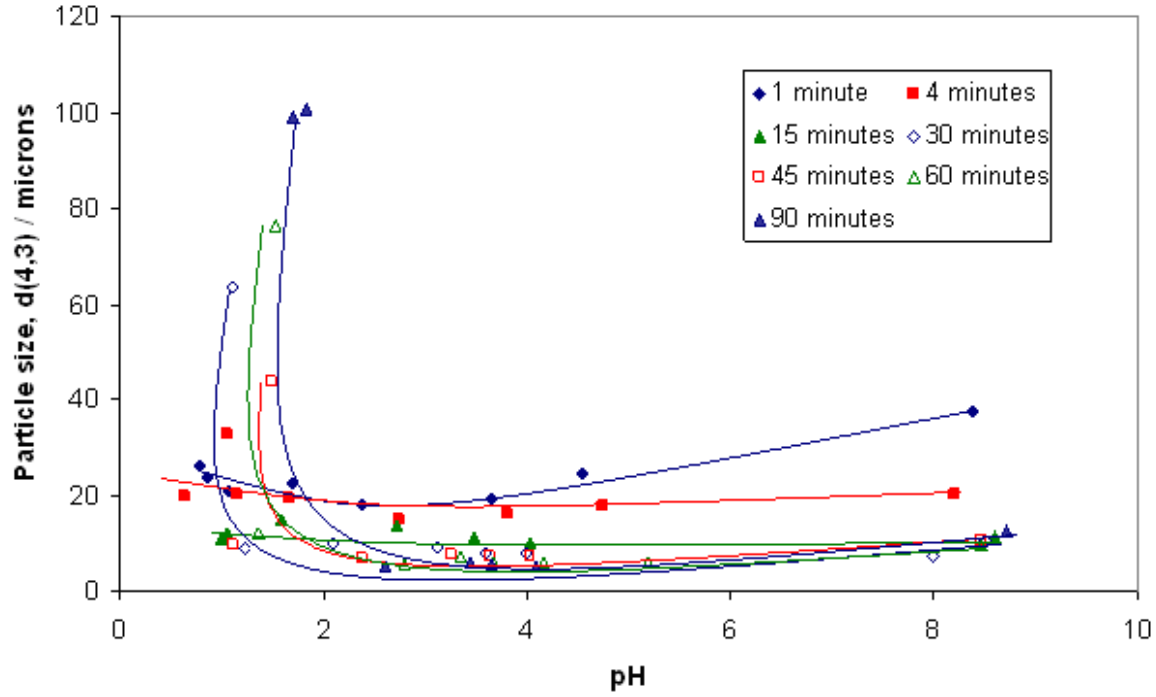

Figure 6.16: Relationship between particle size and pH for G250 samples at various milling times

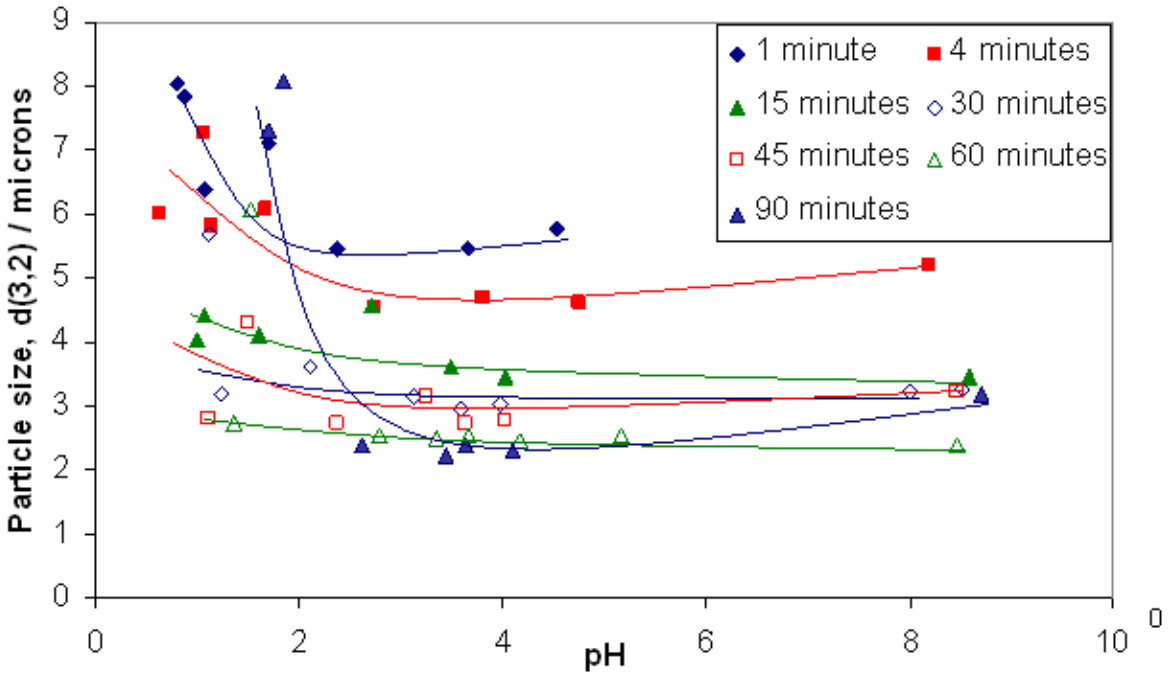

Figure 6.17: Relationship between particle size and pH for G250 samples at various milling times

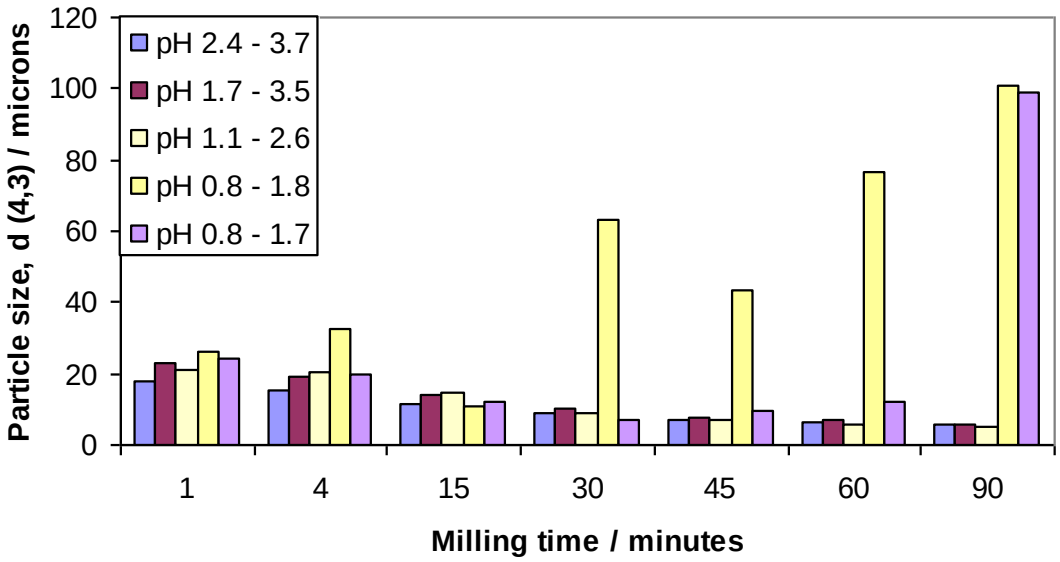

Figure 6.18: Relationship between particle size and milling time for G250 samples at various pH's

The increase in apparent viscosity at 1000 s^{-1} in samples prepared with water as milling time is increased is observed with each of the boehmite powders being investigated and is accompanied by an increase in pH which indicates dissolution of the boehmite under these conditions (boehmite releases OH- groups when it dissolves). Dissolution will alter the rheology of the liquid phase and there is also a considerable reduction in the mean particle size and the width of the particle size distributions, shown in Table 6.8, both of which will contribute significantly to the observed increase in apparent viscosity.

Table 6.8: Effect of milling time on apparent viscosity and size distribution of samples prepared with water

	G250		V250			Dequagel HP		
Milling Time	d (4,3)	Width	Apparent Viscosity at 1000 s^{-1}	d (4,3)	Width	Apparent Viscosity at 1000 s^{-1}	d (4,3)	Width
Mins	μm	μm	Pa.s	μm	μm	Pa.s	μm	μm
1	37.6	80.0	0.24	21.1	53.8	0.029	38.6	123
4	20.3	45.4	0.30	13.8	30.4	0.036	15.9	59.6
15	11.3	25.4						
30	10.3	25.4	0.68	8.90	16.9	0.072	3.40	5.30
45	10.6	25.6						
60	9.8	26.8						
90	12.5	29.4						

The increase in apparent viscosity at 1000 s^{-1} with milling time at pH below 3 is evident in Figure 6.15; also, samples prepared with the same initial acid content have a higher pH after an extended period of milling implying the consumption of acid. The particle size reduces progressively with milling time for all acid concentrations in which the initial pH (pH of the sample milled for 1 minute) is greater than 1, however, samples in which the initial pH was less than 1 (increasing to ~ 2 after 90 minutes of milling) showed evidence of very large particles (d [90] ~ 170 μm) being present after 30 minutes of milling and increasing in size up to 90 minutes of milling. This combined with the consumption of acid strongly supports the theory of the formation of a polymeric species by acidic dissolution and the resulting species being responsible for the observed thickening at acidic pHs. The large

particles observed may be the polymeric species or agglomerates of smaller particles formed due to agglomeration aided by the gelatinous phase.

The ambiguity of trends within the pH region of 3 - 5 suggests that there are a number of competing phenomena occurring and that no single effect is dominant in this range. A combination of mean particle size and size distribution alteration, chemical formation and mechanical breakdown of a polymeric gelatinous phase, change in binder viscosity and solids content due to the dissolution of boehmite and alteration in particle shape and deformability could be responsible for the observed results. Mean particle size and width of distribution both decrease steadily with milling time within this pH range. There is no direct measurement of the dissolution of boehmite or of chemical formation or mechanical breakdown of the gelatinous phase, therefore we cannot be sure to what extent the occurrence of these phenomena is relevant under these conditions. The sphericity of each of the boehmite powders ‘as received’ has been measured and is displayed and discussed in Chapter 5 however, the process of milling will alter the sphericity and measurements of milled samples have not been made preventing any further detailed discussion regarding this relationship.

Boehmites V250 and Dequagel HP exhibit very similar trends in rheological properties to G250 in suspensions prepared with nitric acid when milled for only 1 minute, a similarity which extends to the behaviour observed when milled for longer durations with a few exceptions.

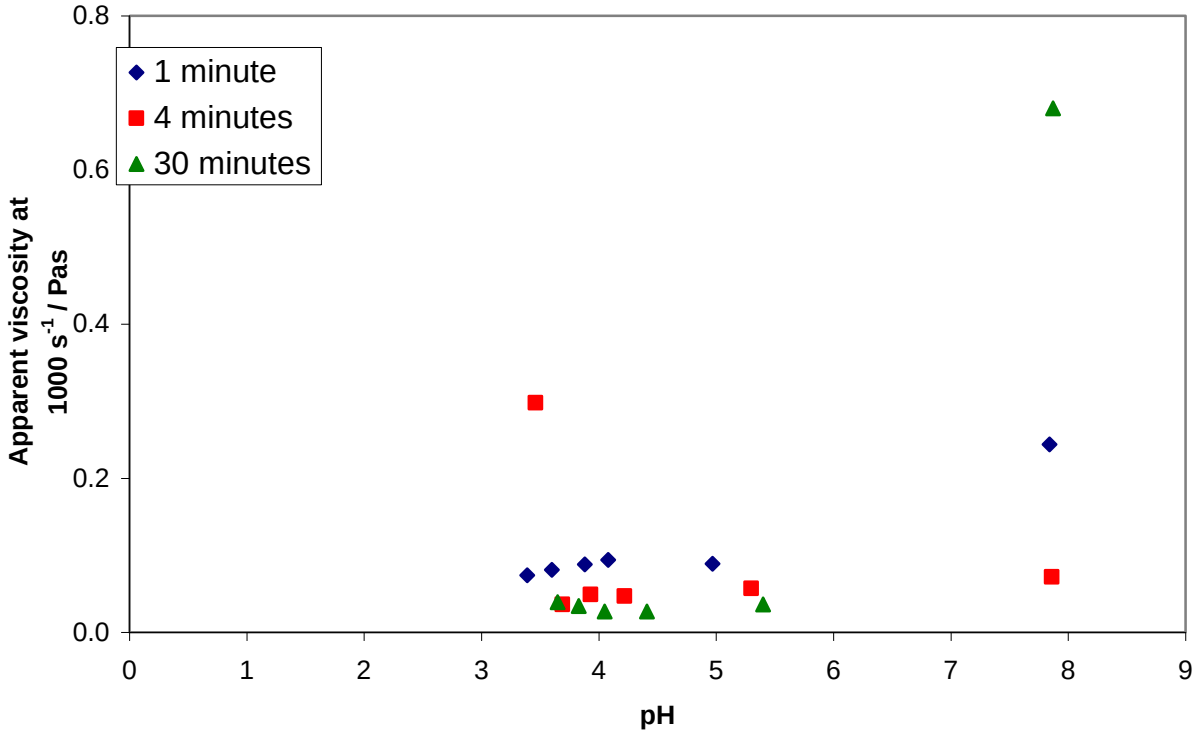

Figure 6.19: Relationship between apparent viscosity and pH for samples prepared with V250 and acetic acid at various milling times

Samples prepared with the boehmite V250 and acetic acid exhibit a reduction in apparent viscosity at 1000 s^{-1} with an increase in milling time shown in Figure 6.19. The same trend is observed with acetic acid in samples prepared with the boehmite Dequagel HP and to a lesser extent with the boehmite G250. This is believed to be due to the dispersive effect of acetic acid in these conditions. The mean particle size and particle size distribution width both decrease with time as expected, which should result in an increase in viscosity, the resulting reduction in viscosity indicates that the dispersive effects are dominant.

The data obtained for samples prepared by milling for 30 minutes has been fitted to the HB model in the same way as the data obtained from the samples prepared by milling for 1 minute described in Section 4.2.1. It can be seen from the data displayed in Table 6.9 that the model fails to fit all samples prepared with water and

samples with high nitric acid content for each of the powders. The model parameters can be seen in Tables 6.10 – 6.12. The model fails in each case at a lower initial molar ratio of acid to boehmite than the samples prepared by milling for 1 minute, which suggests that the additional mechanical energy input has assisted the phenomenon which causes the materials to show a poor fit to the HB model for concentrated suspensions. All of the samples prepared with acetic acid display good fits to the HB model. As was the case with the previous data fitting, the model appears to fit samples which exhibit very low yield stresses, approximating to zero in the majority of cases, seen in Table 6.10. Samples which are not adequately described by the HB model generally display an improved fit to the Cross model, as was the case with the 1 minute samples.

Table 6.9: Standard error of 30 minute samples according to Herschel Bulkley model

molar ratio of acid to boehmie	nitric acid			acetic acid		
	G250	V250	Dequagel HP	G250	V250	Dequagel HP
water	20	60	60	20	60	60
0.02		4	6	8	5	8
0.036	9					
0.048	7	4	10	6	3	8
0.06	6	70	10	10	6	7
0.072	30					
0.084	70	50	20	9	7	6
0.096	20					
0.1			100	9		7
0.13		60		8	5	7
0.25				6		6

Table 6.10: Yield stress (Pa) of 30 minute samples according to Herschel Bulkley model

molar ratio of acid to boehmie	nitric acid			acetic acid		
	G250	V250	Dequagel HP	G250	V250	Dequagel HP
water	7	50	2	7	50	2
0.02		0	0	0	0	0
0.036	0					
0.048	0	0	0	0	0	0
0.06	0	-40,000	0	0	0	0
0.072	-50					
0.084	-700,000	-400,000	-5	0	0	0
0.096	800					
0.1			-1,000,000	0		1
0.13		-700,000		0	0	1
0.25				0		0

Table 6.11: Viscosity constant, k, of 30 minute samples according to Herschel Bulkley model

molar ratio of acid to boehmie	nitric acid			acetic acid		
	G250	V250	Dequagel HP	G250	V250	Dequagel HP
water	5	0	10	2	0	10
0.02		0	0	0	0	0
0.036	0					
0.048	0	0	0	0	0	0
0.06	1	40,000	0	0	0	0
0.072	90					
0.084	700,000	400,000	10	0	0	0
0.096	40					
0.1			1,000,000	0		0
0.13		700,000		0	0	0
0.25				0		0

Table 6.12: Rate index of 30 minute samples according to Herschel Bulkley model

molar ratio of acid to boehmie	nitric acid			acetic acid		
	G250	V250	Dequagel HP	G250	V250	Dequagel HP
water	0	2	0	0	2	0
0.02		1	1	1	1	1
0.036	1					
0.048	1	1	1	1	1	1
0.06	1	0	1	1	1	1
0.072	0					
0.084	0	0	0	1	1	1
0.096	0					
0.1			0	1		1
0.13		0		1	0	1
0.25				1		1

6.6 Oscillatory Rheology, Examining the Microstructure

As discussed in Section 2.2.6 oscillatory rheology, sometimes called mechanical vibrational spectroscopy, can be used to examine the microstructure of a material. A small selection of samples within the range characterised previously by flow rheology has been prepared and studied with oscillatory rheology in an attempt to confirm the proposed gelatinous microstructure. All of the samples examined by oscillatory rheology have been prepared by milling for 30 minutes and the pH has been measured to allow comparison with samples characterised by flow rheology.

As described in Section 4.2.2 a stress sweep was performed on each sample initially to determine an appropriate stress within the linear viscoelastic region (LVR) at which the frequency sweep could be performed. Many of the samples studied did not show a clear or stable LVR over the stress range examined. Issues such as the moduli increasing constantly over the range of frequencies examined, one modulus

being stable and the other varying, and generally noisy data have affected locating the LVR.

Only a selection of samples exhibited an LVR, these were the samples prepared with each of the 3 boehmites and water, and the samples prepared with the boehmite V250 and nitric acid. Acidic samples prepared with the boehmites G250 and Dequagel HP, and samples prepared with V250 and acetic acid, did not display an LVR. The non linear viscoelastic nature of the samples prepared with acid can be attributed to structure deformation and / or destruction under shear, or continued formation of the gelatinous species. The absence of an LVR indicates the dynamic nature of the materials and prevents any further analysis of those samples.

The storage and loss moduli from frequency sweeps of samples exhibiting an LVR have been examined. The loss tangent, tan δ, is the ratio of the loss modulus to the storage modulus, G''/G'. When the loss tangent is greater than 1 the material has a higher loss modulus than storage modulus i.e., is liquid-like. Conversely, a loss tangent of less than 1 implies a gel-like structure. The loss tangent for all samples displaying a linear viscoelastic region in the stress sweep can be seen in Figure 6.20. The vast majority of data displays a loss tangent of less than 1, implying a gel like structure, with the exception of the sample containing V250 and a molar ratio of 0.048 nitric acid which displays liquid like behaviour up to a frequency of ~30 $rads^{-1}$. It is possible that the samples produced with water are displaying gel like behaviour due to the lack of chemical dispersion resulting in a structured material. The addition of a small amount of acid to the boehmite V250 results in a liquid-like response due to the chemical dispersion of particles. Further addition of acid results in a gel like

material, potentially due to the formation of a gelatinuous phase between the boehmite and the acid.

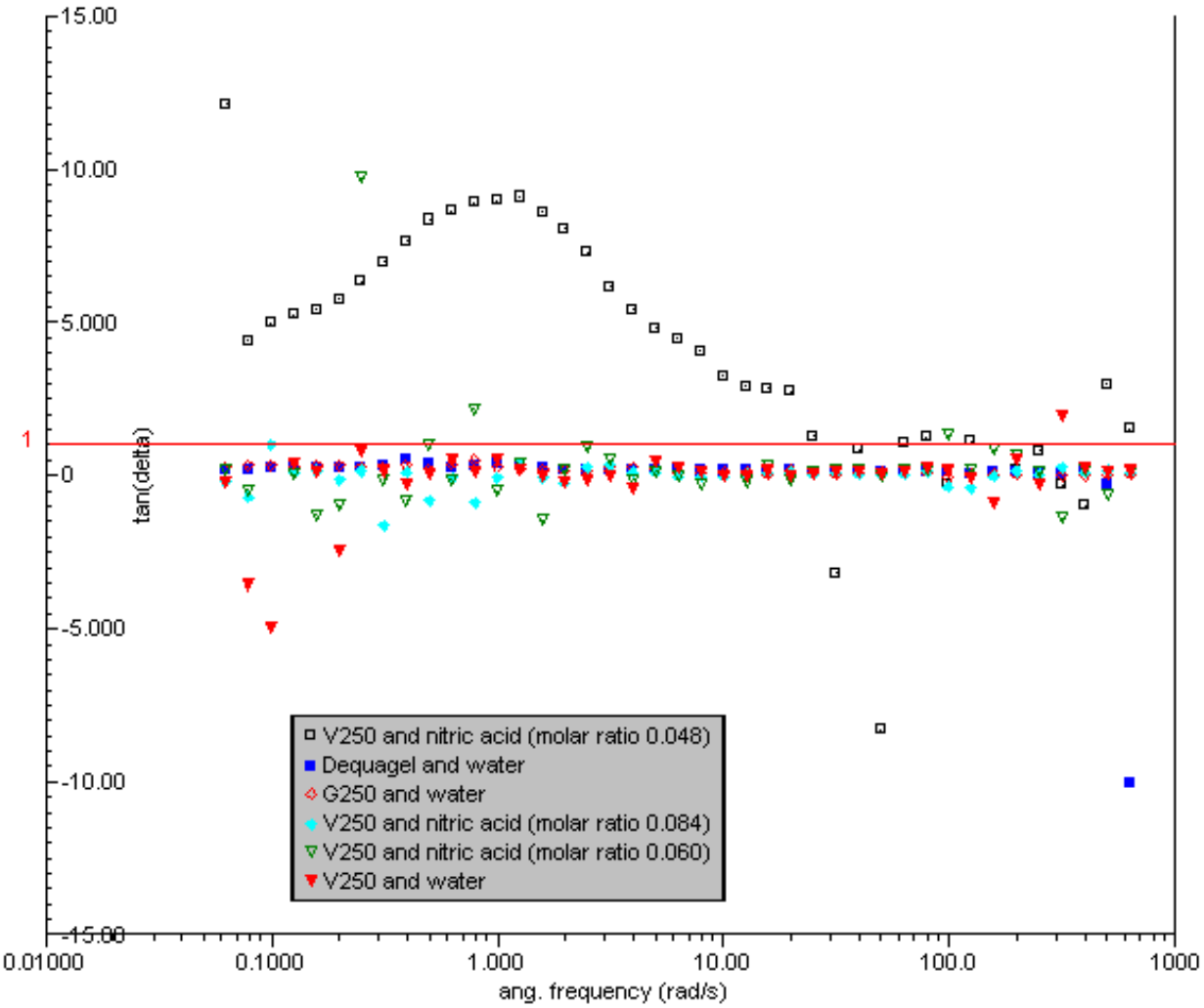

Figure 6.20: Loss tangent of samples displaying a linear viscoelastic region

6.7 Solid State Al Nuclear Magnetic Resonance

Samples prepared under low and high energy input and low and high acid content have been examined.

All samples prepared with low energy input displayed a single peak, similar to that seen in the red curve in Figure 6.21 indicating a purely tetrahedral coordination

regardless of the acid strength with which the sample was prepared. This suggests that by chemical action alone no transition of coordination, or formation of a polymeric cation, was achieved.

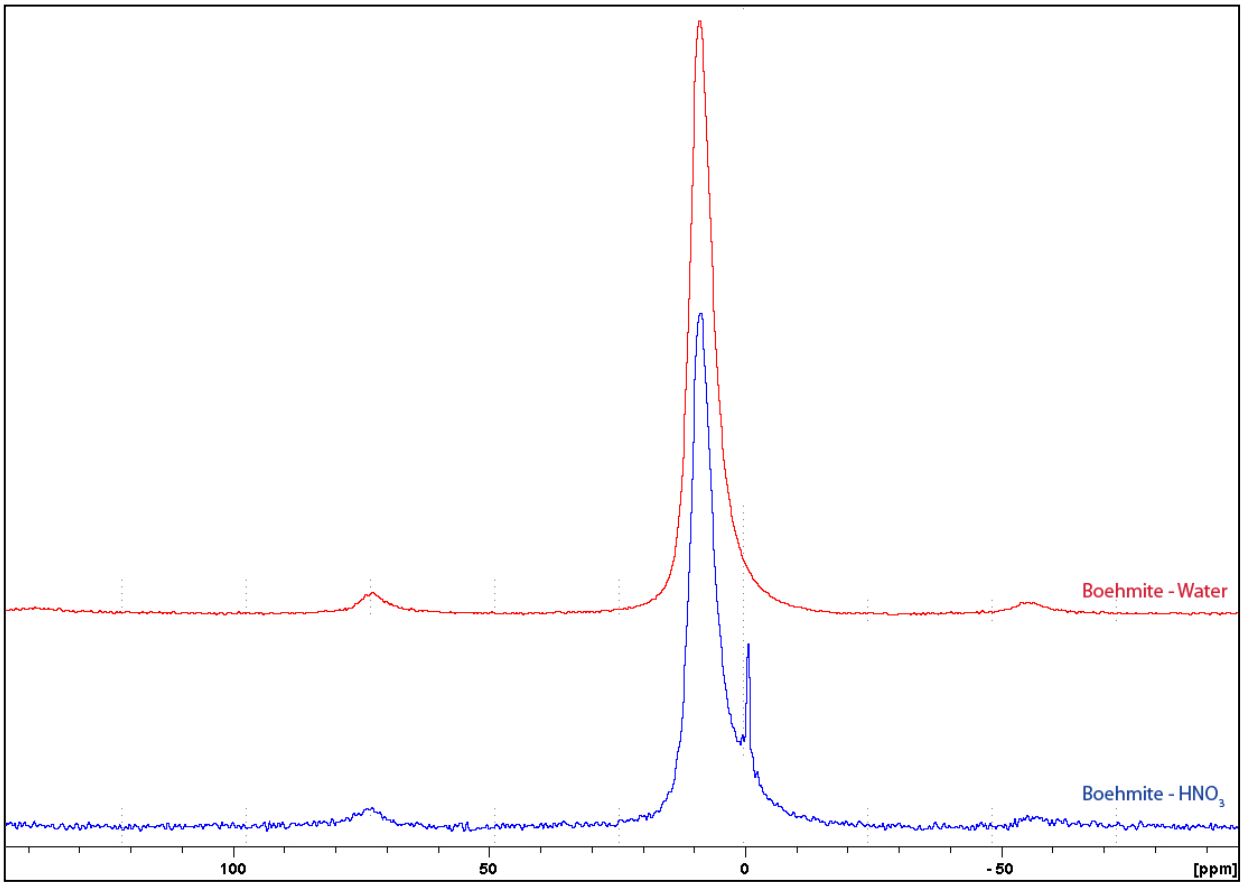

Figure 6.21: Al NMR data

Samples prepared under the same high energy conditions as those characterised rheologically displayed a second peak indicating the presence of octahedral and a five co-ordinated aluminium species (trigonal bi pyramidal). The additional peak cannot be confidently attributed to the presence of a polymeric cation as it may be due to a coordination change in boehmite due to a phase change induced by mechanochemical means.

The lack of coordination change observed in the samples prepared under low energy input suggest that the change is due to mechanochemical changes rather than chemical polymerisation of the aluminium species.

6.8 Cryogenic Scanning Electron Microscopy (Cryo-SEM)

Concentrated slurries were prepared, characterised rheologically and examined by cryo-SEM. One slurry was prepared with only water, and one contained 0.06 moles of nitric acid per mole of boehmite. The rheological characterisation in Figures 6.22 and 6.23 shows the significant variation in rheological properties exhibited by the two samples. The sample prepared with water displays much higher repeatability in the varied shear rate experiments and a lower apparent viscosity at 1000 s^{-1}. The sample containing acid displays a much higher apparent viscosity at 1000 s^{-1}, suggesting a more structured material, and exhibits a small degree of hysteresis during the varied shear rate experiment implying the breakdown and rebuilding of structure as shear is applied.

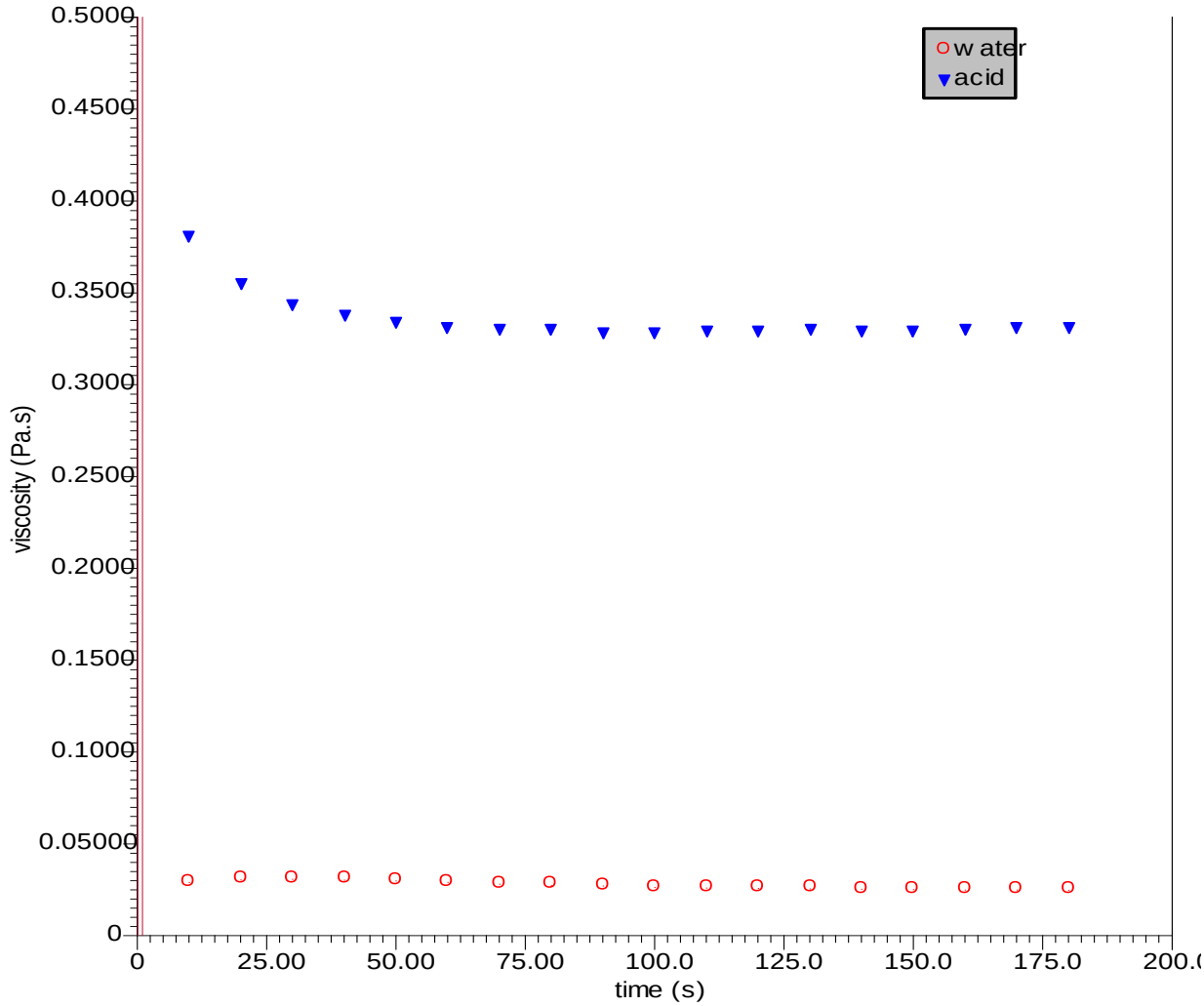

Figure 6.22: Rheological characterisation of samples prepared for examination by cryo-SEM.

(Viscosity presented is apparent viscosity at 1000 s^{-1})

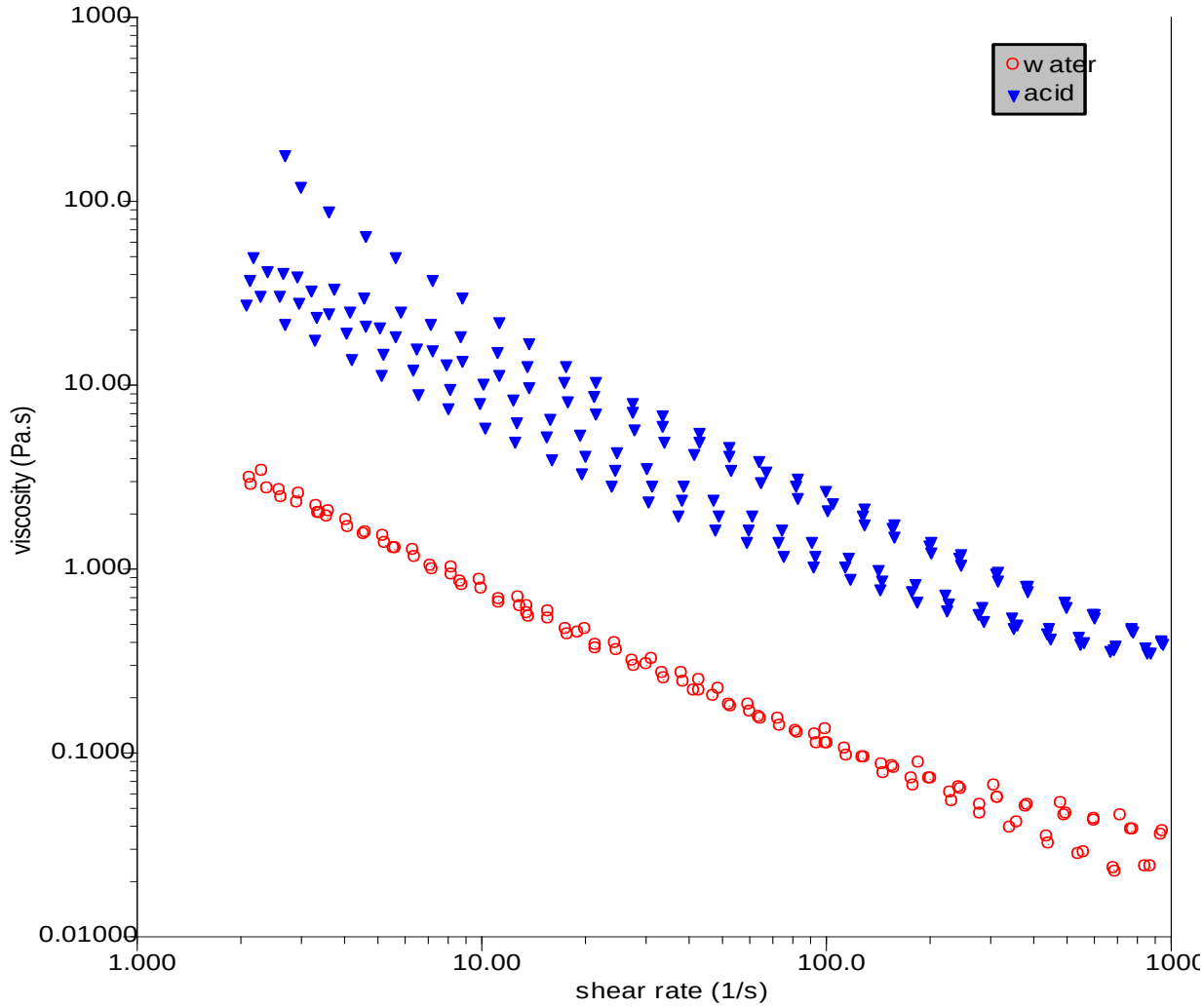

Figure 6.23: Rheological characterisation of samples prepared for examination by cryo-SEM.

The images seen in Figure 6.24 to 6.28 are currently, to the author's knowledge, the best images of their kind. A similar study was performed by Rosenberg *et al.* (1995) showing alterations in the microstructure of boehmite slurries in the presence of acid but the images shown here are at a significantly higher magnification.

Figures 6.24 and 6.25 show each of the samples in a sublimed condition. Figure 6.24 shows the sample prepared with water only with distinct individual particles which shows a very different structure to the sample prepared with acid, seen in Figure 6.25. When prepared with water the sample clearly contains discrete

particles of around 5 μm and below, including evidence of particles in the sub micron range. When prepared with acid, Figure 6.25, the sample still shows evidence of discrete particles but with less distinct edges than in Figure 6.24, and the continuous phase between the particles appears to have structure. This structure is a network structure which is typical of polymeric species. The apparent directionality in the network of the continuous phase structure is an artefact of the technique, the continuous phase has been pushed to the boundaries by the fast cooling ice, forming a 3 dimensional network. There is also evidence of the presence of smaller discrete sub micron particles.

Figures 6.26 and 6.27 also show the samples in the sublimed state, at a higher magnification than Figures 6.24 and 6.25. A distinct particle a few μm in size can be seen in the top right corner of Figure 6.26, and other smaller distinct particles are evident across the top of the image. In the centre of the image we can see evidence of finely dispersed particles, unexpected as this sample was prepared with only water. Although this image is evidence of fine dispersion occurring in a sample containing no acid, the majority of the sample showed discrete particles as seen in Figure 6.25, rather than finely dispersed material.

A closer examination of the structure of the continuous phase observed in Figure 6.25 can be seen in Figure 6.27. On the right hand side of the image the presence of discrete submircon particles within the continuous network can be seen, and the continuous network itself is shown to have a strand-like structure towards the edges created by the sublimation process.

Figure 6.28 focuses on the boundary between a particle and the continuous network observed previously in Figure 6.25. The particle surface can be seen at the top of Figure 6.28 and the network of continuous phase at the bottom of the image with the transition between the discrete and continuous phases across the centre of the image. There is a gradual transition in the nature of the structure from full particle surface to strands within the continuous network.

EDX analysis of these materials confirms the presence of aluminium and oxygen.

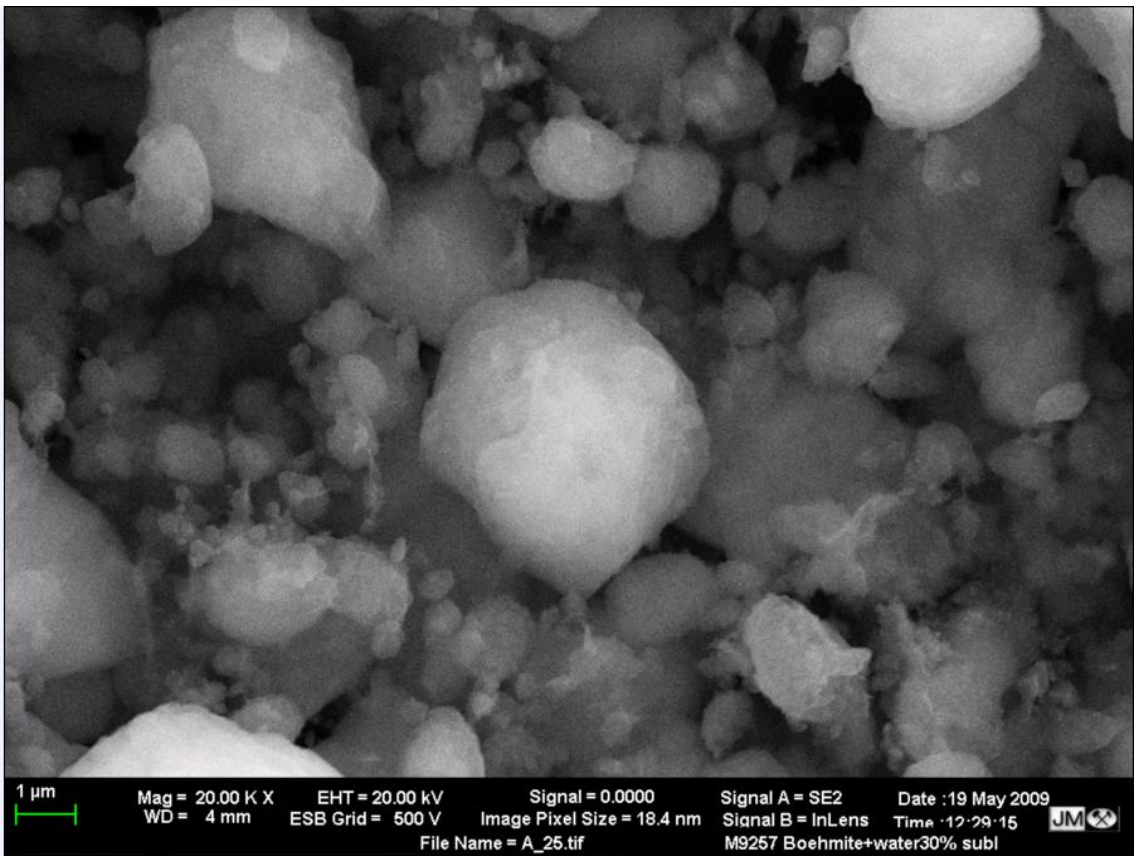

Figure 6.24: Boehmite and water

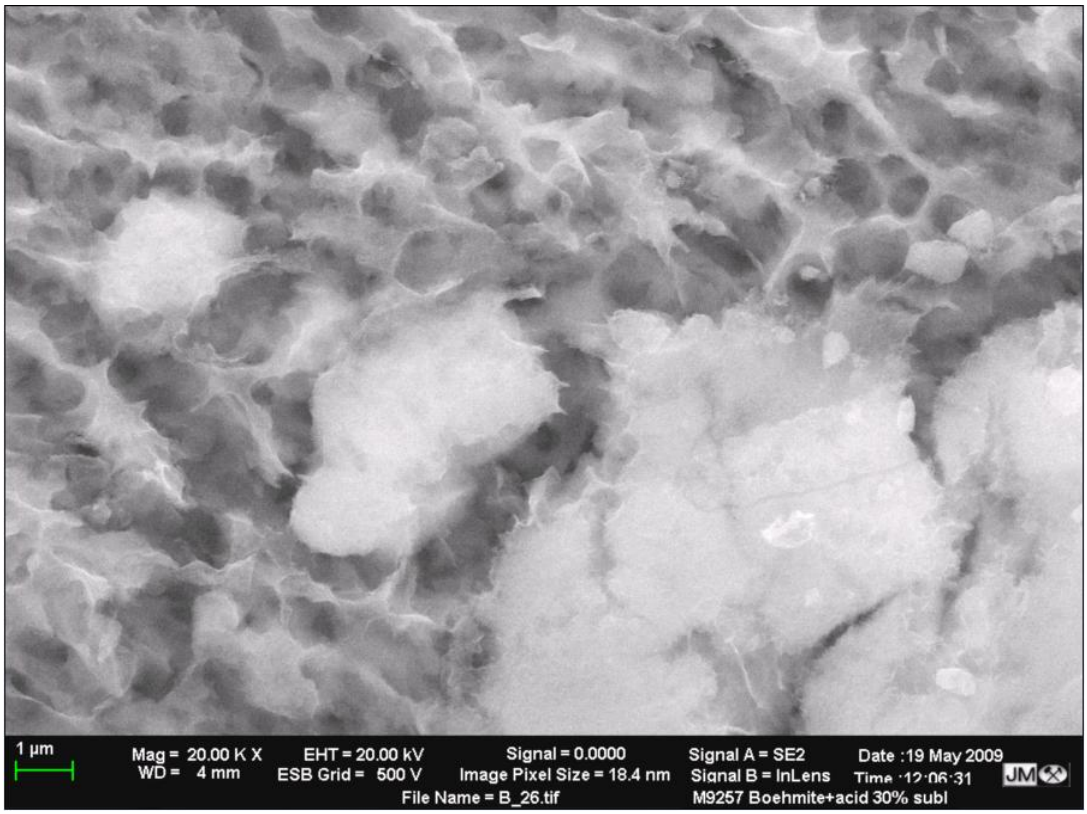

Figure 6.25: Boehmite and acid

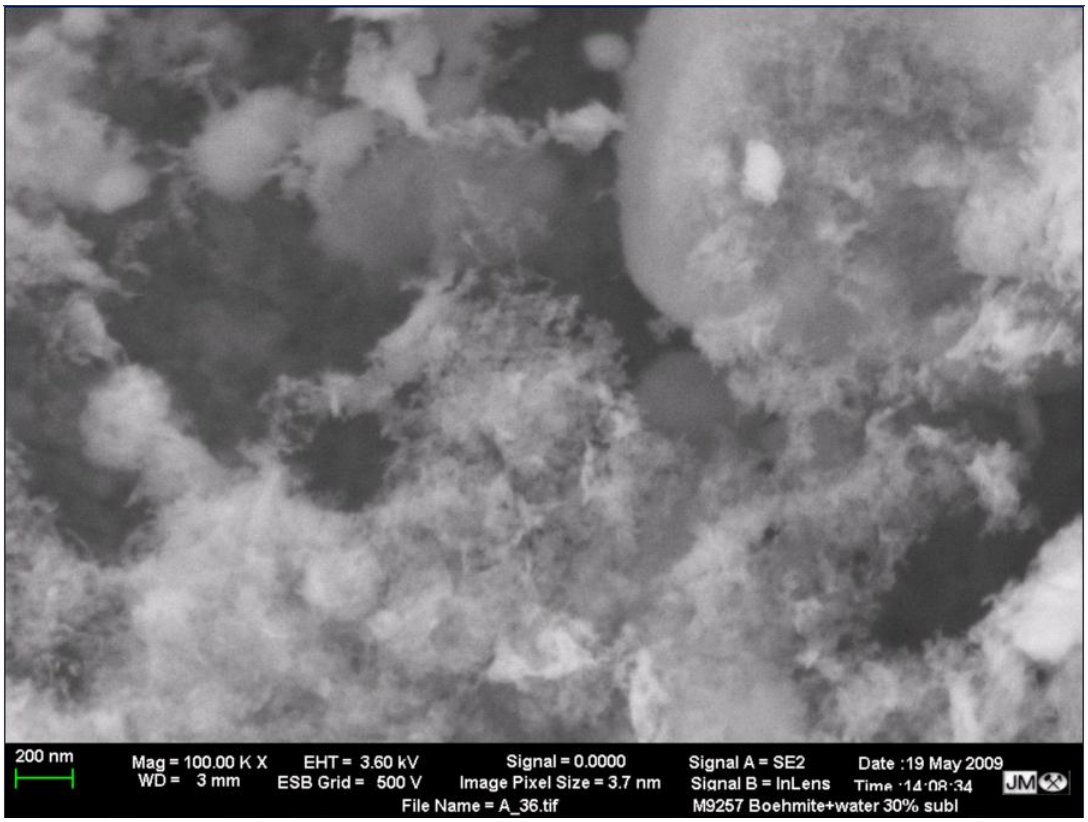

Figure 6.26: Boehmite and water

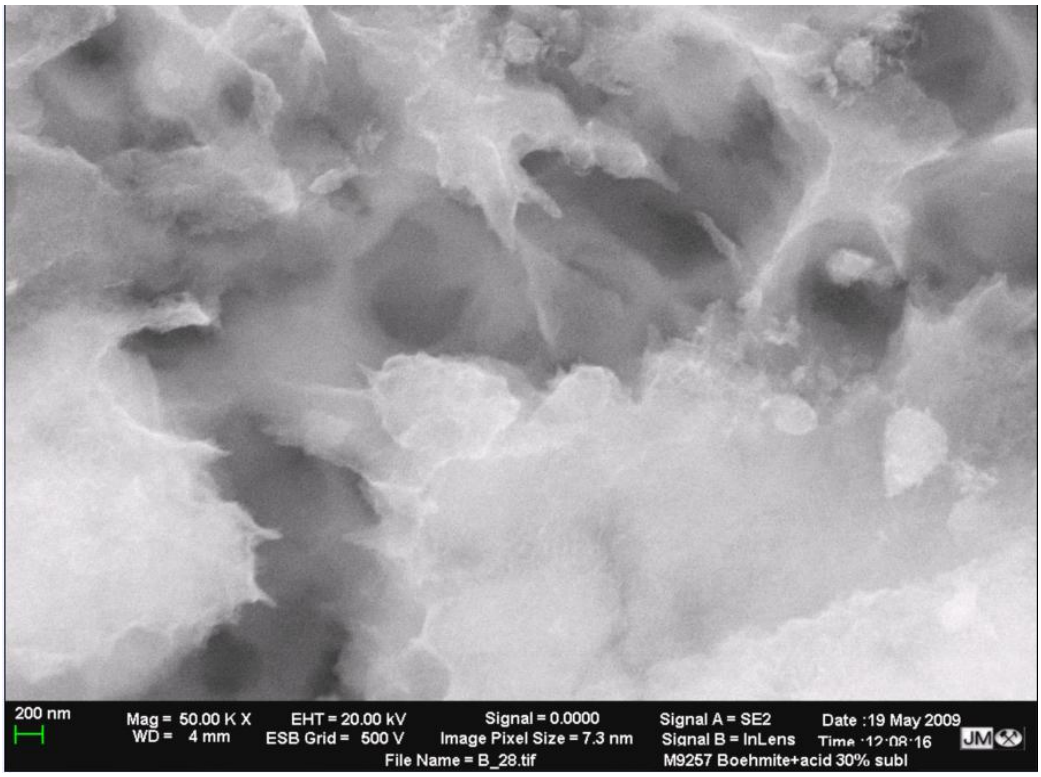

Figure 6.27: Boehmite and acid

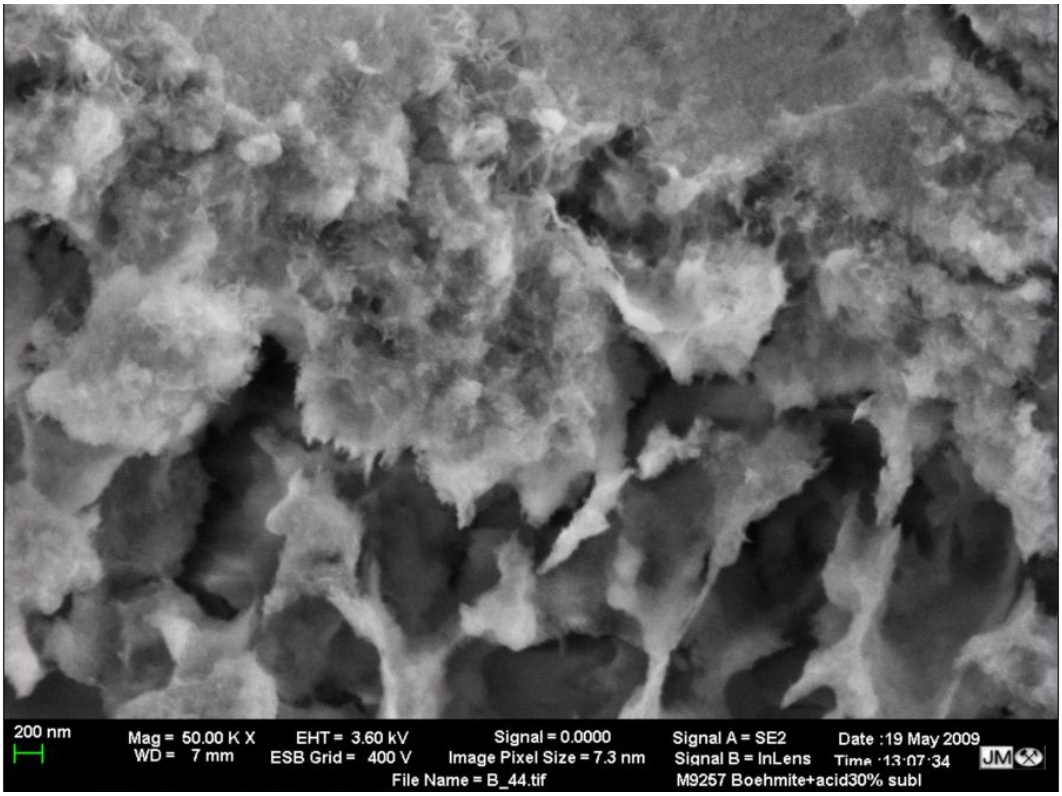

Figure 6.28: Boehmite and acid, interface between remaining particle and amorphous 'gelled' phase.

6.9 Conclusions

Both initial acid content and milling duration result in alteration of the rheological properties of acidic concentrated boehmite suspensions. A combination of rheological characterisation, zeta potential, pH and particle size distribution data has shown that neither the zeta potential, nor particle size changes with acid content can explain the observed increase.

It is believed that the observed increase in apparent viscosity at 1000 s^{-1} and yield stress of acidic concentrated boehmite suspensions is due to the formation of a gelatinous phase of polymeric cations by partial dissolution of boehmite and that these species can adsorb onto particle surfaces. This proposal has been reached, not only by examining and eliminating possible rationalisations, but is also supported by the zeta potential and pH measurements showing surface chemistry changes and consumption of acid. A dissolution – readsorption mechanism is proposed for the interaction between boehmite and acid in which the boehmite surface is dissolved at low acid concentrations and polymeric cationic species are formed in solution at higher acid concentrations and readsorb onto the boehmite surface.

Results show that increasing the sample preparation time enhances the phenomenon, likely due to a combination of the particle size distribution alterations brought about by milling making additional surface area available for the dissolution and mechanical activation and phase changes as a result of milling.

The use of oscillatory rheology to confirm the gelatinous nature of the microstructure was inconclusive due to the absence of a linear viscoelastic region in the shear

stress sweep performed on the majority of the samples, indicating that samples exhibit dynamic characteristics.

Examination of the coordination of the aluminium species by MAS NMR has identified alterations in the coordination, however, it can not be ascertained whether this is due to the presence of the proposed polymeric cation or a mechanochemical phase change resulting from the high energy sample preparation technique.

Cryo-SEM has confirmed textural differences between boehmite slurries prepared with and without acid. These are the first images of these materials to clearly show such differences and support the proposal of the formation of a polymeric species in acidc boehmites. The continuous phase formed in the presence of acid visually appears to be polymeric in nature, and a clear image of the alterations in texture at the interface between a discrete particle and the continuous phase has been captured.

Chapter 7 Mixer Torque Rheometry

7.1 Taguchi

The data obtained from the Taguchi experimental matrix has been processed to ascertain the influence of each of the five input variables on each of the two responses, i.e. 10 influences are assessed. Each influence is calculated as the difference between the average response with the variable set at value 2 and the average response with the variable set at value 1. A negative value of influence gives qualitative information about the relationship between the variable and output, implying that the output is higher when the variable is in condition 1. To compare the significance of each variable on each output the influences have been normalised to the highest influence value for each output.

Table 7.1: Outputs from Taguchi experiments, effect of variable 1 on output A

Experiment Number	Variable 1	Output A
1	1	A1
2	1	A2
3	1	A3
4	1	A4
5	2	A5
6	2	A6
7	2	A7
8	2	A8

Influence of variable 1 on output A (equation 7.1);

$$\frac{(A5+A6+A7+A8)}{4}-\frac{(A1+A2+A3+A4)}{4} \quad \text{.....(equation 7.1)}$$

Table 7.2: Influence of all variables on output A, magnitude of peak mean torque

Variable			Influence	Normalised influence
3	Liquid addition rate	$ml.min^{-1}$	-812	1
5	Acid strength	M	-741	0.91
4	Powder type		260	0.32
1	Temperature	^oC	-69	0.08
2	Paddle rotation rate	rpm	-31	0.04

Table 7.3: Influence of all variables on output B, liquid content at peak mean torque

Variable			Influence	Normalised influence
4	Powder type		51.4	1
5	Acid strength	M	17.9	0.35
3	Liquid addition rate	$ml.min^{-1}$	11.7	0.23
1	Temperature	^oC	10.8	0.21
2	Paddle rotation rate	rpm	-9.4	0.18

The calculated influences show that temperature and paddle rotation rate have the least significant influence on both of the observed outputs. With regards the paddle rotation rate, this is in agreement with results observed by Landin, Rowe and York (1995). The temperature difference investigated in these experiments was expected to have a low influence on the outputs as the range examined was considered small, but within the operating window of interest in the project. This confirms that there is no significant concern with temperature drifting within this range during the experiments.

In the case of output A, the magnitude of the peak mean torque, both the addition rate of the liquid and the type of liquid have the most significant influence. The powder type is significantly more influential than temperature or paddle rotation rate but considerably less so than the liquid conditions. Output B, the liquid content at

which the peak mean torque occurs, is predominantly influenced by the type of powder used, the other four variables all have a comparably small effect on the results.

A higher peak mean torque is achieved at a slow liquid addition rate due to the improvement this allows in the mixedness of the material. The use of acid rather than water, or boehmite rather than alpha alumina, produces a higher peak mean torque, in both cases this is likely due to the chemical interaction occurring between the materials and the resulting structure alteration as observed and discussed previously in Chapter 6. The normalised influences of temperature and paddle rotation rate on the magnitude of the peak mean torque are small enough to consider their influence in either direction as negligible over the range investigated for each parameter.

Boehmite requires more liquid per mass of powder to reach the peak mean torque than alpha alumina and this is the most dominant factor on this response. The use of acid rather than water enables the peak mean torque to be reached at a lower liquid content, the apparently low significance of this influence is likely to be due to the lack of chemical interaction between liquid and powder in the formulations containing alpha alumina. The peak mean torque occurs at lower liquid contents when the liquid is added slowly or the paddles rotated quickly due to the increase in effective mixing reducing the interparticle voids. An increase in temperature results in more liquid required to reach the capillary point, but the variation is not significant.

The findings from this experimental design allowed further experiments, assessing the rheology of various formulations, to be performed at constant temperature,

paddle rotation rate and liquid addition rate with confidence that these parameters would have minimal influence on the experimental results.

7.2 Multiple Addition Tests

7.2.1 Position of Mean Torque Peak

The peak mean torque and the peak torque range have been determined for the multiple addition tests performed on each of the formulations. Both the position (in terms of solids content) and the magnitudes of these peaks are considered. As discussed previously the peak mean torque indicates the material is in a capillary state of saturation, the peak torque range indicates the funicular state of saturation. In addition to the position of these peaks, the shape of the curve, and more specifically the area under the curve up to the peak mean torque is considered, this is a description of the work applied to the material.

Figure 7.1 shows the position of each of the peaks occurring in the 15 multiple addition tests performed. Solids contents have been corrected for loss on drying.

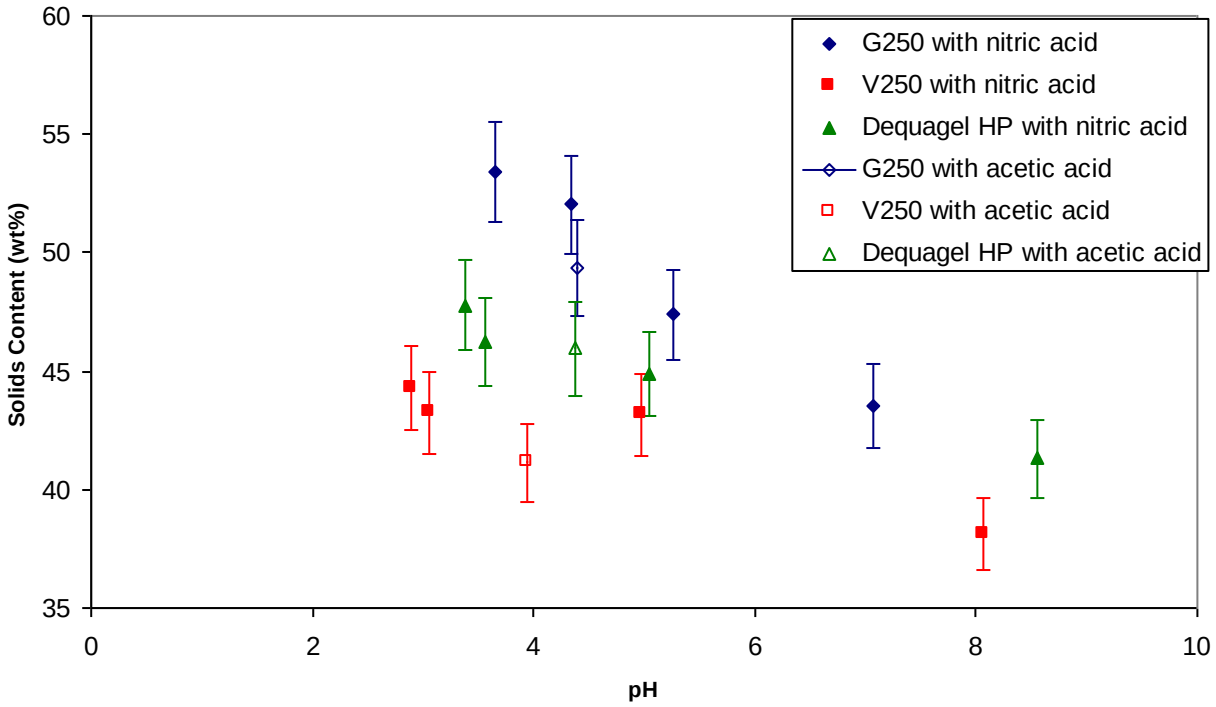

Figure 7.1: Peak mean torque positions for all formulations from MATs

The highest solids concentration at the capillary point is displayed by the boehmite, G250. The boehmite V250 forms a capillary state under the wettest conditions out of the three powders. This trend displayed by the powders is consistent across the range of the liquids tested. The reasons for the change in solids content with pH are discussed further in Section 7.2.4.

Error bars have not been included in this data set as it was not possible to perform repeat measurements on the equipment. Errors in weighing of powder are ± 0.01 g, based on human error. Errors in dispensing of the liquid phase are ± 0.01 ml, based on instrument error. Errors in the position of the peak are ± 4 % based on previous work performed during commissioning and method development on a similar material.

7.2.2 Prediction of Capillary Point with Water

It is theoretically possible to predict the volume of water required to form the capillary saturation state by calculating the volume of voids present in the mass of powder, this can be calculated from the bulk and skeletal densities. The bulk density measurement accounts for all voids in the material, including both inter and intra particle voids, and also closed pores. Inter particle voids are those between particles and intra particle voids the porosity with the particles. The inclusion of closed pores in this measurement means that the available pore volume may be over estimated.

Using the simple relationships that density is mass per volume and the total volume is comprised of only powder volume or void volume the following calculations can be made:

$$\rho_{bulk} = \frac{m_{bulk}}{V_{bulk}} \text{ and } \rho_{skeletal} = \frac{m_{skeletal}}{V_{skeletal}} \quad \text{.....(equation 7.2 and 7.3)}$$

where, ρ is density, m is mass and V is volume. Both bulk and skeletal mass are 20 g and the bulk and skeletal densities of each of the powders have been measured, hence bulk and skeletal volumes can be calculated.

Once bulk and skeletal volumes have been calculated for each of the powders examined the void volume (V_{voids}) can be calculated according to equation 7.4.

$$V_{bulk} = V_{skeletal} + V_{voids} \quad \text{.....(equation 7.4)}$$

The resulting solids content expected at the capillary state calculated for each of the powders using this method can be seen in Table 7.4 along with the experimental results obtained from the multiple addition tests with water.

The poured bulk density of boehmite G250 0.5 $g.cm^{-3}$ (500 $kg.m^{-3}$) and of V250 and Dequagel HP, 0.3 $g.cm^{-3}$ (300 $kg.m^{-3}$). The tapped bulk density of boehmite G250 is 0.6 $g.cm^{-3}$ (600 $kg.m^{-3}$) and of V250 and Dequagel HP, 0.4 $g.cm^{-3}$ (400 $kg.m^{-3}$). The skeletal density of all three boehmite powders is 2.7 $g.cm^{-3}$ (2700 $kg.m^{-3}$).

Table 7.4: Variation between expected and actual solids content at MAT peak, (*correction made for loss on drying)

	Measured solids content at capillary point *	Expected solids content at capillary point		Discrepancy between expected and measured solids content	
		Poured bulk density	Tapped bulk density	Poured bulk density	Tapped bulk density
	wt%	wt%	wt%	wt%	wt%
G250	43.5	38.0	43.6	5.5	-0.1
V250	38.1	25.2	33.0	12.9	5.1
Dequagel HP	41.3	25.2	33.0	16.1	8.3

There is a discrepancy observed between the calculated and measured solids content at the capillary saturation state of the powders and the magnitude of the discrepancy varies between the powders. The discrepancy is significantly reduced when the tapped bulk density is used as opposed to the poured bulk density, indicating that the tapped bulk density behaves as a better predictor for the packing of powders in a mixer torque rheometer. Although the powder is charged to the

mixing chamber by pouring, the work input and rearrangement of particles by mechanical means validates the use of the tapped bulk density rather than the poured bulk density.

With the exception of the prediction of boehmite G250 from tapped bulk density, which is almost exact, the calculation consistently predicts a lower solids content than that measured, i.e. the volume of voids accessible to the liquid is being over predicted.

This discrepancy can be related to the phenomenon of a powder reducing in volume upon addition of liquid. Laboratory tests have been unable to quantify this effect but a qualitative trend between the powders has been observed which supports the trend in the magnitude of the discrepancies in Table 7.4. The boehmites Dequagel HP and V250 shrink significantly upon the addition of water whereas the shrinkage observed with the boehmite G250 was minimal. This phenomenon can be related to the cohesiveness of the powders. A cohesive powder will exhibit inefficient packing as the cohesive forces prevent complete settling of particles into a densely packed system. Examination of the Hausner ratio measured for the powders of interest gives support to this theory. The Hausner ratio is the ratio of the tapped bulk density to the poured bulk density, a large Hausner ratio implies a cohesive powder which is more liable to packing adjustment. The least cohesive powder (G250, Hausner ratio 1.29) exhibits minimal volume reduction upon liquid addition and a low discrepancy is the predicted capillary point, where as the more cohesive powder (Dequagel HP, Hausner ratio 1.35) displays a considerable reduction in volume and a much larger discrepancy in the prediction. Boehmite V250 has an intermediate Hausner ratio of

1.32 and displayed a discrepancy between that of the boehmites G250 and Dequagel HP.

An additional consideration to be made regarding the inaccuracy of this prediction is the variation in particle packing and packing density as a result of changes in particle size distributions resulting from mechanical work input. The technique used to measure tapped bulk density is not thought to alter size distribution, however, the MTR has been shown to affect particle size distribution, results can be seen in Section 7.2.5.

7.2.3 Comparison of Effect of Nitric Acid and Acetic Acid

The MAT mean peak torque results in Figure 7.1 show a strong correlation between the pH and the solids content of a material in the capillary state for all powders. The data for both nitric and acetic acid lie upon the same trend line for a given powder, suggesting that the phenomena responsible for the shift is not anion specific.

7.2.4 Mechanisms Responsible for Shift in Position of Peak Torque

Figure 7.1 shows that the solids content at the capillary point increases as pH decreases, i.e. at lower pH the liquid content required to reach the capillary state is reduced.

A reduction in the liquid content required to reach the capillary state can be achieved either by reducing the pore volume (or accessible pore volume) or increasing in bulk density. Bulk density can be increased by either mechanical or chemical means. The wettability, or contact angle of a powder – liquid combination can also effect the position of the peak torque.

A reduction in pore volume could take place by gelation within the pores or at pore entrances resulting in a reduction of the available intraparticle pore volume. Nitrogen pore volumes of each of the powders have been measured; G250 = 0.59 cm^3g^{-1} ($5.9x10^{-4}$ m^3kg^{-1}). , V250 = 0.82 cm^3g^{-1} ($8.2x10^{-4}$ m^3kg^{-1}) and Dequagel HP = 0.42 cm^3g^{-1} ($4.2x10^{-4}$ m^3kg^{-1}). The difference in void volume resulting from a complete removal of the intraparticle pore volume would be significant.

Rotational rheology performed and discussed in Chapter 6 on slurries containing 30 wt% solids and varying amounts of acid displayed an increase in apparent viscosity and yield stress at high acid contents which was attributed to the gelation of boehmite by nitric acid. It has been considered that the acid content at which the changes occur, and the magnitude of the changes could be used as an indication of a powder's tendency to gel with nitric acid and that this could be used to explain the observed variations in the extent to which the powder responds to the variation in acid concentration within the MTR experiments. In actuality, the gelation behaviour of each of the powders observed within the rotational rheology results is very similar, both in terms of acid content at which a viscosity increase is observed, and the magnitude of the observed increase, this, combined with the issue of variations of MAT data with work input, has prevented any further quantitative analysis being performed in this area.

As discussed previously in Section 2.3.4, the application of work can increase bulk density of powder systems by improving the packing of particles. As seen in Figure 7.2, total work input in a multiple addition test is greater when the mean peak torque occurs at a lower solids content due to the additional time taken to add the liquid (as rate of liquid addition is constant). This is in opposition to the fact that, all other

factors being equal, an increase in work input would result in a drier peak due to the improvements in the particle packing of the system, therefore the work input to the material does not explain the observed trend in the position of the capillary point with pH, i.e. for any given powder, at pH ~ 8 the solids content at the capillary point is lower than at pH ~ 5, despite the fact that this point took longer to reach (due to the constant liquid addition rate), implying a higher work input, which would act to increase the particle packing and reduce the volume of voids to be filled by liquid. The total work input at each of the capillary points has been calculated by measuring the area under the curve up to the capillary point.

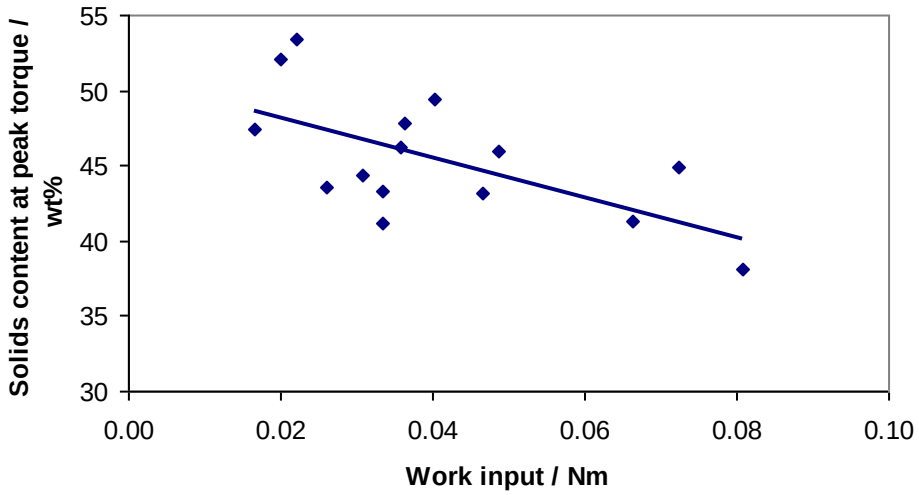

Figure 7.2: Relationship between work input and solids content at peak torque (capillary point)

The relationship between pH and work input can be seen in Figure 7.3. These results highlights the most significant issue with this technique, i.e. that work input varies for each of the peak mean torque positions recorded and as discussed in Section 2.3.4, work input can move the position of the peak mean torque.

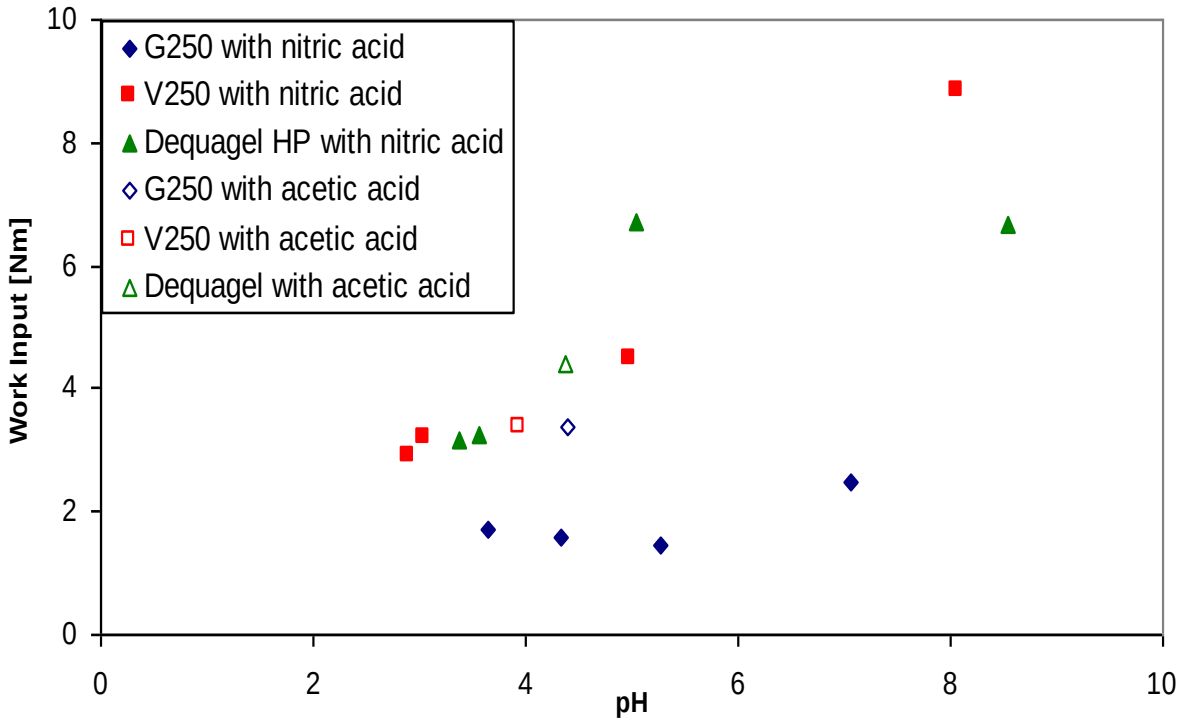

Figure 7.3: Magnitude of work input to reach multiple addition test peak

Chemical dispersion can increase the closeness of packing in a similar way to mechanical dispersion. Qualitatively this would result in a closer packed, drier material at the capillary state with an increase in acid strength, which is in agreement with observations. Closer packing due to the presence of acid is also possible by the mechanism of acid dissolution of boehmite resulting in 'rounding off' of the particles, combined with particle size reduction, resulting in a more effectively packed system. Cryo-SEM images, seen in Chapter 6, confirm the 'rounding off' of particles. The relative dispersiblity of each of the boehmite powders has been measured using an industry standard dispersibility test, as performed by a boehmite manufacturer, this technique is described and discussed previously Section 5.4. The results indicate that variations in the dispersibility of the powders in acid go some way to explaining

the shift observed in the solids content at the capillary point with pH, but it is likely that at least one other phenomena is also involved.

Boehmite is more readily wettable with dilute acid than with water as acid has a lower surface tension than water. In a more wettable system the liquid phase will spread over the solid phase at a faster rate which directionally, due to the inherent nature of the MAT, would result in less liquid addition required to form the capillary state, i.e. a peak mean torque with a higher solids content than a less wettable system. In addition to this, the coverage of powder with liquid results in formation of liquid bridges with capillary forces which may pull the particles closer together and reduce the void volume to be filled by liquid to produce the capillary state.

As discussed in Section 2.3.5 the contact angle between a liquid and a powder can be used as a measure of the wettability of a system. Measurement of this using the DataPhysics tensiometer described in Section 4.3.7 had varying degrees of success with each of the powders. The powder packing consistency of boehmites G250 and V250 was found to be acceptable with packing errors of 7 and 3 % respectively (less than 10 % is considered to be an acceptable error in this technique). However, the Dequagel HP was found to have a packing error of 16 % when packed according to the standard technique, increasing to 33 % when a further 5000 taps were used to pack the powder. This high packing error means that the data obtained for this powder was considered to be unviable for analysis.

The contact angles found for water with the boehmites G250 and V250 were 62 º and 50 º respectively, indicating that V250 is a more readily wettable powder, which would imply a higher solids content at the capillary point as discussed previously.

This is not in agreement with the observed MAT results shown in Figure 7.1, showing that this material parameter is not responsible for the observed variations in solids content at the capillary point. There is no previously published data for the contact angle of water with boehmite powder for these values to be compared to, though Hsiang *et al.* (2007) used boehmite as a surface modifier with anatase and found that the addition of boehmite increased the contact angle of the materials significantly.

Contact angles with 1.0 M nitric and 1.0 M acetic acid were calculated to be close to 90 º (the limit of the instruments' measurement range) in all cases, indicating a non-wetting system. Visually these experiments were observed to uptake a small amount of liquid through the glass frit into the powder but no capillary rise occurred, on cleaning of the samples this bottom layer of powder and liquid was found to be a thick continuous phase rather than a two phase system. Therefore the contact angles calculated by the software for these systems are not valid; the implication of non-wetting behavior from these results is simply due to the lack of liquid uptake due to blocking of the test tube due to the reactive nature of the materials.

According to literature (Hancock, 1991) the distance between the peak torque range and the mean torque peak can be used as an indication of the wettability of a system. It is claimed that a large distance between these points indicates a readily wettable system. Examination of the data produced in this experimental work shows that the peak torque range, indicating the occurrence of the funicular saturation state, occurs at almost the same position as the capillary state in all cases, suggesting that the boehmite / acid system is non-wettable in all formulations

examined. This is not thought to be the case and raises doubts regarding the validity of such an analysis.

Considering each of the phenomena which could explain the observed trends in change of MAT peak mean torque position with pH, it is possible that a combined effect of reduction in pore volume due to gelation, closer packing due to chemical dispersion and increased wettability explain the observed gradients. Alterations in packing due to mechanical energy input cannot explain the increased solids content at the capillary point as already discussed.

7.2.5 Magnitude of Peak Torque

On first inspection the peak mean torque magnitudes appear very similar, with a mean of 0.99 Nm and a standard deviation of 0.27 Nm. However, on closer inspection each powder shows a trend of increasing torque with solids content, and a shift in torque occurs between the different powders.

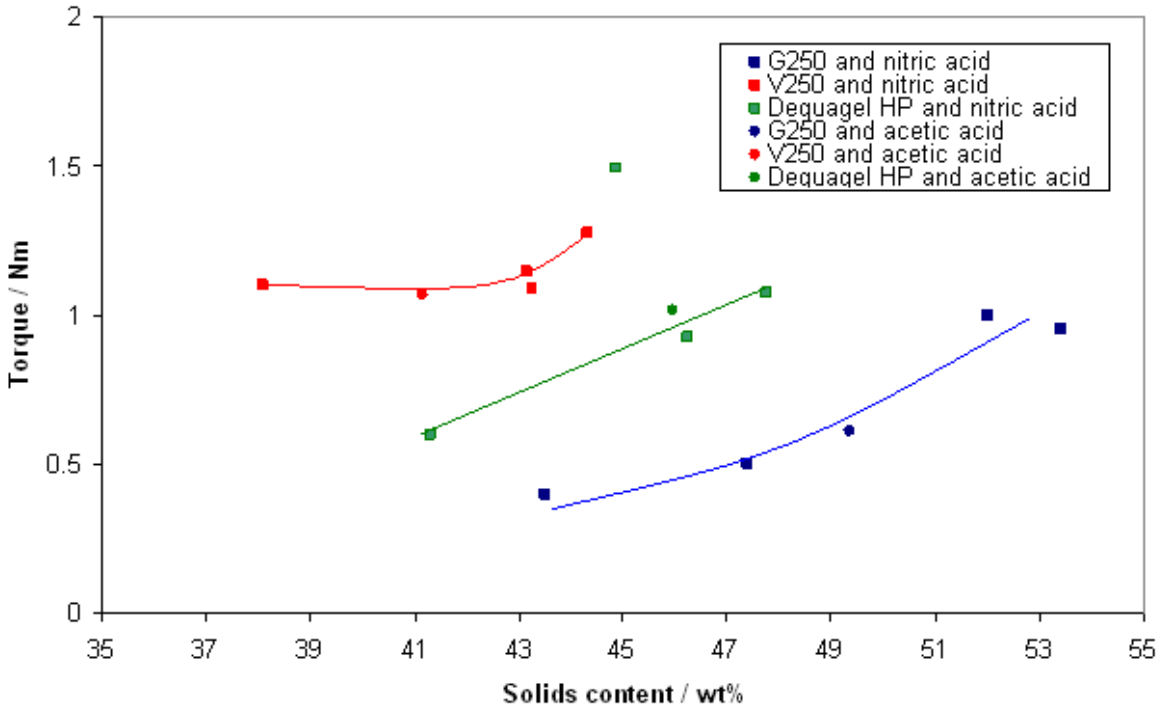

Figure 7.4: Magnitude of torque at capillary point of multiple addition tests

The data displayed in Figure 7.4 indicates that for any particular powder the magnitude of peak mean torque is higher when the peak mean torque occurs at a higher solids content, which has already been shown to increase with acid content. The results obtained with acetic acid indicate that this effect is not anion specific.

The variation of the magnitude of peak mean torque across the range of powders appears counter intuitive; the boehmite G250 shows the highest concentration of solids at the peak but the lowest magnitude of torque. Although boehmite V250 peaks at the wettest formulations, it shows the highest magnitude of torque compared to the other two powders.

The variation between powders can be rationalised by examining the particle size distributions. A formulation containing an equal amount of solids, but with a smaller mean particle size than another, will have a larger number of particles and a larger

number of liquid bridges, with a higher curvature and therefore greater strength in the capillary state.

To verify this hypothesis, MATs with water were performed on ‘as received’ and milled boehmite G250. Particle size distributions were measured before and after the MAT (experimental details in Section 4.3.8). The data shown in Figure 7.5 confirms that a higher torque is observed at the capillary point in the material with a smaller particle size. The results shown in Figure 7.6 also showed that the mixer torque rheometer results in a reduction of particle size, something that is assumed not to be the case in Hancock (1991).

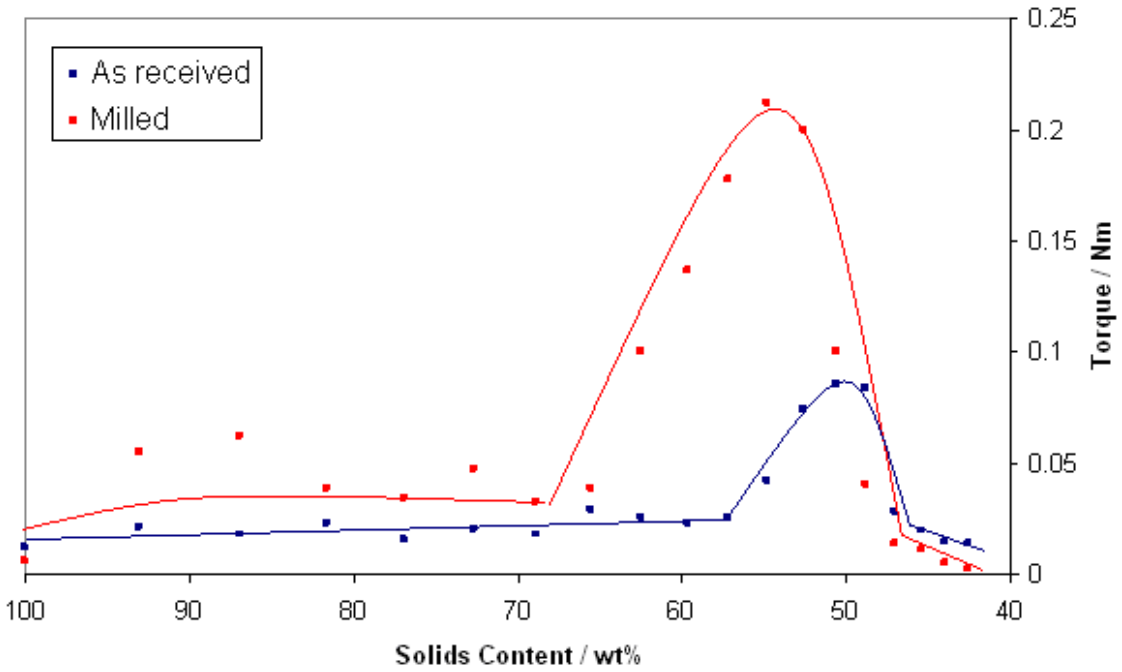

Figure 7.5: Effect of size distribution on mixer torque rheology

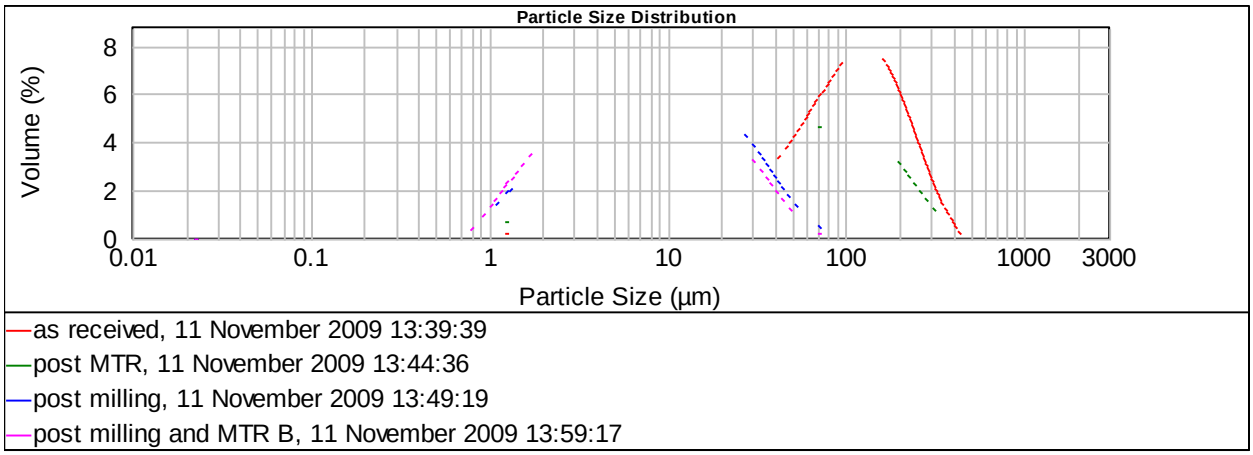

Figure 7.6: Particle size distributions of samples pre and post milling and MTR

7.3 Variable Mixing Time Tests

7.3.1 General Comments on VMT Results

When a variable mixing time (VMT) test is performed on a formulation with significantly more liquid content than is required to reach a capillary saturation state the torque will increase quickly as the materials are mixed into a paste then decrease as the material transforms into the slurry state by mechanical energy and repacking of the particles. As the formulation gets closer to an equilibrium capillary state the torque will increase more gradually as more work input is required to increase the particle packing density to a state which allows the capillary condition with the amount of liquid present. A drier formulation taking longer to peak is illustrated very clearly by the V250 and water system, which can be seen in Figure 7.7. A formulation close to that which is in the capillary state at equilibrium will not only take longer to reach peak mean torque, but will also produce a higher peak. A formulation which has insufficient liquid present to achieve the capillary state of saturation will exhibit a steady climb in torque, reaching a plateau as equilibrium is reached and work input can improve the particle packing no further. When the formulation is too dry to achieve capillary saturation a lower liquid content will

achieve equilibrium more quickly and at a lower torque than a material with a higher liquid content.

Not all of the experiments were performed for long enough for an equilibrium state to be achieved, due to a combination of time limitations on the equipment and consideration of the mixing time of interest, based on the residence time of the extrusion process this investigation pertains to (around 5 minutes). Despite equilibrium state not being reached the shape of the curve up to, and at the point of, the experiments' termination can provide valuable information about the saturation state of the formulation. A quantitative reconstruction of the torque vs. liquid content curve produced from an MAT has not been possible with the data collected, but the results have been given qualitative consideration. A more accurate reconstruction would require variable mixing time tests to be performed on significantly more than 4 liquid contents for each powder liquid combination.

7.3.2 Comparison of Formulations

Each of the data sets displays trends as discussed above, some material combinations display much stronger, more typical trends than others. Figures 7.7 – 7.9 show some typical behaviour as discussed above for particular samples.

Boehmite V250 and water produced clear data, shown in Figure 7.7, with a low level of noise in which each of the experiments reached an equilibrium torque. The results clearly show the equilibrium mean torque and time to reach equilibrium increasing as liquid content is decreased. There is also more noise as the formulation becomes drier. The continuing increase in the magnitude of the equilibrium mean torque indicates that the formulation which produces the capillary saturation state at equilibrium has less than 70 % of the liquid content indicated by

the mean peak torque in the MAT. Figure 7.7 shows each of the formulations reaching a plateau, with the driest formulation taking the longest time to reach the equilibrium. The variations in the shape of the curves prior to the plateau are attrributed to variations in the mixing, particularly evident in the behaviour of the red curve which displays an apparent plateau between 30 and 150 s, this is due to poor initial mixing of the materials.

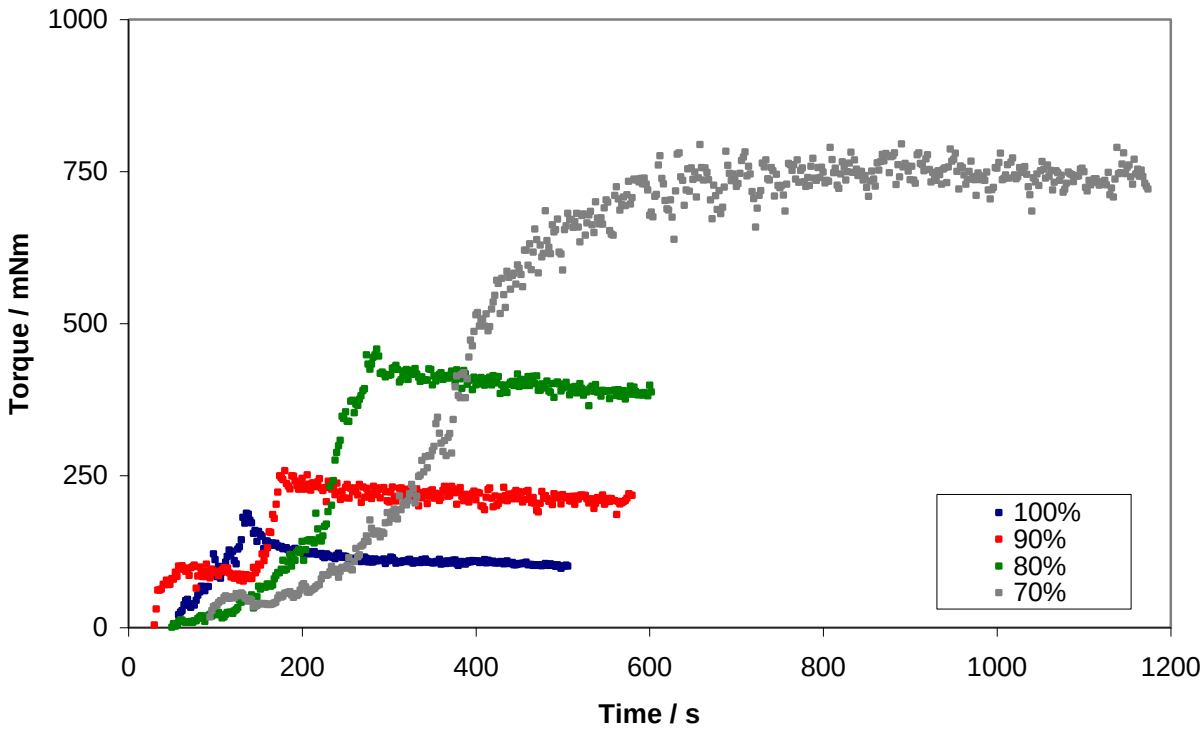

Figure 7.7: VMT data for V250 and water at different liquid contents (% in legend indicates the liquid content as a % of that shown to produce the capillary saturation state in the multiple addition test)

The data produced by boehmite Dequagel and water can be seen in Figure 7.8. The samples prepared with 100 % of the liquid content of the MAT peak mean torque quickly increased in torque and then moved into the saturated state due to the excess liquid, hence the short sharp peak followed by a low torque. When the

moisture content was reduced to 90 % of the liquid content of the MAT peak mean torque, the torque increased steadily for ~ 400 seconds before the excess liquid and work input caused the formulation to transform into the droplet state and torque reduced. At 80 % and 70 % the torque increased steadily to a value higher than that of the 90% sample and remained at a constant high torque for over 600 seconds of mixing before reducing indicating the materials have formed the slurry state.

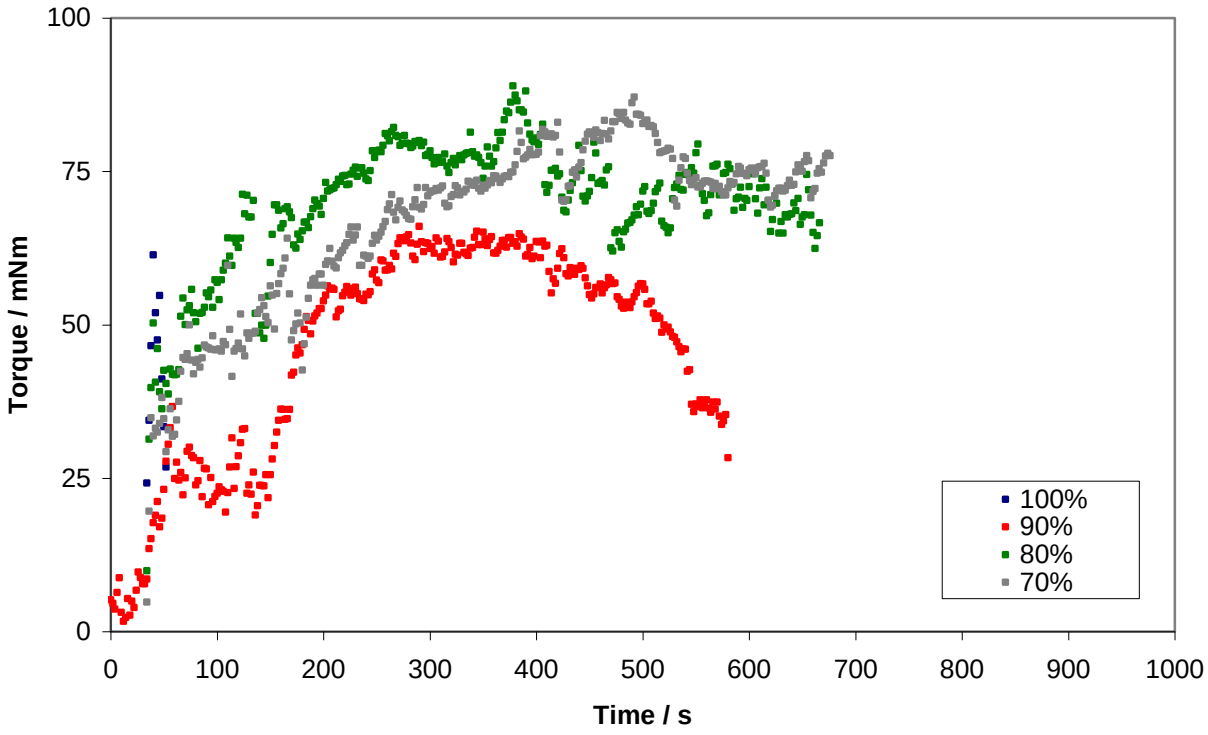

Figure 7.8: VMT data for Dequagel and water at different liquid contents (% in legend indicates the liquid content as a % of that shown to produce the capillary saturation state in the multiple addition test)

A further example of a typical curve produced using this technique is that produced by Dequagel HP and acetic acid seen in Figure 7.9. Similar curves were also produced by Dequagel HP with 0.72 M nitric acid and 1.0 M nitric acid. As the formulation becomes drier, it takes longer, i.e. more work input is required, for the

torque to peak and drop as the saturated state is reached. With 70 % of the liquid content required to reach the peak mean torque in the VMT, the torque almost equilibrates, the shape suggests that the saturated state has been reached as the torque is gradually reducing with time.

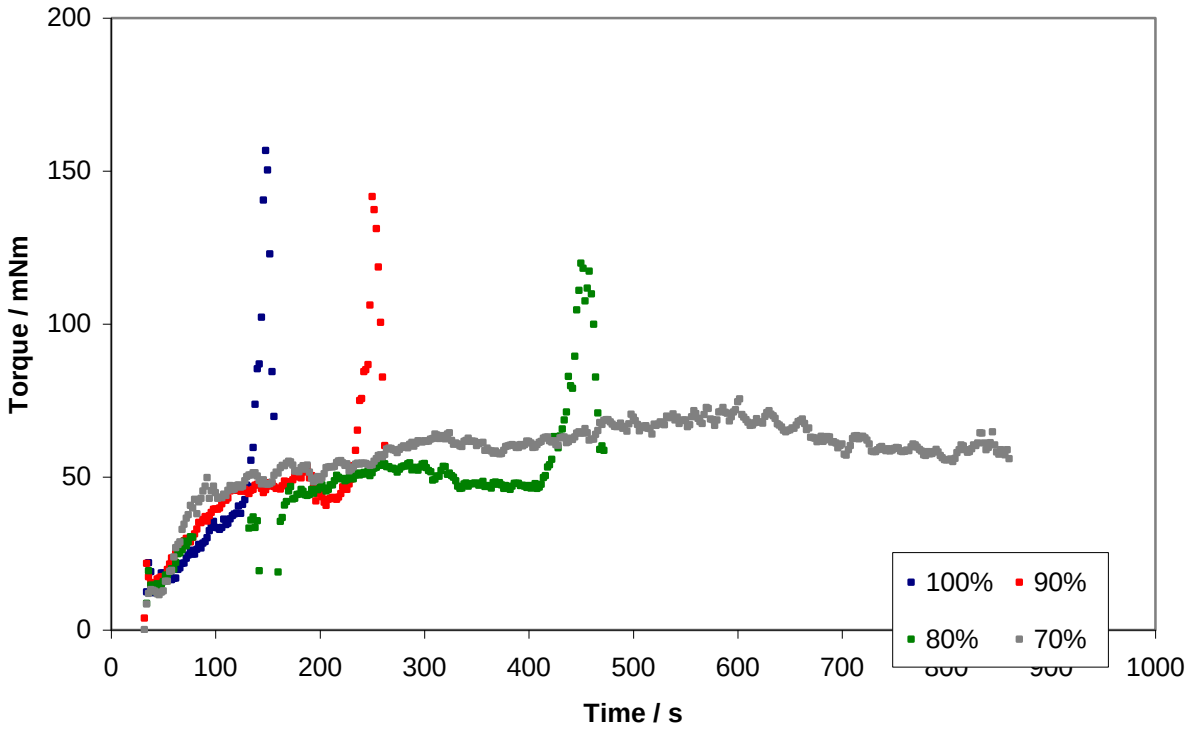

Figure 7.9: VMT data for Dequagel HP and acetic acid at different liquid contents (% in legend indicates the liquid content as a % of that shown to produce the capillary saturation state in the multiple addition test)

The shapes of the curves displayed in Figures 7.7 - 7.9 are all different, the data in Figure 7.7 suggests that the sample prepared with 70% of the liquid content of the MAT peak is approaching an equilibrium condition at the level of work input provided, however more data curves would be needed to suggest how close to the capillary condition this material is. In Figure 7.8 none of the samples prepared display an equilibrium condition, the continued work input results in each of the samples forming the slurry state. Similarly, all but the driest of samples in Figure 7.9 show a

material moved into the slurry state by work input, the sample prepared with 70% of the liquid content of the MAT peak appears to be approaching an equilibrium but, as was the case in Figure 7.7, there is no way of knowing how close to the capillary condition this material is.

For many of the material systems the combination of the high degree of noise, and the experimental setting to automatically end the experiment when torque fell to 50% of a previous max, led to many of the VMT experiments being stopped before an equilibrium was reached, therefore much of the data has had to be disregarded. This situation has meant that a quantitative analysis has not been performed on the data. In order to perform an informative reconstruction of the MAT curve a larger data set similar to that in Figure 7.7 would have to be collected.

7.4 Comparison of MTR Characterisation with Rotational Rheology

MTR data can be converted to give an apparent viscosity by converting speed of rotation into a shear rate and torque into a shear stress. This has been calculated for each of the mean peak torques obtained and also for various other specific data points, for which a comparable formulation has been assessed using rotational rheology, to allow a comparison between the results obtained in each technique.

$$\eta_{app} = \frac{\tau}{\dot{\gamma}} \quad \text{.....(equation 7.5)}$$

$$\tau = \frac{Force}{Area} = \frac{Torque}{Volume} \quad \text{.....(equation 7.6)}$$

where, torque is the measured torque on the MTR and volume is the volume of material within the mixing chamber at the time of the measurement.

$$\dot{\gamma} = \frac{Velocity}{Distance} \quad \text{(equation 7.7)}$$

where, velocity is taken as the tip velocity of the fastest moving paddle and distance is taken as the clearance between the paddle and the wall of the mixing chamber (0.001 m), though in reality the mixing action of the MTR causes compression and expansion of the material within a changing gap. The tip velocity is calculated according to equation 7.8

$$Velocity = \frac{rs \times 2\pi r}{60} \quad \text{(equation 7.8)}$$

where, rs is the paddle rotation rate (125 rpm) and r is the paddle radius (0.015 m), resulting in a shear rate of 196 s^{-1}.

The apparent viscosities at 196 s^{-1} obtained by performing the calculation described on the capillary point of each of the formulations examined can be seen in Figure 7.10. The apparent viscosity generally increases as pH reduces, it is not clear whether this is due to the increase in solids content which accompanies this change, or the increase in the presence of acid. It is not possible with the data available to decouple these two parameters.

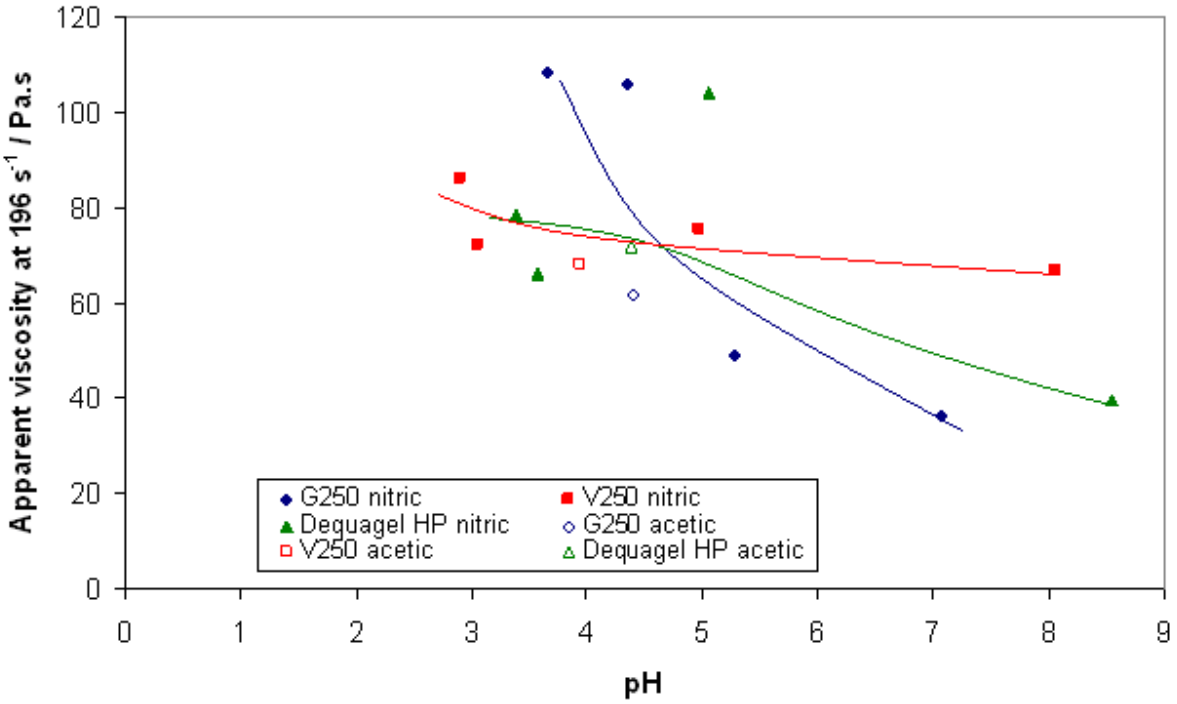

Figure 7.10: Apparent viscosity at 196 s^{-1}, from MTR capillary point data

A more interesting calculation would be the apparent viscosity at 196 s^{-1} of the formulations in the MTR at 30 wt% solids, which would allow a more direct comparison with the rotational rheology data discussed in Chapter 6. Unfortunately the procedure of the MAT is such that the formulation commences at 100 wt% solids and reduces over time. In all cases the peak mean torque was observed at a solids content higher than 30 wt% and the experiment ceased when the torque value reduced to 50 % of the maximum, still at a solids content higher than 30 wt%, therefore this direct comparison is not possible.

7.5 Conclusions

7.5.1 Taguchi Experiments

Taguchi experimental design has been used to determine the effect of five input variables (powder type, liquid type, liquid addition rate, paddle rotation rate and temperature) on two output parameters (magnitude of the peak mean torque and the solids content at the peak mean torque). It was found that the liquid type and liquid addition rate had the most significant influence on the magnitude of the peak mean torque and the powder type had the most significant influence on the solids content of the peak mean torque. Paddle rotation rate and temperature were found to have low impact on both output parameters.

7.5.2 Comparison of Formulations

The bulk and skeletal densities of each powder have been used to predict the solids content at the capillary point found from MATs with water. The tapped bulk density was found to give a more accurate prediction than the poured bulk density, attributed to the work input and particle rearrangement performed by the action of the mixing paddles. The discrepancies between the predicted and measured solids content have been related to the cohesiveness (indicated by the Hausner ratio) of each of the boehmite powders.

The solids content at the capillary point increased as the pH of the binder phase was reduced, this affect appears to be non anion specific. A number of possible mechanisms have been identified as being responsible for the shift in capillary point; reduction of available pore volume due to blockage of intraparticle pores, improvements in particle packing by mechanical work input or chemical dispersion and differences in the wettability of a powder liquid system.

The nature of the test means that work input cannot be used to rationalise the observed trends in the MAT data, though the dispersive action of acid on boehmite supports the alteration of particle packing by chemical dispersion. The highly porous nature of the powders means significant variations in the solids content at the capillary point are possible by making the intraparticle pore volume inaccessible by blocking of pores.

Contact angles between boehmites G250 and V250 and water have been successfully measured as 62° and 50° respectively, though measurements with the boehmite Dequagel HP or acid were unsuccessful. As it has not been possible to take contact angle measurements with acid, it is not clear whether a change in wettability is responsible for the variation in the position of the capillary point as acid content is altered. The indication that the boehmite V250 is a more readily wettable powder than the boehmite G250 implies a higher solids content at the capillary point according to the theory discussed in Section 7.2.4, which is not in agreement with the experimental observations, therefore this phenomenon can not be used to rationalise the observed differences between the powders.

The variation of the magnitude of torque at the capillary point for each of the powders can be rationalised by differences in the particle size distributions. Variations in size distribution have been shown to affect the results obtained in an MAT, and the size distribution of a powder has also been shown to be altered during a MAT.

Much of the VMT test data obtained was redundant for detailed analysis as the experiments had not continued into an equilibrium state. Those data sets which

displayed equilibrium conditions showed higher torques, reached more slowly, when a drier formulation was tested. VMT tests at much smaller increments of liquid content would need to be performed to reconstruct a torque vs. solids content relationship as produced by the MAT.

7.5.3 Comparison of MTR Results and Rotational Rheology Data

Conversion of torque measurements to apparent viscosity has allowed a comparison to be made between rotational rheology data and MTR data. The apparent viscosities calculated in the MTR are at a shear rate of 196 s^{-1}. Apparent viscosities at the capillary point range from 40 – 110 Pa.s.

The data required to calculate the apparent viscosity of slurries with 30 wt% solids is not available, preventing direct comparison with the rotational rheology data discussed in Chapter 6.

7.5.4 Relevance of MTR Results to Extrusion Formulations

The issue of work input affecting the state of saturation of a material formulation has been discussed at various points within this chapter. There are significant differences between the work applied by a twin screw extruder and an MTR, therefore a direct correlation between the prediction of capillary point from a MTR and a successful extrusion formulation on a twin screw extruder is not expected. Further examination of this relationship is performed in Chapter 8.

Chapter 8 Extrusion

8.1 Extrusion Formulations

Solids content and acid content are inherently related for a particular powder type and acid strength combination. The relationship between these parameters can be seen in Figure 8.1. This data is not of significant interest in its own right, however this figure isw designed to aid with the visualisation of the relationship between acid content and solids content throughout this set of experiments, as this will help with understanding the following discussions. As it has not been possible to accurately measure the pH of the extrudates produced the acid content is described as the molar ratio of acid to boehmite, assuming full dissociation of acid, (an accurate assumption for nitric acid, not for acetic acid due to acid strength) and corrected for the mass loss during drying of the boehmite powders. Solids contents reported have also been corrected for the mass loss during drying.

Figure 8.1 shows that the boehmite Dequagel HP is extruded at the highest solids content with water, 0.36 M nitric acid and 1.0 M acetic acid. Extrusions with 0.72 M and 1.0 M nitric acid occur at very similar solids content to boehmites G250 and Dequagel HP. In general the boehmite V250 is extruded at the lowest solids content. This graph is comparable to Figure 7.1 showing the solids content at the peak mean torque identified by the MTR as a function of pH, a comparison between these data sets is presented and discussed in Section 8.2.

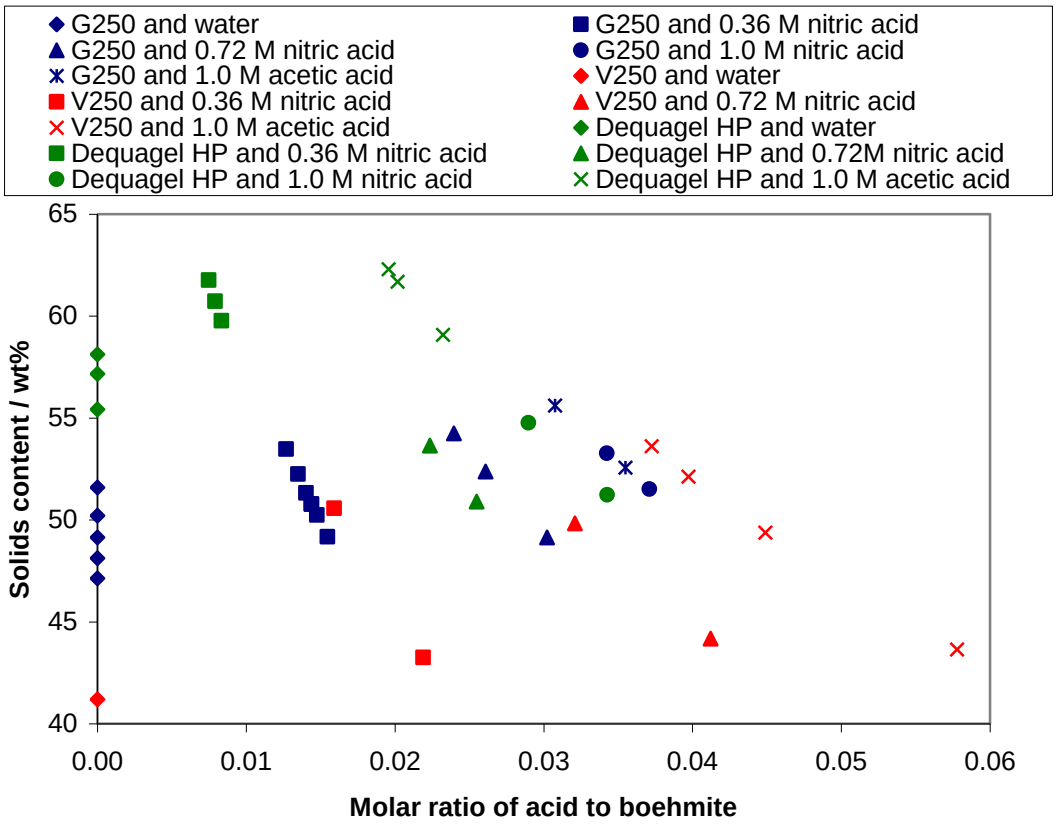

Figure 8.1: Relationship between solids content and acid content of extruded formulations

Figures 8.2 and 8.3 show the relationship between the formulation parameters (solids content and acid content) and a production parameter (torque on twin screw extruder). Figure 8.2 reveals that for a particular system (a combination of a particular powder and liquid) an increase in solids content results in an increase in the extrusion torque, highlighted for certain systems with enlarged data points and best fit lines. This relationship is in agreement with the observations reported by Köster and Thommes (2010). Figure 8.3 shows that for any particular system, an increase in the acid content (note that the scale is molar ratio of acid to boehmite, not pH) results in a decrease in the extrusion torque, a result which can be rationalised by considering the reduction in solids content which inherently

accompanies the increase in acid content when using the same acid strength, as shown previously in Figure 8.1.

Figures 8.2 and 8.3 also both illustrate how a wide variety of solids contents can be extruded at a given extrusion torque depending on the particular powder type and acid strength. In particular, very high solids content extrudates can be produced at low extrusion torques using the boehmite Dequagel HP compared with the boehmites G250 and V250.

The close particle packing required to produce an extrudate with a high solids content can be achieved by either mechanical work input or chemical dispersion of agglomerates. The low extrusion torque, implying low mechanical work input, suggests that the mechanism responsible for achieving the close packing in the boehmite Dequagel HP is chemical dispersion of agglomerates. The dispersiblity test presented and discussed in Section 5.4 confirms that the boehmite Dequagel HP is the most susceptible to dispersion by nitric acid.

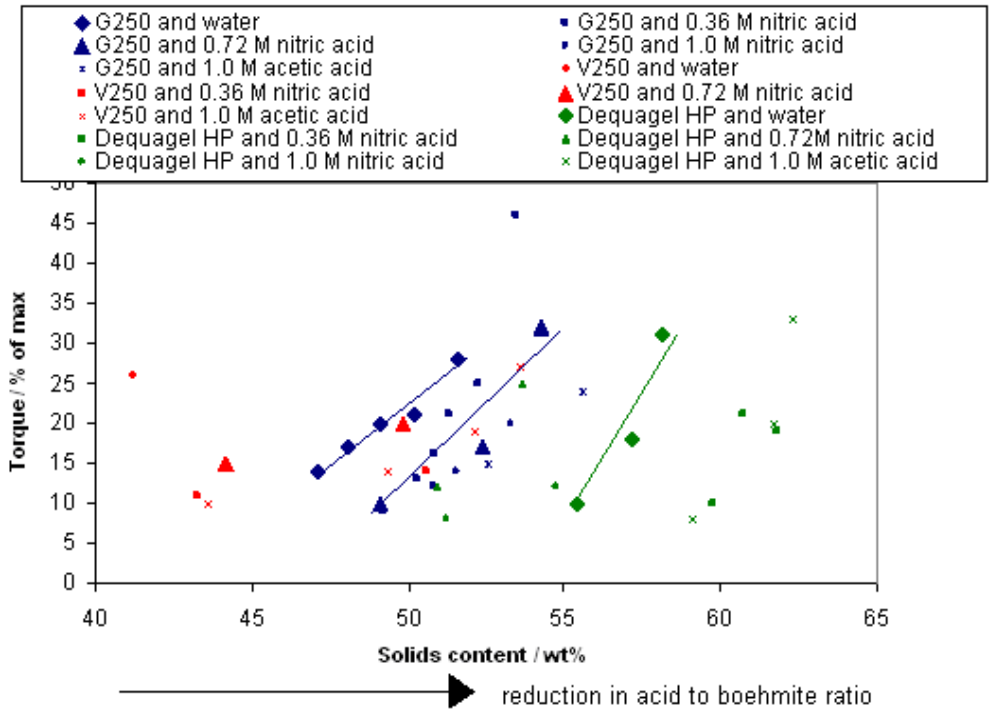

Figure 8.2: Relationship between torque of twin screw extruder and solids content

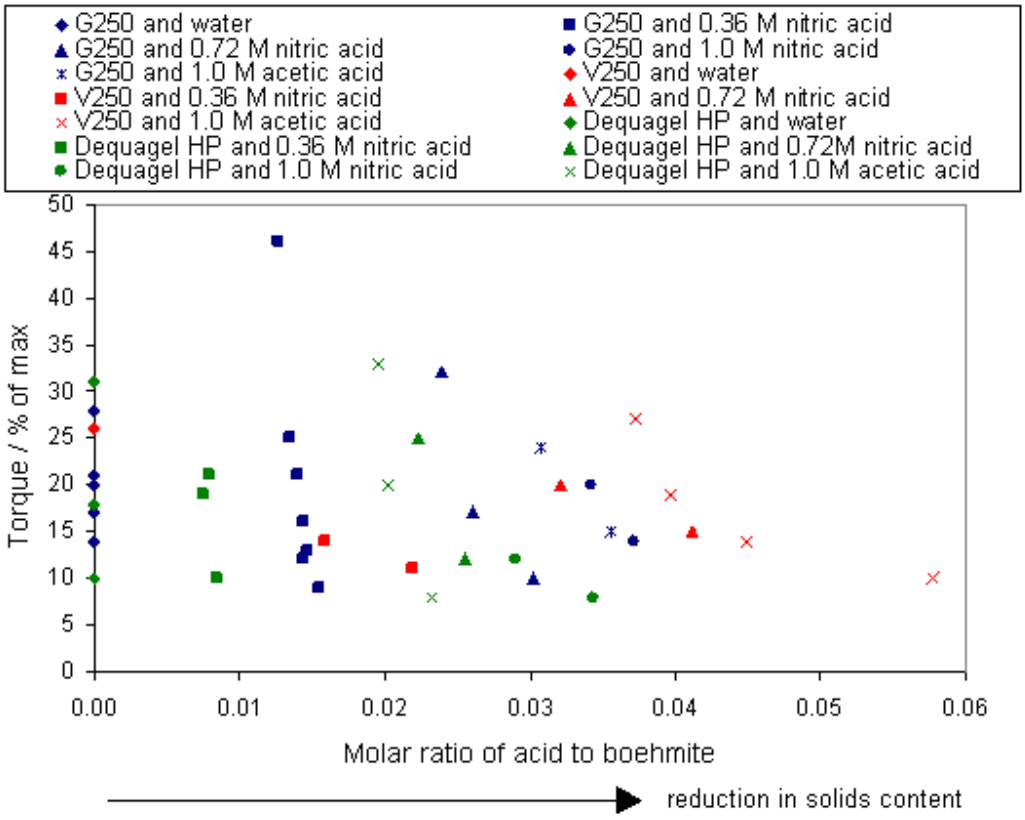

Figure 8.3: Relationship between torque of twin screw extruder and acid content

Photos of samples could not be included, however photos of typical extrudates similar to those produced in this work, of various qualities, can be seen in Benbow and Bridgwater (1993).

8.2 Comparison of MTR Predictions and Extrusion Formulations

Table 8.1 shows the difference between the solids content shown to form the capillary state suitable for extrusion by the MTR (results presented and discussed previously in Chapter 7) and the solids contents found to produce extrudable pastes by twin screw extrusion. This is essentially the difference between the data displayed in Figure 8.1 and Figure 7.1, calculated using equation 8.1. The capillary point on the MTR is a defined position, where as the twin screw extrusion data is subjective and the highest solids content is the closest to the capillary point. The highest solids content extruded is used in the calculation as any value below this would be entirely arbitrary as it is known to be below the capillary point.

$$TSE_{HSC} - MTR_{CP} \quad \text{.....(equation 8.1)}$$

where, TSE_{HSC} is the highest solids content extrusion performed on the twin screw extruder and MTR_{CP} is the solids content at the capillary point found by the multiple addition test performed on the MTR.

A discrepancy between the MTR and twin screw extrusion results was expected, due to the difference in the amount of work applied to the material in each process. The MTR consistently predicted a lower solids content than those successfully extruded, implying a lower work input from the MTR than the TSE. Neither is the work input

applied by each of the techniques consistent across the range of formulations, as the work input is related to the torque which varies in each case. As discussed in Section 2.3.4, the work input to a system affects a materials' state of saturation by altering the particle packing behaviour.

A comparison of the work input per unit mass ($Nmkg^{-1}$) using the MTR and the TSE has been attempted using equations 8.2 and 8.3 respectively. However, the torque reading taken from the TSE is not a true measure of torque, it is a comparative value derived from the voltage drawn by the extruder in operation. Independent torque measurements from the extruder shaft would be required to make a true comparison of the torques drawn in each of these techniques.

$$WI_m = \frac{WI_c.s}{m} \quad \text{.....(equation 8.2)}$$

$$WI_m = \frac{T.r}{\dot{m}} \quad \text{.....(equation 8.3)}$$

where, WI_m is work input per unit mass, WI_c is the work input to the capillary point measured on the MTR, m is the mass of sample present in the MTR, s is the MTR paddle rotation rate, T is the extrusion torque, r is the extruder screw speed and $\dot{m}$ is the total mass flow rate of material in the extruder.

Table 8.1 shows that the discrepancies observed are < 20 %. In general the boehmite G250 exhibits the smallest discrepancy and Dequagel HP the largest, which can be explained by the difference in cohesiveness. This variation in powder behaviour has been discussed previously in Section 7.2.2 when attempting to predict the solids content at the capillary point by considering the bulk and skeletal powder

densities. Cohesiveness affects a powder's susceptibility to particle packing alteration by either mechanical energy input or liquid addition. The Hausner ratios, as previously discussed in Section 7.2.2, shows that qualitatively G250 is the least cohesive powder, therefore the least susceptible to packing alterations. On this principle the results shown in Table 8.1 are as expected.

The discrepancy reduced as the strength of nitric acid is increased. The use of 1.0 M acetic acid results in a discrepancy similar to that exhibited with water for the boehmites G250 and Dequagel HP, and a much larger discrepancy with the boehmite V250. Assuming that the work input is the principal cause of the discrepancy this result suggests that this effect becomes less significant as the formulation becomes more acidic, i.e. chemical alteration of the system reduces the significance of the effect of mechanical energy input on the particle packing.

Table 8.1: Discrepancy between predicted solids content of extrusion formulation by MTR and actual solids content extrused on TSE, wt %

	Water	0.36 M nitric acid	0.72 M nitric acid	1.0 M nitric acid	1.0 M acetic acid
G250	8	6	2	0	6
V250	3	7	7	Not performed	12
Dequagel HP	17	17	7	7	16

8.3 Conditions of Extrusion

Figure 8.4 shows the relationship between twin screw extrusion torque and ram extrusion force. An increase in the torque required to produce a paste on the twin screw extruder unsurprisingly results in an increase in the force required to form extrudates on the ram extruder. The fact that the data does not lie on one master curve suggests that the relationship is formulation dependent. Best fit lines for each data set intersect the x-axis at around 7 % maximum torque suggesting this as a base line torque value for the extruder operating with an empty barrel.

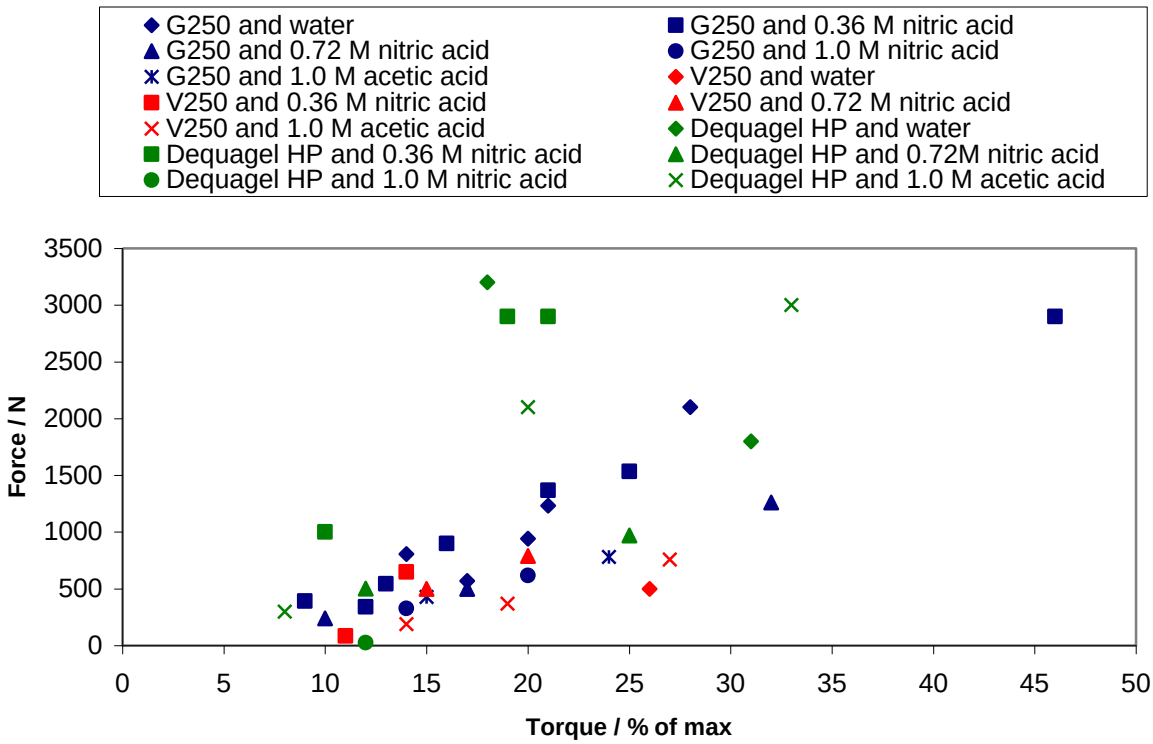

Figure 8.4: Relationship between torque on TSE and force on ram extruder

8.4 Physical Properties of Extrudates

8.4.1 Crush Strength

Figures 8.5 and 8.6 show the relationship between formulation parameters (solids content and acid content) and extrudate crush strength. An increase in solids or acid

content results in an increase in crush strength, presumed to be due to an improvement in particle packing and the binding action of the gelatinous phase formed in an acidic boehmite paste (discussed in Chapter 5) respectively.

Figures 8.7 and 8.8 show the relationship between processing parameters (torque during twin screw extrusion and ram extrusion force) and extrudate crush strength. Strength appears to be almost independent of the torque on the TSE, and only increases very slightly with ram extrusion force for each powder liquid combination. It was expected that a high extrusion force would produce a strong extrudate, however, this relationship is not evident from the results.

The relationship between strength and porosity is discussed in Section 8.5.2, strength is significantly affected by presence of surface defects, illustrated by Griffiths Crack theory which relates strength and toughness and takes into consideration the size of a surface fault. It has been considered to use the Weibull modulus to examine the probability of failure of the samples, however the sample size was not sufficiently large.

These results show that the formulation has a more significant effect on the crush strength of an extrudate than the processing parameters. The nature of the experiments performed means that each of the parameters remain interrelated, a clearer understanding of the factors affecting crush strength could be elucidated by examining the parameters individually.

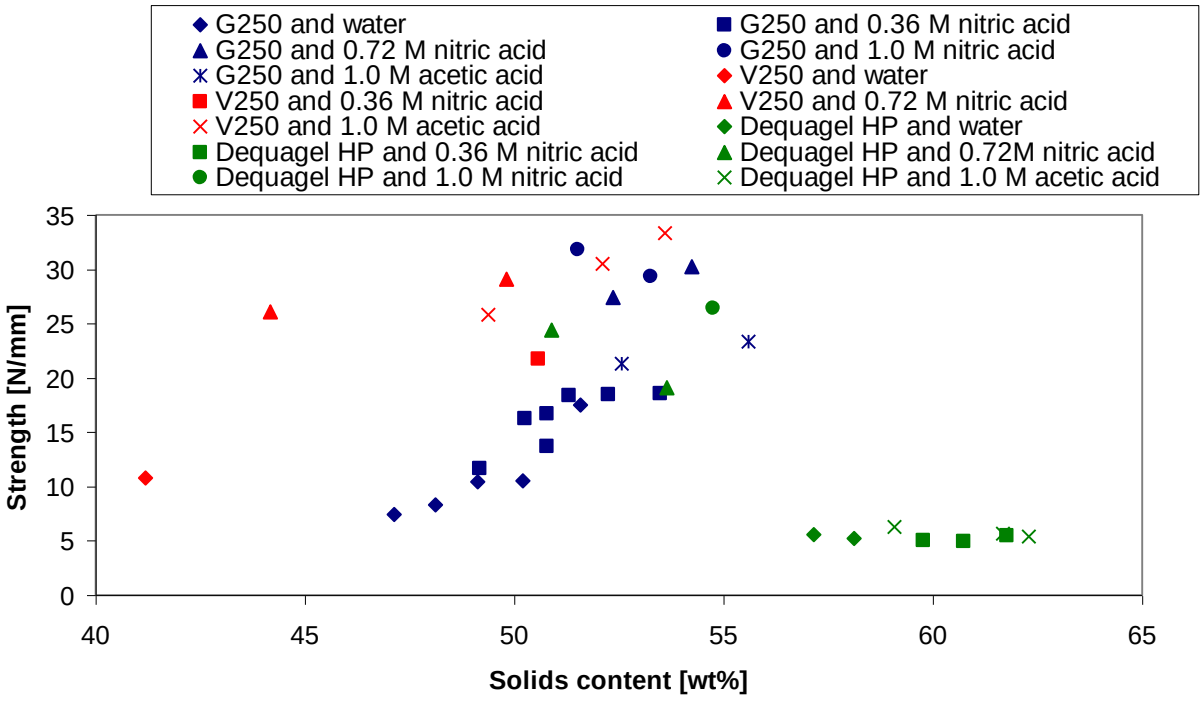

Figure 8.5: Effect of solids content on extrudate strength

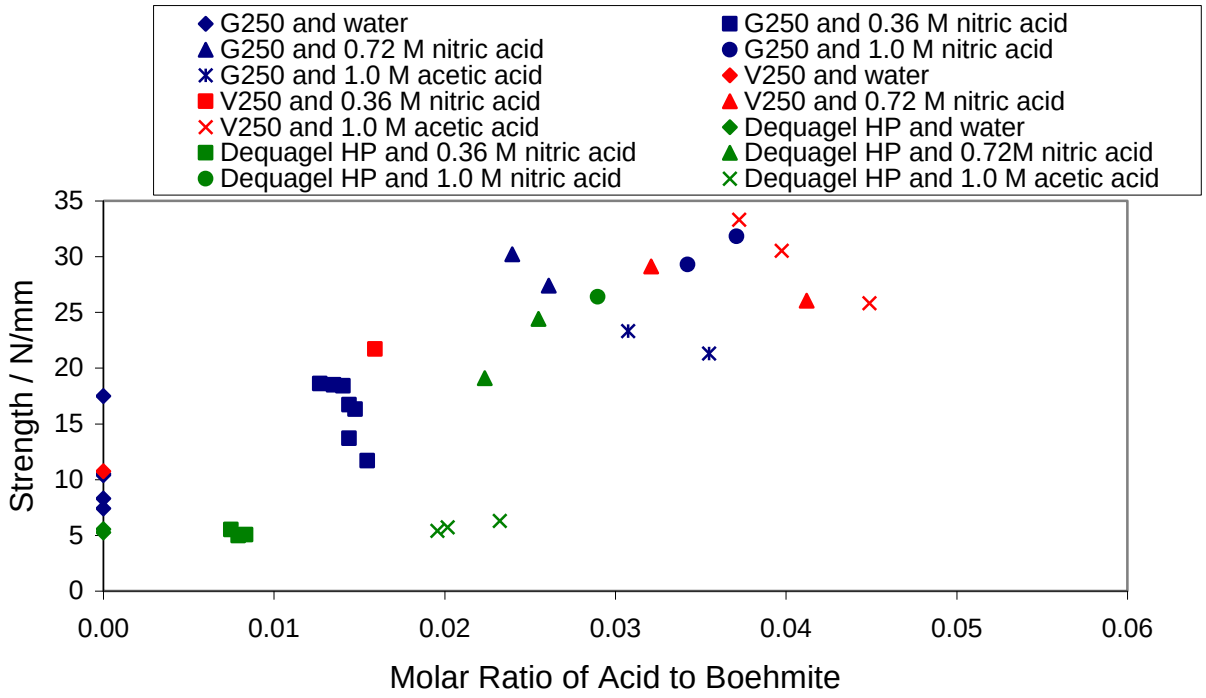

Figure 8.6: Effect of acid content on extrudate strength

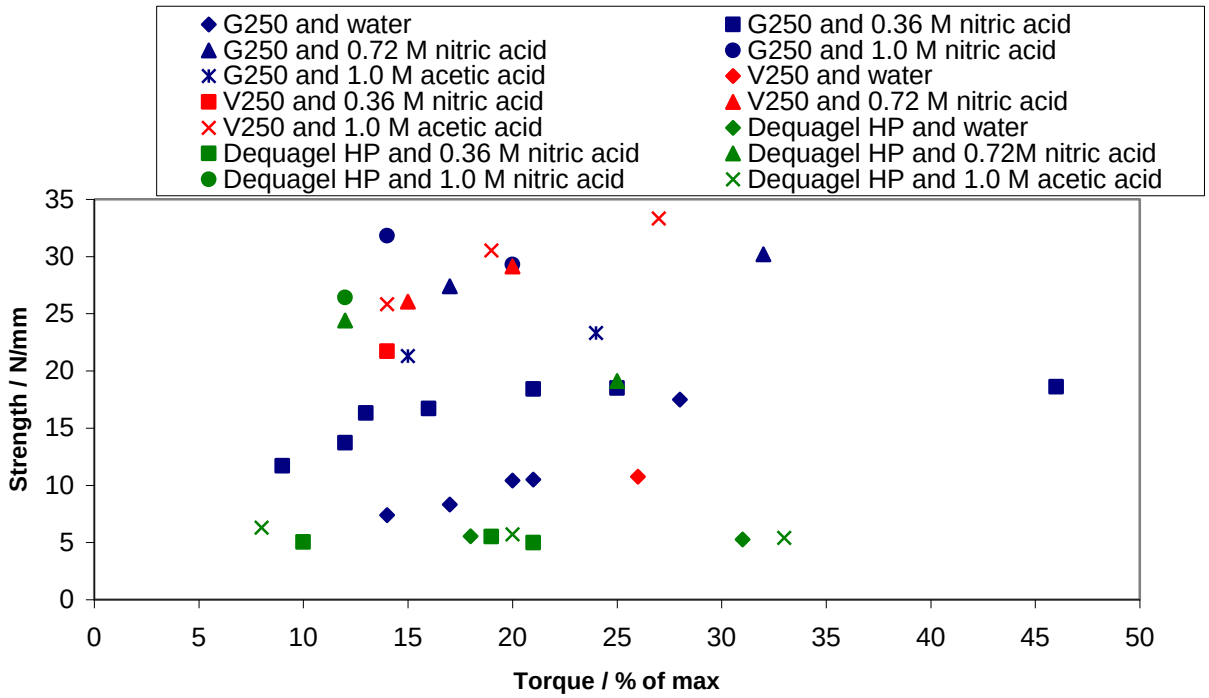

Figure 8.7: Effect of twin screw extruder torque on extrudate strength

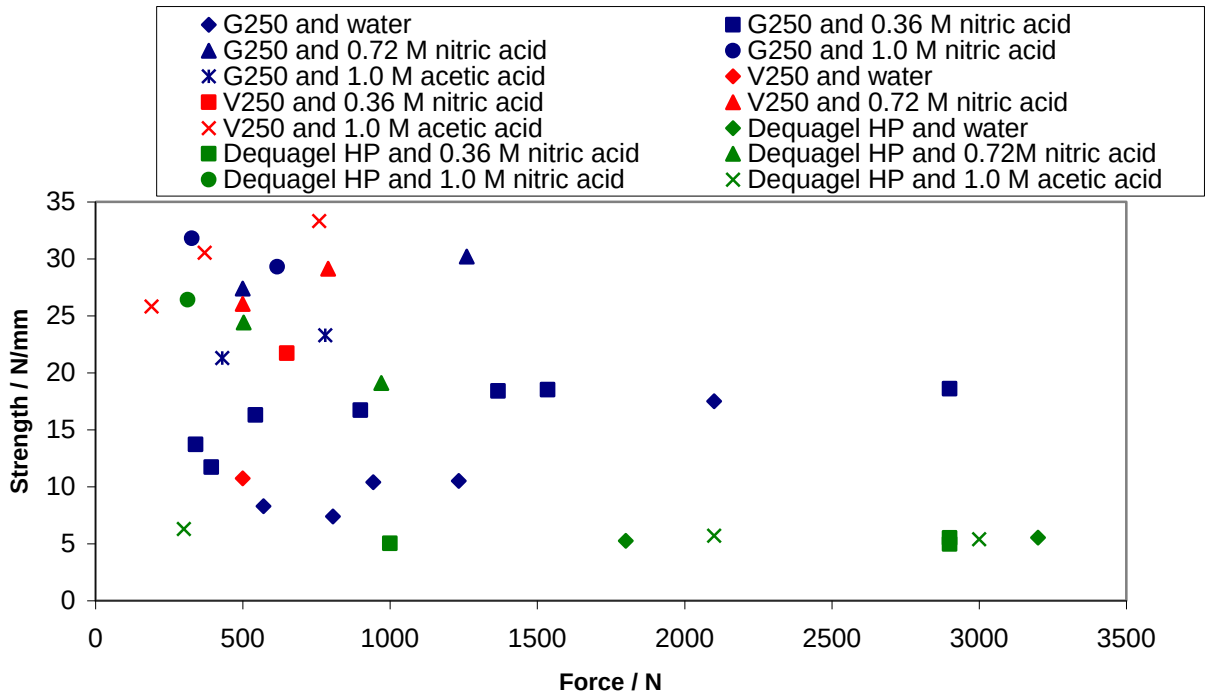

Figure 8.8: Effect of ram extruder force on extrudate strength

8.4.2 Porosity

Figure 8.9 shows how the total pore volume of an extrudate, measured by nitrogen adsorption, varies with solids content of the extruded paste. An increase in solids content causes a small reduction of pore volume, which asymptotes at around 0.5 cm^3g^{-1}, though Dequagel HP exhibits a consistently low pore volume of between 0.3 and 0.5 cm^3g^{-1}. Similar trends are displayed in the total pore volume obtained by mercury intrusion, analysis has focused on pore volume measured by nitrogen adsorption.

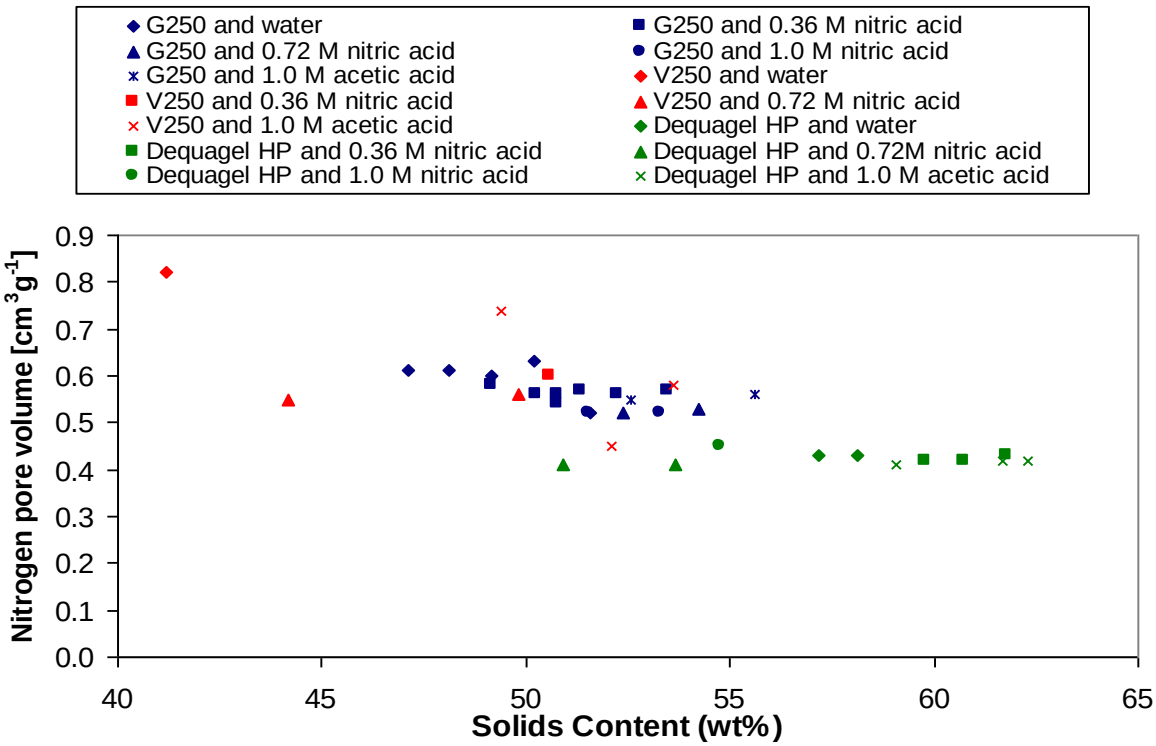

Figure 8.9: Porosity as a function of solids content

The pore size distributions are similar for a particular system (specific combination of powder and liquid), regardless of solids content. However, some sample sets exhibit behaviour as displayed in Figure 8.10, indicating a reduction in pores 10 – 20 nm in size, accompanied by an increase of pores 2 - 6 nm in size, as solids content is

increased. Although this shift appears to be small it is believed to be real by the author based on the number of samples whitch exhibit this shift, not only within this project but other similar samples to which the author has had access. This shift suggests an increase in the closeness of packing, reducing the volume of larger pores and increasing the volume of smaller pores. An increase in solids content under the operating conditions used to produce these samples is inherently accompanied by a reduction in the ratio of acid to boehmite; hence the shift cannot be attributed to an increase in chemical dispersion, rather an improvement in packing density due to the physical presence of more particles.

None of the samples exhibit a plateau as the limits of the technique are reached, implying there is further pore volume present in pores less than 1.7 nm, not detected by nitrogen adsorption. Cumulative pore size distributions of the mesoporous range (2 – 50 nm) are displayed. The volume of pores between 50 – 300 nm removed from the raw data is minimal, less than 0.06 cm^3g^{-1} in all cases. All powders exhibit a reduction in total pore volume as acid strength is increased.

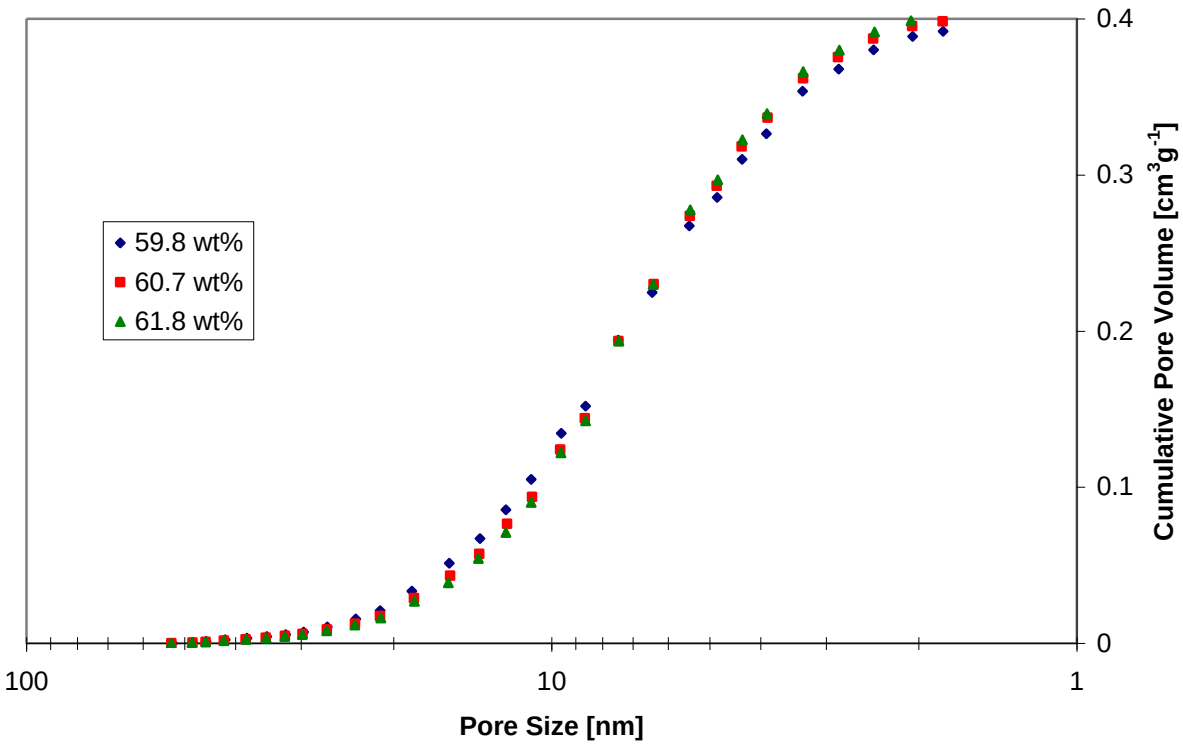

Figure 8.10: Cumulative pore size distribution for Dequagel HP and 0.36 M nitric acid extrudates as a function of solids content

The effect of acid type and strength on the pore size distribution, within the mesoporous size range, of each of the boehmite powders can be seen in Figures 8.11 - 8.13. Each of the pore size distributions displayed for comparison are those of the sample extruded at the highest solids content for each combination of powder and liquid. In Figure 8.11, the pore size distribution of extrudates produced with G250 shows a steady shift and reduction of pore volume as the acid strength is increased. Extrudates produced with V250, shown in Figure 8.12, exhibit a significant change in the pore size distribution when acid is used to produce the extrudates compared to those prepared with water, however, increasing the strength of acid further does not have a significant effect. Extrudates produced with Dequagel HP, shown in Figure 8.13, display very similar pore size distributions when prepared with water, 0.36 M nitric acid or 1.0 M acetic acid and a reduction in the

volume of pores smaller than 10 nm in samples prepared with stronger nitric acid. For each of the boehmite powders the pore size distribution with 1.0 M acetic acid lies in between those with 0.36 M and 0.72 M nitric acid, as was the case in the MAT peak position and pH shown in Figure 7.1. This suggests that the mechanism responsible for the shift in pore size distribution is not anion specific.

Reduction in the pore volume with an increase in acid strength is attributed to an increase in the chemical dispersion of boehmite agglomerates (dispersiblity of boehmites is discussed previously in Chapter 5) reducing the particle size and increasing the particle packing density. This is supported by an increase in the pore volume of the smallest pores, < 2.2 nm, as shown in Figure 8.14 and a reduction in the average pore size as shown in Figure 8.15.

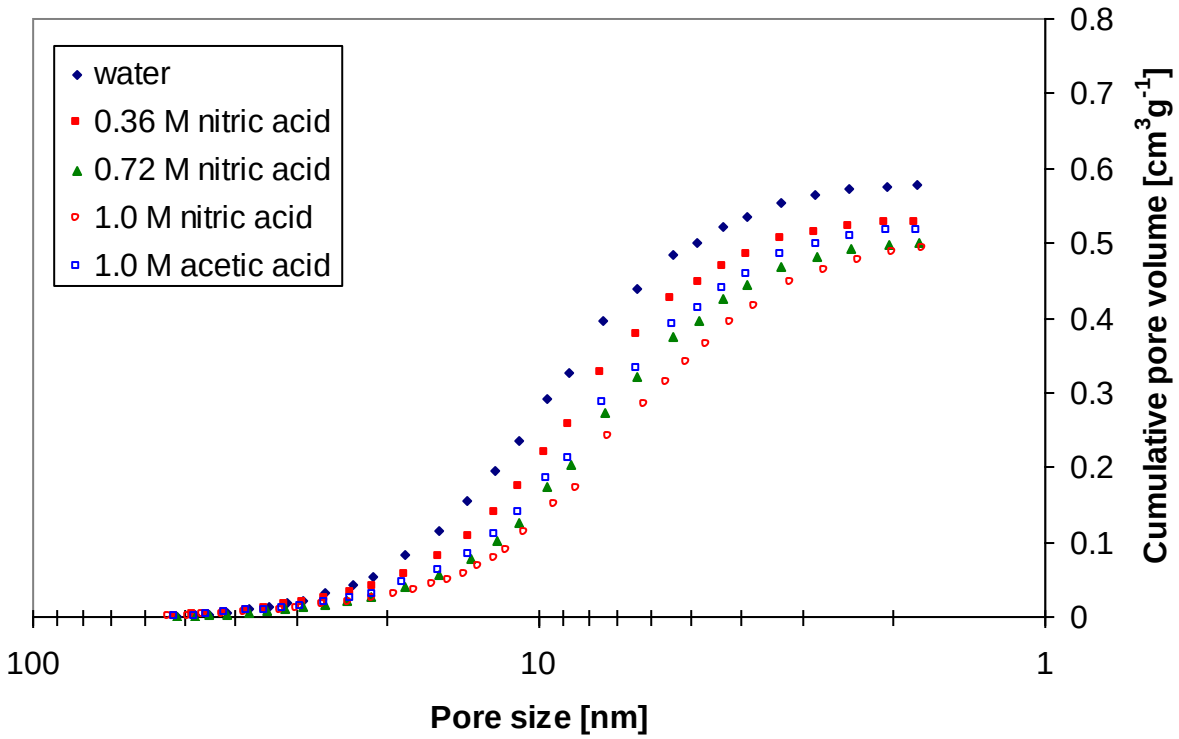

Figure 8.11: Pore size distributions for G250 extrudates with all binders

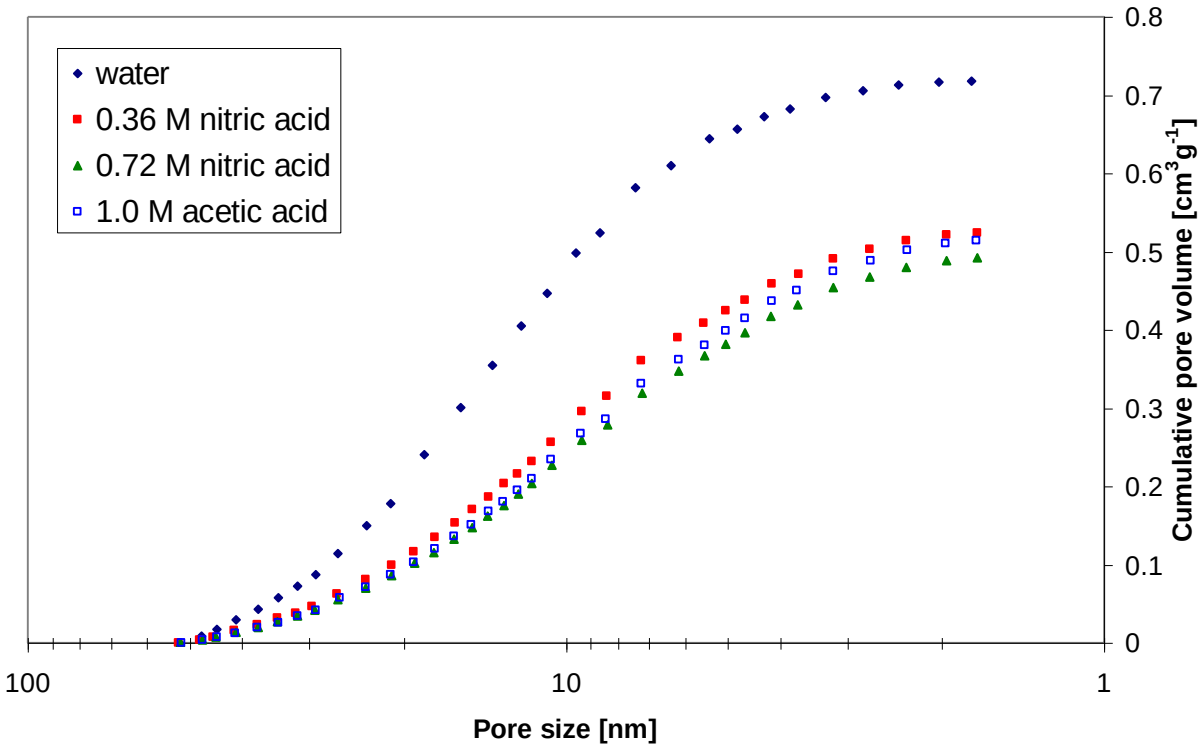

Figure 8.12: Pore size distribution for V250 extrudates with all binders

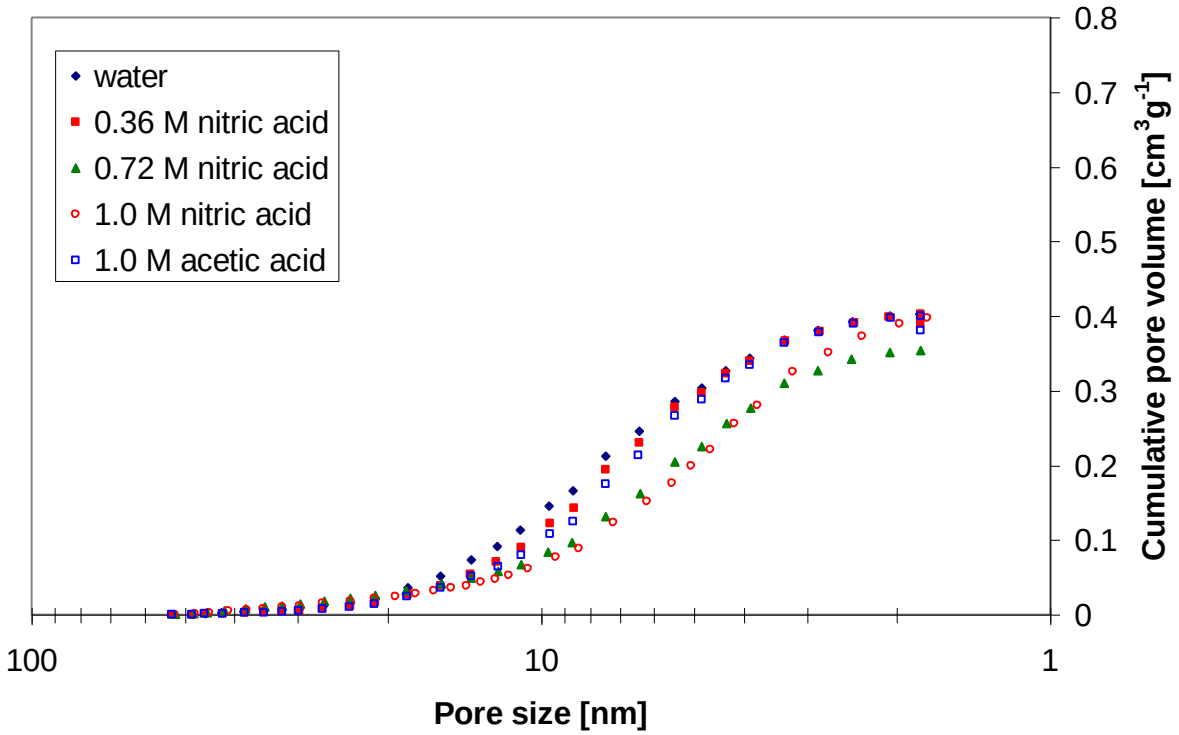

Figure 8.13: Pore size distribution for Dequagel HP extrudates with all binders

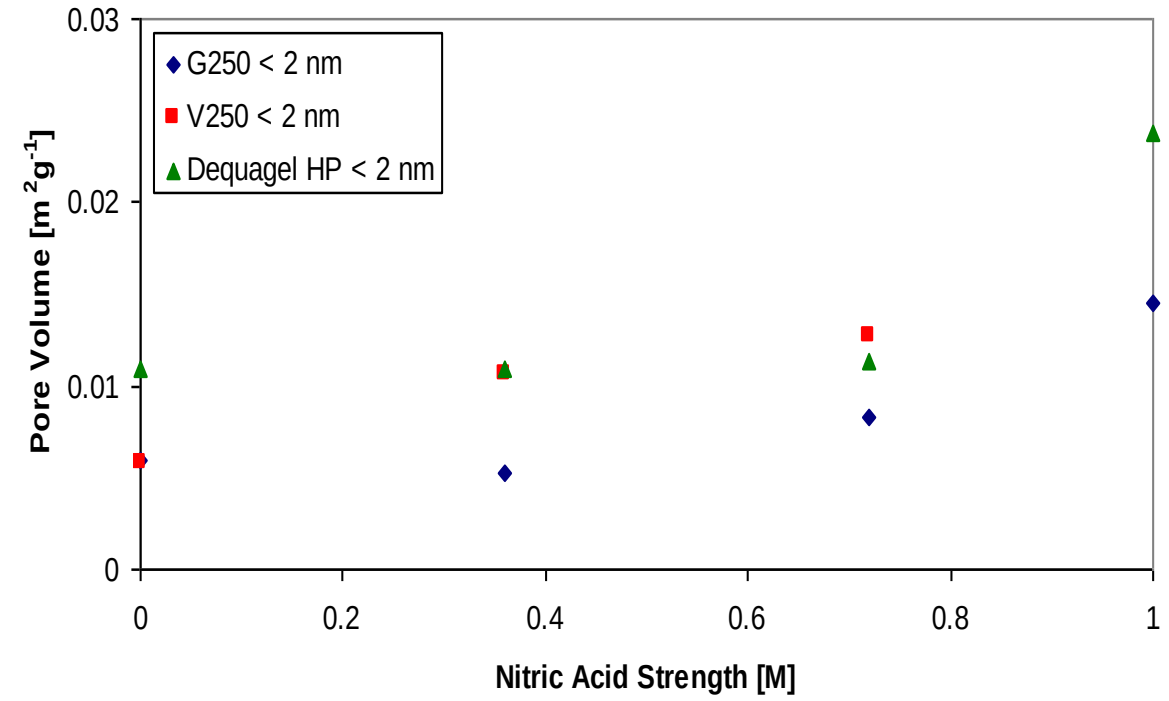

Figure 8.14: Pore Volume < 2.2 nm

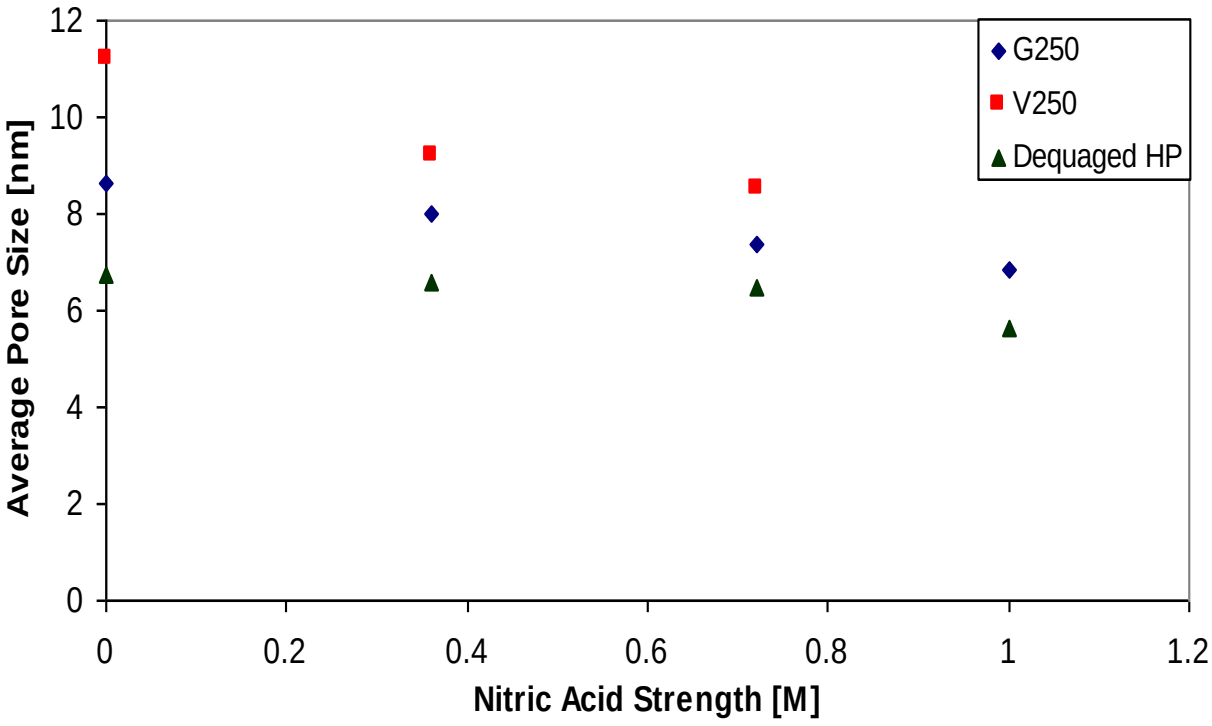

Figure 8.15: Change in pore size with nitric acid strength

The shape of the extrudates' pore size distributions varies depending on the powder feed. Comparisons can be seen in Figure 8.16 and 8.17 of extrudates produced with water and 0.72 M nitric acid respectively. Extrudates produced with the boehmite V250 exhibit a significant volume of pores larger than 10 nm compared with those produced with G250, which has a greater volume of large pores than Dequagel HP.

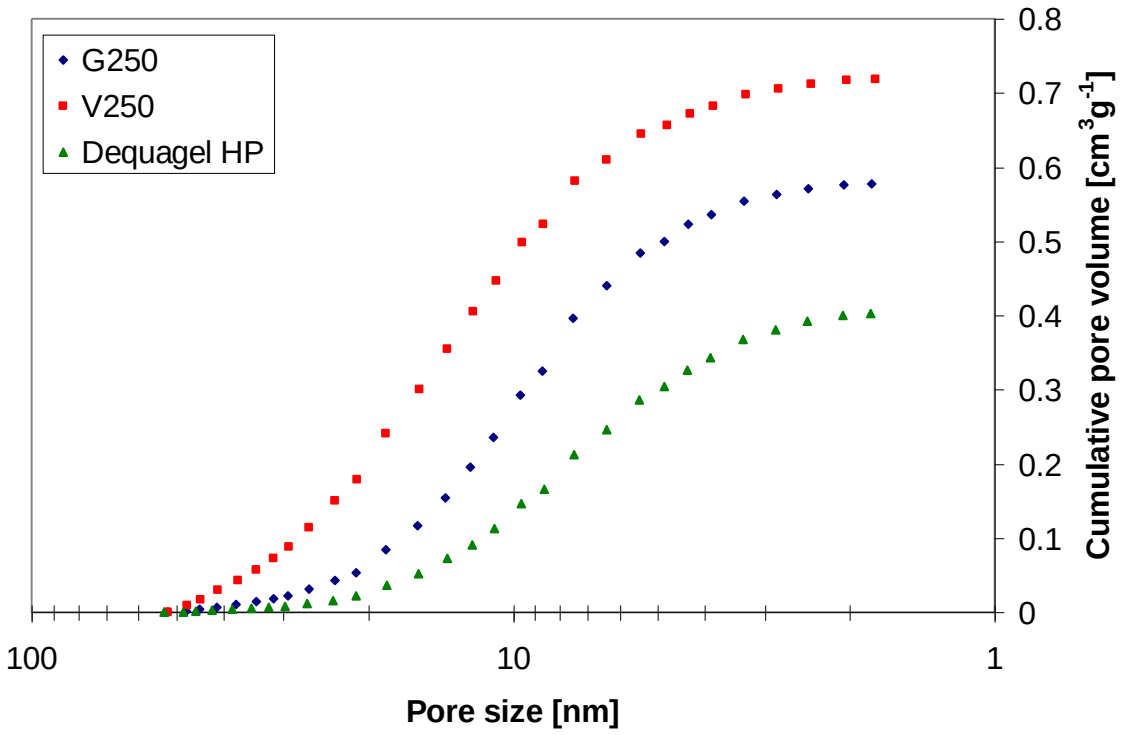

Figure 8.16: Pore size distribution for all boehmite powders with water

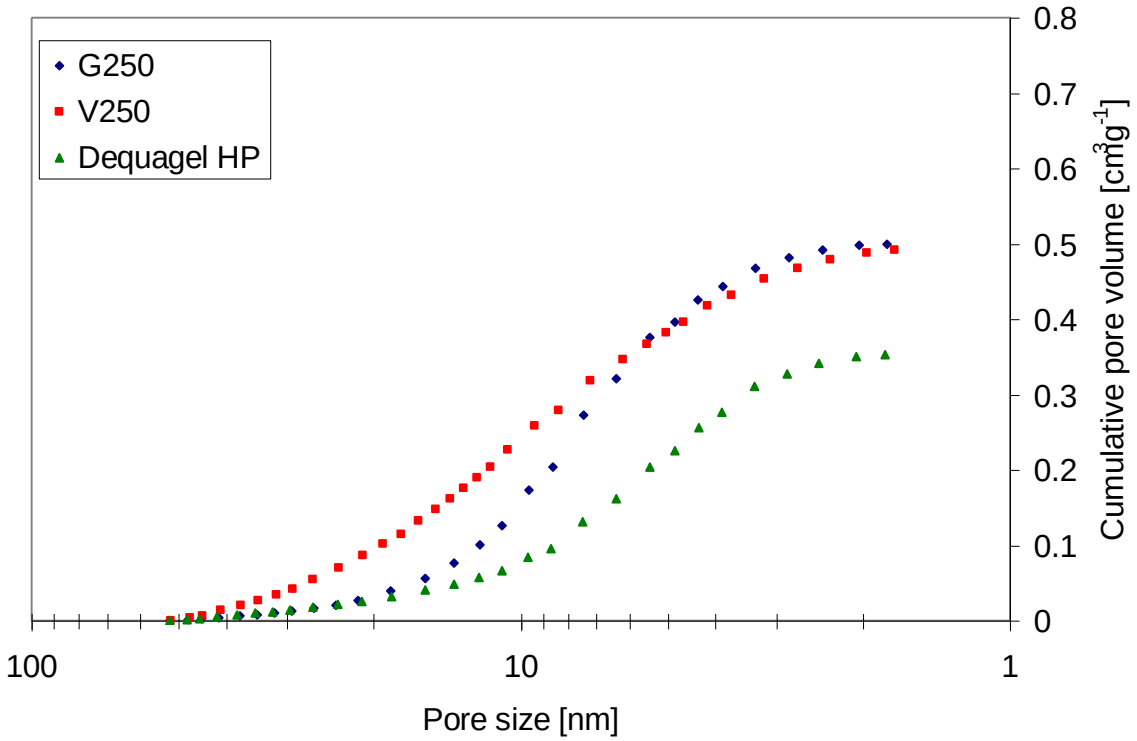

Figure 8.17: Pore size distribution for all boehmite powders with 0.72 M nitric acid

The variation of the surface area of extrudates with strength of nitric acid can be seen in Figure 8.18. Although there is a variation in the surface area, this data displays no evidence of a strong relationship between surface area and acid strength. The surface area of extrudates produced with 1.0 M acetic acid were within the same range as those produced with nitric acid, with values of 300, 272 and 267 m^2g^{-1} for the powders G250, V250 and Dequagel HP respectively.

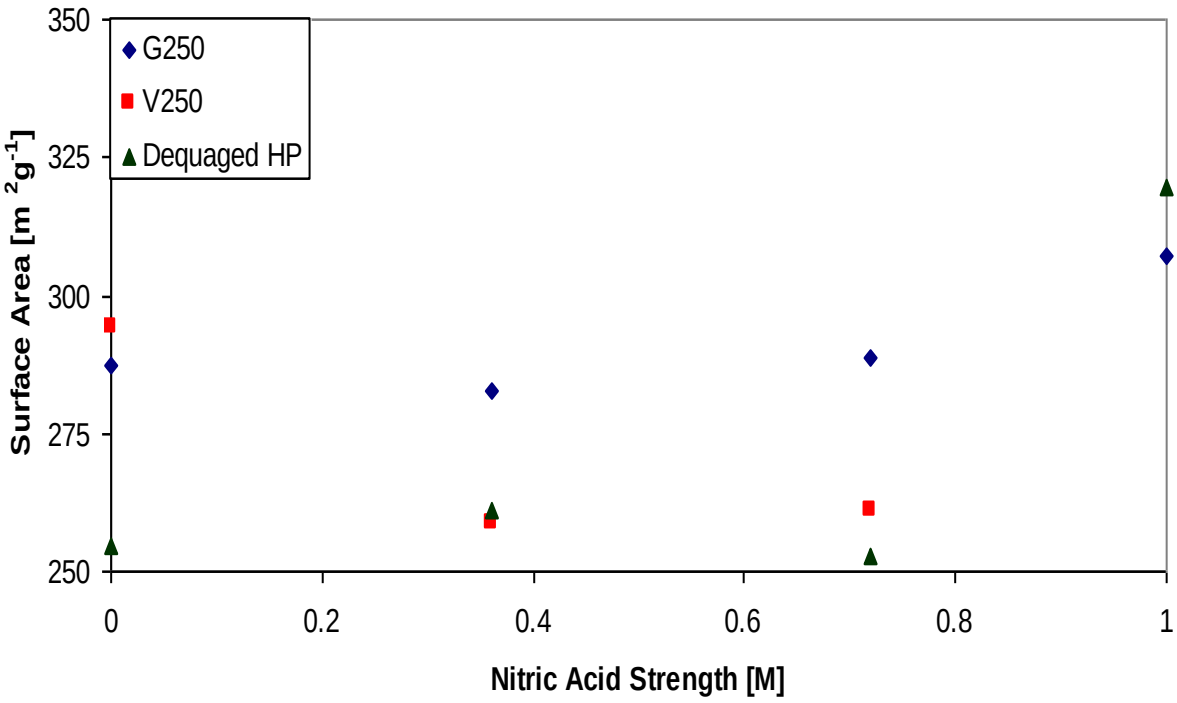

Figure 8.18: Variation of extrudate surface area with nitric acid strength

- It is well understood that there is a compromise to be made between strength and porosity when considering catalyst supports. Figure 8.19 shows the specific compromise between crush strength and total pore volume measured by nitrogen adsorption for the materials under investigation. The data implies a significant loss in crush strength as pore volume, measured by nitrogen adsorption, is increased slightly. Alternatively, this can be viewed as significant increase in crush strength as the total pore volume is decreased only slightly by the use of acid. Extrudates produced with the boehmite G250 shows the clearest relationship between strength and pore volume. Those produced with V250 show a higher strength than those produced with G250 for comparable pore volumes. Extrudates produced with the boehmite Dequagel HP exhibit a wide range of crush strengths with minimal variation in pore volume (note pore volume

is significantly lower than extrudates produced with either of the other two boehmite powders) depending on the acid strength and type. The compromise between crush strength and pore volume appears to be powder specific, with results for extrudates produced with each powder lying on an individual curve for all acid types and strengths. A study of the mechanical srength of ceramics has been performed by Li *et al.* (2004) who identify the importance of this parameter and explore the mechanics of typical failure. The relationship between pores and strength of materials is described by Griffiths (1920) and developments in this area have been made by the concrete industry, for example Liang *et al.* (2011) who provide a model, developed from the basis of Griffith's theory, predicting the strength of concrete with consideration of the porosity. Such specific advancements within the ceramic field can not be found in the literature.

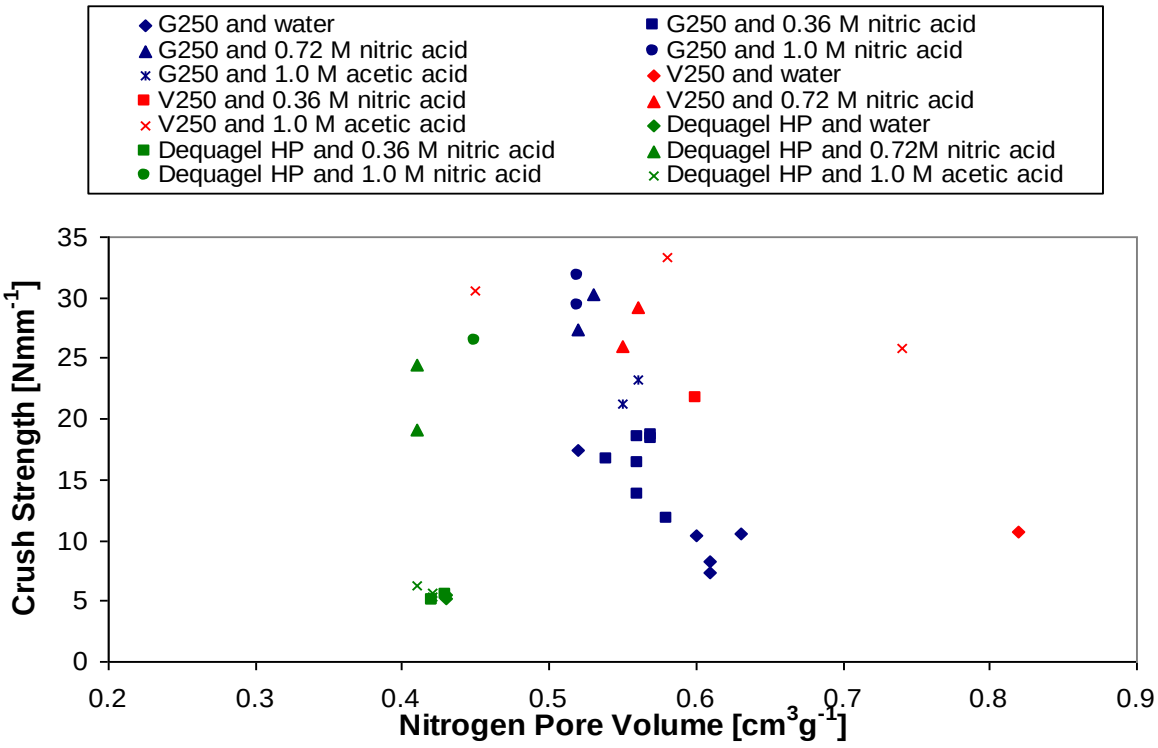

Figure 8.19: Compromise between strength and porosity

8.4.3 Attrition Resistance

The extrudates produced all exhibit a high attrition resistance, with low mass loss experienced during the attrition test. Tables 8.2 – 8.4 show the percentage of mass lost in particles < 1 mm.

Extrudates prepared with the boehmite G250 display very low mass loss on attrition, with the exception of those produced with water. Similarly low mass losses are exhibited by extrudates prepared with the boehmite V250. Extrudates produced with the boehmite Dequagel HP display a much lower resistance to attrition, with the majority of samples losing > 1 % in fines during the test. As shown in Section 8.4.1 these samples also displayed very low crush strength.

Table 8.2: Attrition resistance of extrudates produced with boehmite G250

Liquid	Solids content (wt%)	Acid content (molar ratio of	Attrition loss (%)
Water	47.1	0	11.1
	48.1	0	2.5
	49.1	0	1.4
	50.2	0	3.6
	51.6	0	10.9
0.36 M nitric acid	49.2	0.015	0.4
	50.2	0.015	0.3
	50.8	0.014	0.6
	51.3	0.014	0.6
	50.8	0.014	0
	52.2	0.013	0.4
	53.5	0.013	1.6
0.72 M nitric acid	52.4	0.026	0.5
	54.2	0.024	0.7
1.0 M nitric acid	51.5	0.037	0.5
	53.3	0.034	0.4
1.0 M acetic acid	52.6	0.035	0.1
	55.6	0.031	0.2

Table 8.3: Attrition resistance of extrudates produced with boehmite V250

Liquid	Solids content (wt%)	Acid content (molar ratio of	Attrition loss (%)
Water	41.2	0	0.5
0.36 M nitric acid	43.2	0.022	n/a
	50.6	0.016	0.3
0.72 M nitric acid	44.2	0.041	0.2
	49.8	0.032	0.5
1.0 M acetic acid	43.6	0.058	n/a
	49.4	0.045	0.5
	52.1	0.040	0.2
	53.6	0.037	0.2

Table 8.4: Attrition resistance of extrudates produced with boehmite Dequagel HP

Liquid	Solids content (wt%)	Acid content (molar ratio of	Attrition loss (%)
Water	55.4	0	n/a
	57.2	0	3.7
	58.1	0	9.4
0.36 M nitric acid	59.8	0.008	2.9
	60.7	0.008	0
	61.8	0.007	6.6
0.72 M nitric acid	50.9	0.025	0.9
	53.6	0.022	0.6
1.0 M nitric acid	51.2	0.034	n/a
	54.8	0.029	1.3
1.0 M acetic acid	59.1	0.023	1.5
	61.7	0.020	2.0
	62.3	0.020	2.8

8.5 Particle Size Distribution Profile of Twin Screw Extruder

The particle size distribution of pastes prepared with the boehmite G250 and water along six screw configurations was examined, one configuration was also profiled

using 1.0 M nitric acid as the liquid phase. Details of the configurations examined and operating conditions can be seen in Section 4.4.3.

The particle size distributions suggest that neither the mixing or conveying elements are very effective at reducing particle size. In each case there is evidence of particle size reduction occurring in the short distance of conveying elements between the liquid feed point and the first mixing elements, position 1 and position 2, as displayed in Figure 8.20 for configuration 1, (no particle size distributions were measured upstream of the liquid feed point). There is little further reduction in particle size along the barrel, see position 12 (at the die end) in Figure 8.20.

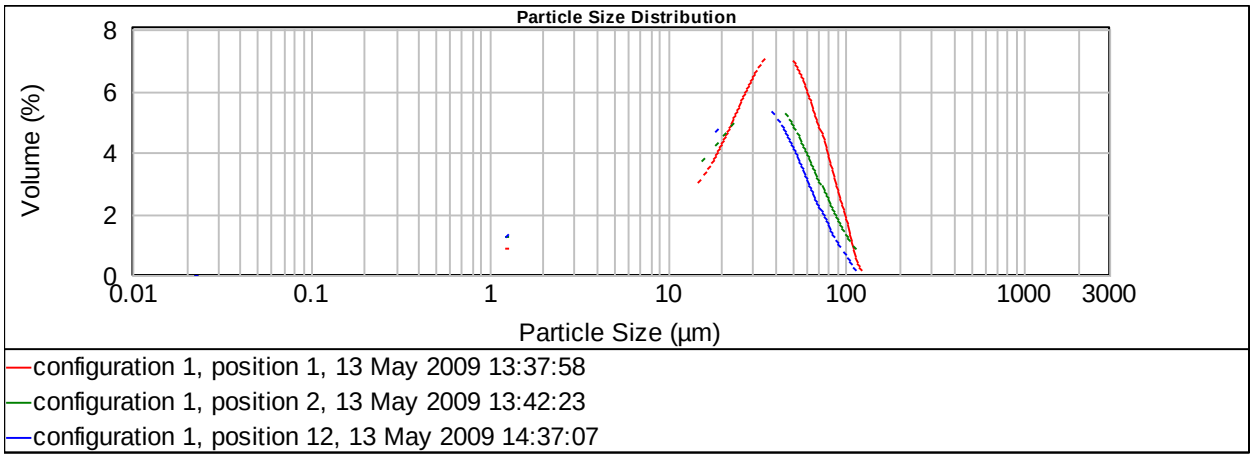

Figure 8.20: PSD profile of TSE using configuration 1, positions can be seen in Figure 5.7 (in experimental section)

Each of the 6 configurations investigated result in very similar size distributions at the die, seen in Figure 8.21, with the exception of configuration 5, which exhibits a distribution with a larger proportion of smaller particles than the other distributions. The change in size distribution between the penultimate and final positions of configuration 5 can be seen in Figure 8.22. The penultimate position in configuration 5 displays a particle size distribution similar to the final distribution of the other

configurations, seen in Figure 8.23. Between the penultimate and final position the material passes through 2 d of 60 º backwards elements. This is theoretically the most aggressive mixing section in all of the configurations, though 60 º backward elements have been used in lengths of 1 d, which did not cause such significant particle size reduction. This suggests that only this most aggressive mixing element is capable of reducing the particle size distribution below that exhibited at the final stage of the other configurations. The use of 5 d of 90 º mixing elements in configuration 3 did not show a reduction as significant as that achieved by configuration 5.

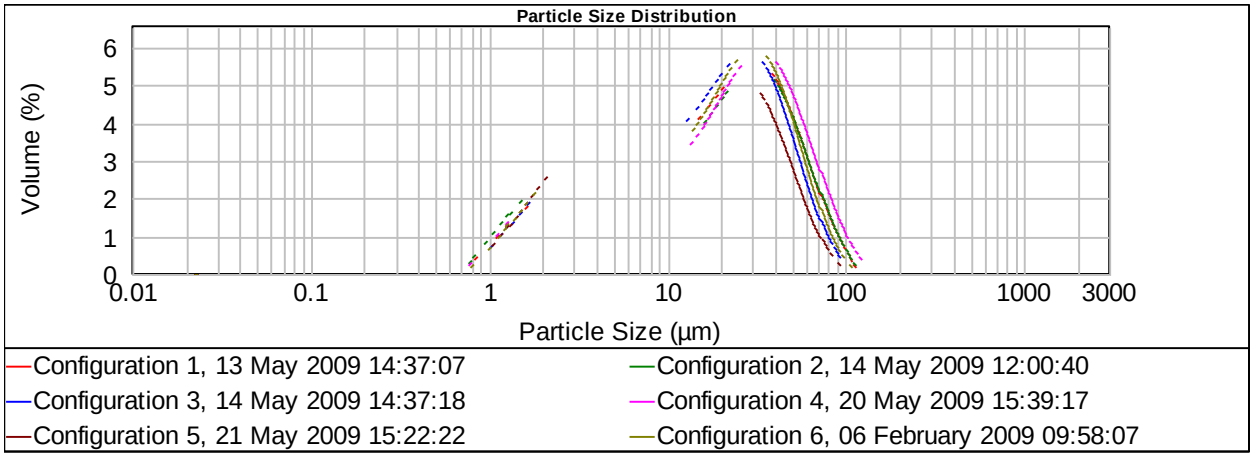

Figure 8.21: Final particle size distributions of all 6 configurations with water

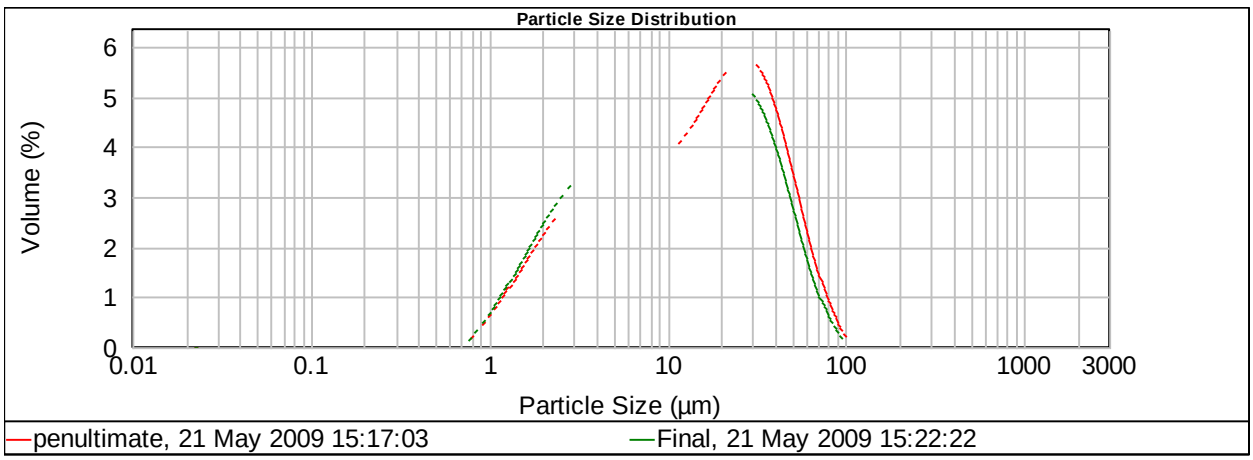

Figure 8.22: Penultimate and final measurement in configuration 5

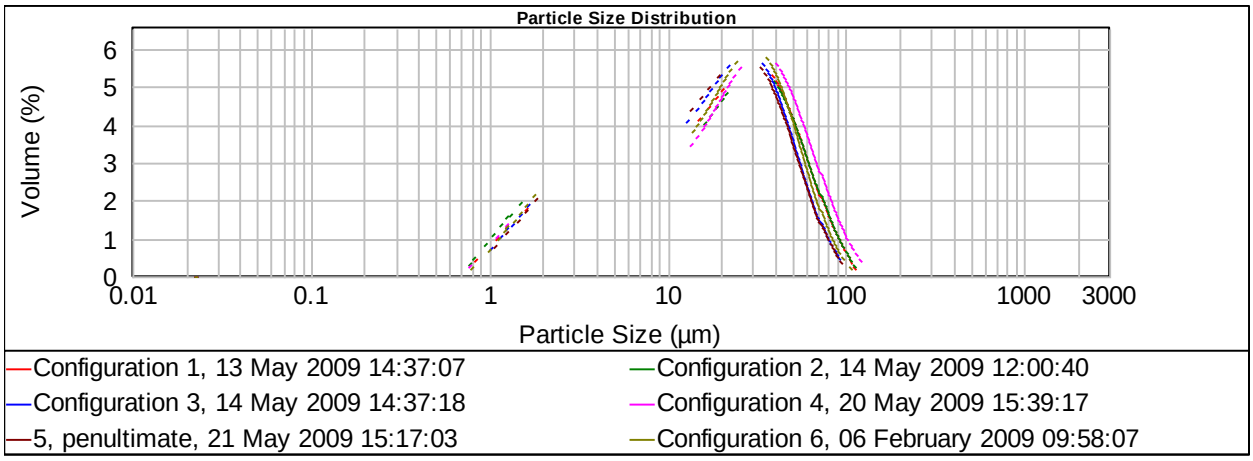

Figure 8.23: Final particle size distributions of all 6 configurations with water, using penultimate data from configuration 5

Although, as discussed in Section 8.2, absolute values of torque cannot be calculated, a comparison between each configuration can be made based on the derived value reported by the instrument. Configuration 5, which produced the most significant particle size reduction, drew the lowest torque. This confirms that the particle size reduction is due to the action of the mixing elements in the configuration rather than additional mechanical energy input.

It has been considered that the similarities between the particle size distributions may be due poor dispersion during presentation of the sample for measurement. Pastes have been redispersed in demineralised water to allow measurements to be taken using the wet dispersion unit and Malvern Mastersizer as described in Section 4.1.2. Work performed by McGuire *et al.* (2007) using X ray tomography to examine the particle size of zirconia particles after twin screw extrusion and found that all particles, initially ~60 µm, were reduced to below 5 µm in size. The work presented here suggests that only a portion of the particles ~30 µm in size are reduced to below 10 µm.

Extrudate samples produced from configurations 1 - 5 all show very similar pore size profiles, seen in Figure 8.24 (data is not available for configuration 6). The similarity of the pore size distributions supports the possibility that the particle size distributions may be as similar as the results displayed in Figure 8.23 suggest.

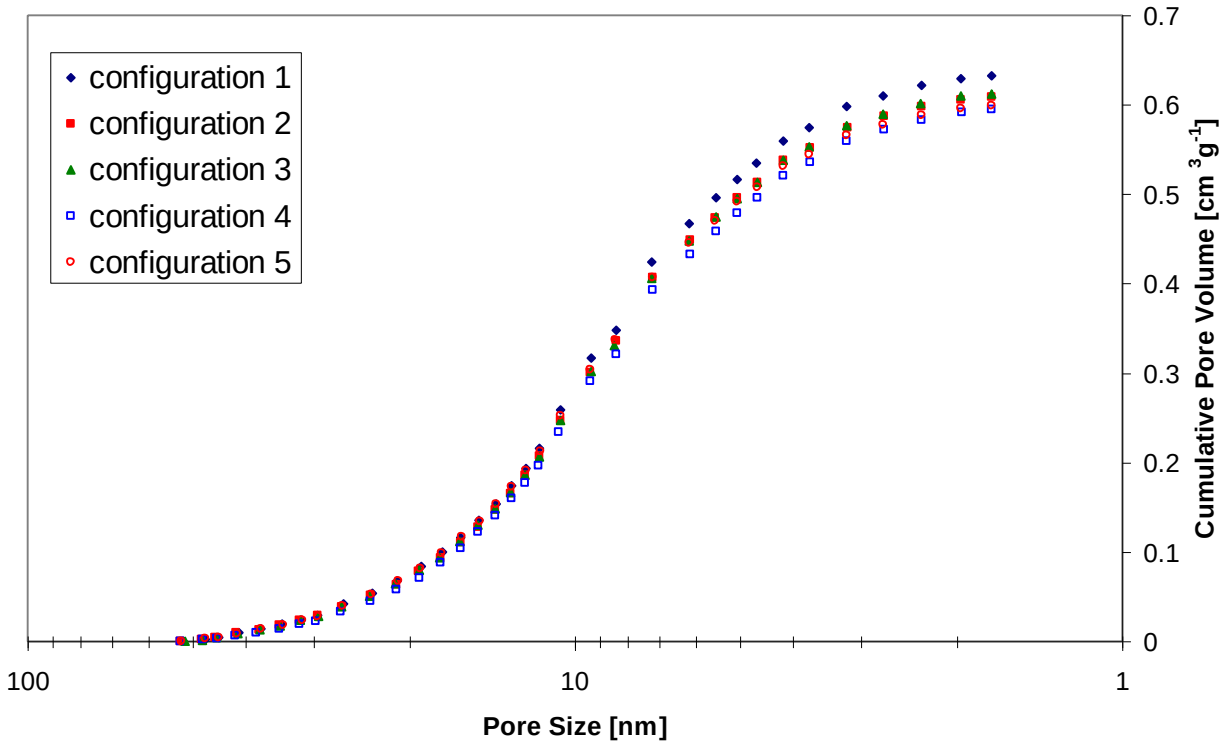

Figure 8.24: Pore size distribution of configurations 1 – 5

A much more significant reduction in particle size was observed in the sample prepared with 1.0 M nitric acid compared with the samples prepared with water, as shown in Figure 8.25, due to the chemical dispersion of boehmite particles by acid. Unfortunately, there is no pore size distribution available for the extrudates prepared with acid.

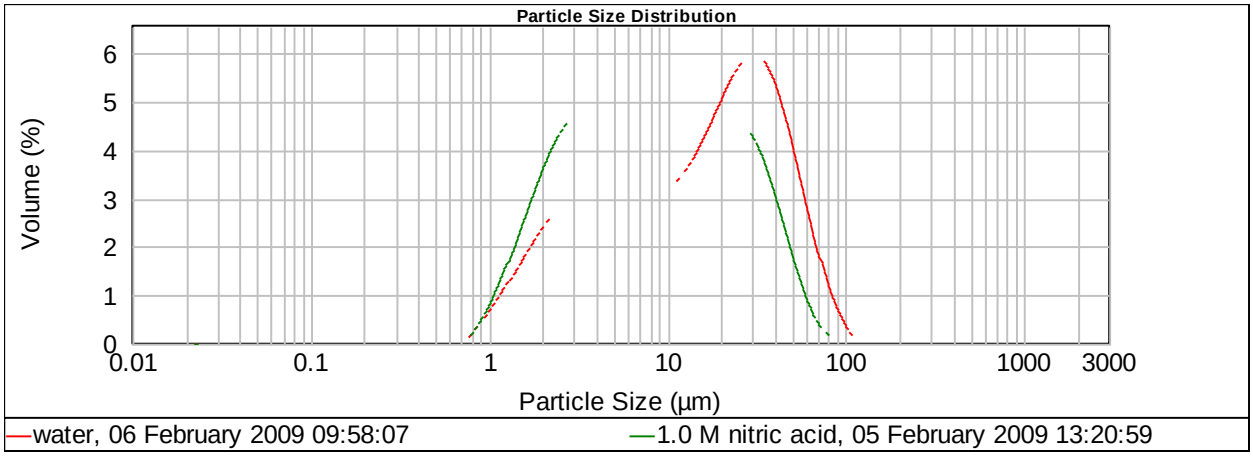

Figure 8.25: Final particle size distributions achieved with water and 1.0 M nitric acid

All of the distributions contain particles of 3-4 µm and 20-30 µm, the shape and change of the particle size distribution suggests that the mechanism of size reduction within the twin screw extruder is the breakdown of 20-30 µm agglomerates to particles which are 3-4 µm in size.

8.6 Conclusions

Extrudates have been successfully produced with each of the powder liquid combinations. A large variety of formulations can be produced at a particular extrusion torque. In general the torque increases with an increase in solids content. Increasing acid content results in a reduction of torque, likely due to the change in the rheological properties caused by the addition of acid.

There is a discrepancy between the solids content predicted to form the capillary saturation state, using the mixer torque rheometer (MTR) discussed in Chapter 7, and the solids contents of successful extrusion formulations due to the difference in the work input of the equipment and the effect this can have on the saturation state of a system as discussed previously in Chapter 7. The MTR consistently predicts a lower solids content at the capillary saturation state than those formulations successfully extruded, implying less work is inputted by the MTR compared to the TSE. The discrepancies are all < 20 wt%. The least cohesive powder, G250, exhibits the smallest discrepancy, as this is the least susceptible to packing density increases by work input. The discrepancy is also reduced when acid strength is increased, as the effect of acid begins to dominate over the physical effect of work input. Despite the discrepancy the author believes the MTR to be a useful tool for predicting successful extrusion formulations, particularly in cases in which there is an understanding of the differences in work input between the equipment and the effect that work input has on the material system.

The force required to extrude a paste on the ram extruder is related to the torque required to produce the pastes on the TSE, however, the relationship appears to be

formulation dependent as the data points for each system lie on an individual curve, there is no single master curve.

Extrudate crush strength is affected by formulation parameters (solids content and acid content) rather than process parameters, (extrusion torque and extrusion force) although it was previously thought that a high torque would produce a strong extrudate.

Total pore volume is reduced by increasing the solids content for a particular powder liquid combination. In many cases the pore size distribution shape remains similar as solids content increases, though some distributions exhibit a shift which implies an increase in the packing density at higher solids content. The nature of the experiments inherently results in a reduction of the acid to boehmite ratio as the solids content is increased, so the observed improvement in packing is not due to an increase in chemical dispersion, but a physical phenomenon. The pore volume is also reduced when acid strength is increased, and the shift in pore size distributions suggest an improvement in packing density, as the volume of the smallest pores increases, in this case due to chemical dispersion. The average pore size reduces with acid strength. The shape of the pore size distributions varies with powder type. Variations in BET surface area do not display a trend related to acid strength.

The compromise between crush strength and pore volume appears to be powder specific, with results for extrudates produced with each powder lying on an individual curve for all acid types and strengths. An increase in crush strength is achieved as the total pore volume is decreased only slightly by the use of acid, particularly for extrudates produced with the boehmite G250 which shows the clearest relationship

between strength and pore volume. Those produced with V250 show a higher strength than those produced with G250 for comparable pore volumes. Extrudates produced with the boehmite Dequagel HP exhibit a wide range of crush strengths with minimal variation in pore volume depending on the acid strength and type. The extrudates displaying the best combination of pore volume and crush strength were produced with the boehmite V250 and acetic acid.

Extrudates produced with G250 and V250 exhibit very high resistance to attrition, with the exception of extrudates prepared with G250 and water. Dequagel HP has much lower resistance to attrition.

Pastes prepared with G250 and water on a TSE all showed very similar particle size distributions at the die end regardless of the screw configuration used, with the exception of configuration 5, incorporating 2 d of 60 ° backwards elements which resulted in further size reduction. The similarity in particle size distribution is accompanied by very similar pore size distributions of the dried samples. The use of nitric acid in the formulation results in a much more significant reduction of particle size, with the distribution still displaying a bimodal form with particles at 3 and 30 µm, but with more particles at 3 µm.

Chapter 9: Conclusions and Further Work

9.1 Conclusions

The interaction between boehmite and acid (nitric and acetic), and the products of this interaction, have been investigated using rheological methods, (rotational, oscillatory and mixer torque), nuclear magnetic resonance and cryomicroscopy. The capability of a mixer torque rheometer to predict successful extrusion formulations has been assessed. The effect of formulation parameters on the resulting extrudate properties has been evaluated.

Three boehmite powders have been studied, each produced by different manufacturing processes. The crystallite size of each of the powders, measured by X ray diffraction, varies by only 1 nm between all powders.

9.1.1 Effect of Acid on Boehmite Slurries

Rheological studies of acidic boehmite slurries observed a significant increase in apparent viscosity and yield stress below pH 4, this result was only observed with nitric acid as acetic acid did not produce slurries with a low enough pH. Measurement of the zeta potential and particle size distribution of acidic boehmite slurries confirmed that the observed rheological changes were not due to surface charge or particle size distribution changes. It is proposed that the observed rheological changes in acidic concentrated boehmite suspensions are due to the formation of a gelatinous phase of polymeric cations by partial dissolution of boehmite and that these species can adsorb onto particle surfaces. The variation of zeta potential with pH is in agreement with the occurrence of a dissolution readsorption mechanism.

The use of oscillatory rheology to confirm the gelatinous nature of the microstructure has been inconclusive due to the absence of a linear viscoelastic region. Examination of the coordination of the aluminium species by magic angle spinning nuclear magnetic resonance (MAS NMR) has identified alterations in the coordination, however, this is most likely due to a mechanochemical phase change resulting from the high energy sample preparation technique and does not confirm the presence of a the proposed polymeric cation. Cryogenic scanning electron microscopy (Cryo-SEM) has confirmed textural differences between boehmite slurries prepared with and without acid. The continuous phase formed in the presence of acid visually appears to be polymeric in nature, and a clear image of the interface between a particle and the continuous phase has been captured.

Additional slurry preparation (milling) time enhanced the observed rheological changes, possibly due to the particle size distribution alterations caused by milling and the exposure of additional surface area for dissolution, mechanical activation and phase changes during milling. Slurries produced with each of the three boehmite powders displayed very similar rheological behaviour.

The interaction between boehmite and acid has also been assessed by examining variations in the solids content required to form the capillary saturation state as measured by the mixer torque rheometer. The solids content at the capillary point increased as the pH of the binder phase was reduced, this effect was non anion specific. Improvement in particle packing density due to chemical dispersion was identified as the primary mechanism responsible for the observed change. Other possible mechanisms such as reduction of available pore volume due to blockage of interparticle pores, improvements in particle packing by mechanical work input and

differences in the wettability of a powder liquid system were also explored. The correlation between the dispersibility of boehmite in nitric acid measured by the dispersibility test and the dispersibility implied by the magnitude of shift in the solids content at the capillary point as measured by mixer torque rheometry strongly suggests that chemical dispersion is responsible for the observed shift.

The variation of the magnitude of torque at the capillary point for each of the powders has been attributed to differences in the particle size distributions. Variations in size distribution have been shown to affect the results obtained by mixer torque rheometry, and the size distribution of a powder has also been shown to be altered during an MTR experiment.

Much of the variable mixing time (VMT) test data obtained was redundant for detailed analysis as the experiments had not continued into an equilibrium state. Those data sets which displayed equilibrium conditions showed higher torques, reached more slowly, when a drier formulation was tested. VMT tests at much smaller increments of liquid content need to be performed to construct a detailed view of the relationship between torque and solids content.

The dissolution rate of boehmite in nitric acid at pH 4 is faster than at pH 2, which is thought to be due to a mass transfer limitation effect at pH 2, due to the rheological changes observed. All boehmite powders have been shown to be more readily dispersed in nitric acid than acetic acid. The boehmite powder V250 is the least dispersible in both acids.

9.1.2 Predictive Capability

Tapped bulk density was found to be a good predictor for the solids content forming the capillary saturation state measured by MTR for powders with low cohesivity. Predictions were less accurate for more cohesive powders due to the low packing density and the susceptibility to packing rearrangements upon the addition of liquid. This prediction was not expected to produced such accurate results as particle packing is strongly affected by particle size distribution which has been found to alter during an MTR experiment, but is unlikely to be altered during tapped bulk density measurements due to the low energy input of this measurement technique.

The capillary saturation state identified by mixer torque rheometry experiments was found to give predictions within 20 wt% solids for successful extrusion formulations. The MTR consistently predicted solids contents lower than those successfully extruded, implying a lower work input using this equipment. The least cohesive powder, G250, exhibits the smallest discrepancy, as this is the least susceptible to packing density alteration by work input. The discrepancy is also reduced when acid strength is increased, as the effect of acid begins to dominate over the physical effect of work input.

9.1.2 Extrusion Behaviour and Extrudate Properties

Extrudates have been successfully produced with each of the boehmite powders and water, nitric acid up to 1.0 M and 1.0 M acetic acid. A large variety of formulations can be produced at a given extrusion torque. Increasing acid strength results in a reduction of torque, likely due to the change in the rheological properties caused by the addition of acid.

The force required to extrude a paste on the ram extruder is related to the torque required to produce the pastes on the TSE, however, the relationship is formulation dependent.

Extrudate crush strength is affected by formulation parameters (solids content and acid content) rather than process parameters, (extrusion torque and extrusion force).

Total pore volume is reduced by increasing the solids content for a particular powder liquid combination, pore size distributions imply an increase in the packing density at higher solids content. The nature of the experiments inherently results in a reduction of the acid to boehmite ratio as solids content is increased, therefore the observed improvement in packing is not due to an increase in chemical dispersion.

The total pore volume is reduced when acid strength is increased, and the shift in pore size distributions suggest an increaes in packing density, as the volume of the smallest pores increases, in this case due to chemical dispersion. The average pore size reduces as acid strength is increased. The shape of the pore size distributions varies with powder type. Variations in the BET surface area do not display a trend related to acid strength.

The compromise between crush strength and pore volume appears to be powder specific, with results for extrudates produced with each powder producing an individual curve for all acid types and strengths. An increase in crush strength is achieved as the total pore volume is decreased slightly by the use of acid, particularly for extrudates produced with the boehmite G250 which shows the clearest relationship between strength and pore volume. The extrudates displaying

the best combination of pore volume and crush strength were produced with the boehmite V250 and acetic acid.

Extrudates produced with boehmite powders G250 and V250 exhibit very high resistance to attrition, with the exception of extrudates prepared with G250 powder and water. Extrudates produced with the boehmite Dequagel HP have much lower resistance to attrition.

Pastes prepared with boehmite powder G250 and water on a TSE all showed very similar particle size distributions at the die end regardless of the screw configuration used, with the exception of configuration 5, incorporating 2 d of 60 ° backwards elements which resulted in further size reduction. The use of nitric acid results in a much more significant reduction of particle size.

9.2 Further Work

The primary focus of this thesis has been on the effect of acid strength and type on boehmite slurries, pastes and extrudates. For a more complete understanding of the area the effect of powder properties on the interaction with acid should be studied, this would require a more systematic approach to the raw materials used for investigation as the powders used in this stuffy have numerous differences, it is difficult to be sure which characteristics are responsible for any differences observed. A full investigation should incorporate a focus on the effect of operational parameters on extrudate properties on specific formulations.

An ongoing issue with the analysis of the data produced during this project has been the lack of ability to decouple the mechanical and chemical effects. The inability to accurately quantify the work input of the sample preparation and

Although there is no definitive boundary between a concentrated slurry and a paste, it is generally true that the measurement of rheological properties of materials with lower solids content are less complex to characterise and predict. The most widely used and well developed paste characterisation technique was considered too laborious for the large volume of samples studied. A better understanding of the paste properties which are most relevant to extrusion behaviour would allow the development of an analysis technique to characterise new formulations.

Chapter 10: References

Absi-Halabi, M., Stanislaus, A. and Al-Zaid, H. Effect of acidic and basic vapours on pore size distribution of alumina under hydrothermal conditions. *Applied Catalysis A: General* **101** *(1993) 117-128*

Akratopulu, K.Ch., Vordonis, L. and Lycourghiotis, A. Effect of temperature on the point of zero charge and surface dissociation constants of aqueous suspensions of γ-Al_2O_3. *Journal of Chemistry Society, Faraday Transactions* **82** *(1986) 3697-3708*

Amarasinghe, A.D.U.S. 1998. Interpretation of paste extrusion data, Thesis, (PhD). University of Cambridge

Amarasinghe, A.D.U.S and Wilson, D.I. Interpretation of paste extrusion data. *Chemical Engineering Research Des.* **76** *(AI) (1998) 3-8*

Ananthakumar, S., Manohar, P. and Warrier, K.G.K. Effect of boehmite and organic binders on extrusion of alumina. *Ceramics International* **30** *(2004) 837-842*

Ananthakumar, D., Menon, A.R.R., Prabhakaran, K. and Warrier, K.G.K. Rheology and packing characteristics of alumina extrusion using boehmite gel as a binder. *Ceramics International* **27** *(2001) 231-237*

Ananthakumar, S. and Warrier, K.G.K. Extrusion characteristics of alumina – aluminium – titanate composite using boehmite as a reactive binder. *Journal of the European Ceramic Society* **21** *(2001) 71-78*

Anklekar, R.M., Borkar, S.A., Bhattacharjee, S., Page, C.H. and Chatterjee, A.K. Rheology of concentrated alumina suspension to improve the milling output in

production of high purity alumina powder. *Colloids and Surfaces A: Physicochemical and Engineering Aspects* **133** *(1998) 41-47*

Assih, T., Ayral, A., Abenoza, M. and Phalippou. Raman study of alumina gels. *Journal of Material Science* **23** *(1988) 3326-3331*

Bakalis, S. and Karwe, M. Velocity distributions and volume flow rates in the nip and translational regions of a co-rotating, self-wiping, twin-screw extruder. *Journal of Food Engineering* **51** *(2002) 273-282*

Baker, B.R. and Pearson, R.M. Water content of psuedoboehmite: A new model for its structure. *Journal of Catalysis* **33** *(1974) 265-278*

Ball, R.C. and Richmond, P. Physics and Chemistry of Liquids **9** (1980) 99-116

Barlow, C.G. Granulation of powders. Chemical Engineering (London) **220** 196 (1986)

Barnes, H.A. A Handbook of Elementary Rheology. The University of Wales Institute of Non-Newtonian Fluid Mechanics, Department of Mechanics, University of Wales, Aberystwyth, Dyfed, Wales. ISBN 0-9538032-0-1. Published 2000. Cambrian Printers

Barnes, E.C., Wilson, D.I. and Johns, M.L. Velocity profiling inside a ram extruder using magnetic resonance techniques. *Chemical Engineering Science* **61** *(2006) 1357-1367*

Baron, R., Vauchel, P., Kaas, R., Arhaliass, A and Legrand, J. Dynamical modelling of a reactive extrusion process: Focus on residence time distribution in a fully

intermeshing co-rotating twin-screw extruder and application to an alginate extraction process. *Chemical Engineering Science* **65** *10 (2010) 3313-3321*

Barrera, M.A., Vega, J.F. and Martinez-Salazar, J. Three dimensional modelling of flow curves in co-rotating twin screw extruder elements. *Journal of Materials Processing Technology* **197** *(2008) 221-224*

Basmadjian, D., Fulford, G.N., Parsons, B.I. and Montgomery, D.S. The control of the pore volume and pore size distribution in alumina and silica gels by the addition of water soluble organic polymers. *Journal of Catalysis* **1** *(1962) 547-563*

Basterfield, R. 2003. Interpretation of mechanical testing measurements for pastes. Thesis, (PhD). Imperial College, London.

Bates, A.J.D. and Bridgwater, J. The radial flow of pastes and gels. *Chemical Engineering Science* **55** *(2000) 3003-3012*

Beattie, J.K., Cleaver, J.K. and Waite, D. Anomalous aggregation behaviour of aluminium oxyhydroxides. *Colloids and Surfaces A: Physicochemical and Engineering Aspects* **111** *(1996) 131-138*

Benbow, J.J. The dependence of output rate on die shape during catalyst extrusion. *Chemical Engineering Science* **26** *(1971) 1467-1473*

Benbow, J.J. and Bridgwater, J. Measurement of paste yield by cone penetration. *Chemical Engineering Science* **42** *(1987) 915-919*

Benbow, J.J., Oxley, E.W. and Bridgwater, J. The extrusion mechanics of pastes – the influence of paste formulation on extrusion parameters. *Chemical Engineering Science* **42** *(1987) 2151-2162*

Benbow, J., and Bridgwater, J. Paste Flow and Extrusion. Oxford Series on Advanced Manufacturing. 1993. ISBN: 0-19-856338-8

Benbow, J.J., Jazayeri, S.H. and Bridgwater, J. Ceramic extrusion mechanics: The effects of paste formulation and liquid phase rheology on die-flow resistance. *Ceramic Transactions* **1** *(1988) 624-634*

Benezeth, P., Palmer, D.A. and Wesolowski, D.J. Aqueous high-temperature solubility studies. II. The solubility of boehmite at 0.03 m ionic strength as a function of temperature and pH as determined by in situ measurements. *Geochimica et Cosmochimica Acta* **65** *(2001) 2097-2111*

Benezeth, P., Palmer, D.A. and Wesolowski, D.J. Dissolution/precipitation kinetics of boehmite and gibbsite: Application of a pH-relaxation technique to study near-equilibrium rates. *Geochimica et Cosmochimica Acta* **72** *(2008) 2429-2453*

Benna, M., Kbir-Ariguib, N., Magnin, A. and Bergaya, F. Effect of rheological properties of purified sodium bentonite suspensions. *Journal of Colloid and Interface Science* **218** *(1999) 442-455*

Bergstrom, L. Shear thinning and shear thickening of concentrated ceramic suspensions. *Colloids and Surfaces A: Physicochemical and Engineering Aspects* **133** *(1998) 151-155*

Bernal, J.D. A geometrical approach to the structure of liquids. *Nature* **183** *(1959) 141-147*

Blackburn, S. and Bohm, H. The influence of powder packing on paste extrusion behaviour. *Transactions of the IChemE* **71** *(1993) 250-256*

Blackburn, S., Burbidge, A.S. and Mills, H. A critical assessment of the Benbow approach to describing the extrusion of highly concentrated particulate suspensions and pastes. *Proceedings of the 13th International Congress on Rheolgy, Cambridge,* **Paper 4** *(2000) 139-141*

Blackburn, S and Wilson, D.I. Shaping ceramics by plastic processing. *Journal of the European Ceramic Society* **28** *(2008) 1341-1351*

Blyler, L.L. and Danne, J.H. An analysis of Brabender torque rheometer data. *Polymer Engineering Science* **7** *3 (1967) 178-181*

Boersma, W.H., Laven, J. and Stein, H.N. Shear thickening (dilatancy) in concentrated dispersions. *American Institute of Chemical Engineering Journal* **36** *3 (1990)*

Böhm, H. and Blackburn, S. Agglomerate breakdown in fine alumina powder by multiple extrusion. *Journal of Materials Science* **29** *(1994) 5779-5786*

Böhm, H. and Blackburn, S. Effect of mixing procedure on fine aluminas paste extrusion. *British Ceramics Transactions* **93** *5 (1994) 169-177*

Bokhimi, X., Toledo-Antonio, J.A., Guzman-Castillo, M.L. and Hernandez-Beltran, F. Relationship between crystallite size and bond lengths in boehmite. *Journal of Solid State Chemistry* **159** *(2001) 32-40*

Botten, A.J., Burbidge, A.S. and Blackburn, S. A model to predict the pressure development in single screw extrusion. *Journal of Materials Processing Technology* **135** *(2003) 284-290*

Bourcier, W.L., Knauss, K.G. and Jackson, K.J. Aluminum hydrolysis constants to 250°C from boehmite solubility measurements. G*eochimica et Cosmochimica Acta* **57** *(1993) 747-762*

Bousima, M., Ait Kada, A. and Faisant, J.B. Determination of shear rate and viscosity from batch mixer data. *Journal of Rheology* **43** *2 (1999) 415-433*

Bowman, E.T., Soga, K. and Drummond, T.W. Particle shape characterisation using Fourier analysis. *(2000) 1-20.* http://www-civ.eng.cam.ac.uk/geotech_new/publications/TR/TR315.pdf

Brenner, H. Rheology of a dilute suspension of axisymmetric Brownian particles. *International Journal of Multiphase Flow* **1** *(1974) 195-341*

Briscoe, B.J. and Ozkan, N. Characterisation of ceramic pastes by an indentation hardness test. *Journal of the European Ceramic Society* **17** *(1997) 1675-1683*

Bruinsma, P.J., Wang, Y., Li, X.S., Liu, J., Smith, A. and Bunker, B.C. Rheological and solid-liquid separation properties of bimodal suspensions of colloidal gibbsite and boehmite. *Journal of Colloid and Interface Science* ***192*** *(1997) 16-25*

Burbidge, A.S. and Bridgwater, J. The single screw extrusion of pastes. *Chemical Engineering Science* **50** *16 (1995) 2531-2543*

Burbidge, A.S., Bridgwater, J. and Saracevic, Z. Liquid migration in paste extrusion. Transactions of the Institution of Chemical Engineers, Part A **73** (1995) 810-816

Burk, R.C. and Apte, P.S. A packing scheme for real size distributions. *American Ceramic Society Bulletin* **66** *(1987) 1389-1392*

Bye, G.C. and Robinson, J.G. The nature of pseudoboehmite and its role in the crystallisation of amorphous aluminium hydroxide. *Journal of Applied Chemistry and Biotechnology* **24** *(1974) 633-637*

Carneiro, O.S., Caldeira, G. and Covas, J.A. Flow patterns in twin-screw extruders. *Journal of Materials Processing Technology* **92-93** *(1999) 309-315*

Casey, W.H. Large aqueous aluminium hydroxide molecules. *Chemical Reviews* ***106*** *1 (2005)*

Chander, S. Challenges in characterization of concentrated suspensions. *Colloids and Surfaces A: Physicochemical and Engineering Aspects* **133** *(1998) 143-150*

Chandler, H.W., George, S.D. and Liddle, J. Deformation and flow of stiff pastes: review of rheology of some soft solids. *British Ceramics Transactions* **101** *(2002) 47-58*

Chapman, M. and Blackburn, S. Extruded design of catalysts. *Proceedings of the European Ceramic Society* **385** *(1991) 385-389*

Chatlapalli, R. and Rohera, B.D. Rheological characterisation of diltiazem HCl/cellulose wet masses using a mixer torque rheometer. *International Journal of Pharmaceutics* **175** *(1998) 47-59*

Chatlapalli, R. and Rohera, B.D. Study of effect of excipient source variation on rheological behaviour of diltiazem HCl-HPMC wet mass using a mixer torque rheometer. *International Journal of Pharmaceutics* **238** *(2002) 139-151*

Chen, Y., Burbidge, A. and Bridgwater, J. The effect of carbohydrate on the rheological parameters of paste extrusion. *Journal of the American Ceramic Society* **80** *7 (1998) 1841-1850*

Chen, A.Y. and Cawley, J.D. Extrusion of alpha alumina ceramics with low organic content. *Ceramic Engineering and Science Proceedings* **10** *(1989) 773-783*

Chen, A.Y. and Cawley, J.D. Extrusion of alpha alumina boehmite mixtures. *Journal of the American Ceramic Society* **75** *3 (1991) 575-579*

Chen, F.R., Davis, J.G. and Fripiat, J.J. Aluminum coordination and lewis acidity in transition aluminas. *Journal of Catalysis* **133** *(1992) 263-27*

Cheng, D.C-H. Further observations on the rheological behaviour of dense suspensions. *Power Technology* **37** *(1984) 255-273*

Cheng, B.J., Zhou, C.X. and Yu, W. Modified calibration technique to evaluate rheological properties of polymer melts in torque-rheometers. *China Synthetic Rubber Industry* **22** *5 (1999) 312*

Cheng, B., Zhou, C., Yu, W and Sun, X. Evaluation of rheological parameters of polymer melts in torque rheometers. *Polymer Testing* **20** *(2001) 811-818*

Chong, J.S., Christiansen, E.B. and Bayer, A.D. Rheology of concentrated suspensions. *Journal of Applied Polymer Science* **15** *(1971) 2007*

Chou, S., Sydow, K., Martin, P.J., Bridgwater, J. and Wilson, D.I. Stress relaxation in the extrusion of pastes. *Journal of the European Ceramic Society* **23** *(2003) 637-646*

Chung, Y.C., Ooi, J.Y. and Favier, J. Measurement and modelling of a particulate assembly under confined compression. *Journal of Physics: Condensed Matter In Particulate Systems Analysis* **20** *28 (2005) 1-5*

Collaborative Publicity Article. PEPT studies. Plastics, Additives and Compounding Volume 11, Issue 4, September-October 2009, 29-31. doi:10.1016/S1464-391X(09)70110-2

Corbato, C.E., Tettenhorst, R.T. and Christoph, G.G. Structure refinement of deuterated boehmite. *Clays and Clay Minerals* **33** *(1985) 71-75*

Dabak, T. and Yucel, O. Modelling of the concentration and particle size distribution effects on the rheology of highly concentrated suspensions. *Powder Technology* **52** *(1987) 193-206*

Danckwerts, P.V. Continuous flow systems: distribution of residence times. *Chemical Engineering Science* **2** *(1) (1953) 1-13*

Das, R. N., Madhusoodana, C.D. and Okada, K. Rheological studies on cordierite honeycomb extrusion. *Journal of the European Ceramic Society* **22** *(2002) 2893-2900*

DeBoer, J.H. and Lippens, B.C. Studies on pore system in catalysis II. The shapes of pores in aluminium oxide systems. *Journal of Catalysis* **3** *(1964) 38-43*

Debrincat, D.P., Solnordal, C.B. and Van Deventer, J.S.J. Characterisation of inter-particle forces within agglomerated metallurgical powders. *Powder Technology* **182** *(2008) 388-397*

DeLiso, E.M., Cannon, W.R. and Rao, A.S. Dispersion of alumina-zirconia powder suspensions. *Advances in Ceramics* **24** *(1988) 335-341*

Dickinson, E. Structure and rheology of simulated gels formed from aggregated colloidal particles. *Journal of Colloid and Interface Science* ***225*** *(2000) 2-15*

Djuric, D., Van Melkebeke, B., Kleinebudde, P., Remon, J.P. and Vervaet, C. Comparison of two twin screw extruders for continuous granulation. *European Journal of Pharmaceutics and Biopharmaceutics* **71** *(2009) 155-160*

Draper, O., Blackburn, S., Dolman, G., Smalley, K. and Griffiths, A. A comparison of paste rheology and extrudate strength with respect to binder formulation and forming technique. *Journal of Materials Processing Technology* **92-93** *(1999) 141-146*

Drouin, J.M., Chopin, T., Nortier, P. Van Damme, H. Rheology and structure of peptized boehmite pastes. *Journal of Colloid and Interface Science* **125** *1 (1987) 314 - 326*

Eise, K., Curry, J. and Nangeroni, J.F. Compounding extruders for improved polyblends. *Polymer Engineering and Science* **23** *(11) (1983) 642-646*

Ekere, N.N., He., D. and Cai, L. The influence of wall slip in the measurement of solder paste viscosity. *Components and Packaging Technologies, IEEE Transactions* **24** *(2001) 468-473*

Fauchadour, D., Pouget, T., Lechaire, J-P., Rouleau, L. and Normand, L. Evaluation of cryotechniques for TEM observation of sols – application to boehmite sols used in catalyst forming. *Oil and Gas Science and Technology – Rev IFP,* **54** *4 (1999) 513-524*

Faure, A., Grimsey, I.M., York, P., Cliff, M.J. and Rowe, R. Mixer torque rheometry: relationships between wet mass consistency in pharmaceutical wet granulation processes and subsequent dry granule properties. *World Congress on Particle Technology* **3** *(1998) 1183-1194*

Fletcher, J., and Hill, A. Making the connection – particle size, size distribution and rheology. http://www.chemeurope.com/en/whitepapers/61207/making-the-connection-particle-size-distribution-and-rheology.html

Forzatti, P., Ballardini, D. and Sighicelli, L. Preparation and characterisation of extruded monolithic ceramic catalysts. *Catalysis Today* **41** *(1998) 87-94*

Frith, W.J. and Lips, A. The rheology of concentrated suspensions of deformable particles. *Advances in Colloid and Interface Science* **61** *(1995) 161-189*

Fu, X., Dutt, M., Bentham, A.C., Hancock, B.C., Cameron, R.E. and Elliot, J.A. Investigation of particle packing in model pharmaceutical powders using x-ray

microtomography and discrete element method. *Powder Technology* **167** *(2006) 134-140*

Gao, J., Walsh, G.C., Bigio, D., Briber, R.M. and Wetzel, M.D. Residence time distribution model for twin screw extruders. *AIChE Journal* **45** *(12) (1999) 2541-2549*

Gasner, G.E., Bigio, D., Marks, C., Magnus, F. and Kiehl, C. A new approach to analyzing residence time and mixing in a co-rotating twin screw extruder. *Polymer Engineering and Science* **39** *(2) (1999) 286-298*

Goodrich, J.E. and Porter, R.S. Rheological interpretation of torque rheometer data. *Polymer Engineering and Science Journal* **7** *1 (1967) 45-51*

Götz, J., Buggisch, H. and Peciar, M. NMR imaging of pastes in a ram extruder. *Journal of Non-Newtonian Fluid Mechanics* **49** *(1993) 251-275*

Götz, J., Müller, D., Buggisch, H. and Tasche-Lara, C. NMR imaging of pastes in steady state flows. *Chemical Engineering and Processing* **33** *(1994) 385-392*

Gramann, P. and Rauwendaal, C. New dispersive and distributive mixers for extrusion and injection moulding. *The Madison Group Publications, ANTEC (2004)1-8.* http://www.madisongroup.com/publications/nrv.pdf

Graule, Th., Hidber, P., Hofmann, H. and Gauckler, L.J. Stabilization of alumina dispersions with carboxylic acids. *European Ceramics* **2** *(1991) 299-305*

Greenwood, R. Review of the measurement of zeta potentials in concentrated aqueous suspensions using electroacoustics *Advances in Colloid and Interface Science* ***106*** *(2003)55-81*

Griffiths, A.A. The phenomenon of rupture and flow in solids. *Phil Trans. Roy. Soc. Lond.* **A221** *(1920) 163-198*

Guzman-Castillo, M.L., Bokhimi, X., Toledo-Antonio, A., Salmones-Blasquez, J. and Hernandez-Beltran, F. Effect of boehmite crystallite size and steaming on alumina properties. *Journal of Physical Chemistry* **105** *(2001) 2099-2106*

Guzman-Castillo, M.L., Hernandez Beltran, F., Fripiat, J.J., Rodriguez-Hernandez, A., Garcia de Leon, R., Navarrete-Bolanos, J., Tobon Cervantes, A. and Bokhimi, X. Physciochemical properties of aluminas obtained from different aluminium salts. *Catalysis Today* **107-108** *(2005) 874-878*

Han, Y.S., Li, J.B. and Chen, Y.J. Fabrication of bimodal alumina ceramics. *Materials Research Bulletin* **38** *(2003) 373-379*

Hancock, B.C. Material interactions and surface phenomena in size enlargement processes. PhD Thesis, University of Bradford (1991)

Hancock, B.C., York, P. Rowe, R.C. and Parker M.D. Characterisation of wet masses using a mixer torque rheometer: 1. Effect of instrument geometry. *International Journal of Pharmaceutics* **76** *3 (1991) 239-245*

Hancock, B.C., York, P. and Rowe, R.C. Characterisation of wet masses using a mixer torque rheometer: 2. Mixing kinetics. *International Journal of Pharmaceutics* **83** *1-3 (1992) 147-153*

Hartman Kok, P.J.A., Kazarian, S.G., Briscoe, B.J. and Lawrence, C.J. Effects of particle size on near wall depletion in moo-dispersed colloidal suspensions. *Journal of Colloid and Interface Science* **280** *(2004) 511-517*

Hatzriakos, S.G. and Dealy, J.M. Wall slip of molten high density polyethylenes II. Capillary rheometry studies. *Journal of Rheology **36** (1992) 703-741*

He, M., Wang, Y. and Forssberg, E. Slurry rheology in wet ultrafine grinding of industrial minerals: a review. *Powder Technology* **147***(2004)94-112*

Hillerova, E., Jiratova, K. and Zdrazil, M. Determination of the surface polarity of peptized aluminas by gas chromatography. *Applied Catalysis* **1** *(1981) 343-354*

Hind, A.R., Bhargava, S.K. and Grocott, S.C. The surface chemistry of Bayer process solids: a review. *Colloids and Surfaces A: Physicochemical and Engineering Aspects* **146 (1-3)** *(1999) 359-374*

Holek, I.S. and Mendoza, C.I. The rheology of concentrated suspensions of arbitrarily-shaped particles. *Journal of Colloid and Interface Science* **346** *(2010) 118-126*

Holt, E.M. The properties and forming of catalysts and absorbents by granulation. *Powder Technology* **140** *(2004) 194-202*

Horrobin, D.J. and Nedderman, R.M. Die entry pressure drops in paste extrusion. *Chemical Engineering Science* **53** *(1998) 3215-3225*

Hotta, Y., Yilmaz, H., Shirai, T., Ohata, K., Sato, K., and Watari, K. State of the dispersant and particle surface during wet jet milling for preparation of a stable slurry. *Journal of the American Ceramic Society* **91** *4 (2008) 1095-1101*

Hotta, Y., Shirai, T., Sato, K., Yilmaz, K. and Watari, K. Hydrodynamic interaction of particles in Al_2O_3 slurries prepared by different milling methods. *Journal of the American Ceramic Society* **92** *6 (2009) 1198-1202*

Hsiang, H.I., Liang, M.T., Huang, H.C. and Yen, F.S. Preparation of superhydrophobic boehmite and anatase nanocomposite coating films. *Materials Research Bulletin* **42** *(2007) 420-427*

Huang, D., Luo, G.S. and Wang, Y.J. Using phosphoric acid to control the structures of mesoporous titanium dioxide materials. *Microporous and Mesoporous Materials* **84** *(2005) 27-33*

Huzzard, R.J. and Blackburn, S. Slip flow in concentrated alumina suspensions. *Powder Technology* **97** *(1998) 118-123*

Isobe, T., Kameshima, Y., Nakajima, A., Okada, K. and Hotta, Y. Extrusion method using nylon 66 fibers for the preparation of porous alumina ceramics with oriented pores. *Journal of the European Ceramic Society* **26** *(2006) 2213-2217*

Isobe, T., Kameshima, Y., Nakajima, A., Okada, K. and Hotta, Y. Gas permeability and mechanical properties of porous alumina ceramics with uni-directionally aligned pores. *Journal of the European Ceramic Society* **27** *(2006) 53-59*

Isobe, T., Takahiro, T., Kameshima, Y., Nakajima, A., and Okada, K. Preparation and properties of porous alumina ceramics with oriented cylindrical pores produced

by an extrusion method. *Journal of the European Ceramic Society* **26** *(2006) 957-960*

Isobe, T., Kameshima, Y., Nakajima, A., and Okada, K. Preparation and properties of porous alumina ceramics with uni-directionally oriented pore by extrusion method using a plastic substance as a pore former. *Journal of the European Ceramic Society* **26** *(2006) 2213-2217*

Jaeger, H.M. and Nagel, S.R. Physics of the granular state. *Science* **255** *(1992) 1523-1531*

James, A.E., Williamson, D.J.A. and Williamson, P.R. Direct measurement of static yield properties of cohesive suspensions. *Rheologica Acta* **26** *(1987) 437-446*

Jin, L., Mao, S., Wang, S and Dong, M. Optimization of the rheological properties of yttria suspensions. *Ceramics International* **35** *(2009) 925-927*

Jiratova, K. The influence of peptizing to physical and chemical properties of extruded alumina. *Chemicky Prumsyl* **31** *(1981) 174-179*

Jiratova, K. and Janacek, L. The influence of peptizing to physical and chemical properties of extruded alumina. *Chemicky Prumsyl* **31** *(1981) 174-179*

Johnhon, S.B., Russel, A.S. and Scales, P.J. Volume fraction effects in shear rheology and electroacoustic studies of concentrated alumina and kaolin suspensions. *Colloids and Surfaces A: Physicochemical and Engineering Aspects* **141** *(1998) 119-130*

Johnson, M.F.L. and Mooi, J. The origin and types of pores in some alumina catalysts. *Journal of Catalysis* **10** *(1968) 342-354*

Johnson, S.B., Franks, G.V., Scales, P.J., Boger, D.V. and Healy, T.W. Surface chemistry-rheology relationships in concentrated mineral suspensions. *International Journal of Mineral Processing* **58** *(2000) 267-304*

Karaman, M.E., Pashley, R.M., Waite, T.D., Hatch, S.J. and Bustamante, H. A comparison of interaction forces between model alumina surfaces and their colloidal properties. *Colloidal Surfaces* **129** *(1997) 241*

Keleb, E.I., Verniere, A., Vervaet, C. and Remon. Continuous twin screw extrusion for the wet granulation of lactose. *International Journal of Pharmaceutics* **239** *(2002) 69-80*

Khan, A.U., Briscoe, B.J. and Luckham, P.F. Evaluation of slip in capillary extrusion of ceramic pastes. *Journal of the European Ceramic Society* **21** *4 (2001) 483-491*

Kiss, A.B., Keresztury, G. and Farkas, L. Raman and i.r. spectra of boehmite. Evidence for the recently discarded D_{2h}^{17} space group. *Spectrochimica Acta* **36** *(1980) 653-658*

Kolenda, F., Retana, P, Racineux, G. and Poitou, A. Identification of rheological parameters by the squeezing test. *Powder Technology* **130** *(2003) 56-62*

Köster, M. and Thommes, M. In-line dynamic torque measurement in twin screw extrusion process. *Chemical Engineering Journal* **164** *(2010) 371-375*

Kristensen, H.G., Holm, P, Jaegerskou, A. and Schaefer, T. Granulation in high speed mixers. Part 4: Effect of liquid saturation on the agglomeration. *Pharmazeutische Industrie* **46** *(1984) 763-767*

Kukolev, G.V. and Karaulov, A.G. The properties of water suspensions of commercial alumina and rational conditions for slip casting. *Ogneupory* **4** *(1963) 168-174*

Kumar, A., Ganjyal, G.M., Jones, D.D. and Hanna, M.A. Modelling residence time distribution in a twin-screw extruder as a series of ideal steady-state flow reactors . *Journal of Food Engineering 84 3 (2008) 441-448*

Lamberov, A.A., Levin, O.V., Egorova, S.R., Evstyagin, D.A. and Aptikasheva, A.G. Effect of peptisation on texture and physicomechanical properties of aluminium hydroxides. *Russian Journal of Applied Chemistry* **76** *(2003) 351-357*

Landin, M, Rowe, R.C. and York, P. Characterisation of wet masses using a mixer torque rheometer: 3. Nonlinear effects of shaft speed and sample weight. *International Journal of Pharmaceutics* **84** *5 (1995) 557-560*

Lange, F.F. Powder processing science and technology for increased reliability. *Journal of American Ceramic Society* **72** *(1989) 3-15*

Laplace, P.S. *Mechanique Celeste*, Paris, (1806)

Laxton, P.B. and Berg, J.C. Gel trapping of dense colloids. *Journal of Colloid and Interface Science* **285** *(2005) 152-157*

Lazghab, M., Saleh, K., Peston, I., Guigon, P., Komumjer, L. Wettability assessment of finely divided solids. *Powder Technology* **157** *(2005) 79-91*

Lee, C.M. and Sohn, Y.S. Preparation and characterization of peptizable alumina. *Bulletin of the Korean Chemical Society* **6** *6 (1985) 329-333*

Lee, G.C.N. and Purdon, J.R. Brabender viscometry: 1. Conversion of Brabender curves to Instron flow curves. *Polymer Engineering and Science* **9** *5 (1969) 360-364*

Leong, Y.K. and Boger, D.V. Surface chemistry effects on concentrated suspension rheology. *Journal of Colloid and Interface Science* **136** *1 (1990) 249-258*

Li, Y., Wu, D, and Lin, Y.S. Mechanical strength and reliability of solid catalysts. *China Particuology.* **2** *(2004) 53-62*

Li, Y.Y. and Bridgwater, J. Prediction of extrusion pressure using an artificial neural network. *Powder Technology* **108** *(2000) 65-73*

Lian, C., Zhuge, Y. and Beecham, S. The relationship betwee porosity and strength for porous concrete. *Construction and Building Materials* **25** *(2001) 4294-4298*

Liang, Y., Hilal, N., Langston, P. and Starov, V. Interaction forces between colloidal particles in liquid: Theory and experiment. *Advances in Colloid and Interface Science* **134** *(2007) 151-166*

Lippens, B.C. Structure and texture of aluminas. *PhD Thesis, University of Delft (1961)*

Liu, F.J. and Chou, K.S. Determining the critical ceramic powder volume concentration from viscosity measurements. *Ceramics International* **26** *(2000) 159-164*

Liu, S. and Ha, Z. Prediction of random packing limit for multimodal particle mixtures. *Powder Technology* **126** *(2002) 283-296*

Loong, C.K. and Ozawa, M. Mass-fractal-like microstructure and proton disorder in nanostructured psuedoboehmite: a neutron-scattering study. *Journal of Electroanalytical Chemistry* **584** *(2005) 5-8*

Luckham, P.F. and Ukeje, M.A. Effect of particle size distribution on the rheology of dispersed systems. *Journal of Colloid and Interface Science* **200** *(1999) 347 – 356*

Lűtzenkirchen, J. Parameter estimation for the triple layer model. Analyiss of conventional methods and suggestion of alternative possiblilities. *Journal of Colloid and Interface Science* **204** *(1998) 119-127*

Luukkonen, P. Rheological properties and the state of water of microcrystalline cellulose and silicified microcrystalline cellulose wet masses. *Academic Dissertation, Department of Pharmacy, University of Helsinki (2001)*

Mackenzie, K.J.D., Temuujin, J., Smith, M.E. Effect of mechanochemical activation on the thermal reactions of boehmite (γ-AlOOH) and γ-Al_2O_3. *Thermochimica Acta* **359** *(2000) 87-94*

Mallette, J.G. and Soberanis, R.R. Evaluation of rheological properties of non-newtonian fluids in internal mixers: an alternative method based on the power law model. *Polymer Engineering and Science* **36** *20 (1996) 1436*

Malvern Article. Ten ways to control the rheology by changing particle properties (size, zeta potential and shape). Malvern Instruments INFORM series. http://www.malvern.com/common/downloads/campaign/MRK1236-01.pdf

Markhoff C.J., Mutsuddy, B.C. and Lennon, J.W. A method for determining critical ceramic powder volume concentration in the plastic forming of ceramic mixes. *Advances in Ceramics, American Ceramic Society* **9** *(1984) 246-250*

Marquez, A. Quijano, J. and Gaulin, M. A calibration technique to evaluate the power law parameters of polymer melts using a torque-rheometer. *Polymer Engineering and Science* **36** *20 (1996) 2556-2563*

Martens, W.N., Frost, R.L., Bartlett, J. and Kloprogge, J.T. The ageing of alumina hydrolysates synthesised from sex-butoxyaluminium. *Journal of Materials Chemistry* **11** *(2001)1681-1686*

Martens, W.N., Kloprogge, J.T., Frost, R.L. and Bartlett, J.R. A crystallite packing model for pseudoboehmite formed during the hydrolysis of trisecbutoxyaluminium to explain the peptizability. *Journal of Colloid and Interface Science* **247** *(2002) 132-137*

Martin, P.J., Wilson, D.I. and Bonnett, P.E. Rheological study of a talc-based paste for extrusion-granulation. *Journal of the European Ceramic Society* **24** *(2004) 3155-3168*

Martin, P.J. and Wilson, D.I. A critical assessment of the Jastrzebski interface condition for the capillary flow of pastes, foams and polymers. *Chemical Engineering Science* **60** *(2005) 493-502*

McGuire, P.A., Blackburn, S. and Holt, E.M. An X-ray micro-computed tomography study of agglomerate breakdown during the extrusion of ceramics. *Chemical Engineering Science* **62** *(2007) 6451-6456*

McGuire, P.A. 2008. Twin screw experimentation for process design. Thesis, (PhD). University of Birmingham.

Mewis, J. and Wagner, N.J. Current trends in suspension rheology. *Journal of Non-Newtonian Fluid Mechanics* **157** *(2009*) 1*47-150*

Meyer, A., Marshall, A., Bush, B.G. and Furst, E.M. Laser tweezer microrheology of a colloidal suspension. *Journal of Rheology* **50** *(2006) 77-93*

Mills, H. and Blackburn, S. Rheological behaviour of γ-alumina/boehmites pastes. *Transactions of IchemE,* **80** *A (2002)*

Mishra, D., Anand, S., Panda, R.K. and Das, R.P. Hydrothermal preparation and characterisation of boehmites. *Materials Letters* **42** *(2000) 38-45*

Mitra, S., Mukhopadhyay, R., Tsukushi, I. and Ikeda, S. Dynamics of water in confined spaces (porous alumina) QENS study. *Journal of Physics* **13** *(2001) 8455-8465*

Mohino, F., Martin, A.B., Salerno, P., Bahamonde, A. and Mendioroz, S. High surface area monoliths based on pillared clay materials as carriers for catalytic processes. *Applied Clay Science* **29** *(2005) 125-136*

Møller, P.C.F., Mewis, J. and Bonn, D. Yield stress and thixotropy: on the difficulty of measuring yield stresses in practice. *Soft Matter* **2** *(2006) 274-283*

Morgado Jr. E., Lau Lam, Y., Menezes, S.M.C. and Nazar L.F. Characterization of peptized boehmite systems: An ^{27}Al nuclear magnetic resonance study. *Journal of Colloid and Interface Science* **176** *(1995) 432-441*

Morgado Jr, E., Lau Lam, Y. and Nazar, L.F. Formation of peptizable boehmites by hydrolysis of aluminium nitrate in aqueous solution. *Journal of Colloid and Interface Science* **188** *(1997) 257-269*

Mooney, M. Explicit formulas for slip and fluidity. *Journal of Rheology* **2** *(1931) 210-222*

Moshkabad, M.E. and Winterbottom, J.M. The behaviour of an intermeshing twin screw extruder with catalyst immobilised screws as a three-phase reactor. *Catalysis Today* **48** *(1999) 347-355*

Musić, S., Dragćević, D. and Popović, S. Formation of boehmite via precipitation from aqueous solutions. *Materials Letters* **24** *(1995) 59-64*

Musić, S., Dragćević, D. and Popović, S. Formation of boehmite via precipitation from aqueous solutions. *Materials Letters* **24** *(1995) 59-64*

Nazar, L.F., and Klein, L.C., Journal of American Ceramic Society. **73** (1988) 187

Newitt, D.M. and Conway-Jones, J.H. A contribution to the theory and practice of granulation. *Transaction of the Institution of Chemical Engineers and the Chemical Engineer* **36** *422 (1958)*

Nguyen, Q.D. and Boger, D.V. Yield stress measurement in concentrated suspensions. *Journal of Rheology* **27** *(1983) 321-349*

Nguyen, Q.D. and Boger, D.V. Measuring the flow properties of yield stress fluids. *Annual Review of Fluid Mechanics* **24** *(1992) 47-88*

Nortier, P. and Fourre, P. Effects of crystallinity and morphology on the surface properties of alumina*. Applied Catalysis* **61** *(1990) 141-160*

Okada, K., Nagashima, T., Kameshima, Y. and Yasumori, A. Effect of crystallite size on the thermal phase change and porous properties of boehmite. *Journal of Colloid and Interface Science* **248** *(2002) 111-115*

Okada, K., Nagashima, T., Kameshima, Y., Yasumori, A. and Tsukada, T. Relationship between formation conditions, properties and crystallite size of boehmite. *Journal of Colloid and Interface Science* **253** *(2002b) 308-314*

Okada, K., Nagashima, T., Kameshima, Y. and Yasumori, A. Effect of crystallite size of boehmite on sinterability of alumina ceramics. *Ceramics International* **29** *(2003) 533-537*

Olson, W.L., and Bauer, L.J., Material Research Society Proceedings. **73** (1986) 187

Omara, N., Hotta, Y., Sato, K., Kinemuchi, Y., Kume, S. and Watari, K. Fabrication of stable Al_2O_3 slurries and dense green bodies using wet jet milling. *Journal of American Ceramic Society* **89** *9 (2006) 2738-2743*

Ouchiyama, N., Benbow, J.J. and Bridgwater, J. On the fracture toughness of extrudates and its relationship to rates of bulk particle attrition. *Powder Technology* **51** *(1987) 103-114*

Ovenston, A. and Benbow, J.J. Effects of die geometry on the extrusion of clay-like materials. *Transactions of the British Ceramic Society* **67** *(1968) 543-567*

Pabst, W., Gregorova, E. and Berthold, C. Particle shape and suspension rheology of short-fiber systems. *Journal of the European Ceramic Society* **26** *(2006) 149-160*

Palmer, D.A., Benezeth, P. and Wesolowski, D.J. Aqueous high-temperature solubility studies. I. The solubility of boehmite as functions of ionic strength (to 5 molal, NaCl), temperature (100–290°C), and pH as determined by in situ measurements. *Geochimica et Cosmochimica Acta* **65***, (2001) 2081-2095*

Panias, D., Asimidis, P and Paspaliaris, I. Solubility of boehmite in concentrated sodium hydroxide solutions: model development and assessment. *Hydromettalurgy* **59** *(2001) 15-29*

Parker, M.D., York, P. and Rowe, R.C. Binder-substrate interactions in wet granulation. 1: The effect of binder characteristics. *International Journal of Pharmaceutics* **64** *2-3 (1990) 207-216*

Parker, M.D. and Rowe, R.C. Source variation in the wet massing (granulation) of some microcrystalline celluloses. *Powder Technology* ***65*** *1-3 (1991) 273-281*

Parker, M.D., York, P. and Rowe, R.C. Substrate-binder interaction in wet granulation III The effect of substrate source variation. *International Journal of Pharmaceutics* **80** *(1992) 179-190*

Parks, G.A. The isoelectric point of solid oxides, solid hydroxides and aqueous hydroxo complex systems. *Chemical Reviews* **65** *(1965) 177*

Patankar, N.A. and Hu, H.H. Rheology of a suspension of particles in viscoelastic fluids. *Journal of Non-Newtonian Fluid Mechanics* **96** *(2001) 427-443*

Patel, M.J., Wedderburn, J., Blackburn, S. and Wilson, D.I. Maldistribution of fluids in extrudates. *Journal of the European Ceramic Society* **29** *(2009) 937-941*

Petrie, C.J.S. The rheology of fibre suspensions. Journal of Non-Newtonian Fluid Mechanics **87** (1999) 369-402

Pierce, P.E. and Holsworth, R.M. Determination of critical pigment by measurement of the density of dry paint films. *Official Digest* **37***-482 (1965) 272-283*

Pierre, A.C. and Uhlmann, D.R. Amorphous aluminium hydroxide gels. *Journal of Non-Crystalline Solids* **82** *(1986) 271-276*

Powell, J. and Blackburn, S. Co-extrusion of multi-layered ceramic micro-tubes for use as solid oxide fuel cell. *Journal of the European Ceramic Society (2010) Doi.10.1016/jeurceramsoc.2010.02.010*

Prabhakaran, K., Ananthakumar, S. and Pavithran, C. Gel casting of alumina using boehmite as a binder. *Journal of the European Ceramic Society* **19** *(1999) 2875-2881*

Prabhakaran L, Prushothaman M, Sriganesan P. Pharmaceutical Micropellets : An Overview. Latest Reviews **7** 4 (2009)

Previdi, F., Savaresi, S.M. and Panarotto, A. Design of a feedback control system for real-time control of flow in a single-screw extruder. *Control Engineering Practice* **14** *(2006) 1111-1121*

Quemada, D. and Berli, C. Energy of interaction in colloids and its implication in rheological modelling. *Advances in Colloid and Interface Science.* **98** *(2002) 51-85*

Ramal Jr. F.T., Pileggi, R.G., Gallo, J.B. and Pandolfelli, V.C. The particle size distribution effect on the rheology of refractory castables. *Ceramica* **48** *308 (2002)*

Ramsay, J.D.F., Daish, S.R. and Wright, C.J. Structure and stability of concentrated boehmite sols. *Journal of Chemical Society, Faraday Discussions.* **65***, 65 (1978)*

Reynolds, G.K., Fu, J.S., Cheong, Y.S., Hounslow, M.J. and Salman, A.D. Breakage in granulation: a review. *Chemical Engineering Science* **60** *(2005) 3969-3992*

Rosenberg, E.***,*** Kolenda, ***F.,*** Szymanski***, R.*** and Walter***, M.*** Characterization of alumina paste by cryomicroscopy, *Preparation of Catalysts VI (1995) 843-850*

Rough, S.L., Wilson, D.I. and Bridgwater, J. A model describing liquid phase migration within an extruding microcrystalline cellulose paste. *Chemical Engineering Research and Design* **80** *(2002) 701-714*

Rowe, R. and Sadeghnejad, G.R. The rheology of microcrystalline cellulose powder / water mixes – measurement using a mixer torque rheometer. *International Journal of Pharmaceutics* **38** *1-3 (1987) 227-229*

Rowe, R.C. Characterisation of wet masses using a mixer torque rheometer: 4. Effect of blade orientation. *International Journal of Pharmaceutics* **133** *1-2 (1996a) 133-138*

Rowe, R.C. Mixer Torque Rheometry – Further Advances. *Pharmaceutical Technology Europe* **8** *8 (1996b) 38-48*

Rumpf, H. The strength of granules and agglomerates. Knepper, W. (Ed.) Agglomeration. AIME, Interscience, New York (1962) 379-418

Russel, B.D., Lasenby, J., Blackburn, S. and Wilson, D.I. Characterising paste extrusion behaviour by signal processing of pressure sensor data. *Powder Technology* **132** *(2003) 233-248*

Russel, B.D., Lasenby, J., Blackburn, S. and Wilson, D.I. Monitoring structural aspects of pastes undergoing continuous extrusion using signal processing of pressure data. *Chemical Engineering Research and Design* **82** *(A6) (2004) 770-783*

Rutgers, I.R. Relative viscosity and concentration. *Rheologica Acta* **2** *(1962) 305-349*

Sato, Katsuya., Hotta, Y., Yilmaz, H., Sato, Kimiyasu., Watari, K. Fluidity of methyl cellulose contained suspensions and pastes prepared from differently milled Al_2O_3 powder. *Journal of Colloid and Interface Science* **331** *(2009) 221-226*

Scales, P.J., Kapur, P.C., Johnson, S.B. and Healy, T.W. Shear yield stress of partially flocculated colloidal suspensions. *American Institute of Chemical Engineers Journal* **44** *(3) (1998) 538-544*

Schefe, C.R., Kappen, P., Zuin, L., Pigram, P.J. and Christensen, C. Addition of carboxylic acids modifies phosphate sorption on soil and boehmite surfaces: A solution chemistry and XANES spectroscopy study. *Journal of Colloid and Interface Science* **330** *(2009) 51-59*

Servais, C., Ranc, H., Sansonnens, C., Ravji, S., Romoscanu, A. and Burbidge, A. Rheological methods for multiphase materials. *3rd International Symposium on Food Rheology and Structure (2003) 137-141*

Shah, A. and Gupta, M. Comparison of the flow in co-rotating and counter-rotating twin-screw extruders. Society of Plastics Engineering Annual Technical Papers (*ANTEC) (2004) 443-447*

Sharp, D.W.A. The Penguin Dictionary of Chemistry, 3rd edition. Penguin (2003)

Shearer, G. and Tzoganakis, C. Relationship between local residence time and distributive mixing in section of a twin screw extruder. *Polymer Engineering Science* **41** *(2001a) 2206-2215*

Shearer, G. and Tzoganakis, C. Distributive mixing profiles for co-rotating twin screw extruders. *Advanced Polymer Technology* **20** *(2001b) 169-190*

Slade, R.C.T. and Halstead, T.K. Evidence for proton pairs in γ-AlOOH (Boehmite) from NMR absorption spectra. *Journal of Solid State Chemistry* **32** *(1980) 119-122*

Snabre, P. and Mills, M. Rheology of concentrated suspensions of viscoelastic particles. *Colloids and Surfaces A: Physicochemical and Engineering Aspects* **152** *(1999) 79-88*

Soh, J.L.P., Liew, C.V. and Heng, P.W.S. Torque rheological parameters to predict pellet quality in extrusion – spheronisation. *International Journal of Pharmaceutics* **315** *(2006) 99-109*

Stenger, F., Mende, S., Schwedes, J. and Peukert, W. The influence of suspension properties on the grinding behavior of alumina particles in the submicron size range in stirred media mills. *Powder Technology* **156** *(2005) 103-110*

Stoepler, R. and Unger, K.K. The properties of commercial alumina base materials and their effect on the manufacture of active porous alumina supports by means of extrusion. *Preparation of Catalysts III (1983) 643-651*

Strenge, K. and Bollmann, U. A rheological investigation of peptized boehmite suspensions. *Colloids and Surfaces* **57** *(1991) 139-148*

Sunil Kumar, C., Balagopal, N., Damodaran, A.D. and Warrier, K.G.K. Processing and densification of ceria - zirconia ceramic through extrusion of ceramic - polymer mixture. *Ceramics International* **20** *(1994) 183-187*

Sunil Kumar, C., Hareesh, U.S., Damodaran, A.D., Warrier, K.G.K. Monohydroxy aluminium oxide (boehmite, AlOOH) as a reactive binder for extrusion of alumina ceramics. *Journal of the European Ceramic Society* **17** *(1997) 1167-1172*

Sunil Kumar, C. Hareesh, U.S., Damodaran, A.D., Warrier, K.G.K. Aqueous extrusion of alumina – zirconia (12 mol % ceria) composite using boehmite as an extrusion aid. *Ceramics International* **24** *(1998) 583-587*

Sweeney, S.M. and Martin, C.L. Pore size distribution calculated from 3-D images of DEM-simulated powder compacts. *Acta Mater* **51** *(2003) 3635-3649*

Tang, H.S. and Kalyon, D.M. Estimation of the parameters of Herschel Bulkley fluid under wall slip using a combination of capillary and squeeze flow viscometers. *Rheologica Acta* **43** *(2004) 80-88*

Theuerkauf, J., Witt, P., Schwesig, D. Analysis of particle porosity distribution in fixed beds using the discrete element method. *Powder Technology* **165** *(2006) 92-99*

Tischer, R.E. Preparation of bimodal aluminas and molybdena / alumina extrudates. *Journal of Catalysis* **72** *(1981) 255-265*

Tomita, N., Guo, L., Zhang, Y., Uchida, N. and Uematsu, K. Effect of temperature on characteristics of alumina slurry. *Science, Technology and Applications of Colloidal Suspensions* **24** *(1994) 103-109*

Tottenhorst, R.D. and Hoffman, D.A. *Clays and Clay Minerals* **28** *(1980) 373*

Trimm, D.L. and Stanislaus, A. The control of pore size in alumina catalyst supports: a review. *Applied Catalysis* **21** *(1986) 215-238*

Tsesekou, A., Agrafiotis, C. and Milias, A. Optimization of the rheological properties of alumina slurries for ceramic processing applications Part I: Slip casting. *Journal of the European Ceramic Society* **21** *(2001) 363-373*

Tsukada, T., Segawa, H., Yasumori, A. and Okada, K. Crystallinity of boehmite and its effect on the phase transition temperature of alumina. *Journal of Materials Chemistry* **9** *(1999) 549-553*

Unlu, E. and Faller, J.F. RTD in twin screw food extrusion. *Journal of Food Engineering* **53** *(2002) 115-131*

Vainio, T.P., Harlin, A. and Seppala, J.V. Screw optimisation of a corotating twin-screw extruder for a binary immiscible blend. *Polymer Engineering Science* **35** *(1995) 225*

Van Bruggen, M.P.B., Donker, M., Lekkerkerker, H.N.W. and Hughes, T.L. Anomolous stability of aqueous boehmite dispersions induced by hydrolyzed aluminium poly-cations. *Colloids and Surfaces A: Physicochemical and Engineering Aspects* **150** *(1999) 115-128*

Van Kao, S., Nielsen, L.E. and Hill, C.T. Rheology of concentration suspensions of spheres I: Effect of the liquid-solid interface. *Journal of Colloid and Interface Science* **53** *(1975) 358-366*

Vergnes, B. and Berzin, F. Modelling of reactive systems in twin screw extrusion: challenges and applications. *C.R. Chimie* **9** *(2006) 1409-1418*

Villmow, T., Kretzschmar, B. and Pötschke, P. Influence of screw configuration, residence time, and specific mechanical energy in twin-screw extrusion of polycaprolactone/multi-walled carbon nanotube composites. *Composites Science and Technology* **70** *14 (2010) 2045-2055*

Wang, X. and Rackaitis, M. Gelling nature of aluminum soaps in oils. *Journal of Colloid and Interface Science* **331** *(2009) 335-342*

Wefers, K. and Bell, G.M. Oxides and Hydroxides of Aluminium; *ALCOA Technical Paper 19 (1972)*

Wefers, K., Misra, C. Oxides and Hydroxides of Aluminum; ALCOA Laboratories, Pennsilvania, USA, (1987)

Wildman, R.D., Blackburn, S. Breakdown of agglomerates in ideal pastes during extrusion. *Journal of Materials Science* **33** *(1998) 5119-5124*

Wildman, R.D., Blackburn, S., Benton, D.M., McNeil, P.A. and Parker, D.J. Investigation of paste flow using positron emission particle tracking. *Powder Technology* **103** *(1999) 220-229*

Wilson, D.I. and Rough, S.L. Exploiting the curious characteristics of dense solid-liquid pastes. *Chemical Engineering Science* **61** *(2006) 4147-4154*

Wood, R., Fornasiero, D. and Ralston, J. Electrochemistry of the boehmite-water interface. *Colloids and Surfaces* **51** *(1990) 389-403*

Worrall, W.E. and Khan, R.A. An extrusion method of assessing the plasticity of clays. *Transactions and Journal of the British Ceramic Society* **71** *(1972) 159-161*

Xu, X. and Hilmas, G.E. The rheological behaviour of ceramic / polymer mixtures for coextrusion processing. *Journal of Material Science* **42** *(2007) 1381-1387*

Yaras, P., Kalyon, D. and Yilmazer, U. Flow instabilities in capillary flow of concentrated suspensions. *Rheologica Acta* **33** *(1994) 48-59*

Yasuoka, M., Okada, K., Hayashi, T. and Otsuka, N. Property changes of machanochemically treated alumina powders by annealing. *Ceramics International* **18** *(1992) 131-135*

Ye, G., Xin, H., Bao-lin, Z., Bao-gui, M. amd Hong-bo. Method for calculating packing density of powder particles in paste with continuous particle size distribution. *Powder Technology* **187** *(2008) 88-93*

Yilmazer, U. and Kalyon, D.M. Dilatancy of highly filled suspensions with Newtonian matrices. *Polymer Composites* **12** *(1991)*

Youssef, A.M. Effect of addition of water-soluble organic polymers on the porosity and adsorption properties of alumina. *Journal of Colloid and Interface Science* **54** *(1976) 447-449*

Yu, A.B., Bridgwater, J., Burbidge, A. and Saracevic, Z. Liquid maldistribution in particulate paste extrusion. *Powder Technology* **103** *(1999) 103-109*

Zakharchenya, R.I. Influence of peptization on the properties of alumina produced from boehmite gels. *Journal of Sol-Gel Science and Technology* **6** *(1996) 179–186*

Zheng, J., Carlson, W.B. and Reed, J.S. Dependence of compaction efficiency in dry pressing on the particle size distribution. *Journal of the American Ceramic Society* **78** *9 (1995) 2527– 2533*

Zhou, Z., Scales, P.J. and Boger, D.V. Chemical and physical control of the rheology of concentrated metal oxide suspensions. *Chemical Engineering Science* **56** *(2001) 2901-2920*